

**GEOLOGY, METAMORPHISM
AND TECTONIC EVOLUTION OF
A SEGMENT OF THE PALGHAT GAP, KERALA**

Thesis submitted to
the Cochin University of Science and Technology
for the degree of
DOCTOR OF PHILOSOPHY
in
GEOLOGY

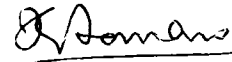
By
THARA K. G.

CENTRE FOR EARTH SCIENCE STUDIES
TRIVANDRUM, INDIA

MAY, 1992

C E R T I F I C A T E

This is to certify that this thesis submitted to the Cochin University of Science and Technology for the award of the Ph.D Degree is an authentic record of research carried out by Smt. K.G. Thara under my supervision and no part of it has previously formed the basis for the award of any other degree in any University.



Dr. K. Soman,
Research Guide &
Scientist-in-charge,
Geodata Information Group,
Centre for Earth Science
Studies,
Thiruvananthapuram - 695031.

Thiruvananthapuram,
22nd June, 1992.

CONTENTS

	PAGE NO.
Acknowledgement	i - iii
Abstract	1 - 16
Chapter I Introduction	17- 26
Chapter II General Geological Setting	27- ..
II.1 Regional Geology & Geomorphology	27- 30
II.2 Geology of the study area	30- 49
II.3 Structure & tectonic framework of the area	49- 63
Chapter III Petrography	64 - ..
III.1 Khondalites	64- 82
III.2 Calc granulites	82- 93
III.3 Crystalline limestones	93- 98
III.4 Migmatitic gneisses	98-106
III.5 Amphibolites	106-110
III.6 Granites	110-115
III.7 Pegmatite	115-118
Chapter IV Geochemistry & Petrogenesis	119 -...
IV.1 Khondalites	119-133
IV.2 Calc granulites	133-149
IV.3 Crystalline limestones	149-155
IV.4 Migmatitic gneisses	155-168
IV.5 Amphibolites	168-175
IV.6 Granites	175-189
IV.7 Pegmatites	189-190

Chapter	V	Mineral Chemistry	191-...
	V.1	Garnet	192-199
	V.2	Biotite	199-204
	V.3	Alkali feldspar	204-207
	V.4	Plagioclase	207-211
	V.5	Cordierite	211-...
	V.6	Clinopyroxene	211-217
	V.7	Amphibole	217-221
Chapter	VI	Conditions of Metamorphism	222-224
	VI.2	Geothermometers	224-238
	VI.3	Limitations: Possible sources of errors and precautions	238-243
	VI.4	Geobarometry	244-256
	VI.5	Accuracy and precision	256-261
	VI.6	Results	261-282
	VI.7	Fluid inclusion studies	282-292
	VI.8	Discussion and Conclusions	292-304
Chapter	VII	Age	305-316
Chapter	VIII	Conclusions	317-328
Appendix			329-336
References			337-370

ABSTRACT

Palghat Gap is the only major breach within the Western Ghats, and constitutes a very conspicuous geomorphic feature in the landscape of Peninsular India. Widely contrasting and contradicting hypotheses exist on its origin, advocating marine and fluvial erosion, crustal upwarp and consequent development of joints and fractures, as well as tectonic processes such as block faulting. This clearly shows that the origin of the Palghat Gap is still a controversy, and evinces further geological interest. The present study was initiated in this backdrop, with the prime object of elucidating the geologic setting and metamorphic evolution of a segment of the Palghat Gap with contrasting geological features.

Geological mapping of the study area (about 100 km²) in 1:25,000 scale, comprising a part of the Gap proper and a part of its northern flank within Kerala, reveals the presence of two distinct rock units: 1. Garnet-biotite-sillimanite ± graphite gneisses (*khondalite sensu stricto*), ubiquitously associated with calc granulites and crystalline limestones, with a subordinate group of sillimanite-free gneisses and pockets of cordierite-bearing gneisses, exposed towards the flank, and 2. Fissile migmatitic rocks comprising biotite and biotite-hornblende gneisses showing discontinuous and boudinaged bands of amphibolites and associated granites and pegmatites occurring within them.

Field investigations indicate that the rocks of this area experienced three deformation episodes with certain geological evidences in favour of mylonitisation in khondalites and intense fracturing of calc granulites in the northern flank. The first phase (D_1) resulted in a compositional layering (S_1), observed more distinctly in khondalites and migmatitic gneisses. The second phase (D_2) is evidenced by E-W symmetrical to isoclinal folds, defined by S_1 with an easterly gentle plunge, observed in calc granulites and migmatitic gneisses with an associated lineation L_1 . The third phase (D_3) is marked by the development of gentle or open N-S folds and N-S, NE-SW and NW-SE trending fractures. Boudinage in amphibolites is attributed to D_1 -deformation stage whereas the D_1 - D_2 transition is characterised by extensive migmatisation. More pervasive migmatisation is coeval with the D_2 -event.

Equal area lower hemisphere projection of 184 measurements of joints in the Gap and 50 measurements in the flank, revealed the presence of two prominent sets trending ENE-WSW and N-S in the flank and the additional presence of NW-SE joints in the Gap.

Khondalites are medium-to coarse-grained, typically polymetamorphic, porphyroblastic rocks showing extreme dynamic effects like crushing and granulation of minerals. The sillimanite-free varieties are constituted mainly by

quartz and feldspar (50-60 modal %) with 15-22 % of biotite, as compared to khondalites (*sensu stricto*) with 40% quartz and about 9% biotite. Sillimanite percentage is highly variable from 0 to 21%. Two generations of sillimanite are distinguished, an earlier generation of prismatic and elongate crystals and a later fibrolitic sillimanite associated with biotite, as a breakdown product. Three generations of biotite are identified; one as inclusions in garnet, the second as a phase coexisting with garnet as well as sillimanite and the third is formed after garnet. Cordierite appears to have grown by a progressive mineral reaction involving consumption of biotite, sillimanite, quartz and plagioclase. Characterised by a wide variation in SiO_2 values (46-66 wt %) and high wt % of Al_2O_3 (13-39 %), the khondalites correspond closely to the Al-rich petrochemical types. A pelitic - to arenite parentage is suggested by the geochemical plots.

Intimately associated with the garnet-biotite-sillimanite \pm graphite gneiss (*khondalite sensu stricto*) and crystalline limestones, the calc granulites are characterised by their fine-grained, xenomorphic granular texture. Based on mineralogy and modal proportions, two types (type I and type II) have been distinguished. Type I is characterised by K-feldspar + calcite + vesuvianite + scapolite + diopside + grossularite + sphene assemblage while in type II, garnet is conspicuously absent and sphene is present in much more

abundant proportions. Geochemical data reveal a predominance of K_2O (2.87 wt %) over Na_2O (1.76 wt %) for type I while, the reverse holds true for type II with Na_2O (2.51 wt %) predominating over K_2O (1.97 wt %). Petrogenetic characterisation implies a protolith of impure, silica-rich calcareous sediments admixed with phyllosilicates and clays.

Crystalline limestones are medium-to coarse-grained rocks with typical crystalline texture, often passing over to elongated granoblastic texture. Geochemical characterisation of the limestones into two groups, based on elemental concentrations, is also borne out by the modal analyses. Group I marbles are richer in CaO and poor in other major elements. Presence of diopside, sphene, hornblende, magnetite, muscovite and higher percentages of quartz are characteristic of group II marbles. The ubiquitous association of dolomite with silicates suggests that dolomite is a product of silicate + calcite reaction and is presumed to be not of primary origin. Geochemical plots imply a protolith consisting of an admixture of limestone with variable proportions of marly impurities.

Migmatitic rocks comprise biotite - and biotite-hornblende gneisses. A stromatic structure, often grading into surreitic and schollen types is exhibited with rafts of amphibolite boudins preserved in them. They are medium-to coarse-grained rocks, displaying xenomorphic granular texture. Biotite gneiss is typically coarse-grained with a

mineralogy of K-feldspar (46 modal %), quartz (36 %), plagioclase (12 %) and biotite (5 %). Biotite-hornblende gneiss is an intensely deformed, medium- to coarse-grained rock, chiefly composed of quartz + plagioclase + biotite + hornblende + K-feldspar assemblages with accessory phases of apatite, magnetite and sphene. Increased proportions of hornblende towards the flank and occurrence of biotite as an alteration product of amphibole are noteworthy features. A calc-alkaline trend is indicated by the AFM and Ca - Na - K plots. Negative linearity is indicated by almost all the major elements. Decreasing trend of Al_2O_3 and CaO with SiO_2 indicate anorthite fractionation. Depletion trends of MgO, FeO and TiO_2 as well as increasing trend of K_2O are consistent with the progressive removal of hornblende, with synchronous K-enrichment.

Amphibolites occur as xenolithic masses of various sizes and shapes within the migmatitic gneisses. Intricately permeated by granitic material, typifying a paleosome-neosome relationship, these lenticular, discontinuous patches or boudins pass quite imperceptibly into migmatitic gneisses. Medium - to coarse-grained, they exhibit an inequigranular, xenoblastic texture. Petrographic observations reveal textures suggestive of partial or complete replacement of clinopyroxene by hornblende and biotite is observed to occur as a hornblende-break down reaction product. Major and trace element signatures speak of a basaltic and more distinctly, a

quartz normative tholeiitic origin. In the absence of REE data, their tholeiitic nature could not be established conclusively. However, a general basic igneous trend is indicated by the ACF and Niggli mg-c plots while, TAS and AFM plots suggests a possible, homogeneous mantle source for them.

Granites have intrusive relationships with the amphibolites and exhibit faint foliation towards periphery. These are phanero-crystalline, medium - to coarse-grained rocks with typical granitoid texture. Mineralogical peculiarities include a two-feldspar composition with perthites dominating over plagioclase. Plots in K_2O Vs. CaO and K_2O Vs. Na_2O as well as normative An-Ab-Or diagram show a range between granodiorite and granite. High ratios of K_2O/CaO (1.43) and Fe_2O_3/CaO (0.69) are also characteristic. Increase in A/CNK values from 1.114 to 1.29 towards periphery, compared to the core portions reflect the increasing peraluminous nature of biotite-hornblende granites. This is attributed to the removal of the metaluminous phase (hornblende) through fractional crystallisation, which is also consistent with the observed increase in Na_2O and decrease in TiO_2 and Sr contents. Exsolution textures, general high potash contents exceeding soda and formation of microcline after plagioclase argue in favour of a late potash metasomatism. They typically correspond to late-post kinematic types (Marmo, 1971), while

discrimination of tectonic environments based on their geochemical characteristics point to their classification as POG (post orogenic granitoid) groups. Alkali feldspar (av) - plagioclase (av) temperature of 527°C obtained for one of the granites (Ps.11) at 5 Kbars closely corresponds to the retrogressive reequilibration event in granulitic rocks and to the temperature estimated for the migmatites of the Gap proper.

Pegmatites exhibit concordant to discordant relationships with the country rocks and are assigned to two intrusion episodes; one with predominantly white feldspar, folded along E-W direction and another, with pink feldspar, showing pinch and swell effects. They are unzoned and have a simple mineralogy with quartz (40-42 modal %), microcline (25-35 %), perthite (14-25 %), biotite (4-10 %) and plagioclase (3-8 %) as the major minerals. Pegmatites within the metasedimentary sequence contain additionally garnet (2-10 %) and muscovite (6 %). Mineralogical composition supports a migmatitic origin of the pegmatitic melts. Temperature estimates obtained for the pegmatites (av.547°C) correspond well with the retrograde temperatures of khondalites (av.521°C).

Microprobe analyses of garnets in khondalites and associated gneisses show that they are almandine-rich, with low Mn contents. Zoning profiles provided for garnets from the metapelitic rocks show many characteristics typical of

granulite terrains. Enrichment of almandine from core to rim is also expressed in chemical terms by a lower X_{Mg} . Garnet in calc granulites are remarkably high in grossular content (59-61 %) while, almandine is distinctly low at 36-38 mol %.

Individual grains of biotite show the effect of redistribution of elements during retrogression. The general Mg-enrichment trends observed in biotite from matrix - to contact zones - to inclusions indicate chemical exchange with host garnets and is well illustrated also by plots of Al^{iv} Vs. $Mg/(Mg + Fe)$ and X_{Mg} Vs. Ti, where the matrix biotite composition corresponds to the Fe-rich varieties (Mg:Fe < 2:1) while, the rims and especially the inclusions tend towards Mg-rich (Mg:Fe > 2:1) or phlogopite composition. On the basis of their increasing Mg and decreasing Ti and Fe concentrations (atomic proportions), three groups of biotite (biotite I, II and III) have been distinguished, an assumption which goes well with the petrographic evidences too.

The alkali feldspars are characterised by small Ca (0.013 p.f.u, average) and Fe (0.004 p.f.u, average). Anorthite content of alkali feldspar is largely controlled by the rock chemistry, especially the $Na_2O/(Na_2O + K_2O)$ ratio of the host rocks. Towards plagioclase contacts, 'Or' increases and 'Ab' shows a corresponding decrease. Higher Fe concentrations in perthites of granites, compared to matrix

alkali feldspar, is reflected in the higher temperature estimates for the former.

Plagioclase grain is unzoned and exhibits more or less a uniform composition. In sillimanite-bearing and absent-metapelitic rocks, plagioclase composition corresponds to oligoclase and in cordierite-bearing rocks, it becomes albitic. In calc granulites, an andesine composition is reported.

Cordierites are Mg-rich (8.43 wt % MgO) and contain appreciable amounts of FeO also (7.84 wt %). They are relatively poor in Na and K (< 0.03 p.f.u and 0.001 p.f.u respectively) and Mn is reported only in trace amounts (< 0.004 p.f.u). X_{Fe} shows a slight decrease from core to rim.

Clinopyroxene of calc granulites shows a wide variation from hedenbergitic to diopsidic composition. The large variation in $Mg/(Mg + Fe)$ and $Ca/(Ca + Fe + Mg)$ of the two sets of clinopyroxene implies that the mechanism of equilibration was a combination of cation exchange and solution regrowth. More specifically, the change in composition may be related to the incomplete re-equilibration during decrease in temperature (from 808 to 775°C) and a pressure drop from 4.39 to 2.20 Kbars, whereby the clinopyroxene changed by diffusion processes, towards a diopsidic composition.

Amphiboles of both the calc granulites and migmatitic gneisses correspond to calcic types with a calcium content in the range of 1.9-2.0 (p.f.u). In the binary plot of (Na + K) Vs. Al^{iv} of Robinson et al (1971), amphiboles from granulites lie close to the hornblende composition and the amphiboles from migmatitic gneisses lie towards pargasite field. In the Giret et al (1980) diagram, they plot respectively in the fields of hornblende and ferro-magnesio-hastingsite field. Total aluminium content of amphiboles in calc granulites is higher, compared to that in migmatitic gneiss, reflecting their higher temperature and increased grade of metamorphism.

Based on an approach of 'centre to centre' compositions of equilibrium assemblages and 'rim to rim' compositions of contacting grains of cordierite, garnet, biotite etc., quantitative data on the peak, as well as the retrograde temperature of metamorphism were estimated through the use of a variety of exchange and solvus thermometric methods.

A peak metamorphic temperature of $\sim 800^{\circ}C$ has been assumed, based on phase equilibria constraints such as the coexistence of plagioclase and scapolite in calc granulites, X_{Mei} content of 74-79% in scapolite of calc granulites and absence of evidences in favour of anatexis in the granulites. The ubiquitous presence of sillimanite in the granulites and its stability relations along with the P-T constraints exerted by cordierite + almandine + sillimanite + quartz

assemblages, limits the peak pressure to ~ 8 Kbars.

However, average temperatures calculated at peak pressures of ~ 8 Kbars by various garnet-biotite thermometers (Thompson, 1976; Ferry & Spear, 1978; Holdaway & Lee, 1977; Hodges & Spear, 1982; Perchuk & Lavrente'va, 1983; Indares & Marignole, 1985; Bhattacharya & Raith, 1987) reveal a temperature range from 759°C to 1000°C for the khondalites and associated gneisses. Garnet-cordierite 'pressure-independent' thermometers (Holdaway & Lee, 1977; Perchuk & Lavrente'va, 1983; Bhattacharya et al, 1988) yield a lower range from 802 to 813°C for the cordierite-bearing khondalite, which is conformable to the perthitic alkali feldspar-plagioclase (average) temperatures (828°C) of Green & Usdansky's (1986) Na-distribution model, at 5 Kbars. Garnet-clinopyroxene temperatures of the calc granulites, estimated by Ellis & Green (1979) method also indicate a peak temperature of 792°C.

Retrogressive metamorphic conditions estimated by various methods, using mineral phases in contact with each other, give a mean temperature value of 652°C (av). Garnet (rim)-biotite (secondary) temperatures of khondalite are lower at 521°C, comparable to the garnet (rim)-newly formed biotite (biotite III) temperatures of pegmatite (547°C, av). Plagioclase-amphibole equilibrium temperature by amphibole Al_T content (Plyusnina, 1982), from one of the hornblende-biotite migmatitic gneiss samples (close to a granite

occurrence), is estimated to be 530°C. This is comparable to the alk-Fs (av)-plag (av) temperature (527°C) obtained for the granite sample at 5 Kbar pressure. Neomineralisation associated with migmatisation and granitic emplacement is therefore, fixed at 532°C (mean).

Core pressures estimated for the khondalites and associated gneisses using Ghent (1976), Newton & Haselton (1981), Mckcenna & Hodges (1988) and Koziol & Newton (1988, 1989) barometers yield values ranging from 7.58 to 9.99 Kbars at 800°C. Cordierite-bearing gneisses yield peak pressures in the range from 5.7 to 8.15 Kbars. Geobarometric calculations at $P_{H_2O} = P_{total}$ conditions, based on garnet-cordierite geobarometers of Bhattacharya & Sen (1985) and Bhattacharya (1986) bracket equilibrium pressures within reasonable limits (9.07 & 10.38 Kbars), thus fixing the peak pressure approximately at 8.4 Kbars. Application of clinopyroxene-garnet-plagioclase-quartz method of Perkins & Newton (1981) yields a mean pressure value of 3.3 Kbars for the calc granulite sample occurring close to the Gap proper. Extensive application of Moecher et al (1988) geobarometer for the present study has been limited due to the compositional constraints introduced by extensive solid solution between hedenbergite and diopsidic compositions of clinopyroxene grains.

Rim pressures corresponding to peak temperatures, calculated for the khondalites and associated gneisses are

estimated to be 6.50 Kbars. Pressure values by plagioclase-hornblende geobarometer of Plyusnina (1982) for one of the migmatitic gneiss samples close to a granite occurrence, is 4.66 Kbars at a temperature of 530°C. Barometers of Hammarstrom & Zen (1986) and Hollister et al (1987) yield closely corresponding values of 4.72 and 4.92 Kbars respectively. Pressures estimated by the cordierite-garnet geobarometers for $P_{H_2O} = 0$ conditions range from 2.84 to 3.84 Kbars which approximate to the average neomineralisation pressures of pegmatites. Thus, the neomineralisation episode associated with migmatisation and attendant granitic emplacement is fixed at an average pressure of 4.97 Kbars.

Results obtained from the garnet-biotite thermometers indicate a pressure dependence of 3.6 to 5.4°C/Kbar. It is 5.1°C/Kbar for garnet-cordierite and 12-14°C/Kbar for two - feldspar thermometers. Ghent's (1976) pressure estimates have a dependence of 12.5 to 14 bar/degree and for Koziol & Newton (1989), it is 14.5-16.5 bar/degree. Precision and accuracy determinations of the various thermometric sensors indicate that uncertainties do not exceed $\pm 60^\circ\text{C}$ and the obtained results have been confirmed by the use of intersecting GPAQ pressure-temperature lines as well. The reported values of peak metamorphism of 800°C and 8.4 Kbars are comparable to the P-T conditions of granulites world over and also fall in Bohlen's (1987) best fit P-T box of 7.5 ± 1 Kbar and $800^\circ\text{C} \pm 50^\circ\text{C}$ for granulites.

Fluid inclusion studies in selected quartz plates from granulitic rocks reveal the presence of three types of inclusions: 1. An early CO₂-rich inclusion 2. Mixed carbonic-aqueous inclusions and 3. H₂O-rich inclusions, which have a bearing on the fluid evolution history of granulitic rocks. Freezing and heating studies suggest CO₂ density of 0.8-0.9 g/cm³ for the carbonic inclusions, which in turn fixes the pressure at 4.9 and 4.1 Kbars respectively, corresponding to peak as well as retrograde temperatures obtained by mineral thermometry.

Since P-T estimates of granulites are the minimum estimates of the actual metamorphic conditions (Frost & Chacko, 1989), the presently estimated values can be suggested as the lower limit of the P-T maxima attained by the granulites of the study area. The possibility is further amplified by the high P-T values for the pelitic units of the Nilgiri Hills reported by other workers.

The overall P-T array defined by the maximum and minimum pressure-temperature limits of the granulitic rocks of the study area suggests a steep cooling curve corresponding to isothermal depression (ITD) path, which is corroborated by the crossings of P-T lines also. The obtained P-T path is consistent with the typical evolution path of south Indian khondalites and can be ascribed to the net result of tectonic thickening combined with the vertical redistribution of heat

through syn to post-thickening magmatism, followed by extension. Lack of correspondence between the geometry of the ITD paths with the model paths of erosion (England & Thompson, 1984) preferentially favour a tectonic extension setting, which is also consistent with the findings of Van Reenan et al (1987), Sonder et al (1987) and Harley (1989). An element of IBC component generally observed towards the closing stages of an ITD path, as the one obtained for the study area, coinciding with the reequilibration-granite emplacement stage, further supports this.

K-Ar dating of muscovite and biotite samples from pegmatites belonging to the post D₂ syn-D₃ deformation episode, located within the migmatitic gneisses and the metasedimentary sequence yields ages ranging from 484-512 m.y. Field relations preclude the possibility of any significant metamorphic or tectonic episode to have affected the pegmatites, which is also substantiated by the close correspondence of age results from the central and peripheral portions of large mica flakes and concordance of ages between muscovite and biotite samples.

The reported K-Ar ages (484-512 m.y.) of biotite and muscovite from the Palghat Gap region correspond with the prominent Late Precambrian-Early Paleozoic acid magmatic emplacement phase observed in Kerala and elsewhere in south India. Since, pegmatite emplacement is known to be

associated with the closing stages of tectono-magmatic cycles, it is reasonable to suggest that the reported ages represent the closing stages of a tectono-magmatic event in Palghat Gap, presumably related to isothermal depression during crustal uplift associated with the retrogressive event. This inturn would suggest that the tectonic framework for the formation of the Palghat Gap was initiated during this period.

CHAPTER I

INTRODUCTION

Palghat Gap is a prominent geomorphic feature in the landscape of South India (Fig.1). This low level landform having a width of about 30 km and a length of over 80 km in an east-west direction and bordered by the Nilgiris to the north and the Anaimalai massif to the south, constitutes the only major break in the Western Ghats. The Gap proper has a subdued profile (Fig.2 a & b) with an average elevation of 60 m in the western part and 120 m in the eastern part, with well-defined scarp faces towards southern and northern flanks. Origin of this interesting geomorphic feature is still a controversy with the present day discussions centering around apparently conflicting hypotheses:

(1) Fluvial action model of Jacob and Narayanaswamy (1954) attributed the origin of the Gap to a large easterly flowing and a probable westerly flowing drainage systems with their source very close to the Palghat region. Absence of strike trends and other structural features indicative of faulting were taken as supporting evidences in favour of a fluvial origin.

(2) Supported by the geomorphological and structural evidences in favour of uplift of the Nilgiris flanking the Palghat Gap to the north, through large-scale faulting and



Fig.1 Landsat (MSS band 4) image of Palghat Gap. Scale : 1:1 million.



Fig.2(a) A view of a part of the Palghat Gap close to the northern flank.



Fig.2(b) View of the northern flank from the Malampuzha reservoir site.

the suggested presence of a wide shear zone in the Mangalam (10° 34'; 70° 31') and Walayar (10° 51'; 76° 51') dam sites within the Gap (Balasundaram, 1953; 1954), Arogyaswamy (1962) emphasised the role of structural control and marine erosion subsequent to the uplift of the mountains in sculpturing of the 'Gap' area. Presence of terraces at an elevation of 375 m in the Gap was taken as an indication of large-scale block faulting (Arogyaswamy, 1962), coinciding with that of the west coast, resulting in horst and graben like structures. Presence of bedded concretionary 'tuffaceous limestones' and black clays typical of backwaters and estuarine lagoons close to the Gap, in Coimbatore Dist., was taken as indication of shallow marine conditions.

The unlikely possibility of river erosion being the sole cause for the formation of the Gap was furthered by Ahmed (1966), Bose and Kartha (1977), Rao (1978) and others. The possibility of upheaval of the plateau landforms on either side of the Gap by tectonic processes was considered by Demongeot (1975) while Vaidynandhan (1977) viewed it as due to repeated uplifts along major fault zones.

Fluviatile or marine erosion as the sole cause for the reduction of the order of 1900 m of land masses was also ruled out by later workers (Subramanian et al, 1980; Subramanian & Muraleedharan, 1985). Absence of structural features indicative of faulting (Jacob &

Narayanaswamy, 1954), paucity of mylonites (Mani, 1975) the tectonically undisturbed character of the rocks of the Gap area (Venkata Rao & Subramanian, 1979) and consideration of the steep northern scarp faces as probable escarpment slopes (Gopalakrishnan, 1979), rule out major faulting and uplift of the Jurassic plateau landform. Absence of displacement features in limestone bands traceable from Madukkarai in Tamil Nadu to Walayar in Palghat Gap (Subramanian & Muraleedharan, 1985) and continuity of structural trends of the Pre-cambrian crystalline from the north-eastern part of the hills into the Gap (Gopalakrishnan, 1981), were taken as substantiating evidences of this hypothesis.

(3) Following the model of King (1962), the possibility of upward doming of the lithosphere in this region as a result of vertical thermal plumes with related volcanic activity (Wyllie, 1976) and the passing of Indian plate near a mantle thermal plume around 65 m.y ago (Dietz & Holden, 1970) were taken as supplementary arguments by Subramanian & Muraleedharan (1985) to postulate a 'crustal upwarp' theory. Arogyaswamy's (1962) emphasis on marine erosion as a dominant sculpturing agent of 'Gap' was also ruled out since, the bedded concretionary limestones and black clays containing gypsum occurring near the Gap, on which his theory was mainly based, were shown to be nothing but kankar and desiccated inland lake clays by later workers. Crustal upwarp of the surface in Post Jurassic times along an E-W axis and consequent development of joints and fractures

in the weak rocks such as hornblende and biotite gneisses exposed in the area were explained to have facilitated speedy erosion by fluvial agents. Their model also explained the same level of elevation of high lands on either side as due to the proximity of these hills to the axis of upwarp. The elevation of Jurassic surface was attributed to be a consequence of the accumulation of thick lithic sediments in taphrogenic basins such as that of the Cauvery, leading to crustal imbalance and isostatic adjustments by way of elevation of the continental crust. Presence of a thinner crust in the Gap area has also been suggested by the reported positive Bouger anomaly over the Gap and negative Bouger anomaly over the elevated areas (Subramanian, 1978).

P.S. Rao (1978) indicated that at least the structural foundation of the Gap was laid in Precambrian times, and its present profile as a compressional graben between two E-W trending shear zones was attributed to repetitive movements along the shear zones in early Tertiary times and subsequent erosion.

(4) Palghat Gap as a possible outcome of repeated differential uplifts of the plateau on both sides and subsequent erosional cycles through the fluvial action of a westerly flowing stream (Nageswara Rao and Srinivasan, 1980) had its basis on a theory proposed by Medlicott and Blanford (1893) advocating combined headward erosion of two

opposite flowing drainage systems as responsible for the origin of the Gap. The tectonic framework, geomorphic features and development of soil types typical of river valleys in the Gap area as reported by the authors, were cited to reiterate this line of argument. Rejuvenation features observed along the river courses of the three physiographic horizons identified within the Gap area were taken as probable indications of similar rejuvenation of the Gap proper.

Recent investigations point to the lack of correspondence between P-T data on rocks lying south and north of the Palghat-Cauvery 'shear zone' (Harris et al, 1982; Janardhan et al, 1982; Raith et al, 1983; Chacko et al, 1987) facilitating arguments in favour of its being a tectonic boundary between two distinct terranes within the southern shield (Ramakrishnan, 1988), a view which concurs with the gravity data (Mishra, 1988) also.

Drury et al, (1984) envisaged it as a zone of strong E-W striking planar tectonic fabric connected to the N-S thrust system of the Eastern Ghats by many arcuate shears at its eastern extremity (Drury & Holt, 1980). Its relation to the Eastern Ghat mobile belt was also emphasised by curving of the N-S fabric of the northern block into the E-W shear system, which is consistent with an E-W crustal shortening (Mukhopadhyay, 1986; Reddi et al, 1988) and a dextral sense

of movement.

Aeromagnetic data of Reddi et al (1988) also show a conspicuous downfaulted region extending from west of Palghat through Tiruchirappalli region and beyond, in an E-W direction. Contrary to the view points presented by Drury and Holt (1984), a continuity of structural trend lines across Palghat Gap has been cited by Nair (1990), through visual interpretation of LANDSAT imagery, supplemented by aerial photographic data, in support of an absence of a shear zone.

The review of the present status of the origin of Palghat Gap presented above, highlights the diversity of opinions among geologists on its origin and shows that it still offers a subject of debate and challenge to geologists working in the area. The present study attempts to unravel the geologic evolution of the area, through field geological investigations and attendant geochemical, geothermobarometric and geochronological components.

I.1 Location and methodology:-

The study area (Fig.3) comprises part of the Gap proper and a part of its northern flank exposing the meta-sedimentary sequence. This region, covering an area of 100 km² (falling within longitudes 76° 45' and 76° 50' and latitudes 10° 47' 30" and 10° 52' 30") was chosen after a

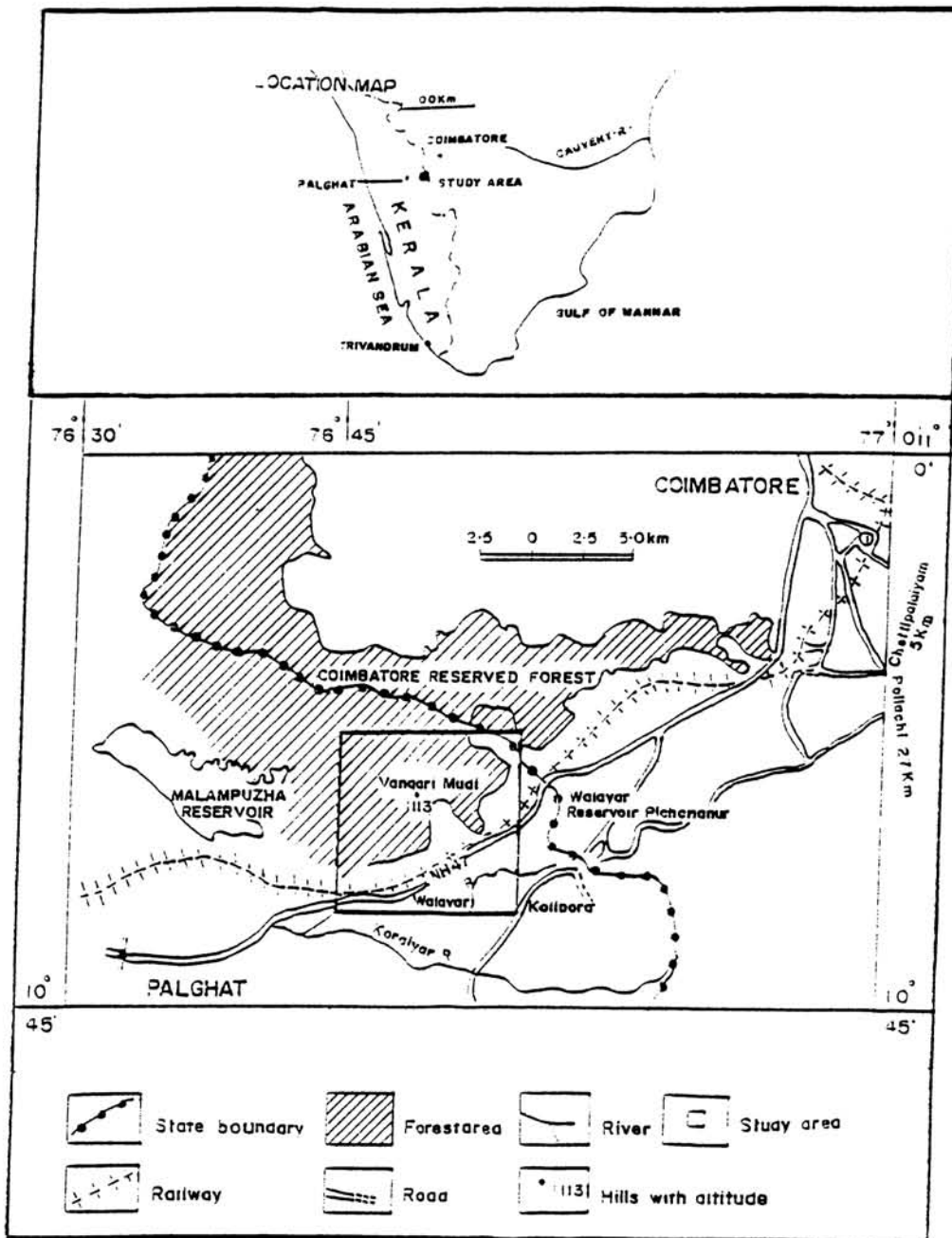


Fig.3 Location map of the study area.

careful perusal of the available geological and geomorphological data. The areal limits of the chosen territory however, has not constrained data collection from areas to its west and east.

Methodology:

- (I) Geological mapping in 1:25,000 scale in order to delineate the lithological units outcropping in the area and to bring out the broad structural features.
- (II) Systematic collection of representative samples from the various lithological units for :-
 - (a) Petrographic studies (about 120 thin sections)
 - (b) Geochemical investigations for protolith characterisation of rocks (50 whole rock analyses)
 - (c) Microprobe analyses of coexisting mineral phases to deduce pressure-temperature conditions of metamorphism/rock formation (about 389 mineral analyses from the garnet-biotite-sillimanite + cordierite gneisses, garnet-biotite gneisses, hornblende-biotite migmatitic gneisses, granites and pegmatites)
 - (d) Fluid inclusion studies to supplement the mineral P-T data (about 10 quartz and garnet plates from various rock samples) and
 - (e) Geochronologic investigations (age determinations of biotite and muscovite mineral samples from 5 pegmatites by K-Ar method).

CHAPTER II

GENERAL GEOLOGIC SETTING

II.1. Regional Geology and Geomorphology

The Kerala region, forming the southern tip of the peninsular Archaean gneiss-granulite terrane (Radhakrishna, 1989), constitutes probably one of the oldest regions in the Indian shield and has undergone repeated events of tectogenesis (Rao, 1978). Falling south of the notional line separating the low grade terrain of "Dharwar Schist Belts" and Peninsular Gneisses to the north, from the high grade granulitic terrain lying to the south, it is constituted chiefly by charnockite (interbedded orthopyroxene and garnet-bearing granulites) and ancient supracrustals (Radhakrishna, 1989); the latter comprising metapelites, calcareous rocks, quartzites and banded iron formations (Sinha Roy, 1983; Srikantappa et al, 1985). Other rocks include mafic/anorthositic intrusive suites, late potassic granites, post-tectonic alkaline rocks comprising carbonatites and nepheline syenites, pegmatites, mafic alkaline dykes and quartz veins. Many of the acid intrusives are spatially related to major lineaments (faults/shear zones). Miocene-Pleistocene tectonic province of sedimentary rocks (sandstone, clays and sub-recent sands and gravels) is confined to a narrow coastal belt.

Repeated events of tectogenesis affecting Kerala had been envisaged by Rao (1978) of which, the earliest 'recognisable' tectonic activity is the E-W folds (f_1) in the charnockite-khondalite and Wynad-sargur units, followed by NNW-SSE folds (f_2) and a third set of f_3 -folds interfering with the minor folds of the first set. Structural analyses by Sinha Roy (1979) shows the imprints of at least four deformational stages; (1) regional gneissosity and secondary compositional layering related to the first stage, (2) NW-SE reclined to steeply inclined folds of second deformation, (3) large upright folds with NNW-SSE and WNW-ESE conjugate axial surfaces and (4) fractures, oblique shear zones and strike-slip faults, parallel to the coast. Naha (1990) discerned three temporal relations of charnockites exposed in the Precambrian metamorphic terrain of Kerala, the first of these being represented by isoclinal folds with thickened hinges which are affected locally by near co-axial open folds, followed by an ubiquitous set of upright folds with axial planes striking between NNW - SSE.

Rao (1978) identified 5 sets of shear zones in the NW - SE, N-S, E-W, NNW - SSE and NE - SW directions, of which the Periyar, Achenkovil and Tenmalai are the prominent ones in south Kerala.

Earlier studies on Kerala charnockites (Jacob, 1962; Mahadevan, 1964; Narayanaswamy & Lekshmi, 1967) speak of

retrogression of charnockites to gneisses, while isochemical, progressive conversion of gneiss to charnockite, has been suggested by Ravindra Kumar et al, (1985); Srikantappa et al (1985) and Ravindrakumar & Chacko, 1986).

Published geochronological data for the charnockite and khondalite rocks of the Kerala region include whole rock Rb-Sr ages of 2155 and 3070 m.y. reported by Crawford (1969) and U-Pb zircon dates of 2838 ± 40 and 2930 ± 50 m.y for the garnet - biotite gneiss and charnockites (Odom, 1982). The schistose rocks exposed in Kasargod - Mercara and Cannanore - Wynad (Sargur) belts have been observed to be older than the rocks of the main Dharwar Schist belt and are also seen overlying the charnockite and biotite gneiss groups, as doubly plunging syncline, with their regional trends cutting across the boundary between the charnockites and biotite gneisses (Rao, 1978). The basic and ultrabasic intrusives represented by dykes of dolerite, anorthosite, peridotite and pyroxenite occurring in all the rock groups and more commonly in the charnockite and biotite - gneiss group, belong to Tertiary age. In addition to the mafic and ultramafic intrusives of Precambrian age, granitic to syenitic intrusives of Late Precambrian - Early Palaeozoic episode (Odom, 1982) have also been identified. The sedimentary tract of the coastal plains have been assigned a Miocene - Pliocene age.

Bounded by the Western Ghats, the Kerala region has been divided into four distinct geomorphic zones from east to west namely, the high lands (600-2500m altitude), midlands (300-600m altitude), low lands (30-300m altitude) and the coastal strip with lagoons and sand dunes. Evidences of polycyclic development of planation surfaces in Kerala have also been reported by various workers (Vaidyanadhan, 1967; Demongeot, 1975; Sinha Roy, 1979). Except for the prominent break at Palghat Gap area, the Western Ghats and the fringing high land terrains of Kerala are extensive from north to south. Palghat Gap is the only major break within the Western Ghats. Topo analysis of the Palghat area has brought to light remarkable linear, consequent rivers of high orders in the Gap proper, as compared to closely spaced, lower order streams of trellis, dendritic, obsequent and subsequent patterns of the hill ranges (Nageswara Rao & Srinivasan, 1980). Geomorphologically, three distinct physiographic horizons of both erosional and depositional types with characteristic soils have been discerned in the Gap area; a calcareous crust overlain by red brown loamy soil towards east, lateritic soil towards west and yellowish - brown clayey soil derived from the weathering of the gneisses towards the central part.

11.2 Geology of the study area

Earlier studies by various authors (Nageswara Rao & Srinivasan, 1980) also indicate that the geological

formations of the Palghat area belong chiefly to the Precambrian metamorphic complex with the sedimentaries forming a narrow belt along the coastal plains. The Gap proper, composed mainly of migmatitic gneisses and associated granites is flanked to the north by khondalite, associated calc granulites and crystalline limestones while, the Nilgiri massif is predominately composed of enderbitic charnockites, showing enclaves of mafic rocks such as gabbro, garnetiferous and ultramafic rocks represented by rare pyroxenite to common hornblende pyroxenite as well as minor meta sedimentary rocks. The southern hill ranges of Anamalai are also made up of charnockite and gneisses of granitic composition. Occurrence of discontinuous bands of magnetite - quartzite has been reported from the central and northern part of the area, and lenticular bands of crystalline limestones intimately associated with calc granulites have been observed in the north - eastern and eastern part of the area. Basic intrusives (gabbro, dolerite and norite) and acidic intrusives (granitic pegmatites and quartz veins) have also been reported.

Within the study area, two major rock units are observed (Fig.4) namely, the meta - sedimentary sequence of khondalite (garnet + sillimanite ± graphite gneiss), calc granulites and associated crystalline limestones towards the northern flank and the migmatitic suite consisting of biotite

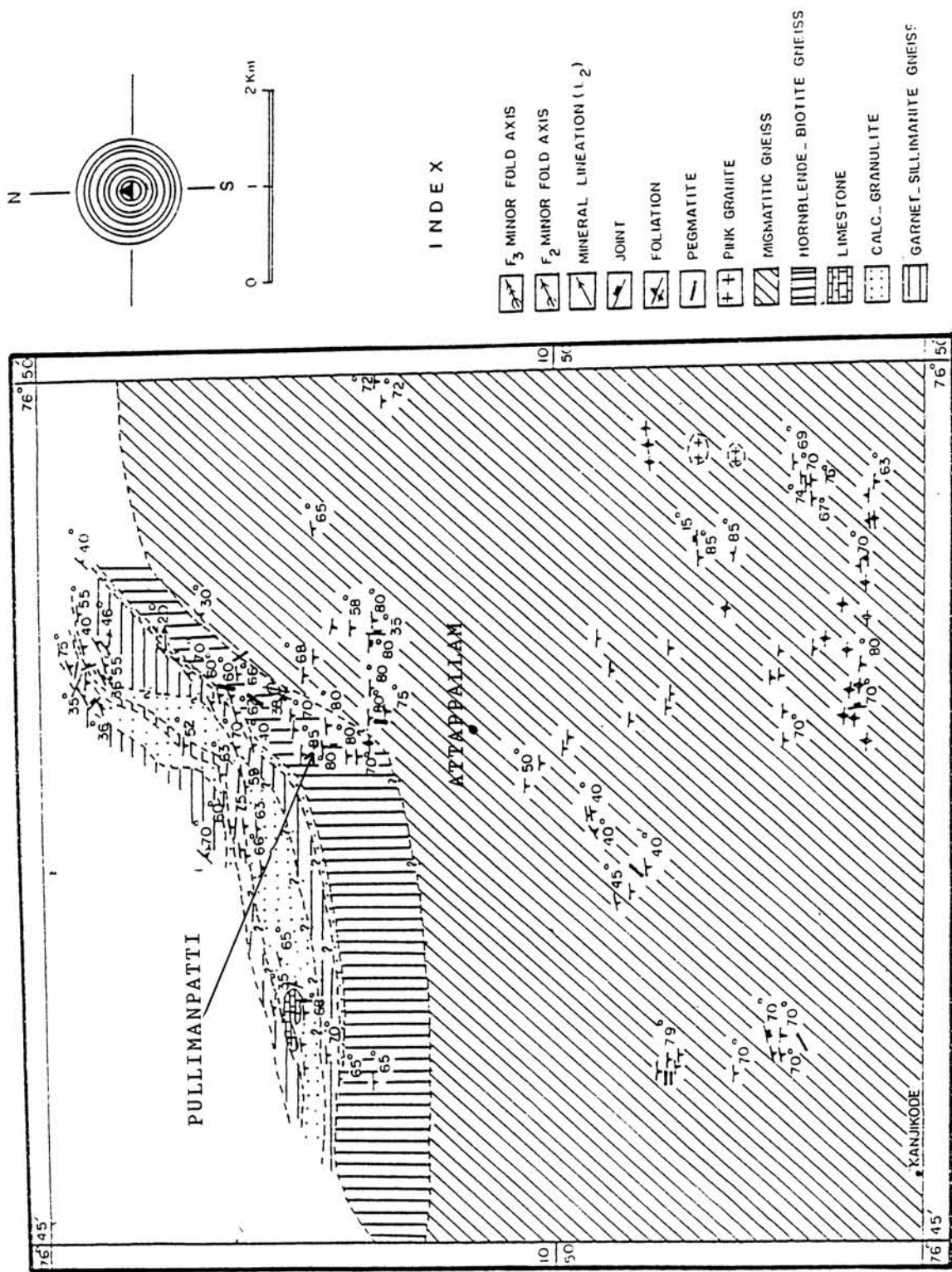


Fig.4 Geological map of the study area.

and hornblende gneisses containing concordant enclaves of amphibolite and associated granites, in the Gap proper. Transition from the meta - sedimentary granulites to the migmatitic gneisses is marked by a sequence of hornblende - biotite gneisses.

Khondalites are meta sedimentary gneisses consisting of two major units namely, garnet - biotite gneisses and garnet - sillimanite gneisses. The latter is exposed in the northern flank of the Palghat Gap with an E - W strike of foliation in the west and NW - SE trend in the east, showing sharp contacts with the calc granulites. Contact between the E - W trending calc granulites and khondalite has been established near Pullimanpatti as well as to its west and north east. Khondalite often passes into a garnet - gneiss, with the disappearance of sillimanite and increase in the amount of feldspars. Eventually, with the appearance of cordierite as an essential constituent, it becomes cordierite - garnet - sillimanite gneiss, as observed in the Walayar limestone quarry region.

The characteristic assemblage of these rocks is garnet + quartz + plagioclase + K-feldspars + biotite ± sillimanite ± graphite, with accessory phases including zircon, pyrrhotite, apatite, sphene and ilmenite. Development of cordierite is considered to be a result of progressive mineral reaction (see chapter III). Sillimanite defines the compositional

layering (S_1) and garnet grains are usually deformed into elongate, lens-shaped bodies lying within the sillimanite layers. The rock is intensely sheared, and often displays garnet and sillimanite porphyroblasts measuring 1 to 3 cm across. Coarsening of grain size, especially of sillimanite, is seen near contact with later pegmatites traversing the khondalites. Occurrences of 'sillimanite - augens' (Fig. 5) were noticed along the river course near the water fall on Kerala - Tamil Nadu border. In the check-dam quarry west of the Walayar limestone deposit, E-W trending garnet-biotite gneiss without sillimanite, showing joint planes roughly parallel to foliation, has been observed. Exposures of sillimanite - absent gneisses trending E-W, with steep dips (70° , S 15° E), are also observed in certain other localities such as those near the Aduppukutti Malai. These occurrences show well-developed joint sets, oblique and parallel to foliation.

Massive calc granulites form individual, laterally continuous bands upto scores of metres thick, interbanded with crystalline limestones and garnet-biotite-sillimanite + graphite gneisses (Khondalites *sensu stricto*). The noteworthy features include its intense fracturing (Fig. 6) and fine-grained nature. Exposures near Pullimanpatti, Pandarettu etc., roughly show an E-W alignment with fold closures plunging east. Near Marappalam, calc - granulites



Fig.5 Coarsening of sillimanite in Khondalite-pegmatite contact zone (1) and occurrence of sillimanite 'augens' (2).



Fig.6 Intense fracturing in calc granulites.

are interbanded with quartzo-feldspathic layers. Other occurrences are observed near Kerala-Tamil Nadu border in the Walayar Reserve Forest. Occasional bands of intensely fractured calc granulites are reported from south of the limestone deposit, closer to the migmatitic gneisses. Further, occurrence of calc granulites and associated limestones is known from the Gap proper near Gopalapuram. Towards the eastern part of the study area, in the plains near Madukkarai, calc granulites veined by pegmatites (Fig.7) both across and along the foliation, are seen. A few of these show minor scale displacement (~ 30 cm) along NE - SW trending fractures (Fig.8). A second set of prominent joints in the E - W direction, with a dip of 20° N and a third set in the $N 58^{\circ}$ E - $S 58^{\circ}$ W direction with a dip of 58° SE direction, are also observed here.

Crystalline limestones:- presence of commercially exploitable crystalline limestone deposits in Kerala is rather scarce. The largest among the known deposits is located at Pandarettu (Mani, 1962 a & b; Rao et al, 1974; 1975) falling within the study area, towards the northern flank of the Palghat Gap. It occurs within calc granulites, interbanded with garnet-sillimanite-graphite gneiss as an isoclinal antiform, with limbs steeply dipping (70° - 80°) towards south and plunging towards east (Fig.9). The limestone band (Fig.10) has a strike length of about 630 m

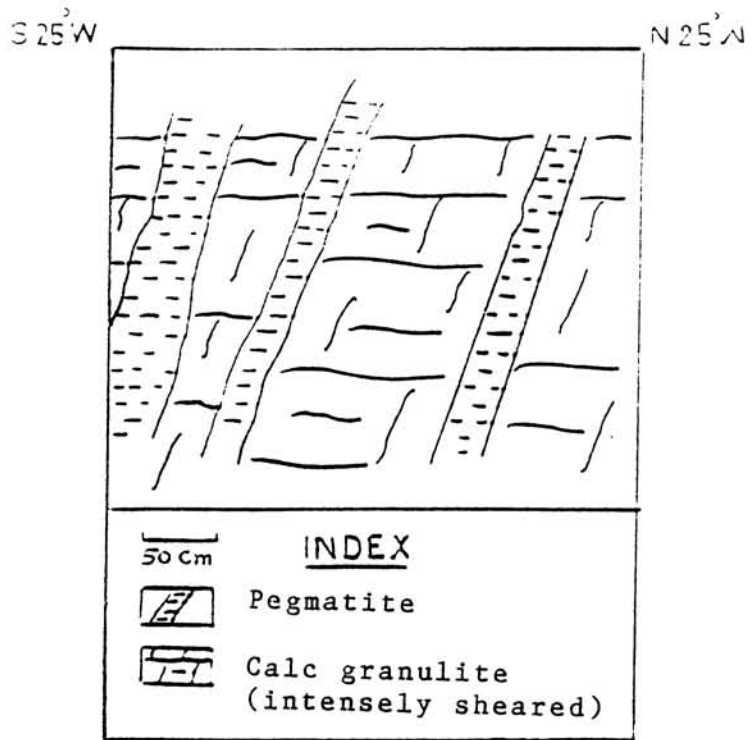


Fig.7 Sketch of pegmatite emplacement along the joint planes of intensely sheared calc granulite.



Fig.8 Displacement of calc granulite and thin concordant pegmatite veins along NE-SW trending fractures (near Madukkarai).

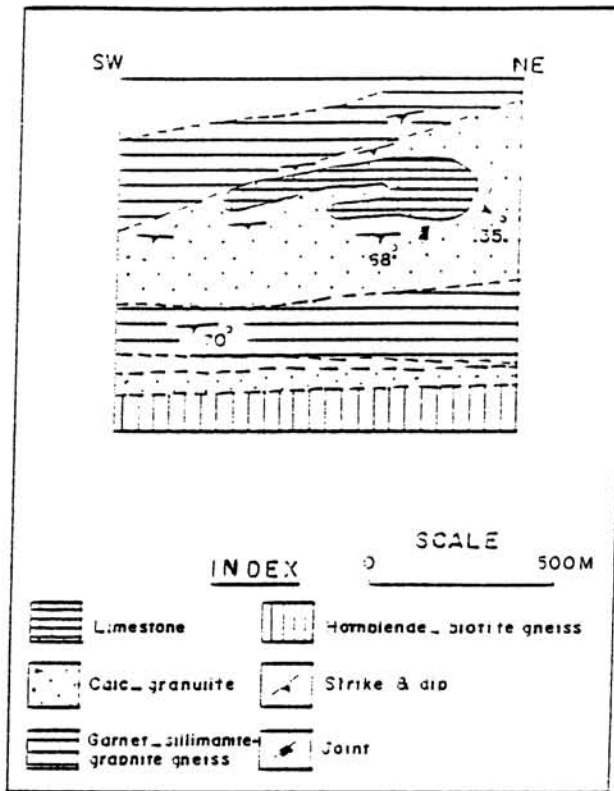


Fig.9 Sketch map showing interrelationship between calc granulites and crystalline limestones at Pandarettu. Index and scale are shown in figure.



Fig.10 Open cast mining of crystalline limestones from Pandarettu.

and a proven vertical extent of more than 155 m in the eastern part. The calc granulite horizon enclosing the Pandarettu limestone deposit is traceable to the WNW and ESE (Fig.11) and contains another major deposit at Madukkarai in Tamil Nadu. The main limestone band is intruded near the fold closure by a wide pegmatite (quartz + feldspar + biotite) body along a major NE - SW trending joint. Smaller limestone occurrences are also known to occur within the stretch of the two deposits, as well as to the south and WNW of Pandarettu.

In hand specimens, the crystalline limestone is typically medium-grained and massive. At Madukkrai, limestone form bands upto 2 km long with a width of 18 - 20 m and shows the presence of biotite and calc silicate minerals such as green coloured amphibole towards contact with calc granulites. Banding is prominently developed. At Pandarettu quarry, vertical joints trending N-S are frequently observed along with NW-SE trending joint sets with dip angles of 25° E and 30° NE respectively.

Migmatitic gneisses consist of biotite and biotite-hornblende varieties and occur as medium - to coarse - grained, grey to pink coloured, banded rocks. These well-foliated gneisses (Fig.12) are commonly folded and impregnated by granitic material, the latter, often cutting across the main E-W foliation. These rocks are characterised

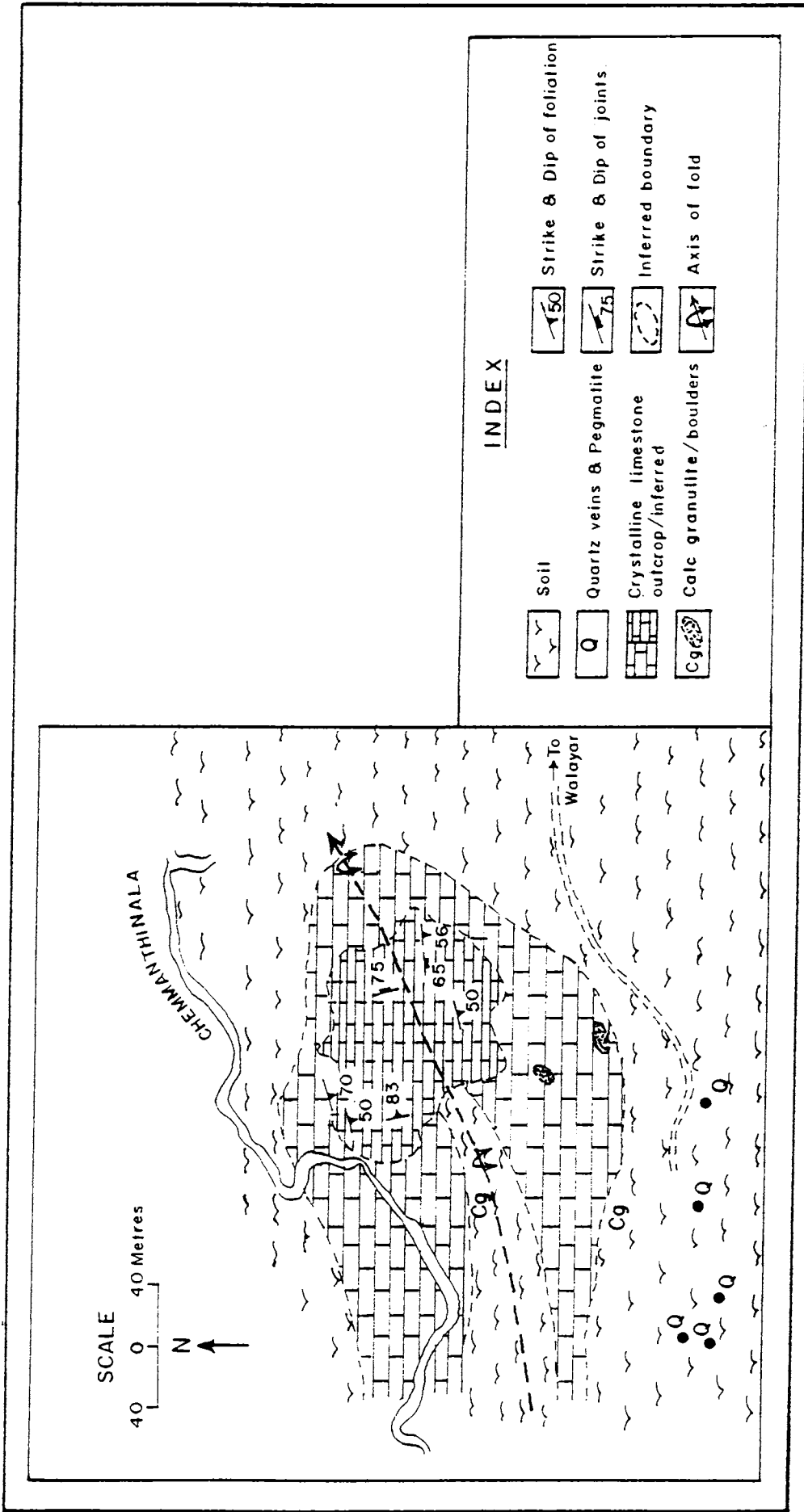


Fig.11 Geological Map of Pandarettu limestone deposit.

by the presence of bands and boudins of amphibolites constituting the paleosome and anastomosing networks of material constituting the neosome. These are pervasively inhomogeneous on a macroscopic scale, and fit the definition of typical migmatites of Ashworth (1985).

Biotite-gneiss is typically a coarse-grained (>4mm), leucocratic rock with foliation indicating a general E - W trend. Coarsening is much more distinct near contact with the pegmatite veins. Occurrence of biotite-gneiss has been observed at Kanjikkode, Attappallam, Chandrapuram, Chullimada and Pampupara localities. Exposure at Kanjikkode shows an intensely deformed structure with numerous pegmatitic veins intruding into it. Another major outcrop, partly weathered and extending over 65 m as isolated patches observed near Chandrapuram, shows an E-W trend with a dip of 62° towards south. Here, two episodes of folding with NE-SW and N-S trending axial planes and NW-SE trending joint/fracture system are also observed. Exposures at Pampuppara locality show 3 sets of well-developed joints; parallel, perpendicular and oblique to foliation.

Biotite - hornblende gneiss is an intensely deformed, medium to coarse -grained rock occurring around Kongampara, Pulamparapudur and nearby localities. Increased mineral proportions of hornblende towards flanks, is especially noteworthy. Exposure at Pulamparapudur exhibits only two sets

of joints (horizontal and oblique). Near Malampuzha dam site, the exposed biotite - hornblende gneisses shows minor displacement in N 60°E direction (Fig. 13).

Mainly stromatic (layered) in structure, the migmatitic gneisses often grade into surreitic (dilatational) and schollen varieties (Mehnert, 1968; Ashworth, 1985). Since, molten and unmolten portions of these irregularly layered rocks can still be distinguished petrographically, these are broadly categorised as metatexites.

Amphibolites are localised within the gneisses and occur as medium - to coarse - grained xenolithic masses of various sizes and shapes. Rarely, some fine-grained schistose types are also observed. Intricately permeated by granitic material, these lenticular, discontinuous patches pass quite imperceptibly into migmatitic gneisses (Fig. 14, 15). These enclaves are generally dark and often show boudinage (Fig. 16). Some of these enclaves located within the hornblende - biotite migmatitic gneiss, measure upto 40 to 75 cm in length and 10-15 cm in width and often pinch out along foliation within outcrop level. Near Pulamparapudur locality, amphibolite patches in migmatitic gneisses attain a maximum width of 10 m which get progressively reduced to smaller patches towards the eastern extremity of the quarry, due to progressive transformation of amphibole to biotite. Amphibolite bands of 2-3 m thickness showing weathering effects are also seen. Some of the bands show displacement



Fig.12 Hornblende - biotite gneiss showing well-developed E-W foliation. Location : SE of Malampuzha reservoir.

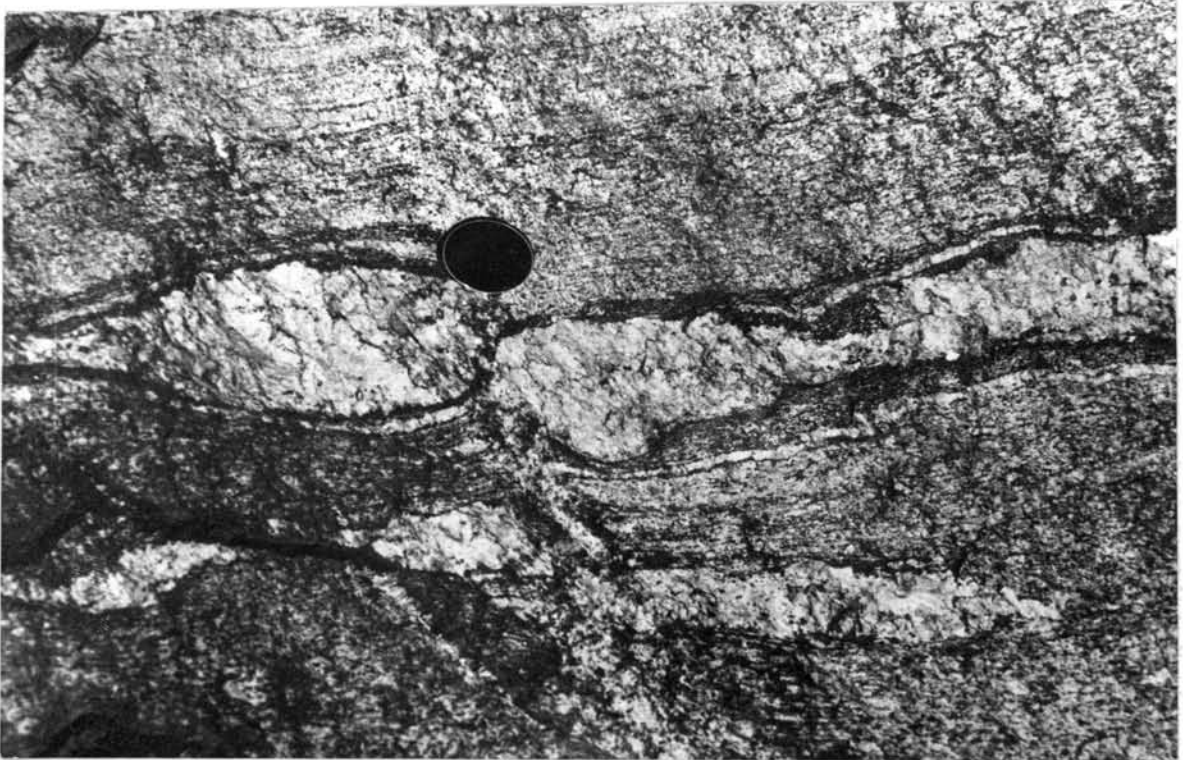


Fig.13 Displacement of gneissic layers and pegmatite in migmatitic gneiss, along fracture.



Fig.14

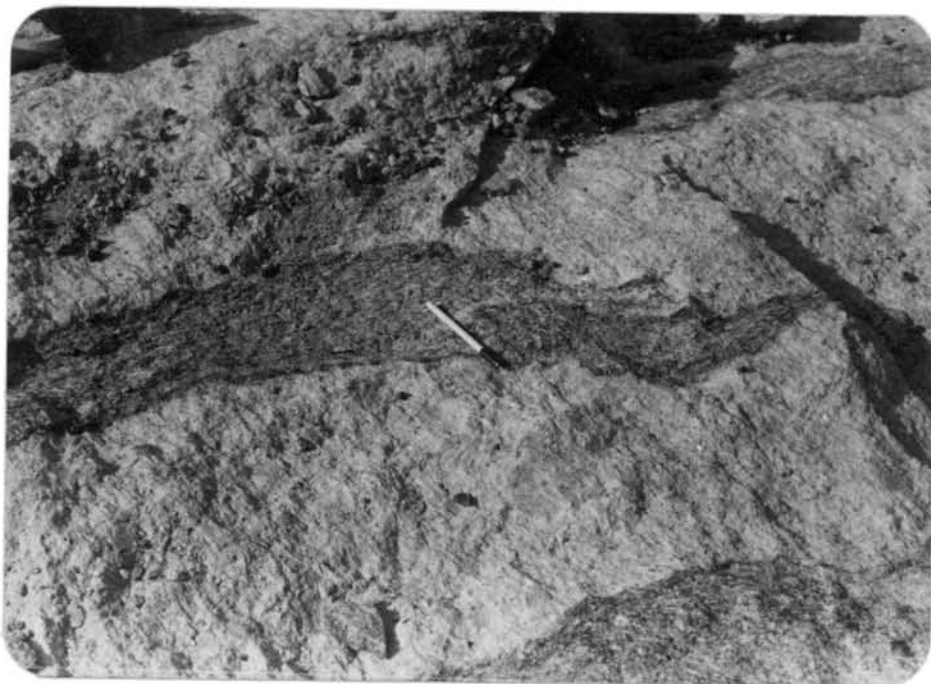


Fig.15

Fig.14 & 15 Amphibolite patches grading into migmatitic gneisses (Paleosome represented by amphibolite associated with a leucosome [quartz + feldspar] and melanosome [biotite + hornblende]). Location : south west of Pandarettu.

of 0.75 m, along NE-SW trending fractures. A few of the amphibolite bands and boudins are also intersected by later joints and transverse tensional cracks. Filling of incompetent neosomatic material along these ruptures developed in competent fragments of amphibolites (Fig. 17), result in the formation of structures similar to ladder veins (Holmquist, 1920). Coarsening of plagioclase and hornblende along contacts of granitic and pegmatitic injections showing intrusive relationship with the amphibolites, is also noticed. In certain localities like Kanjikkode, enclaves of amphibolite boudins in pegmatitic veins are seen.

Granites are leucocratic, homogeneous rocks, pink in colour. Thick bands and sub-parallel lit - par-lit injections of granite show intrusive relationships with the amphibolites (see Fig. 15 and 18). They are biotite - or amphibole - bearing and often occur as small isometric intrusions into the gneisses. Huge boulders of granitic composition are exposed along the road to Aduppukutti Malai. These are medium grained, with quartz and feldspar as essential constituents, with specks of mafic minerals. Exposures are also reported from the Madukkarai and Pullimanpatti areas. In the former locality, feldspar is generally pink in colour. The general alignment of the granite bodies in the western part of the Gap proper is in an east-west direction, while in the eastern part of the Gap proper, it is in NE-SW direction, conformable with the broad

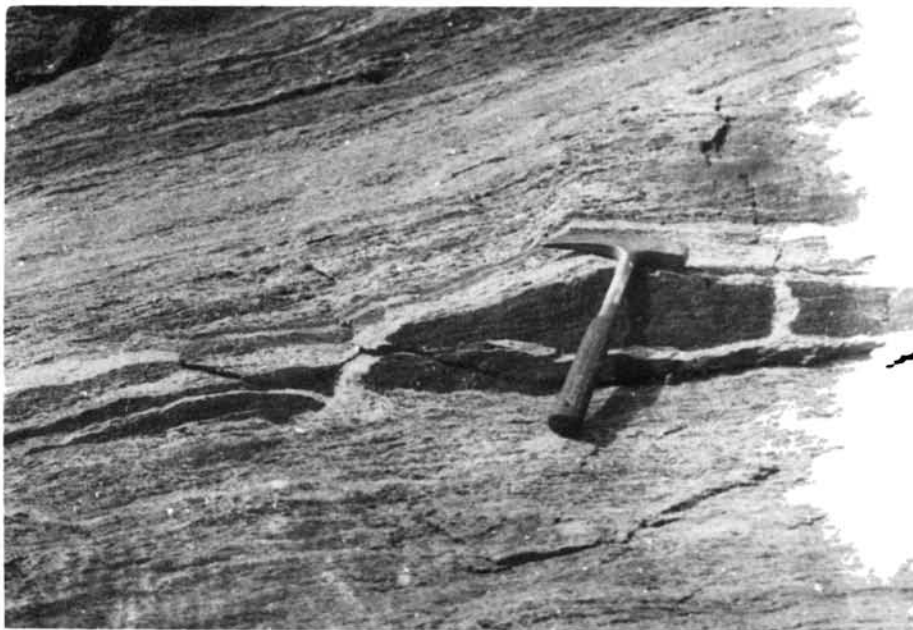


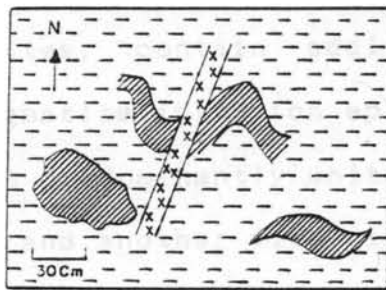
Fig.16 Boudins of amphibolite in migmatitic gneisses. Location : SE of Malampuzha reservoir.



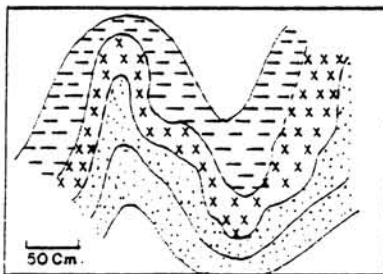
Fig.17 Filling of neosomatic material along the tensional cracks developed in amphibolite.



Fig.18 Thick bands of granitic material intruding the amphibolites.



a



b

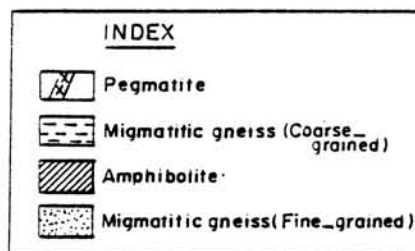


Fig.19 (a) Pegmatite showing discordant relationship with amphibolite and (b) concordant pegmatite folded along migmatitic gneisses.

direction of fracture planes. Within the hills of the northern flank, granite bodies appear to have emplaced parallel to foliation. They also exhibit subhorizontal joints and fractures facilitating sheet-weathering. Though, the core portions of the granite bodies are massive in appearance, ill-defined foliation is observed towards the periphery. Field relationships of granites show characteristics of late to post-kinematic types (Marmo, 1971).

Pegmatites occur as massive and coarse veins of quartz + feldspar + plagioclase + biotite mineralogy, showing sharp contacts with the country rocks. Pegmatites traversing the khondalites, contain additionally garnet and sillimanite. Two pegmatite intrusion episodes have been identified; the one with predominantly white feldspar showing effects of E-W folding and another with pink feldspar, showing only feeble effects of possible E-W stress regime. Localised both within the meta-sedimentary sequence and the migmatites, they show both discordant as well as concordant relationships (Fig. 19 a & b) and often show extensions from a few metres to more than a kilometre and width, from a few centimetres to a few metres. Some of the pegmatite veins tranersing the hornblende - biotite ridges are 150 to 200 m long and 1 m wide, with offshoots cross-cutting the foliation. Near Marappalam, a massive pegmatite body, 10 m across and

extending to more than 14 m is seen intruding into the calc granulites, along a possible weak zone coinciding with a saddle between two hillocks. Large crystals of glassy quartz and white - to pink feldspars, the latter showing well-developed cleavage traces, are observed in this body. Some of the pegmatite bodies have lenticular shapes and thin out both along the dip and strike directions. Many of the thin, concordant pegmatite veins emplaced along strike directions of calc-granulites and folded migmatitic gneisses, exhibit pinch and swell structures. Towards the south-eastern edge of Malampuzha reservoir, on the left side of the road from Malampuzha to Kawai, pegmatite veins evidently later than the main mass of migmatites are seen traversing the amphibolite bands. Some of the thin, concordant veins of pegmatites (10 cm wide), within biotite - hornblende gneiss, show evidence of displacement (~1.4 m) along N 60° E-S 60° W direction. Near Pullimanpatti, a wide pegmatite body folded along N-S direction is observed.

II.3. Structure and tectonic framework of the area

Oldham (Krishnan, 1953) noticed the E-W strike of certain rocks in South Malabar to the west of Nilgiris and the bending of foliation round the rocks of the Dharwarian strike (Fig. 20) and suggested the E-W foliation to be younger than the latter. Possibility of the E-W strike to be the westerly continuation of the ENE strike of the Nilgiris

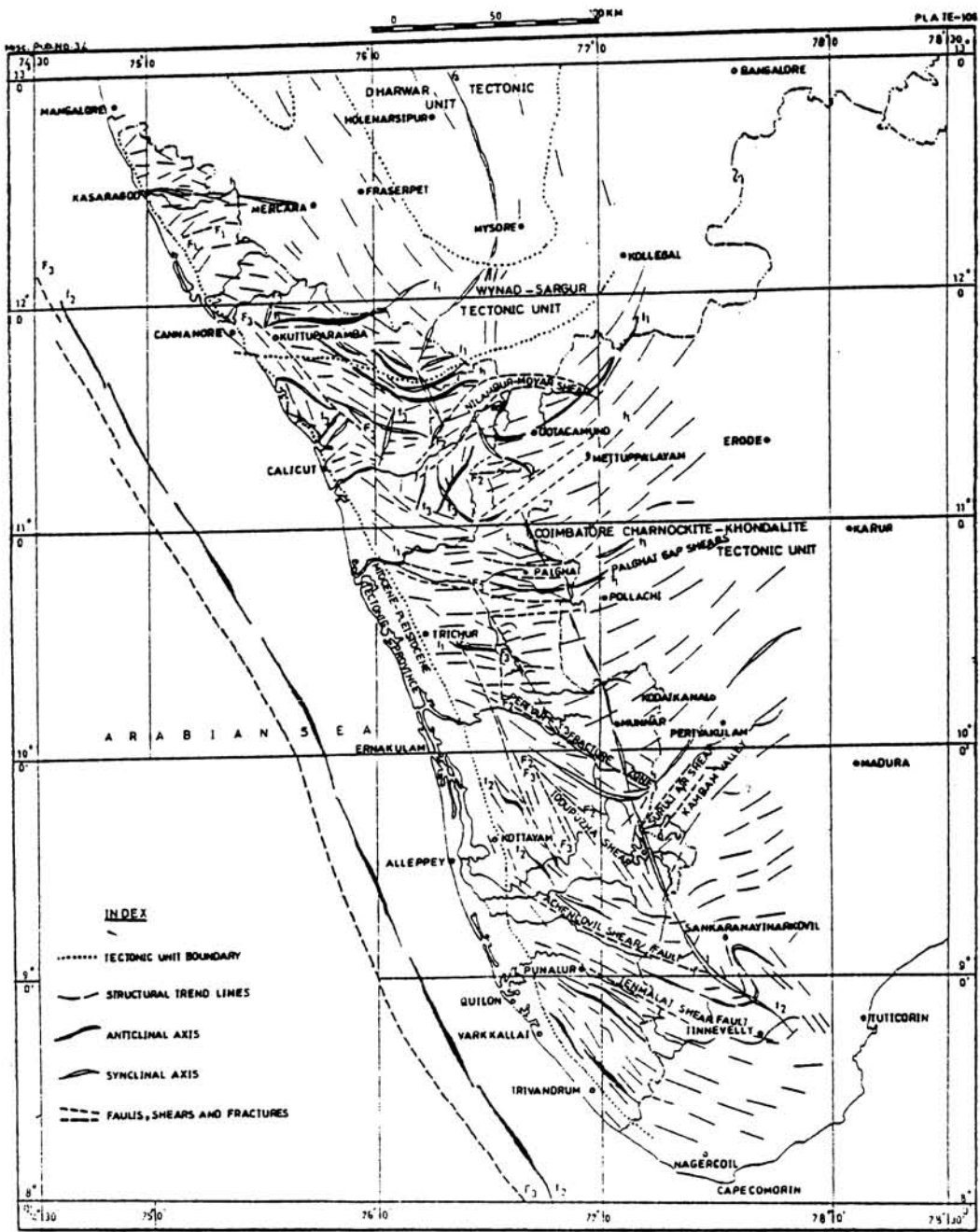


Fig.20 Structural trend map of Kerala showing the bending of E-W strike around the Dharwarian trend (after Rao., 1978).

has also been considered by various workers (Lake, 1890, p.812; Mukhopadhyay, 1986; Reddi et al, 1988; Nair, 1990).

Different generations of planar and linear structures are recognised in the rocks of the study area. Based on the geometry, orientation and superposition characteristics of the folds, the planar and linear structures of the study area have been grouped into three generations, corresponding to three deformation phases.

II. 3.a. Structures of first deformation.

All rock units contain a high-grade gneissosity defined by millimetre to decimetre-scale secondary compositional layering which is identified as the earliest recognisable planar structure (S_1). In migmatitic gneisses, S_1 is defined by alternating biotite/hornblende and quartzo-feldspathic layers (see Fig. 12) and in khondalite, by quartz, feldspar, garnet and sillimanite-rich layers. Strike of the secondary compositional banding of the rocks in the Gap proper is E-W and in the northern flank, it swings generally from NW-SE in the western part to NE-SW in the eastern part. Dip of S_1 is generally steep. Pervasive nature of the foliation in all the rock types and its conformity to the general trend of Palghat Gap speaks of a genetic linkage between the two. The relatively thick quartzo-feldspathic bands in migmatites, resembling rootless isoclinal folds (Fig. 21) and showing axial plane cleavage traces, can be considered as fold

closures of an earlier generation (F_1), following Campbell's (1980) lines of argument. However, the possibility of these structures resembling remnant fold closures, resulting from the mechanical permeation of melanosome by a molten leucosome or incorporation of melanosome into leucosome, in a melt dominated system (Mc Lellan, 1984) also cannot be ruled out. Presence of a regular relationship between wave length and layer thickness and the consistent orientation of the axial planes of multilayers, within a single outcrop of migmatites however, supports the earlier contention (De caprariis, 1974). Presence of deformational structures predating secondary compositional banding, is also favoured by the observed occurrence of co-axially folded, minor isoclinal folds in the hinge zone of a major, east-west isoclinal fold, within calc granulites and the associated meta-sedimentary rocks near Madukkarai.

II. 3.b. Structures of second deformation (D_2)

Small scale, symmetrical - to isoclinal folds (F_2) defined by S_1 , are the D_2 structures of the area. Their axial planes strike broadly E-W with steep inclinations ($70-75^\circ$) and the fold axes show an easterly gentle plunge of 20° .

In calc-granulites and migmatitic gneisses they are defined mostly by similar styled, isoclinal folds (Fig. 22 & 23). In calc granulites, these are also seen as



Fig.21 Rootless isoclinal folds (F_1) in migmatitic gneiss. Location : SE of Malampuzha reservoir.

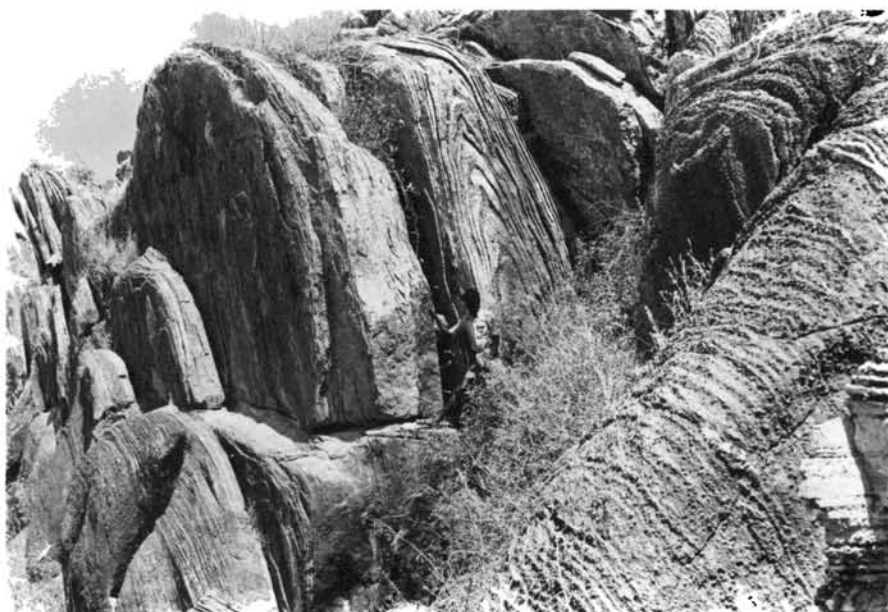


Fig.22 Isoclinal folds (F_2) in calc granulite with E-W axial plane. Location : Outcrop near Kerala - Tamil Nadu border.

symmetrical folds (Fig. 24). In migmatites, both the melanocratic and leucocratic layers have been affected by F_2 folds and are also disrupted by later fracture systems. Long axes of feldspar and quartz and biotite/hornblende, are also co-planar with the axial surfaces. The concordant amphibolite bands enclosed within the migmatitic gneisses show widespread effects of boudinage. Fragments or boudins of amphibolites are seen folded into F_2 -folds (Fig. 25) attributing boudinage to the D_1 - deformation stage. Emplacement of pink granitic material (neosome) along the cracks in the hinge and interboudin spaces of amphibolites and disruption of migmatitic layerings (see Fig. 25) bear evidences of subsequent deformation of migmatitic matrix through later injections. Field data thus, indicate a superposed history of migmatisation during D_1 and D_2 - deformation periods of which, a more pervasive migmatisation episode is attributed to the D_2 - stage, later than boudinage and coeval with F_2 folding.

Many pegmatite bodies of quartz + feldspar (mostly plagioclase) + very little biotite mineralogy, occurring in the Gap proper, display D_2 - structural elements, particularly F_2 minor folds. These are, in the relative sequence of emplacement, the first set of pegmatites in the study area and predate the D_2 - deformation episode. Pinch and swell structures observed in thin, concordant (2-5 cm thick) pegmatoid (Fig. 26) intruding into medium to coarse



Fig.23 Isoclinal folds (F_2) in migmatitic gneiss with E-W axial plane. Location : SE of Malampuzha reservoir.



Fig.24 Symmetrical folds (F_2) in calc granulite.

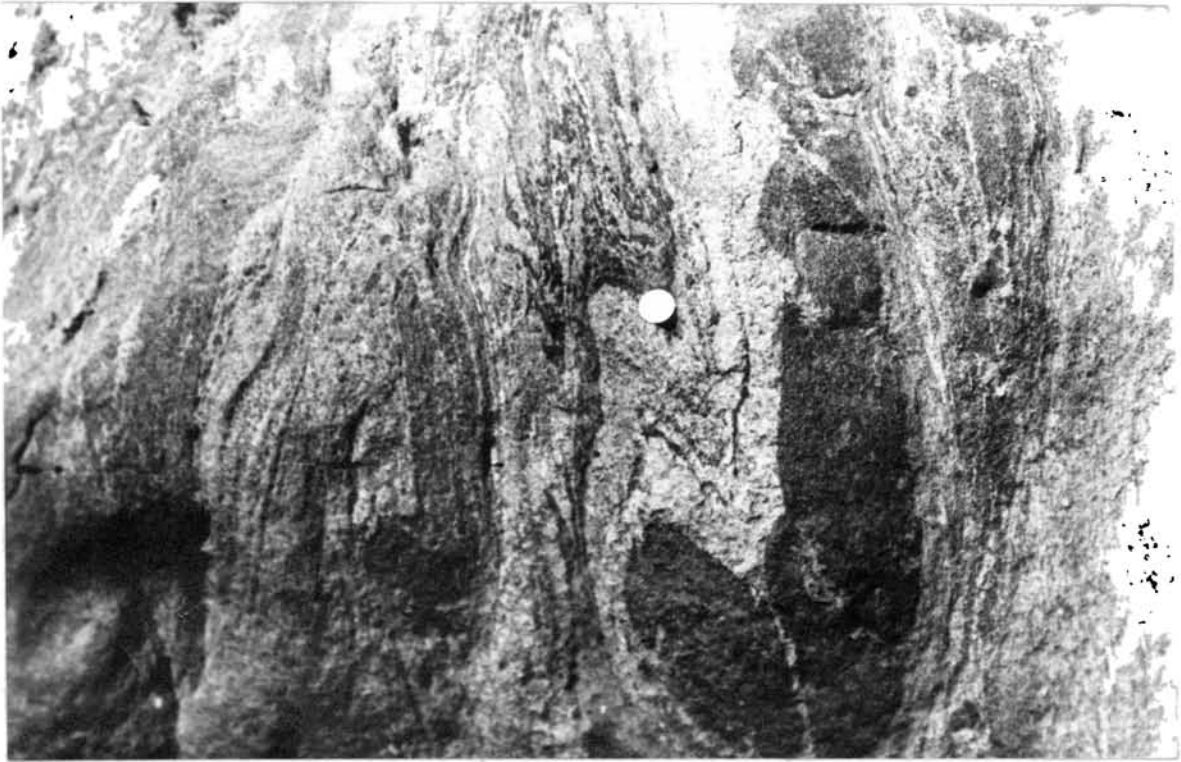


Fig.25 Boudins of amphibolite folded into F_2 - folds. Emplacement of granitic material along the cracks in hinge zone and interboudin space, is also seen. Location : Gap proper, within the SW part of the study area.



Fig.26 Thin concordant pegmatites intruding into the migmatitic gneisses, showing pinch and swell structures.

grained migmatitic gneisses may be related to the last stages of D_2 - deformation. Some of these pegmatite bodies also contain enclaves of amphibolites. Another set of pegmatites, consisting of quartz + feldspar + biotite \pm muscovite, transects the F_2 - folds. Many of the concordant pegmatites in the Gap proper, unaffected by D_2 - deformation, belong to this set of later (post - D_2) pegmatites (Fig. 27).

The important D_2 -linear structure is a mineral lineation (L_1) defined by biotite or hornblende and the long axes of quartz and feldspar porphyroblasts.

11. 3.c. Structures of third deformation (D_3)

The planar surfaces of D_1 and D_2 structures are folded by D_3 deformation leading to F_3 - folds; which are gentle or open, with N-S strike of the axial plane. Some of the concordant, post - D_2 -pegmatites with sharp contacts with the country rocks are seen affected by this deformation. A 10 metre thick pegmatite with large crystals of quartz and pink feldspar, showing D_3 deformation in the form of broad N-S, open fold structure is observed near Pullimanpatti (Fig. 28). Field and petrographic data do not indicate any intense alteration in the pegmatite.

Formation of fracture systems is attributed to the late brittle response of rocks to the continuous D_3 -deformation. The major fracture systems of this deformation stage are in



Fig.27 Concordant pegmatite belonging to post- D_2 syn- D_3 deformation phase. Locality near Chandrapuram.



Fig.28 Pegmatite body showing impact of D_3 -deformation. Locality near Pullimanpatti.

the N-S (parallel to the F_3 - fold axis), NE-SW and NW-SE directions. Equal area lower hemisphere plot of 184 measurements of joints in the Gap and 50 measurements in the flank (Fig. 29 a & b) show that in the flank area, two joint sets trending ENE-WSW and N-S are prominent while, the Gap proper shows the additional presence of NW-SE trending joints. The E-W trending pegmatite veins and the country rocks in the Gap area are displaced along these fracture systems (see Fig. 13). Within the less competent calc-granulite sequence in the northern flank of the study area, intense fracturing and subsequent displacement of strata appear to have given rise to a set of open mesofolds with E-W axial plane (Fig. 30 a & b). Some of the large blocks of calc granulites, detached from the flank, near the denuded plains of the Gap proper towards Mudukkarai, display cross-folded meso-scale openfolds (Fig. 31) which are suggested to represent the thickened inner hinge of the above mentioned folds.

Though occurrence of extensive and conspicuous features of faulting are absent, intense fracturing of rocks, presence of slickensides in the flank and formation of sillimanite augens in khondalite with a steep mineral lineation, are suggestive of mylonitisation and vertical movement close to the flank during /later to D_3 deformation stage. Presence of open mesofolds with E-W axial plane is characteristic of rocks of the flank only.

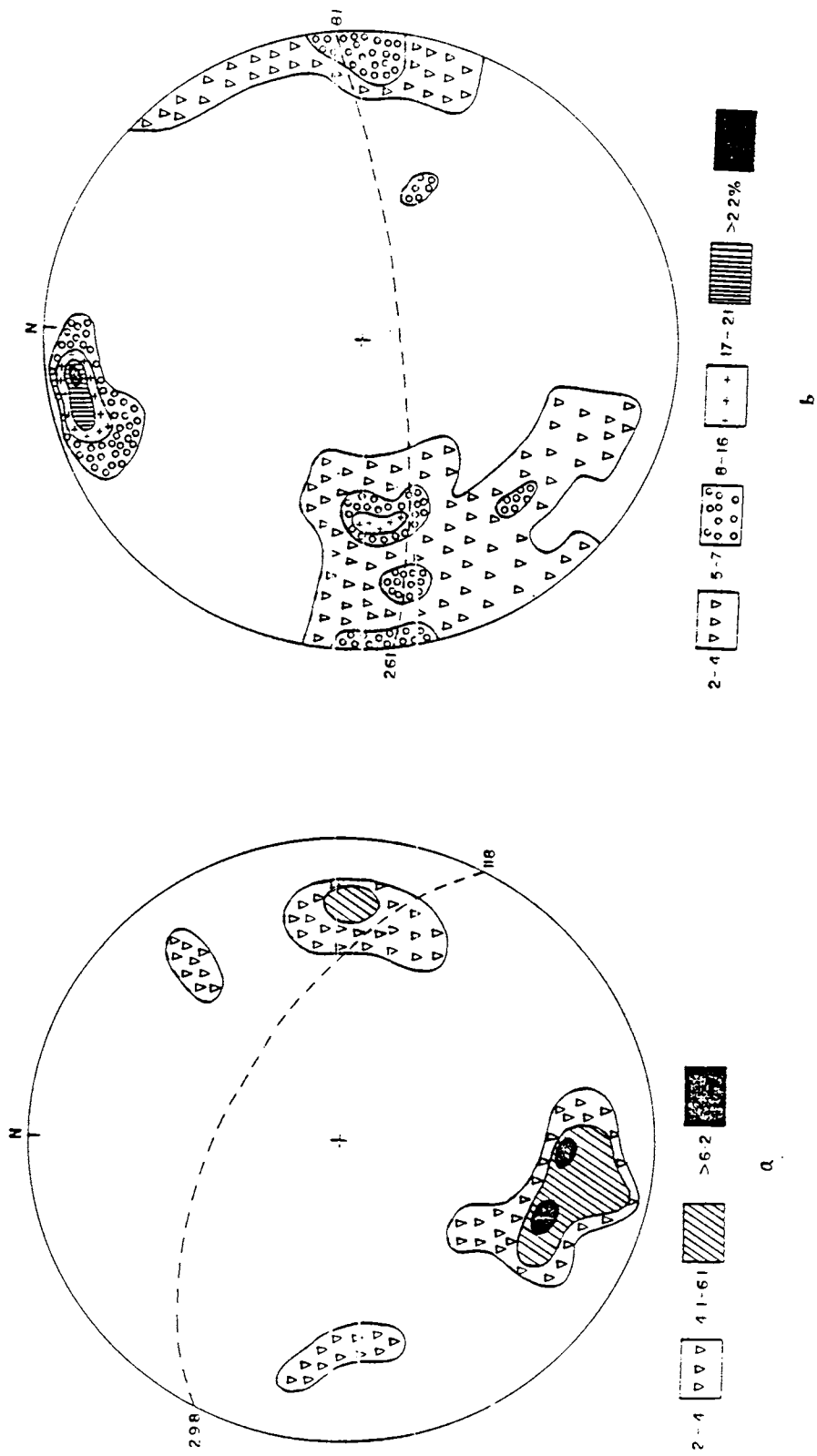


Fig.29 Equal area lower hemisphere plot of joints
 (a) 184 measurements in the Gap
 (b) 50 measurements in the Flank.

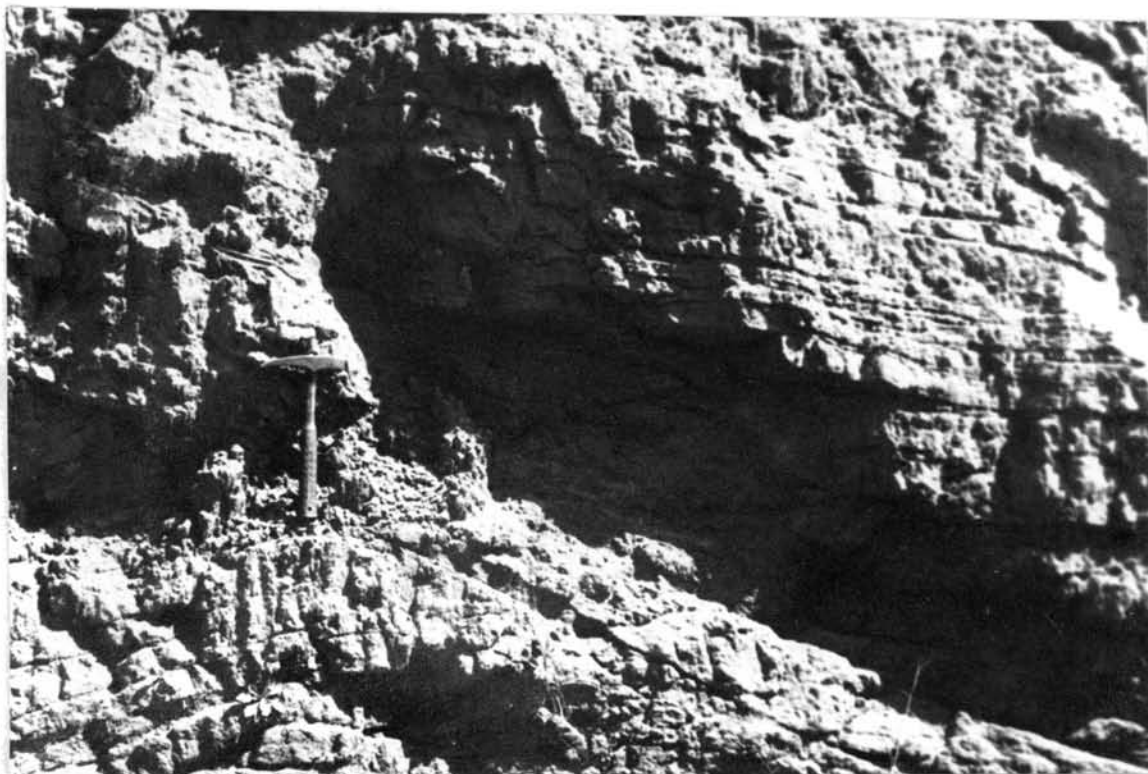


Fig.30 (a) Photograph of open mesofold associated with fractures in calc granulites in the northern flank. Locality near Pandarettu limestone deposit and (b) its sketch.

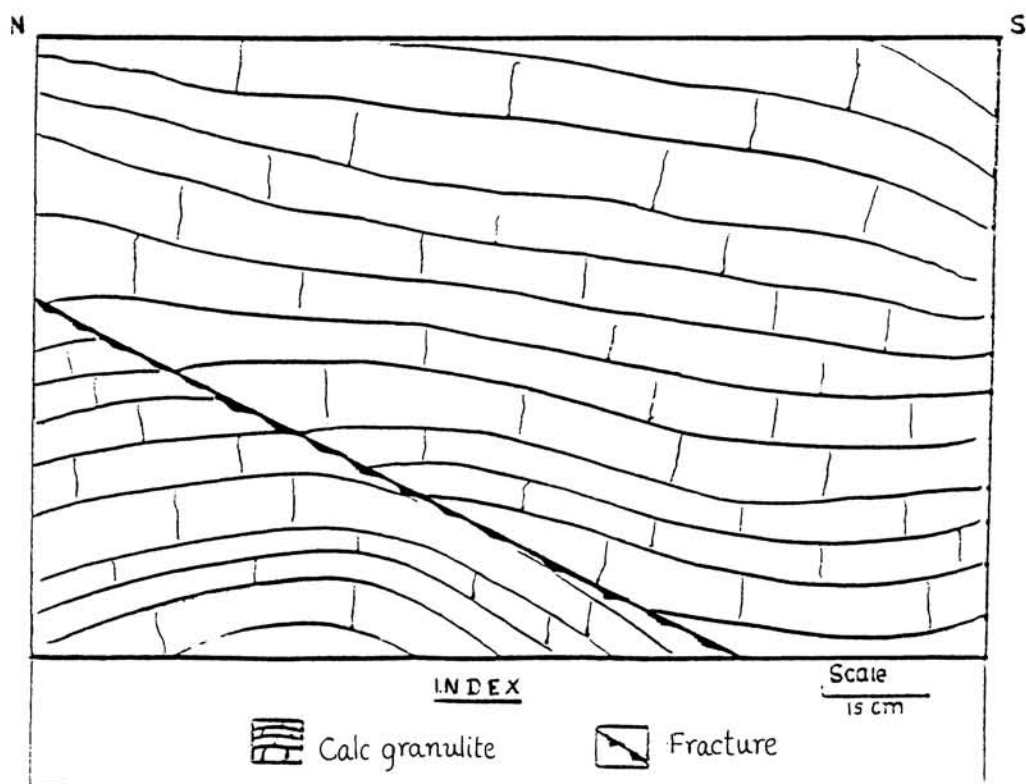


Fig.30 (b) Sketch of open mesofold after photograph.



Fig.31 Cross - folding of open mesofold in the flank.

The tectonic framework of the area may be suggestive of a deep rooted rupture in E-W direction. The general foliation trend of the gneisses in the E-W direction with steep dip to both sides, also led the earlier workers (Nageswara Rao & Srinivasan ,1980) to infer the presence of a first order fold system in the Gap area, across which prominent N-S lineaments were identified. Folds in the south were reported by them to be overturned to the north and fractures in the NNW-SSE, N-S, NNE-SSW, NE-SW and ENE-WSW directions were indicated to be subsequent tectonic features. The postulated presence of prominent southern and northern shear zones (Nageswara Rao & Srinivasan, 1980) of pre-Cretaceous age is also suggestive of faulting in the Gap.

CHAPTER III

PETROGRAPHY

Petrographical investigations of about 120 thin sections of khondalites, calc granulites, crystalline limestones, migmatitic gneisses, amphibolites and granites were made, and the results have been compiled.

III.1. KHONDALITES

Medium to coarse - grained (2 to 4 mm and more), the khondalites (*sensu stricto*) represent texturally complex and typically poly-metamorphic, porphyroblastic rocks (Fig.32), which frequently grade into granoblastic and occasionally into mylonitic texture (Fig.33). Extreme dynamic effects like crushing and granulation of minerals (quartz and sillimanite) are seen in some of the khondalite sections.

Modal percentage of quartz is 40 and garnet is as high as 20. Biotite is subordinate with 9% and the feldspar grains constitute 14%. Sillimanite percentage is highly variable from 0 to 21%. The sillimanite-free varieties (garnet - biotite gneisses) are constituted mainly by quartz and feldspar (50-60%), with lesser proportions of biotite (15-22%), garnet (10-12%) and opaques (8%); the rest of the volume being occupied by the accessories (2-5%).

Quartz consists of subhedral to anhedral (0.03 to 0.4 mm) grains of 1st order colours. They often contain

inclusions of plagioclase as well as sillimanite (Fig.34). Vermicular intergrowths of quartz and feldspar are observed in one of the sections. Grains are intensely fractured and show embayed boundaries. Recrystallization effects along the rim are observed, especially in cordierite-bearing samples.

Garnet occurs as xenomorphic porphyroblasts which are occasionally poikiloblastic (Fig.35) with inclusions of quartz, plagioclase and sillimanite. Back scattered electron images (BEI) of a garnet grain surrounded by quartz and biotite, showing inclusions of quartz and ilmenite are shown in Fig.36 and 37. Garnet metacrysts do not strictly follow the general trend of foliation and show cracking and rotation (Fig.38). In the khondalite (*sensu stricto*), garnet is seen associated with one generation of biotite, quartz and feldspar and in the sillimanite - free gneisses, with biotite and quartz. Fibrolitic sillimanite (Fig.39) and flakes of biotite around garnet grains (see Fig.32) are observed in the sillimanite-bearing sections. Microprobe analyses of garnets (See Table.14, Chapter.V) reveal that Ca content decreases from core to rim in all garnets, except in two samples (PS.16 and PS.76), where a slight enrichment from 0.111 to 0.123 and 0.079 to 0.089 (p.f.u) respectively, is noticed towards biotite contacts. This slight enrichment may be related to the plagioclase formation after garnet, through

- Fig. 32 Porphyroblastic texture in khondalite.
Parallel nicols. Scale : 1 cm = 0.2 mm.
- Fig. 33 Mylonitic microtexture in khondalite. Crossed
nicols. Scale : 1 cm = 0.03 mm.
- Fig. 34 Thin section of khondalite showing inclusions
of sillimanite in quartz. Parallel nicols.
Scale : 1 cm = 0.03 mm.
- Fig. 35 Garnet porphyroblasts in khondalite showing
poikilitic texture with quartz inclusions.
Parallel nicols. Scale : 1 cm = 0.2 mm.

Fig. 32

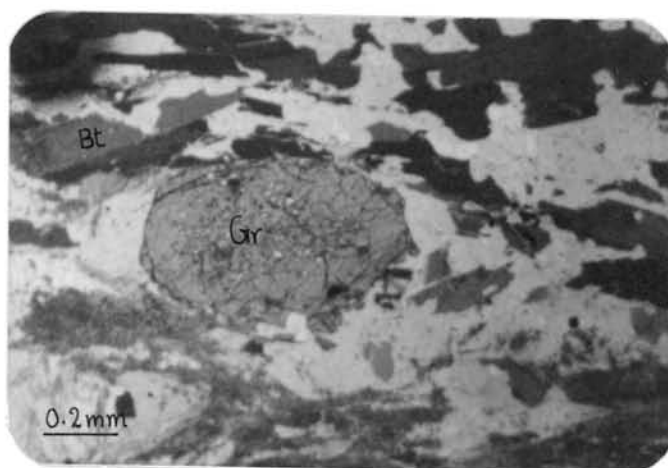


Fig. 33

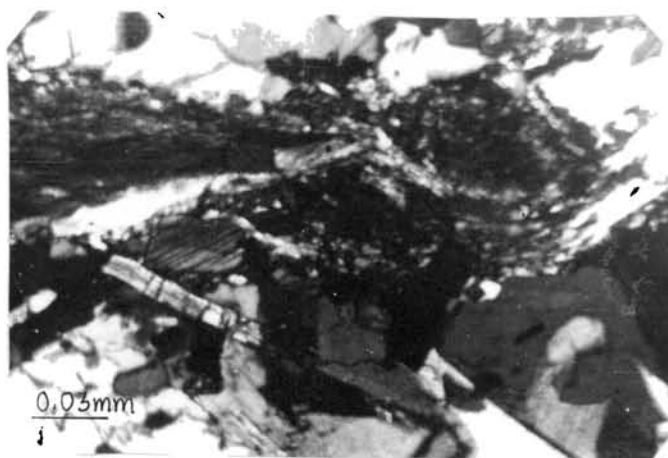


Fig. 34

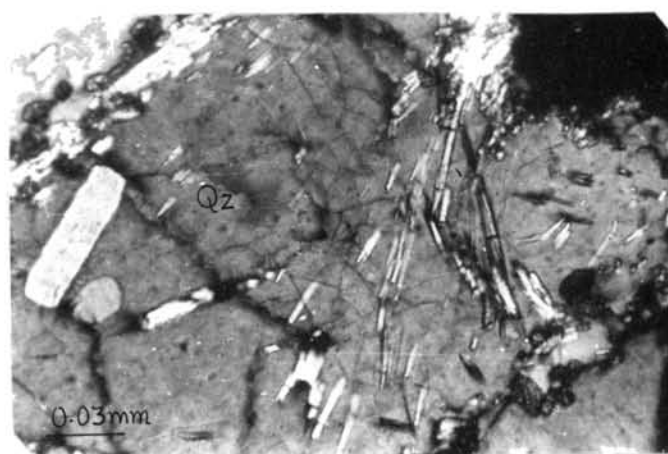
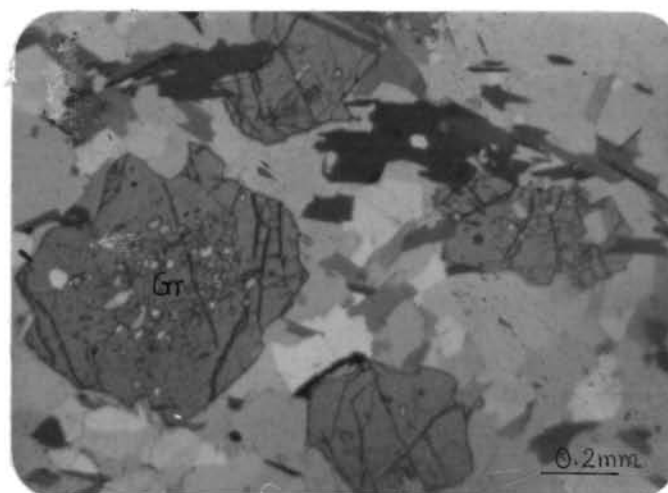
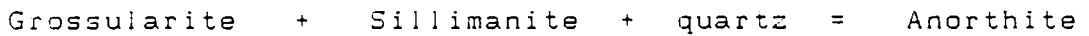


Fig. 35



the reaction:-



as illustrated by the presence of tiny plagioclase symplectitic rims around some resorbed garnets. Garnet zoning profiles in one of the samples (PS.76) show sinuous paths of MnO and CaO (Fig.114, see chapter.V) proceeding from biotite to quartz contacts while, Feo follows a depletion trend. In cordierite-bearing assemblages, garnet shows an increase in almandine (from 72 to 75 mol %) content towards rims adjacent to biotite while, pyrope and grossularite show a corresponding decrease from 25.5 to 22.3 and 2.1 to 1.90 (mol %) respectively. Towards cordierite contacts, almandine is increased to 78 mol % while pyrope is much lowered to 20 mol%. Zoning with respect to grossularite is rather insignificant (See Figure.113, Chapter.V).

K-feldspars:- Orthoclase is the predominant phase. The grains vary in size from 0.98 to 2 mm and exhibit 1st order grey colour. Microperthites (Fig.40) are frequent. Local variation to coarse blebs and patches (patchy perthites) is also observed. In khondalite (*sensu stricto*), anorthite content of K-feldspar ranges between 0.1 and 0.6 mol%. Average composition of matrix alkali feldspar is represented as Or_{82.2} Ab_{17.46} An_{0.34} which is shifted to Or_{87.91} Ab_{15.2} An_{3.11} towards plagioclase contacts. In sillimanite - free assemblages, megacrysts are not zoned

Fig. 36 Back scattered electron image (BEI) of a garnet grain surrounded by quartz (dark grey) and biotite (medium grey). Inclusions in garnet : quartz (dark) and ilmenite (bright). Scale bar : 1 mm.

Fig. 37 Enlarged portion of garnet showing an ilmenite inclusion which in turn contains a small plagioclase crystal. Scale bar : 10 μ m.

Fig. 38 Cracking and rotation of garnet (Gr) in khondalite. Plane polarised light. Scale : 1.1 cm = 0.2 mm.

Fig. 39 Fibrolitic sillimanite (Sill) wrapping around garnet porphyroblast in khondalite. Parallel nicols. Scale : 1.1 cm = 0.2 mm.

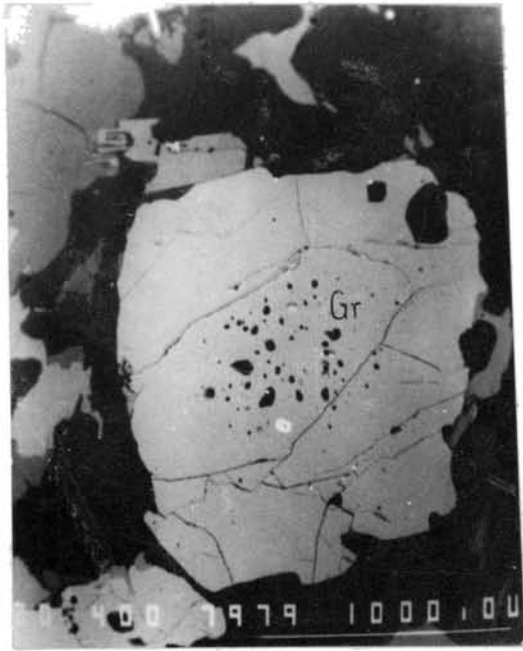


Fig. 36

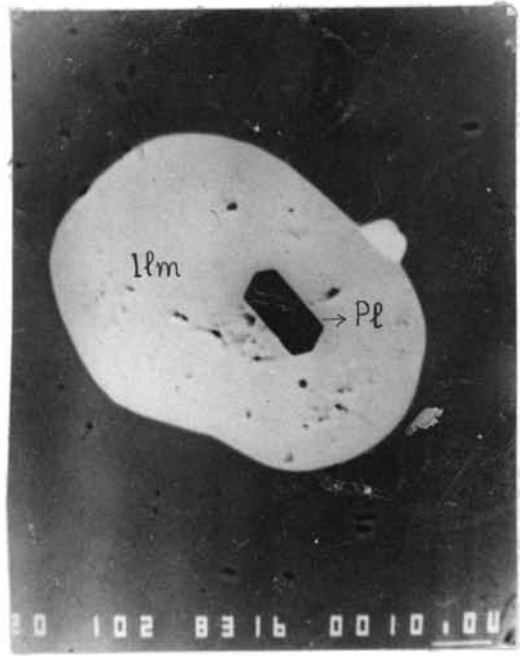


Fig. 37

Fig. 38

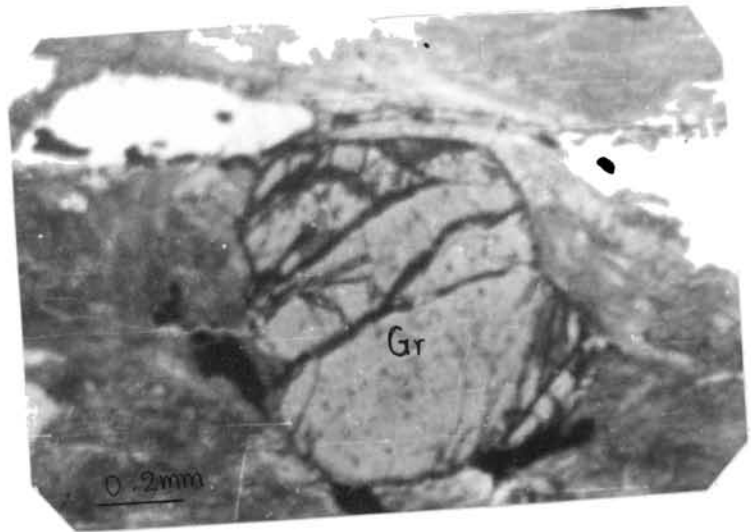
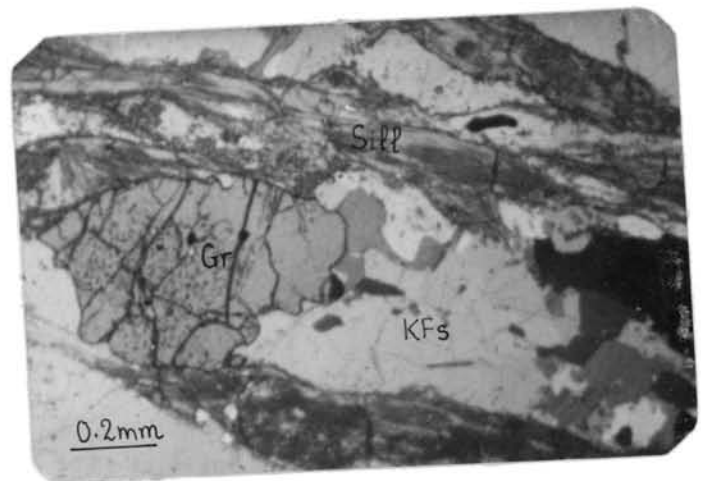


Fig. 39



optically but, contain numerous inclusions of plagioclase and quartz, oriented parallel to the crystallographic planes. In cordierite - bearing assemblages, occurrence of K-feldspars is limited. Back scattered electron image of a perthitic alkali feldspar (PS.79) is shown in Fig.41. Microprobe data (See Table.16, Chapter.V) show that the perthites correspond to a composition of Or_{51.2} Ab_{47.6} An_{1.2}. Frequency of exsolved plagioclase lamellae is less towards plagioclase grains.

Plagioclase occurs in lesser quantities compared to orthoclase and often shows simple carlsbad twinning. Discontinuous- to continuous-pericline twinning is also observed. Grain size varies from 0.08 to 0.8 cm, some of them having broad lamellae of 0.08 to 0.4 mm size. No zoning is observed. In khondalites (*sensu stricto*), An in plagioclase ranges between 23 and 34%. In one of the samples (Ps.76), An content of plagioclase inclusion in garnet is found to be 32 mol %, while the matrix plagioclase has a much lower An content of 23 mol %. Back scattered electron image of a small grain of plagioclase characterised by a high An content (32 mol %) and a total absence of Feo, preserved by an ilmenite shell is shown (see Fig.37). In sillimanite-absent assemblages, compositional variation ranges from An₃₀ to An₃₇. In cordierite-bearing samples, strain twinning is observed in large grains and the average composition approximates to An₂₃ mol %.

Sillimanite constitutes 0-21% modal composition with grain size ranging from 0.05 to 2.4 mm. Coarsening of grain size often leading to 'augens', is seen in khondalites near the contact with later pegmatites (Fig.42). It is seen intimately associated with garnet and is also seen as a replacement product of biotite in contact with quartz (Fig.43 & 44). Two generations of sillimanite are observed; an earlier generation of prismatic and elongated crystals and a later fibrolitic sillimanite, associated with biotite as a breakdown product. Fibrolitic sillimanite anastomose around garnet and commonly truncates larger plagioclase and k-feldspar grains. Petrographic properties such as perfect unidirectional cleavage, straight extinction, absence of pleochroism, moderate relief and yellow to pink interference colours are characteristic. Back scattered electron image of cordierite, in sillimanite and quartz are shown in Fig.45 & 46 respectively. Microprobe data [Table.1] show that Ti, Mn, K and Zn are absent while, Cr (0.001 p.f.u) and Mg (0.003 p.f.u) are found only in traces. Atomic proportions of 'Si' occupies less than 1 p.f.u. and Al_{V_i} occupancy is around 2 p.f.u.

TABLE:- 1 MICROPROBE ANALYSES OF SILLIMANITE WITH ATOMIC PROPORTIONS

Rock type	Gar-Bt-Gn		Gar-Bt-Sill-Gn
Sample No.	PS.14 (av.3)	PS.16(av.6)	PS.25a (av.3)
<u>Elements</u>			
SiO ₂	35.93	36.22	38.17
Al ₂ O ₃	61.44	61.40	61.76
Cr ₂ O ₃	0.03	0.03	0.05
FeO	0.28	0.17	0.16
MgO	0.01	0.00	0.00
CaO	0.00	0.00	0.01
Total	97.70	97.51	98.16
on the basis of 5 oxygens			
Si ^{vi}	0.994	0.999	0.995
Al ^{vi}	2.003	1.997	2.003
Cr	0.001	0.001	0.001
Fe	0.006	0.004	0.003
Mg	0.003	0.000	0.000

Biotite is ubiquitously present in all the sections and defines the main foliation. Size ranges from 1-2 mm and the colour is pale to red-brown. It shows second order green to orange interference colours and is pleochroic from yellow to brown. Intergrowth of biotite and sillimanite, mantled by feldspar is observed in some sections. In some, intergrowths with quartz resembling cuneiform textures (Fig.47) are also seen. Three generations of biotite are noticed; one as inclusions in garnet grains; and the second as a phase co-existing with garnet and sillimanite. The latter tend to be segregated as discontinuous streaks and curving lenses, often enclosing garnet prophyroblasts (see Fig.32) and coarse

- Fig. 40 Microperthites in khondalite. Crossed nicols.
Scale : 1.25 cm = 0.2 mm.
- Fig. 41 Back scattered electron image of perthitic
feldspar in cordierite - bearing gneisses.
White (on the left) : biotite (Bt), dark grey :
plagioclase, black : quartz. Scale bar : 100 μ m
- Fig. 42 Sillimanite augens in khondalite. Crossed
nicols. Scale : 1.25 cm = 0.2 mm.
- Fig. 43 Sillimanite as a replacement product of biotite
& 44 in contact with garnet and quartz (Qz).
Parallel nicols. Scale : 1.25 cm = 0.2 mm.

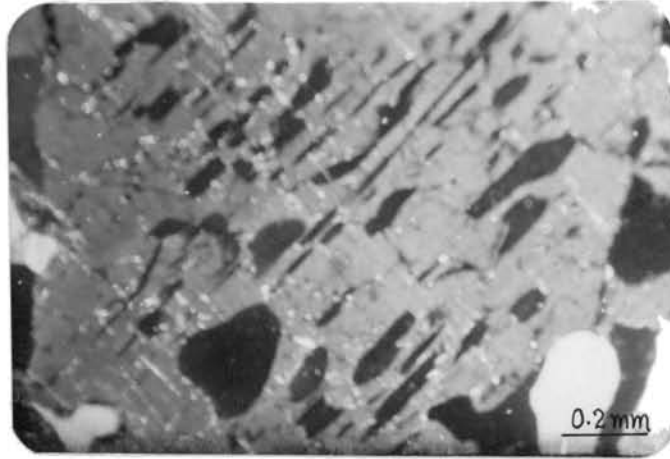


Fig. 40

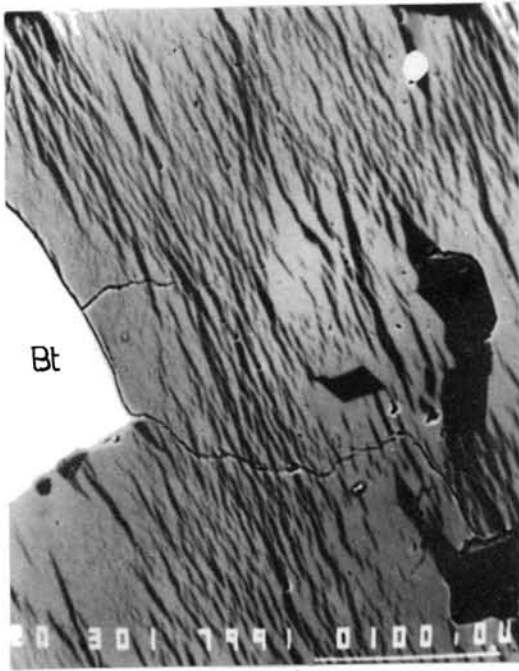


Fig. 41

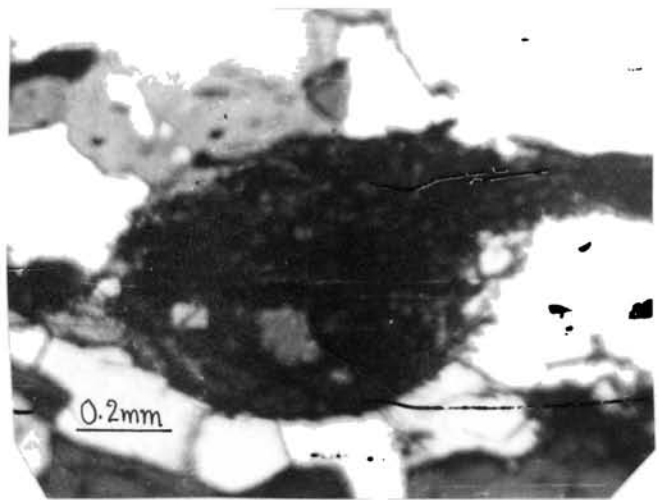


Fig. 42

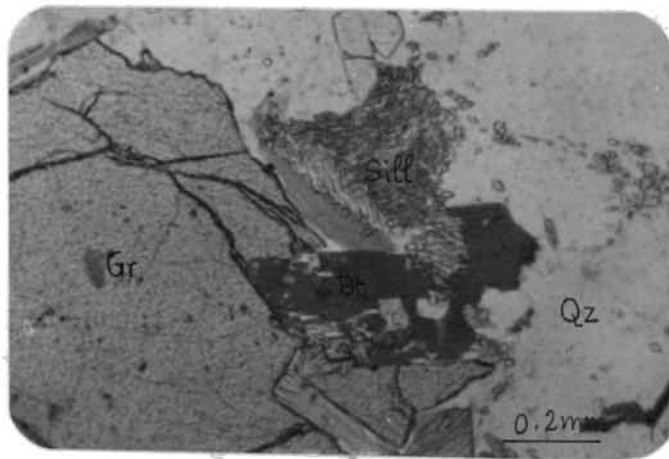


Fig. 43

Fig. 45 BEI of cordierite inclusions in sillimanite (dark grey). Ti-rich biotite (on the right) and chlorite (on the left). Scale bar : 100 μ m.

Fig. 46 BEI of cordierite in quartz (dark) and sillimanite. Ti-rich biotite (white) is shown. Scale bar : 100 μ m.

Fig. 47 Intergrowth between biotite and quartz resembling cuneiform textures. Crossed nicols. Scale : 1.1 cm = 0.03 mm.

Fig.44

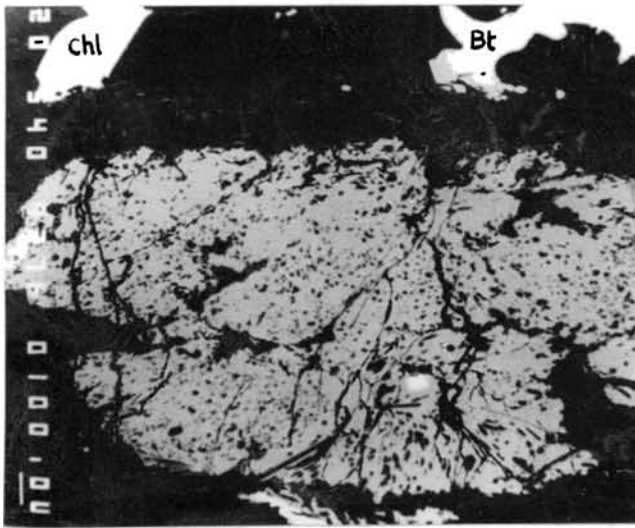
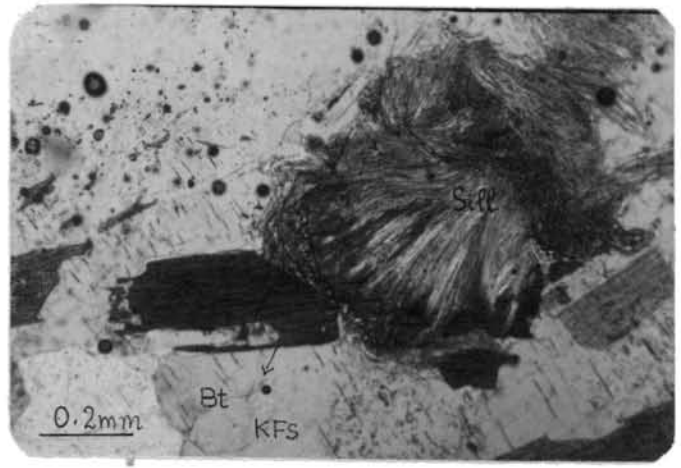
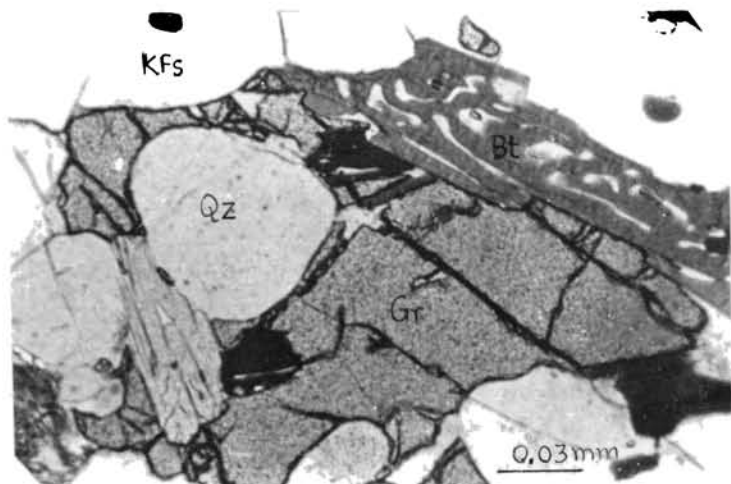


Fig.45



Fig.46

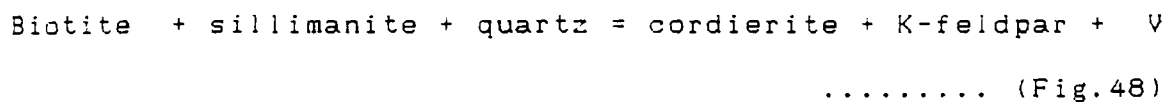
Fig.47



quartzofeldspathic augens. Kinked and fragmented lamellae are frequent. The third generation biotite is formed after garnet.

In cordierite - bearing khondalites, biotite is observed as automorphic grains coexisting with sillimanite. Microprobe analyses of biotites from sillimanite -bearing rocks (see Table.15, Chapter.V) also show higher Fe and Ti contents (av.2.2382 and 0.5644 p.f.u.) for matrix biotite compared to biotites adjacent to garnets (av.2.0445 and 0.3028 respectively). Biotite inclusions contain an average Fe of 1.4313 (p.f.u.) and has still lower proportions of Ti (av.0.2677 p.f.u.). In sillimanite - absent assemblages. Mg/Fe content decreases from 0.97 in matrix biotite to 0.94 in biotite adjacent to garnet.

Cordierite forms large grains in the matrix and rarely appears around garnet as a typical mineral of reaction textures. In one of the samples (PS.79) however, a slightly decomposed cordierite is found among sillimanite, garnet, biotite and quartz grains. It is seen as a white to grey coloured, optically positive mineral, showing weak birefringence and polysynthetic twinning. $2V$ is 72° . Cordierite appears to have grown by a reaction involving consumption of biotite, sillimanite, quartz and plagioclase:



where biotite is almost completely transformed into sericite. In terms of metallic ions (see Table.18, Chapter.V), bigger grains of cordierite tend to have relatively homogenous composition with an av. $Mg/(Mg + Fe^t)$ of 0.64 in the core, which increases to 0.67 towards the rim adjacent to garnet.

Accessory phases of the khondalites include zircons, apatite, sphene, ilmenite and graphite. Zircons, often enclosed in biotite, occur as colourless, euhedral crystals occasionally showing terminal rounding. Characteristic features include parallel extinction, positive elongation and high relief.

Apatite Tiny, euhedral, prismatic crystals of apatite are seen in association with sphene. Distinguishing features include uniaxial negative nature, high relief and weak to moderate birefringence.

Sphene occurs as wedge-shaped grains of pale-brown colour. Distinct birefringence (0.187), biaxial positive nature and very high relief are noteworthy features.

Ilmenite: In addition to the above mentioned accessory phases, a variety of oxide minerals are present, among which the most abundant is ilmenite.

Sericite is present as a secondary mineral in variable amounts. It is seen as very fine-grained, randomly oriented

Fig. 48 Reaction showing the possible formation of cordierite (Crd) by the consumption of sillimanite and biotite. The latter is completely converted into secondary calcite and sericite. Crossed nicols. Scale : 1 cm = 0.2 mm

Fig. 49 Sericite development as an alteration product of biotite, along the interstices between sillimanite and cordierite. Crossed nicols. Scale : 1 cm = 0.03 mm.

Fig. 50 Fine grained granoblastic texture of calc granulite. Crossed nicols. Scale : 1 cm = 0.2 mm

Fig. 51 Intensely sheared calc granulite with granulated quartz and feldspars. Crossed nicols. Scale : 1 cm = 0.2 mm.

Fig. 48

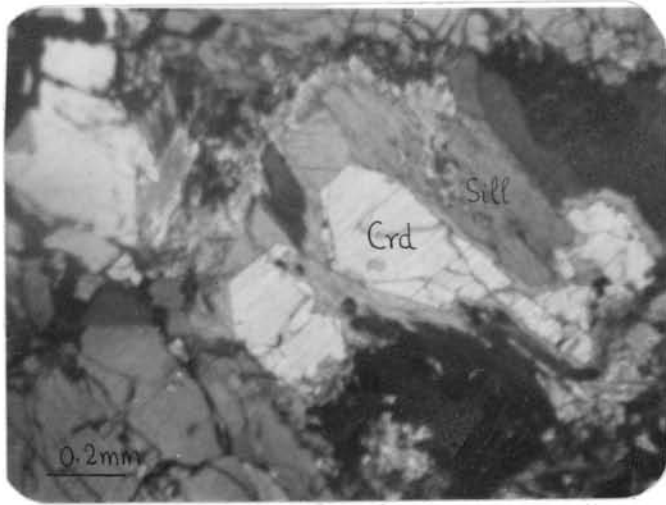


Fig. 49

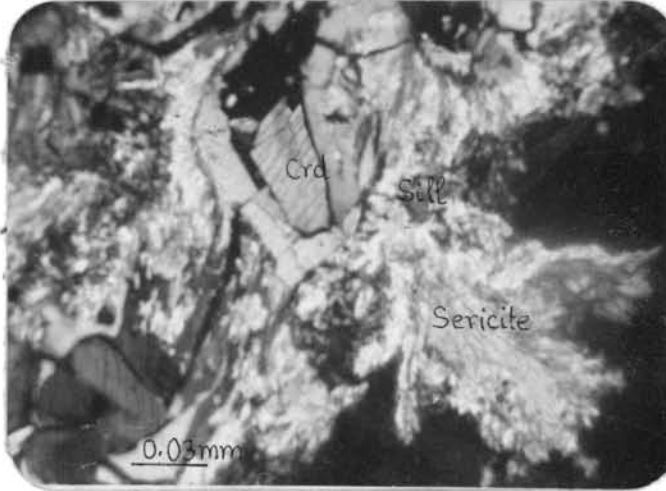


Fig. 50

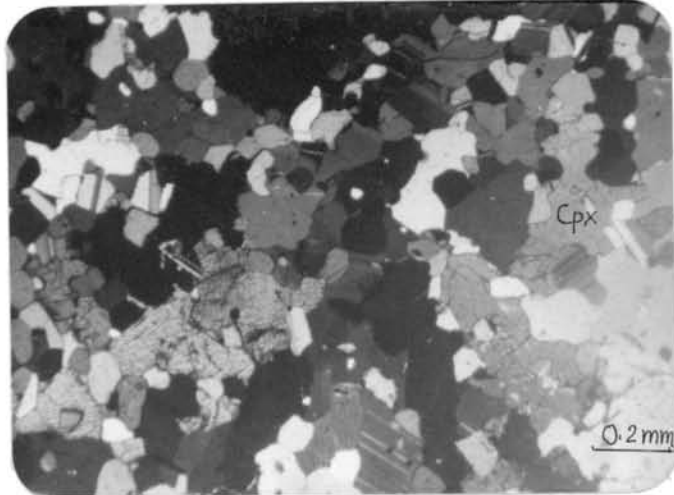
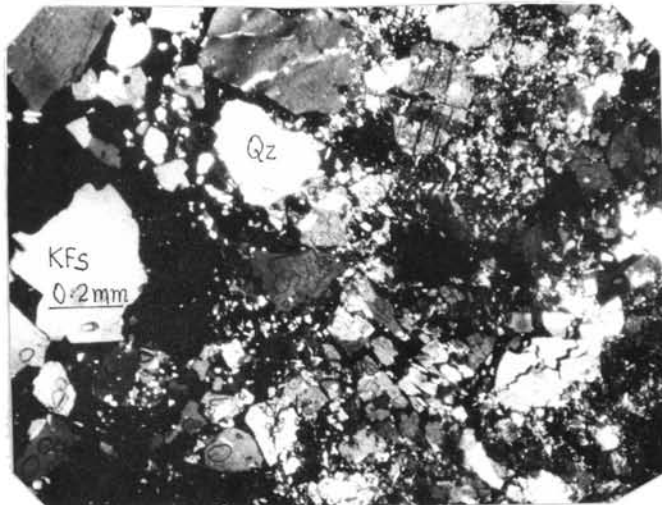


Fig. 51



flakes, filling the interstices between sillimanites, biotite and K-feldspars. (Fig.49).

III. 2. CALC-GRANULITES

Megascopically, they are fine-grained (1-2 mm) and petrographically exhibit a granoblastic texture with xenomorphic, granular grains (Fig.50). Some are massive while, others show a faint trace of foliation with a rough segregation of leucocratic and melanocratic minerals. Where the rock is foliated, quartz occur as lenticular shreds parallel to foliation. Granoblastic texture of the massive rock is also favoured by the lack of micaceous minerals. Thin section study of rocks reveal, locally pronounced granulation effects (Fig.51) Most of the grains show fractures and cracks. Many of the quartz, plagioclase and orthoclase grains with coherent grain boundaries meet at equigranular triple points. High modal percentages of quartz and plagioclase are characteristic.

Diagnostic mineral assemblages include diopside + hornblende + alkali feldspar + plagioclase + quartz + vesuvianite + scapolite ± biotite ± garnet ± calcite ± orthopyroxene with sphene, epidote and magnetite in accessory amounts.

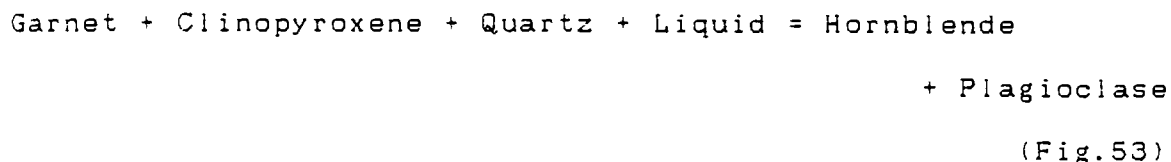
Based on microscopic examination, two types of calc-granulites with differing mineralogy and modal proportion

have been distinguished. Type I varieties are characterised by K-feldspar + calcite + vesuvianite + scapolite + diopside + grossularite + sphene assemblage while, in the type II, garnet is conspicuously absent. The latter also shows sphene in larger proportions.

Clinopyroxene:- Grains range in size from 0.4 to 0.9 mm and constitute the most abundant mineral (40-45% modal composition). It has an extinction angle of $30-38^{\circ}$ and second order yellow to bluish - yellow interference colours. Feebly pleochroic from pale green to green (X=pale green, Y = brownish green and Z = yellowish green), it is optically positive with $2V_z = 59^{\circ}$. Poikiloblastic grains of diopside with plagioclase inclusions are also common. These pyroxenes show a primary association with garnet and exhibit a variation from hedenbergite to diopside in composition (see mineral chemistry and structural formulae in Chapter.V). Alteration to hornblende is noticed (Fig.52) and sericitisation is limited to the cleavage planes.

Amphiboles (10-11% of modal composition), with grain size ranging from 0.12 to 0.36 mm, are light to dark green in colour. Small fragments often show pinkish to bluish colours. Birefringence ranges from 0.015 to 0.022. It is pleochroic from X = Yellowish green, Y = pale green to Z = dark green to bluish green and occurs along the borders of diopside as an alteration product of the latter, (see Fig.52). Hornblende is also seen developing in the contact of garnet and

clinopyroxene, possibly suggesting the reaction:-



Poikiloblastic of hornblende showing inclusions of spinel, are also observed (Fig.54). Microprobe analysis show a calcium content of 1.9-2.0 p.f.u and hence, correspond to the calcic types.

Both alkali feldspar (20-23% of modal composition) and plagioclase (16-20% modal composition) are present in the rocks. Alkalifeldspar crystals are generally anhedral, with size ranging from 0.15 to 0.9mm. Diffuse isogyres are suggestive of a very large 2 V angle. Microperthites are very few in occurrence. Cracks and partings are common. Some marginally granulated crystals show conversion to microcline along the rims. Graphic intergrowths resulting from the intergranular crystallisation process are also observed. Microprobe analyses reveal an orthoclase content of 90-95% (also see Table.16, Chapter.V).

Plagioclase also is usually anhedral with a maximum size of about 0.75 mm. They show albite to pericline 'discontinuous' twinning and are replaced by scapolite in a few sections. Alteration to sericite is observed in a few sections (Fig.55). Composition ranges from An₅₃ to An₆₄

- Fig. 52 Alteration of clinopyroxene (Cpx) to hornblende (Hb) with sphene (Sp) developing along deformation cracks. Parallel nicols. Scale : 1 cm = 0.2 mm.
- Fig. 53 Development of hornblende by the reaction :
Garnet + Clinopyroxene + Quartz + Liquid =
Hornblende + Plagioclase (Pl). Parallel nicols.
Scale : 1 cm = 0.1 mm.
- Fig. 54 Poikiloblastic hornblende showing inclusions of spinel. Sc = Scapolite. Crossed nicols. Scale : 1 cm = 0.1 mm.
- Fig. 55 Extensive development of sericite after plagioclase. Crossed nicols. Scale : 1 cm = 0.1 mm.

Fig. 52

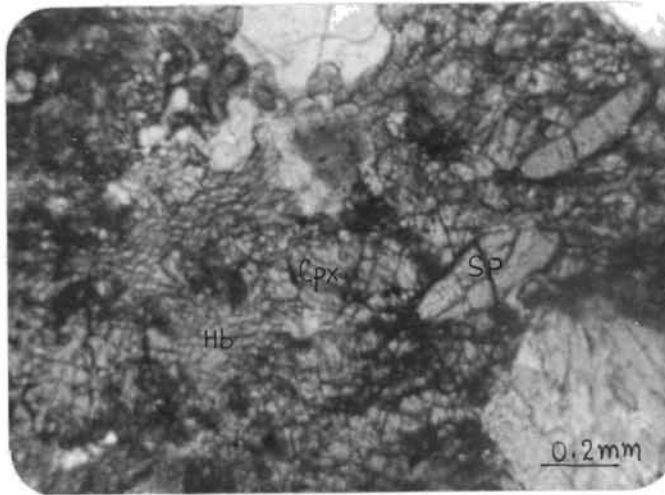


Fig. 53

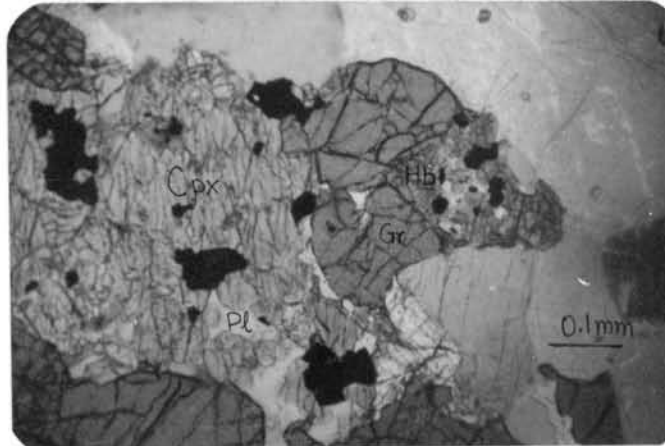


Fig. 54

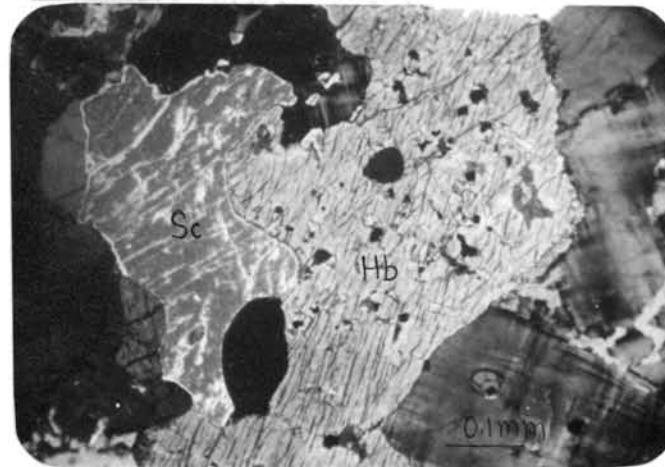
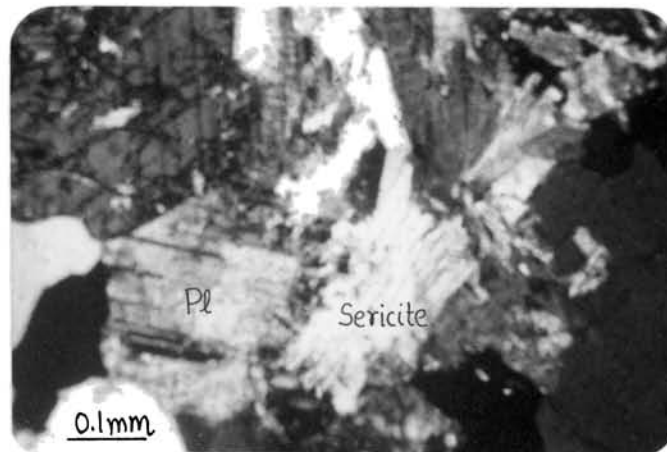


Fig. 55



Labradorite) as indicated by microprobe data (see Table.17, Chapter.V).

Quartz, exhibiting polygonal and irregular grain boundaries measure up to 0.3 to 0.5mm in size. They occupy 25-35% of the total volume. Minute fractures are noticed. Some contain inclusions of calcite. In some sections, quartz is seen almost completely surrounded by biotite with associated secondary calcite and sericite.

Garnet: Porphyroblasts of garnet are observed in only one section. Common association are feldspars and clino- as well as orthopyroxenes (see Fig.53). Grain size varies from 0.3 to 2.515 mm and deformation cracks are frequently seen. Microprobe data (see Chapter.V, Table.14) indicate remarkably high grossularite value (59-61 mol%). Average composition is expressed as $Alm_{36} Spess_3 Gross_{60.2} Pyr_1$.

Biotite is rarely present, except where metasomatic or retrogression changes have taken place. It is deep brown in colour with no pleochroism or cleavage traces. Another set consisting of tabular, flaky grains with greenish brown colour, perfect cleavage and pleochroism (in shades of yellowish green to greenish brown) is also seen (Fig.56).

Vesuvianite is seen as independent grains (Fig.57) associated with quartz and orthoclase. They are colourless with high relief, often showing anomalous Berlin blue

colours (Fig.58). Cleavage parallel to elongation, uniaxial negative nature and moderate pleochroism are characteristic.

Orthopyroxenes occur mostly as anhedral grains, in close association with diopside. Cleavage (87-90°), second order yellow interference colours and parallel extinction are characteristic. In some, these are partially or completely surrounded by clinopyroxene. The retrogression in some samples is so intense that hypersthene is completely destroyed and clinopyroxene is largely degraded to hornblende and quartz (see Fig.59).

Scapolite is found as independent grains in association with hornblende, sphene and microcline (see Fig.54). Analysis on the basis of 12 (Si + Al) shows Si content to be less than 7 p.f.u and Al, less than 6 p.f.u. Ti is absent while Cr (~0.005 p.f.u), Mn (~0.006 p.f.u) and Mg (0.0018 p.f.u) are reported in trace amounts only. Ca/Na ratio ranges between 2.87 and 3.82 and Ca + Na varies between 3.95 and 4.04. Ca/Ca+Na averages around 0.769. Me% ranges between 74 and 79 and are hence designated as mizzonite (Me₅₀- Me₈₀).

Calcite belongs to two generations; primary and secondary. Primary calcite, with a size ranging from 0.35 to 1.2 mm is associated with diopside and secondary calcite is a

- Fig. 56 Calc granulite showing two generations of biotite. Crossed nicols. Scale : 1 cm = 0.1 mm.
- Fig. 57 Vesuvianite (Vt) coexisting with quartz and orthoclase. Crossed nicols. Scale : 1 cm = 0.2 mm.
- Fig. 58 Section of calc granulite showing vesuvianite (anomalous berlin blue colour) and development of hornblende (Hb). Crossed nicols. Scale : 1 cm = 0.2 mm.
- Fig. 59 Clinopyroxene almost wholly replaced by hornblende. Crossed nicols. Scale : 1 cm = 0.1 mm.

Fig. 56

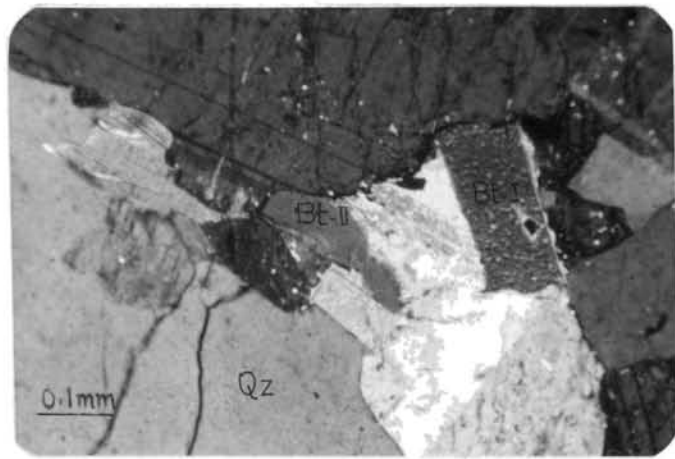


Fig. 57

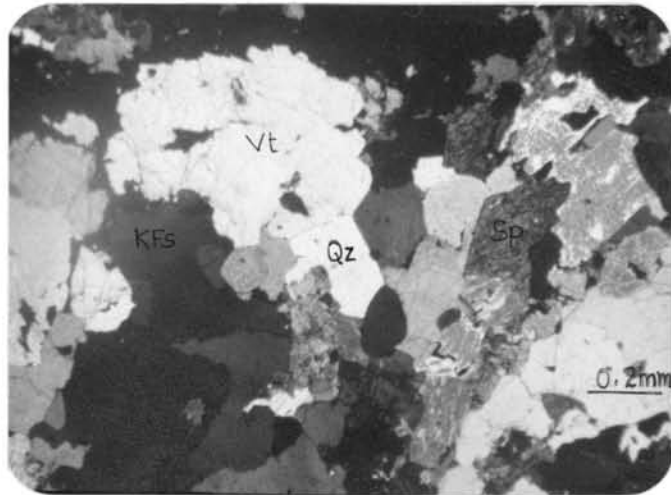


Fig. 58

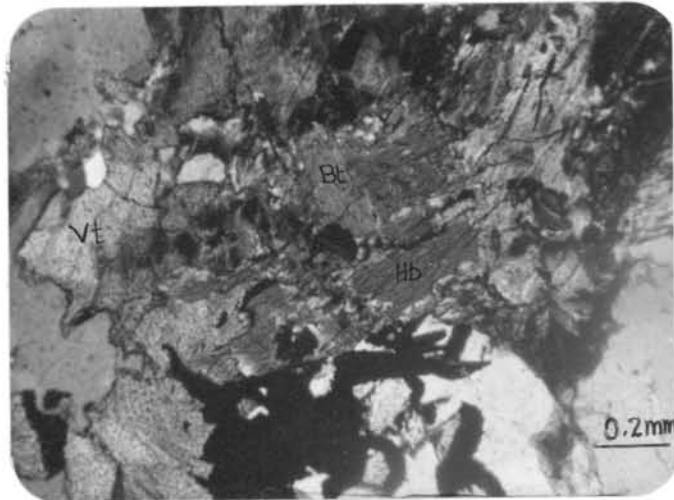
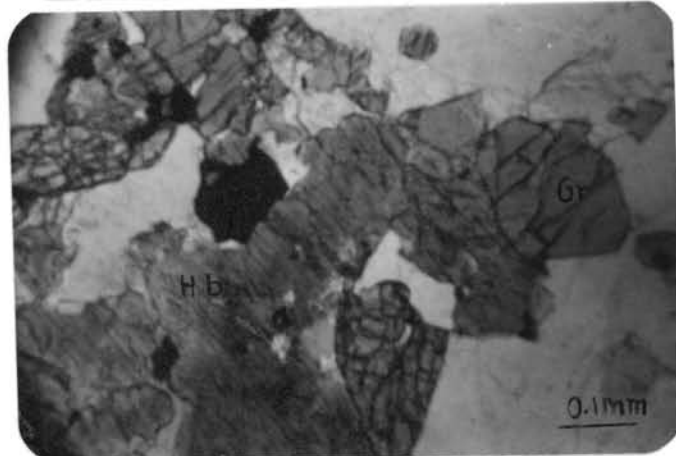


Fig. 59



product of biotite alteration (see Fig.60).

Sphene is interlocked in grain boundaries between clinopyroxene and plagioclase (see Fig.54). Grains are upto 2 mm in size and show symmetrical extinction and wedge-shaped form. Pleochroism is weak from grey to light brown (X= colourless; Y= pale-brown and Z= pinkish brown; Z>Y>X). Microprobe analyses of sphene is shown below (Table.2).

Table.2 MICROPROBE ANALYSES OF SPHENE WITH ATOMIC PROPORTIONS.

Rock type with sample No	Calc granulite (PS.35)	
Anal.No.	25	29

SiO ₂	29.41	30.02
TiO ₂	32.33	32.33
Al ₂ O ₃	3.34	3.63
FeO	2.33	2.50
MnO	0.07	0.10
CaO	26.61	26.87

Total	94.00	95.45

on the basis of 5 oxygens		
Si ^{iv}	0.022	1.028
Al ^{iv}	0.405	0.405
Al ^{vi}	0.268	0.258
Ti	0.845	0.832
Fe	0.068	0.072
Mn	0.002	0.003
Ca	0.991	0.986

Epidote: Columnar in shape, it exhibits a size range from 1.26 to 2.08 mm and is associated with plagioclase and hornblende. It is yellow to greenish-yellow in colour and shows good cleavage, bright interference colours (rather

unevenly distributed) and pale yellow to pale green pleochroism (X=pale yellow, Y=brownish-green, Z=pale yellow-green). It is biaxial negative, with an extinction angle of 38° with respect to cleavage. Microprobe data (Table.3) show that CaO ranges between 22-23 and MgO is less than 0.05 wt %. Tetrahedral Al occupancy (0.0013 p.f.u) is less than Al^{vi} occupancy (2.264 p.f.u). Ti is low (~ 0.006 p.f.u) and Cr is almost absent, except in one of the analyses (0.003 p.f.u). Fe is <1 with a range from 0.802-0.936 p.f.u. Range of Mn is limited between 0.018 and 0.029 p.f.u. Microprobe analyses of epidote is shown below.

Table.3 MICROPROBE ANALYSIS OF EPIDOTE FROM CALC-GRANULITE
(PS.35)

Elements	Av(7 Analyses).
SiO ₂	36.54
TiO ₂	0.09
Al ₂ O ₃	22.82
Cr ₂ O ₃	0.01
FeO	12.17
MnO	0.33
MgO	0.01
CaO	22.75
Total	94.70

on the basis of 12.5 oxygens

Si	3.080
Al ^{iv}	0.001
Al ^{vi}	2.264
Ti	0.005
Cr	0.001
Fe	0.858
Mn	0.023
Mg	0.001
Ca	2.053

Magnetite is present ubiquitously as an idiomorphic grain with or without exsolution lamellae. Mineral composition obtained through microprobe analysis shows traces of Mg (0.001 p.f.u) and Ti (0.001 p.f.u). Al (total) is 0.003 p.f.u and Mn is less than 0.02 p.f.u. Fe_2O_3 and FeO are 66.51 and 29.58 (mol %) respectively. Since X_{Mt} is greater than 0.96, magnetite is considered almost a pure phase.

Mineral parageneses characteristic of the calc granulites include:-

Quartz - Orthoclase - Diopside

Plagioclase - Diopside - Garnet

Diopside - Plagioclase - Calcite - Quartz

Hornblende - Sphene - Quartz - Plagioclase - Microcline

Quartz - Orthoclase - Garnet

III.3 CRYSTALLINE LIMESTONES

Limestone is medium to coarse grained (grain size varies from 2 to 4 mm) and its colour ranges from white to pink. The texture is typically crystalline with interlocking polygonal crystals (Fig.61). Occasionally, granoblastic, elongate texture is observed. In some lensoid outlines of calcites define a crude foliation (Fig.62) and in some other sections, quartz and feldspars are seen segregated into thin bands. Mechanical fragmentation of quartz and feldspar grains (Fig.63) giving rise to a 'mortar texture' is noticed in a

- Fig. 60 Quartz grain completely surrounded by biotite with associated secondary calcite (Cc). Crossed nicols. Scale : 1 cm = 0.1 mm.
- Fig. 61 Crystalline limestone showing interlocking polygonal crystals. Crossed nicols. Scale : 1 cm = 0.5 mm.
- Fig. 62 Stained thin section showing crude foliation in crystalline limestones, defined by lensoid outlines of calcites (Cc). Hornblende (Hb) occurs as an alteration product of diopside (Di). Parallel nicols. Scale : 1 cm = 0.5 mm.
- Fig. 63 Mechanical fragmentation of quartz and feldspar in crystalline limestones (stained thin section). Parallel nicols. Scale : 1 cm = 0.5 mm.

Fig.60

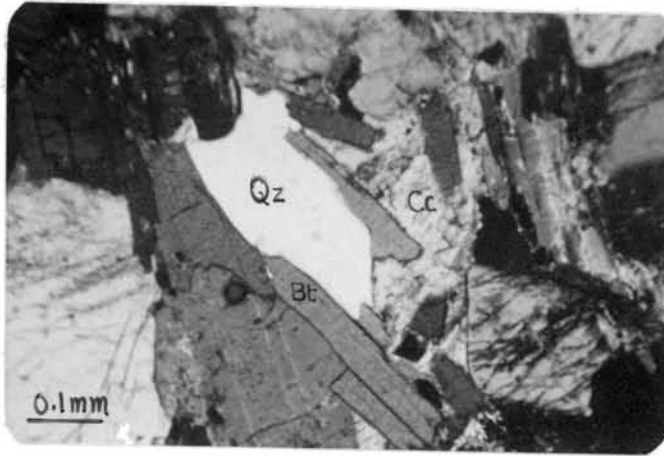


Fig.61

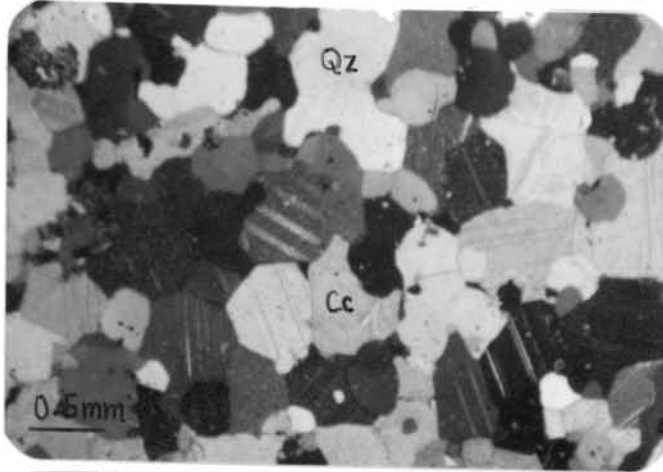


Fig.62

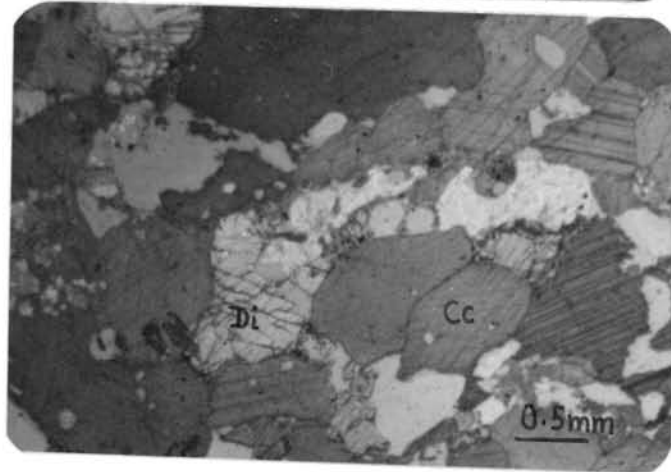
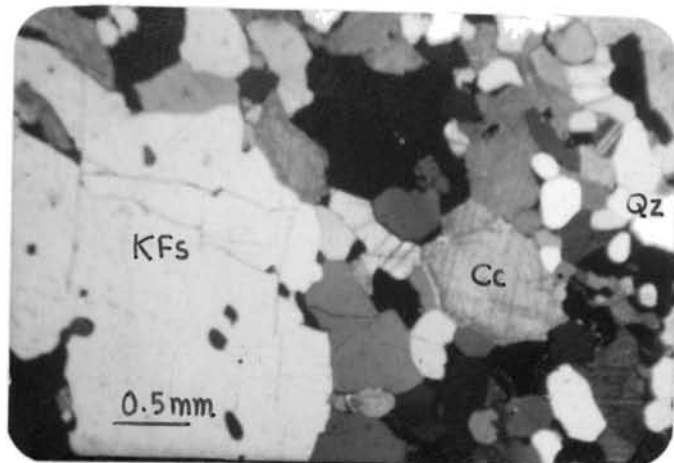


Fig.63



few cases.

Principally composed of calcite (46 to 72 modal %), it contains 1-10 % dolomite and various amounts of quartz (4-8 %), alkali feldspar (3-6 %), plagioclase (0-2%), diopside (0-3 %), scapolite (0-3 %), hornblende (0-2 %), sphene (0-2 %), sericite (0-0.5 %) and iron oxides (0.9-2 %). Towards contact with the country rocks, the content of impurities increases.

Calcite:- Coarse calcite displays typical twin lamellae and is characterised by the presence of perfect rhombohedral (1011) cleavages. Size varies from a fraction of a millimetre to 2.87 mm; the crystals being equidimensional with amoeboid outlines. Larger grains are poikiloblastic with inclusions of quartz, feldspars, and accessory minerals. Perceptible biaxiality and brittle fractures (Fig.64) are observed in strained calcites.

Dolomite is distinguished by the presence of twin lamellae parallel to the short diagonal and presence of zonal structure (Fig.65). Identification of dolomite has also been done by staining with alizarin red S solution (Dickson, 1965, Ref:Appendix I.3). Textural relationship of dolomites with the silicates suggests that they have formed from silicate + calcite reactions and are not of primary origin.

Quartz is the major impurity in the limestones. The

grains are inequigranular with crenulate margins. They occur as strained, xenomorphic to hypidiomorphic fragments, interstitial to calcite grains or as poikiloblastic inclusions in feldspars. Some of the grains carry arrays of liquid inclusions.

Alkali feldspars occur as xenomorphic to hypidiomorphic grains. Carlsbad twinning and perthitic intergrowths are seldom met with. Some of them contain inclusions of quartz and carbonates. Alteration to sericite is observed.

Plagioclase has been observed in minor amounts, occupying interstitial spaces between calcite crystals. They are characterised by symmetrical extinction (4° - 8°) and biaxial positive nature. Composition (Michel-Levy's method) ranges between An₂₈ to An₃₂ (oligoclase). Sericitisation of plagioclase has been observed.

Scapolite is noticed as hypidiomorphic to panidiomorphic prisms occurring in close association with calcite and quartz. Textural relation observed in thin sections suggest the following reaction:-

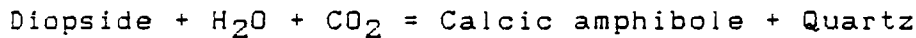
Plagioclase + Calcite = Scapolite (Fig.66)

It is uniaxial and optically negative with low refractive index and birefringence. Its composition in terms of Me content, estimated using the maximum birefringence values (Deer et al, 1966) is Me₅₈, which is lower than that of the

scapolite in the calc-granulites.

Diopside occurs as isolated, hypidiomorphic grains with conspicuously high R.I and bright interference colours. Its presence is restricted to sections relatively poor in CaO.

Hornblende occurs in trace amounts and is associated with diopside as a dissociation product and also with sphene. Based on textural relationship, the reaction:-



(see Fig.62)

may be suggested.

Sericite is seen occupying intergranular spaces of calcites, and calcite-feldspar boundaries.

III.4 MIGMATITIC GNEISSES

Migmatitic gneisses consist mainly of two varieties, (1) biotite gneiss and (2) biotite-hornblende gneiss. Texturally, they are medium-to coarse-grained and display xenomorphic granular texture, displaying well-defined foliation by alignment of biotite or hornblende. Myrmekitic intergrowths, corrosion edges and embayments of mineral contacts are frequent. Undulose extinction of quartz and suturing of grain boundaries are commonly observed. Recrystallisation effects are limited to some quartz and mica flakes.

- Fig. 64 Brittle deformation fractures in calcites (stained thin section). Parallel nicols. Scale : 1 cm = 0.2 mm.
- Fig. 65 Dolomite (Dol) grain in crystalline limestone showing broad twin lamellae. Crossed nicols. Scale : 1 cm = 0.5 mm.
- Fig. 66 Development of scapolite (Sc) after plagioclase and calcite (Plagioclase + Calcite = Scapolite). Crossed nicols. Scale : 1 cm = 0.2 mm.
- Fig. 67 Microclinisation of plagioclase in biotite - gneiss. Crossed nicols. Scale : 1 cm = 0.2 mm.

Fig. 64

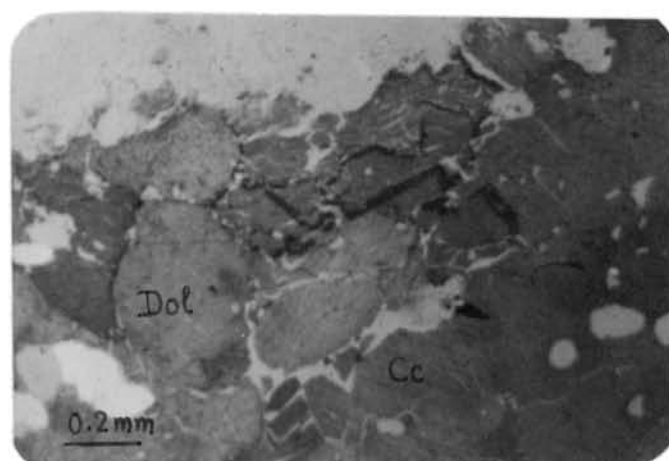


Fig. 65

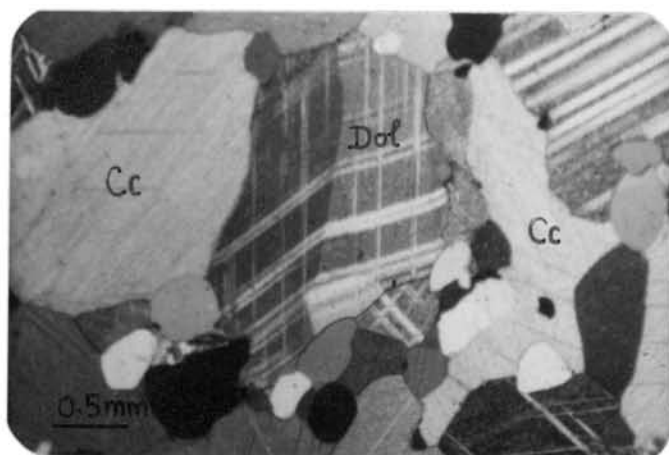


Fig. 66

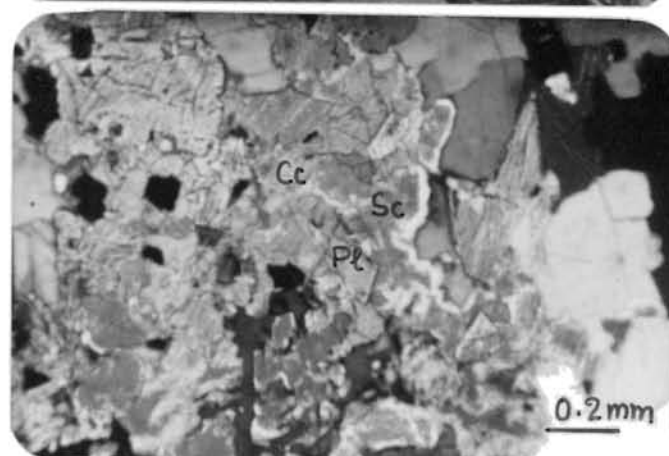
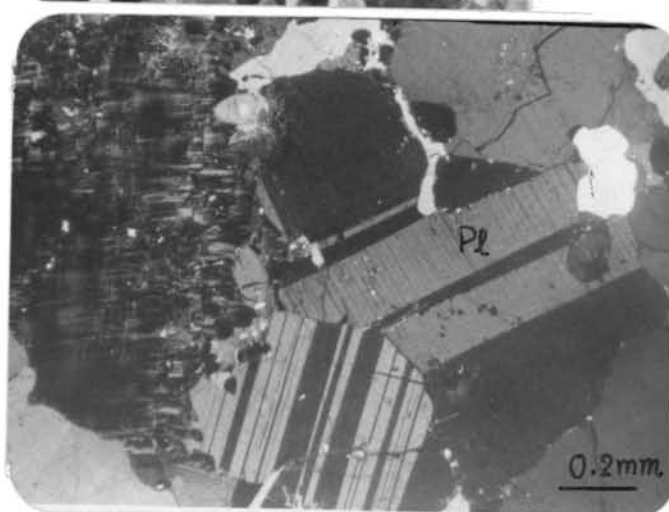


Fig. 67



Biotite gneiss is typically a coarse-grained (>4mm), leucocratic rock. Feldspar is generally pinkish in colour. Major minerals of biotite-gneiss include K-feldspar (46 modal %), quartz (36%), plagioclase (12%) and biotite (5%) with apatite occurring in accessory amounts.

K-feldspar is mostly composed of microcline. Xenomorphic to porphyroblastic, it contains inclusions of quartz. Maximum birefringence is 0.010. It is optically negative and biaxial with a large $2V(40^\circ)$, and is partly altered to sericite. Often, it remains as large, strained augens.

Quartz consists of xenomorphic grains with size ranging from 0.4 to 0.8 mm. Strain effects such as fracturing and undulose extinction are common. It shows yellowish to 1st order grey interference colours. Rounded 'drop-like' forms included in feldspars are frequent. It is also seen as interstitial, xenomorphic grains between plagioclase megacrysts.

Plagioclase is medium - sized, with a composition corresponding to oligoclase. Some of the plagioclase show signs of microclinisation (Fig.67).

Biotite shows typically reddish brown colours and perfect unidirectional cleavage traces. Relatively coarse flakes of upto 1.2 mm in extent, are seen cutting across

large plagioclase and quartz grains (Fig.68). Some flakes show bending effects too.

Biotite - hornblende gneiss is an intensely deformed, medium - grained rock. Cataclasis induced marginal granulation is observed in quartz and feldspar.

These are mainly quartz - plagioclase - biotite - hornblende - k-feldspar assemblages with accessory phases of apatite, magnetite and sphene.

Quartz constitutes 30-35 modal % of the rock. Xenomorphic quartz grains of 0.03 to 0.2 mm size occupy interstitial spaces. Some of them contain inclusions of opaques and biotite.

Plagioclase (20 to 25 modal %) occurs as sub-hedral grains which are often bent or kinked. Its dimension vary from 0.32 to 0.5 mm. Extinction angles determined by Michel - Levy method indicate an oligoclase composition which is corroborated by microprobe data (see Table.17, Chapter.V) and the composition is represented as $Ab_{73.8} An_{24.78} Or_{1.42}$ (mol %). Partial twins of albite and pericline laws are frequent. Cross-cutting lamellae possibly induced by deformation are also seen. Secondary transformation of plagioclase like sericitisation and microclinisation effects are observed.

Biotite occurs as an alteration product of amphibole (Fig.69). It constitutes 10 - 12 % of the total modal composition. Grain size ranges from 0.3 to 1.2 mm. Microprobe data indicate that the titanium content is low (<0.4 p.f.u) and total aluminium occupancy is 2.531 (p.f.u). Ratio of Mg:Fe is 1.13.

Hornblende occupies 1-9% of the total modal composition and occurs as sub-idioblastic grains with size varying from 0.1 to 2.12 mm. Increase in hornblende proportion is observed towards the flag. Microprobe analyses (see Table.20, Chapter.V) indicate a correspondence to calciferous to sub-calciferous types.

K-feldspar is represented mainly by orthoclase which tends to remain as large porphyroblasts showing deformation features. A few grains are transformed to biotite (Fig.70) and some others are sericitised. Perthitic (string perthites), antiperthitic and myrmekitic intergrowths are frequently observed.

Apatite is the main accessory mineral and is associated with biotite and hornblende. Pitted surface, straight extinction with respect to crystal faces, unidirectional cleavage and first order grey colours are characteristic.

Sphene is commonly seen with hornblende - biotite alteration process. It exhibits subhedral crystal outline and prominent partings.

- Fig. 68 Coarse biotite flakes transecting the feldspars
 in biotite - gneiss. Crossed nicols. Scale :
 1 cm = 0.2 mm.
- Fig. 69 Microfabric of the melanosomes in biotite -
 hornblende gneiss showing conversion of
 hornblende into biotite. Parallel nicols.
 Scale : 1 cm = 0.2 mm.
- Fig. 70 K-feldspar porphyroblasts showing cross-cutting
 biotite streaks in biotite - hornblende gneiss.
 Crossed nicols. Scale : 1 cm = 0.2 mm.
- Fig. 71 Fine grained variety of amphibolite showing
 faint foliation defined by streaks of
 hornblende and biotite. Parallel nicols. Scale:
 1 cm = 0.2 mm.

Fig. 68

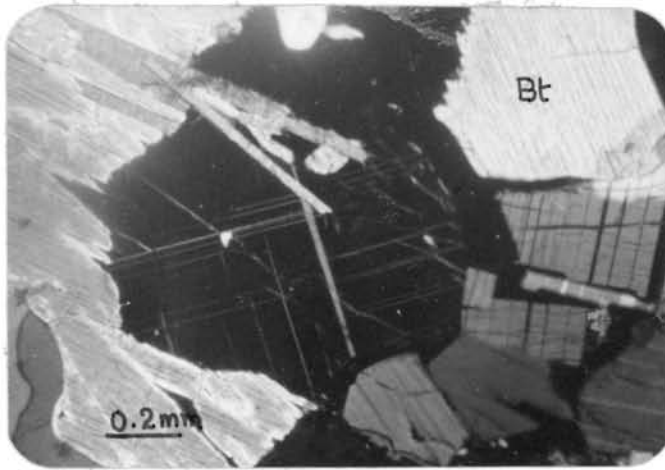


Fig. 69

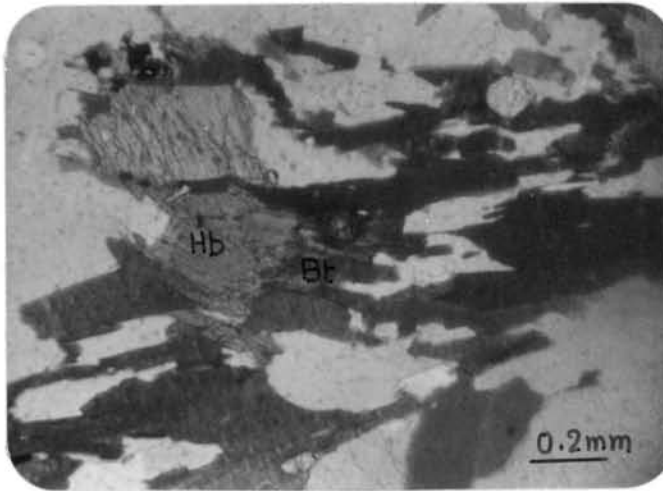


Fig. 70

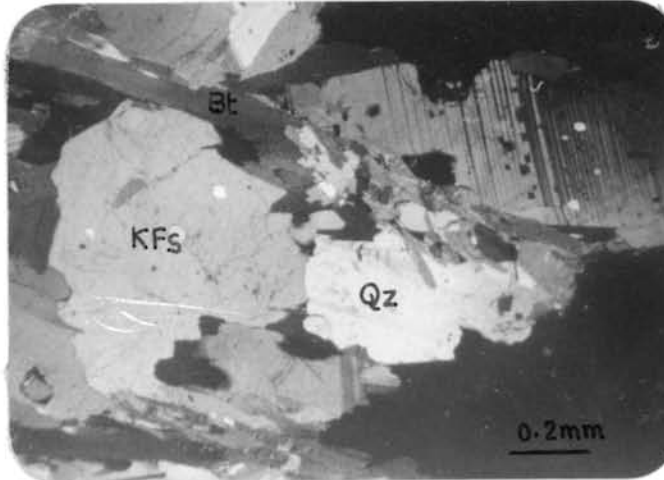
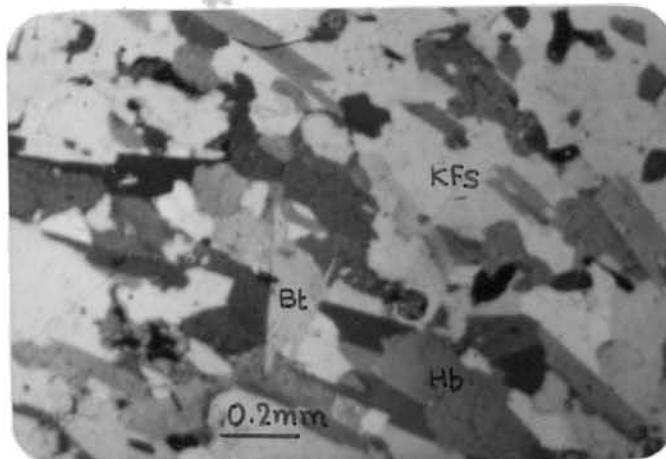


Fig. 71



III.5 AMPHIBOLITES

These are medium to coarse - grained rocks with an inequigranular, xenoblastic texture, consisting chiefly of hornblende (20-48 modal %), plagioclase (13-49%), k-feldspars (3-16%), quartz (8-12%) and clinopyroxene (0 -7%), with or without biotite (0-31%). Scapolite, sphene (1-2%), apatite (< 1-2%), secondary calcites (0-6%) and opaques (0-6%) occur as minor and accessory minerals.

Amphibole in granular varieties occurs as porphyroblasts set in the plagioclase matrix. In the fine - grained varieties, fine needles of amphiboles are aligned parallel (Fig.71). It is commonly green to greenish brown and is strongly pleochroic with X = yellowish green, Y = brownish green and Z = dark green. Extinction angle varies between 16° and 26° and 2V is 72°. In some sections, a sieve texture impregnated with quartz, apatite and iron ores (Fig.72) is observed.

Plagioclase is abundant and forms rather an even grained mosaic. Grain size ranges from 1.25 to 2.35 mm and commonly shows twinning. Extinction angle varies between 7° and 19°. Sericitisation is observed in some grains, and in some cases, muscovite is developed along the grain boundary.

Alkali feldspar is mainly represented by anhedral to subhedral orthoclase. Size varies from 0.2 - 1.2 mm . . It

occurs in association with quartz, hornblende and apatite. Cuneiform structures are observed along the periphery. Microcline (3 modal %) is observed rarely.

Quartz forms about 8 to 12 modal percentage and often exhibits anhedral crystal outlines. Size ranges between 0.04 and 0.8 mm. Recrystallization effect is also seen. Sutured margins and undulose extinction are characteristic.

Clinopyroxene is limited in occurrence (0 to 7 modal %) and is usually seen partially or wholly replaced by hornblende (Fig.73). Well developed prisms showing first order yellow to grey interference colours are also noticed. Extinction angle varies from 38° to 43° .

Biotite occurs as subhedral grains. Its size ranges from 1.5 to 2mm. Pleochroism is from light brown to dark brown. It occurs as a 'hornblende-breakdown' reaction product (Fig.74), in close association with secondary calcites.

Sphene is greenish pink in colour and is seen as euhedral grains or as irregular masses (see Fig.74) at the plagioclase - biotite boundary. Apatite is restricted to hornblende-biotite interface with grains of upto 0.24mm size.

Secondary calcite is developed at the grain boundaries of plagioclase and biotite with hornblende or as an alteration product of k-feldspars.

- Fig. 72 Sieve structure in -hornblende (Hb) showing inclusions of opaques and quartz. Parallel nicols. Scale : 1 cmm = 0.2 mm.
- Fig. 73 Replacement of clinopyroxene (Di) by hornblende. Parallel nicols. Scale : 1 cm = 0.2 mm.
- Fig. 74 Hornblende (Hb) breaking down to biotite (Bt). Sphene (Sp) is developed at the interface between biotite and plagioclase. Parallel nicols. Scale : 1 cm = 0.2 mm.
- Fig. 75 Typical granitoid texture of core portions of granite. Crossed nicols. Scale : 1 cm = 0.1 mm.

Fig.72

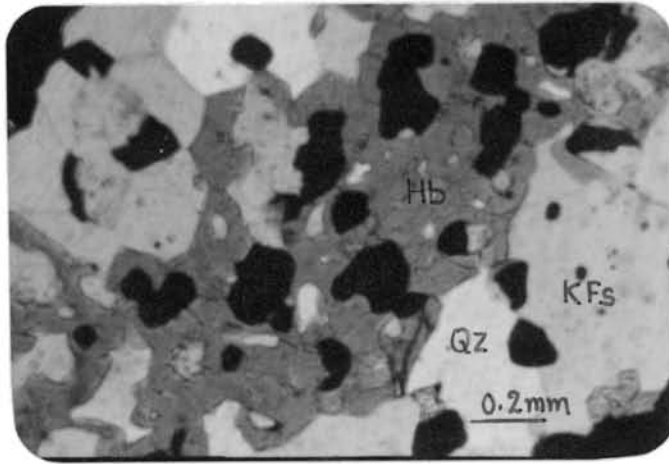


Fig.73

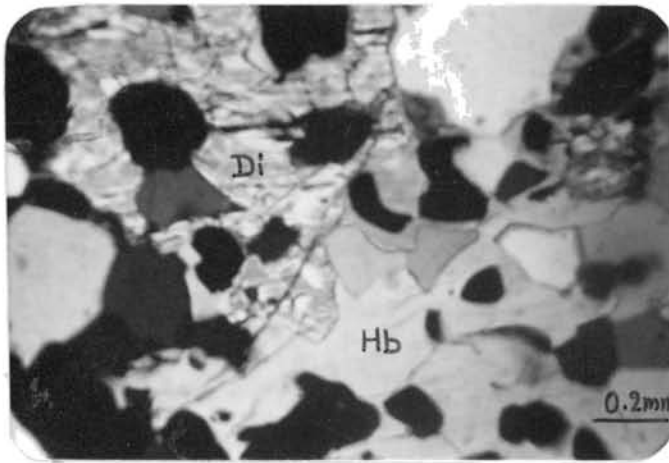


Fig.74

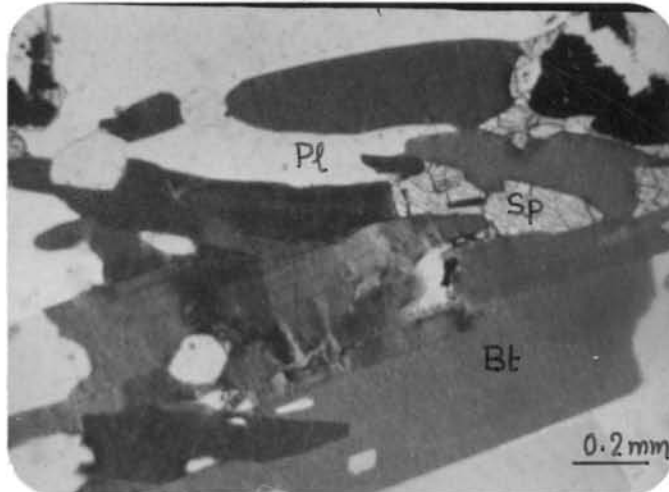
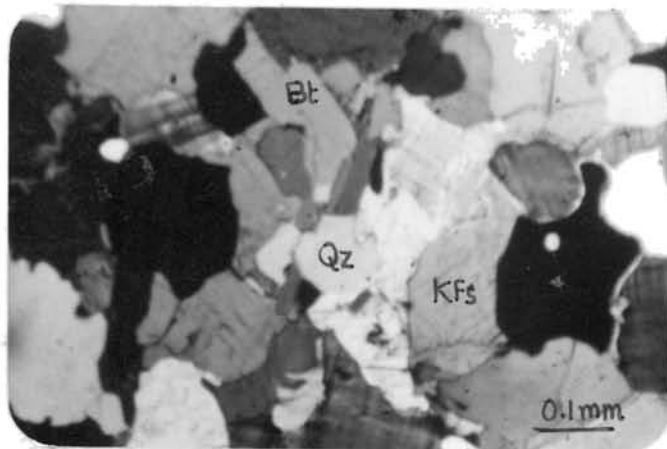


Fig.75



Opaques constitute 0 to 6 modal percent of the total volume of the rocks and occur as xenomorphic masses intimately associated with hornblende - biotite breakdown textures. Scapolite forms granular aggregates of low first order colours replacing plagioclase.

III.6 GRANITES

These are phanerocrystalline, with typical granitoid texture (Fig.75). Towards periphery, faint foliation due to the parallel alignment of biotite flakes is observed (Fig.76). They are medium to coarse-grained, the shapes of grains being equant, tabular or prismoid. Constituent minerals (modal %) include quartz (40-45%), feldspars (20-34%), hornblende (10%), biotite (3-10%), and opaque (2-6%).

Quartz:- It is mainly interstitial and occasionally found as inclusions within feldspars. It is invariably anhedral and the grain size varies from 0.18 to 0.9mm. Most of the grains show marginal granulation and strained polarisation. Inclusions of quartz in plagioclase, showing graphic outlines are frequent.

Feldspars consist of plagioclase and alkali feldspars. Plagioclase is the second most abundant mineral, characterised by low birefringence (0.008) with a size range from 0.12 to 0.36mm. These white to very light grey coloured grains are twinned according to albite and pericline laws. Partial twinned lamellae are also frequent. Some grains

appear to corrode amphiboles. Alteration to sericite is also observed. Extinction angle determinations (Michel-Levy and combined Carlsbad-Albite twin methods) suggest the composition to be varying between oligoclase (An_{10-30}) and andesine (An_{30-50}), which is substantiated by microprobe analyses (see Table.17, Chapter.V). Myrmekitic intergrowths are locally developed along the junctions of microcline and plagioclase. Alkali feldspar:- The most common alkali feldspars are microcline and microperthite, occurring as subhedral grains of 1.3 to 2.5 mm size. In some, it is sporadically distributed as small sized anhedral plates. The grain boundaries are often corroded by quartz and the fractured large grains enclosing plagioclase show sericitisation. String and patch perthites are frequent. Large area microprobe analyses of alkali feldspars give estimated bulk composition of $Or_{85.2} Ab_{14.9} An_{0.6}$ (Table.16, Chapter.V). The included plagioclase found within the potash feldspars (Fig.77) has a higher sodium content (0.576 p.f.u) than the independent plagioclase (0.276 p.f.u) or alkali feldspar grains (0.447 p.f.u). Back scattered electron image of an enlarged portion of alkali feldspar resembling string perthite is shown in Fig.78. Microperthites have a composition of $Or_{79.7} Ab_{19.4} An_{0.9}$ which show a shift to $Or_{90.7} Ab_{9.1} An_{0.2}$, near plagioclase contacts.

Hornblende:- It forms subhedral grains upto 0.5 mm length and has strong pleochroism in yellow and green shades

(X= yellowish green, Y= brownish green and Z= dark green). Extinction angle varies from 21 to 34°. A few grains show twinning. Biaxial negative nature and 2V of 75° are characteristic. It is seen partially or completely replaced by biotite (Fig.79).

Biotite:- Greenish black biotite is an ubiquitous mafic phase forming 3 to 10 modal % of the granites. Size ranges from 0.316 to 0.581 mm. Two generations, one as a primary crystallisation product associated with plagioclase, quartz and alkali feldspar and the other as an alteration product of hornblende, have been observed. Pleochroism from brown to brownish-green and second order yellow to green interference colours are characteristic. Birefringence is in the order of 0.06. Elongation is positive and the acute bisectrix figures yield 2V of 20°. The Fe/(Fe+Mg) ratios (see Table.15, Chapter.V) of biotites is in the range of 0.51-0.57. Plot of biotite composition in terms of solid solution end-members annite-phlogopite shows a shift towards annite field (See Fig.117 b, Chapter.V).

Accessory minerals include apatite and zircon. Apatite, characterised by straight extinction and strong relief, is found associated mainly with the opaques. Magnetite is the chief opaque mineral. Muscovite also occurs rarely as flakes of medium size (0.212-0.305 mm) with pink to yellow (second order) interference colours surrounding biotite and plagioclase, suggesting its secondary origin.

- Fig. 76 Peripheral portion of granite showing faint foliation defined by biotite flakes. Crossed nicols. Scale : 1 cm = 0.2 mm.
- Fig. 77 Back scattered electron image (BEI) of perthitic alkali feldspar in granite. A plagioclase grain is shown at the top right corner. Dark grey border of the plagioclase is pure albitic in composition. Scale bar : 100 μ m.
- Fig. 78 Back scattered electron image of an enlarged part of string perthite in granite. Scale bar : 10 μ m.
- Fig. 79 Microfabric of granite showing hornblende, with biotite developed along rim. A slender biotite flake is also seen cutting across the hornblende grain. Parallel nicols. Scale : 1 cm = 0.2 mm.

Fig.76

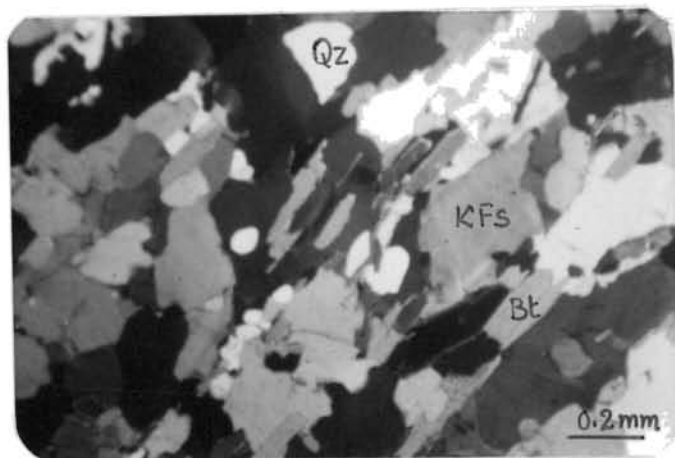


Fig.77

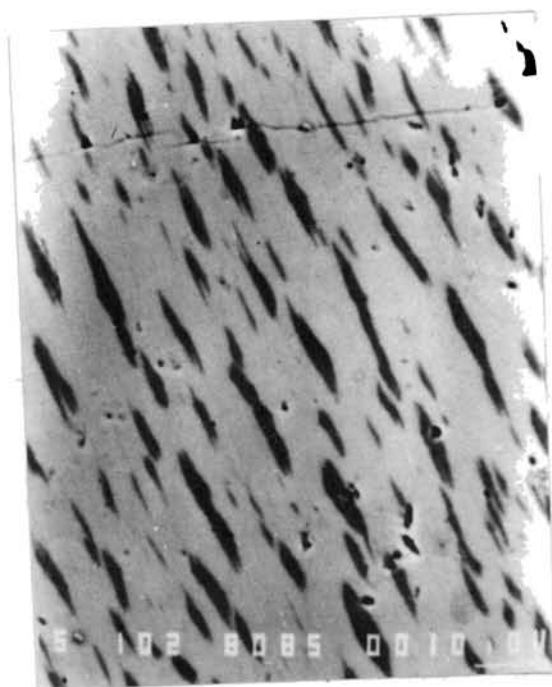
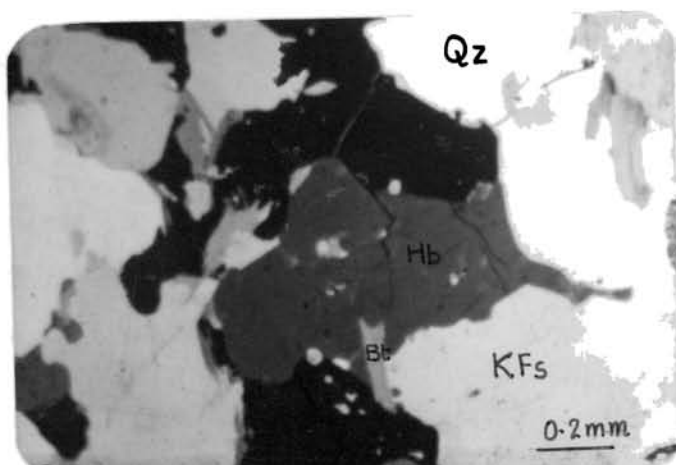


Fig.78

Fig.79



III.7 PEGMATITE

Pegmatites are unzoned and have a simple mineralogy with quartz (40-42 modal %), microcline (25-35%), perthite (14-25%), biotite (4-10%) and plagioclase (3-8%) as the major minerals. Pegmatites within the meta-sedimentary sequence contain additionally garnet (2-10%) and muscovite (6%).

Quartz (subhedral to anhedral) grains are surrounded by microcline and in some cases are rimmed by thin layers of myrmekite. Rounded blebs of quartz in feldspar are also observed.

Microcline is found as anhedral grains showing first order white to grey colours. Graphic intergrowths of quartz and feldspars are frequent. Grid like twinning pattern, length fast nature and weak birefringence (0.007) are diagnostic. Development of myrmekite due to replacement of microcline by oligoclase is also seen (Fig.80). Microperthites showing extensive development of strings of exsolved Na-rich plagioclase are also observed (Fig.82).

Biotite is seen at quartz-microcline interface as well as partially surrounding quartz. It shows second order green to pink colours and yellow to brown pleochroism. Pleochroic haloes are frequently observed. In some cases, it is developed after garnet (Fig.82). Slight bending of biotite plates is also seen. Intergrowths resembling cuneiform

- Fig. 80 Pegmatite showing development of myrmekite at the microcline (Ml) - oligoclase (Ol) boundary. Crossed nicols. Scale : 1 cm = 0.1 mm.
- Fig. 81 Microperthite (Perth) in pegmatite. Crossed nicols. Scale : 1 cm = 0.1 mm.
- Fig. 82 Biotite developed after garnet in pegmatite. parallel nicols. Scale : 1 cm = 0.5 mm.

Fig. 80



Fig. 81

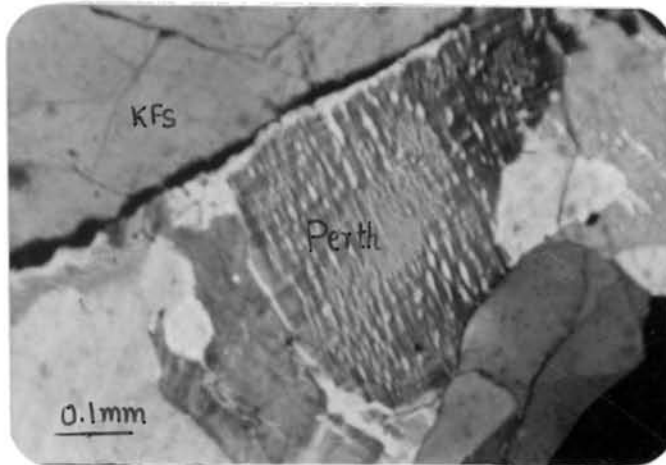
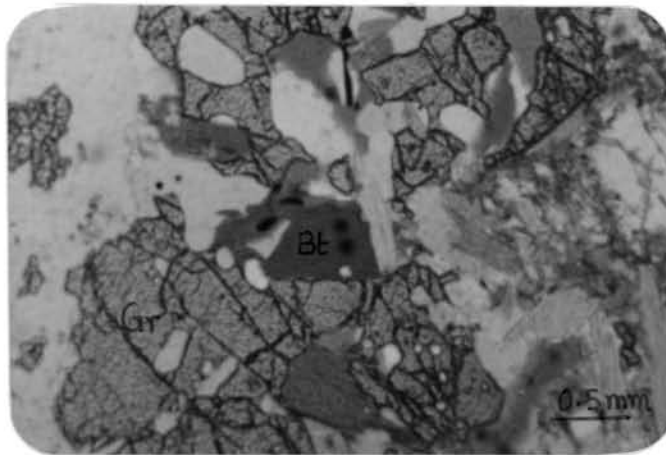


Fig. 82



structures are noticed in a few sections. Matrix biotite has a TiO_2 content of 3.52-3.73 (wt %) and comparatively low X_{Mg} ratio (0.45-0.47). Average compositional shift to phlogopite is observed from matrix to garnet-biotite contact zones (Ref.Chapter.V, Fig.117 a & b). Temperature determinations fixes the garnet (core)- matrix biotite temperature at 784°C and garnet (rim)-biotite (inclusion) temperature at 527°C for a pressure of 8 kbar (also see chapter.VI).

Plagioclase occurs as euhedral to subhedral phenocrysts showing well-developed polysynthetic twinning. Sometimes, it is seen corroding biotite flakes. Extensive development of sericite is also observed.

Garnet occurs as subhedral crystals showing medium to coarse grain size (see Fig.82). First order colours and multiple fractures are frequently observed. Inclusions of a host of minerals such as plagioclase, biotite etc., are also observed. Microprobe analyses (see Table.14, Chapter.V) show garnet rims slightly enriched in Ti (by 0.02 mol %) and compositionally correspond to almandine (73-75 mol %).

Muscovite development is limited to plagioclase-quartz interface.

CHAPTER IV

GEOCHEMISTRY AND PETROGENESIS

Geochemical analyses for major and trace elements of khondalites and associated gneisses, calc granulites, crystalline limestones, migmatitic gneisses, amphibolites, granites and pegmatites were undertaken by wet chemical as well as XRF methods and the results have been processed for protolith characterisation of the rocks. (Analytical techniques and precision are discussed in Appendix I a & b).

IV.1.a KHONDALITE

Results of whole - rock analyses of 10 samples of khondalite (*sensu stricto*) and associated sillimanite -absent and cordierite - bearing gneisses, show a wide variation in SiO_2 values from 46 to 66 wt% (Table.4). In sillimanite - bearing samples, Al_2O_3 , FeO and Fe_2O_3 tend to exhibit average values of 14.54, 6.02 and 3.12 wt% respectively, while the corresponding values in sillimanite - absent assemblages are 14.18, 5.84 and 2.62 wt%. The former is also characterised by relatively lower CaO (2.24 wt%) and Na_2O (1.11 %), as compared to the sillimanite - free types (3.28 and 2.19 wt% respectively). Cordierite - bearing sample (Ps.149), exhibits a very low proportion of SiO_2 (46.36 wt%) while, FeO and Fe_2O_3 are 8.68 and 1.29 wt% respectively. CaO is very low (0.68 wt%) and Na_2O value is still lower at 0.33 wt%. However, the sample shows a very high Al_2O_3 value (38.56 wt%).

TABLE.4 RESULTS OF MAJOR ELEMENT ANALYSES OF KHONDALITES

No.	PS.13	PS.14a	PS.14b	PS.16*	PS.37	PS.125*	PS.149**	PS.25*	PS.112	PS.142
Elements										
SiO ₂	59.94	59.14	65.12	65.48	61.4	65.91	46.36	61.98	61.8	62.34
Al ₂ O ₃	15.29	15.29	13.26	12.93	13.77	16.72	38.56	14.43	14.25	13.87
FeO	2.99	2.59	2.87	3.66	2.87	3.79	1.29	2.47	2.27	3.12
Fe ₂ O ₃	6.21	7.22	5.60	6.32	5.46	5.29	8.00	5.96	5.82	5.73
CaO	2.02	2.47	2.24	2.92	3.11	0.67	0.68	3.59	3.12	3.14
MgO	2.58	3.06	2.58	1.93	2.74	2.52	3.00	2.26	2.90	2.56
Na ₂ O	0.63	1.59	1.40	0.59	1.83	0.63	0.33	2.43	2.13	2.02
K ₂ O	5.25	4.75	2.79	2.31	3.9	1.66	0.02	4.34	4.17	4.31
TiO	1.49	1.50	1.45	1.47	1.55	1.09	0.27	0.99	0.80	0.46
MnO	0.05	0.07	0.04	0.06	0.04	0.13	0.07	0.07	0.08	0.08
P ₂ O ₅	0.25	0.28	0.23	0.17	0.52	0.09	0.03	0.43	0.33	0.15
S	0.06	0.05	0.08	0.61	0.08	0.09	0.00	0.00	0.00	0.00
Moi	0.16	0.16	0.07	0.21	0.24	0.00	0.03	0.15	0.71	0.27
Loi	1.97	1.07	1.23	0.08	1.18	0.90	0.43	1.07	0.99	0.99
CaO/Mgo	0.78	0.81	0.87	1.51	1.13	0.27	0.23	1.58	1.08	1.23
Niggli Parameters										
al	34.00	31.21	34.57	32.04	30.53	42.08	62.14	31.82	30.55	29.94
fm	42.83	43.76	40.88	46.17	40.86	47.68	34.97	36.39	40.06	40.44
c	8.18	9.18	10.64	13.17	12.55	3.08	1.99	13.63	12.18	12.35
alk	14.98	15.84	13.91	8.62	16.06	7.16	0.90	18.16	17.21	17.28
k	0.85	0.66	0.57	0.72	0.59	0.63	0.04	0.54	0.56	0.58
mg	0.34	0.36	0.26	0.26	0.38	0.34	0.35	0.33	0.40	0.35
A	36.07	29.47	38.53	38.57	30.32	51.92	63.81	28.33	28.63	27.72
C	10.63	12.29	13.95	15.74	16.03	3.11	3.22	21.74	21.18	20.18
F	53.31	58.23	47.52	45.69	53.65	44.97	32.96	49.93	50.19	52.10
A	18.71	11.51	20.35	20.08	4.31	44.29	64.18	0.05	2.91	0.73
K	21.91	19.57	16.03	12.17	21.30	6.32	0.04	24.74	24.44	23.91
F	59.38	68.91	63.63	67.75	74.38	49.32	35.78	75.19	72.65	75.36

* Sillimanite absent varieties ** Cordierite-bearing varieties

Average values of CaO/MgO ratios for the sillimanite-bearing and - absent types are 0.90 and 1.30 respectively, while that of cordierite - bearing gneiss is 0.22. On the whole, these samples correspond to the petrochemical type of Al-rich series, with $Al_2O_3 / [3(K_2O) + Na_2O + (FeO + MgO)/2]$ values greater than 1 (Long Kang and Zhendong, 1988).

Chromium and nickel of khondalite samples (*sensu stricto*) are high (Table.5), showing a range from 107 to 178 and 68 to 148 ppm respectively. In sillimanite - absent assemblages, these values are respectively 175 and 189 ppm and in cordierite - bearing samples, they assume values of 125 ppm and 40 ppm. The average Cr values reported for shales and sandstones (90-400 ppm; Krauskopf, 1955; Turekian & Wedepohl, 1961) as well as for granulite facies rocks of sedimentary origin (115 ppm; Drury, 1973) are also in the same range [90-400 ppm (Krauskopf, 1955; Turekian & Wedepohl, 1961) and 115 ppm (mean) resp.]. Sr exhibits a range from 13-126 ppm in sillimanite -bearing assemblages and 114-156 ppm in sillimanite - absent assemblages. In cordierite-bearing assemblages, it is reduced to 11 ppm. The overall range of Sr exhibited by the samples is in general, consistent with the range reported (37-210 ppm) for sandstones (Gebauer & Grunfelder, 1974; Peterman et al, 1967) but, is lower than that of pelites (416), as reported by Shaw (1956) or the mean value (543 ppm) reported for granulites (Sighinolfi, 1970; in Wedepohl, 1969). Ba

TABLE.5 RESULTS OF TRACE ELEMENT ANALYSES OF KHONDALITES

No.	PS.13	PS.14a	PS.14b	PS.16	PS.37	PS.125	PS.149	PS.25	PS.112	PS.142
Rb	116	77	71	52	86	36	14	83	106	18
Sr	63	126	55	13	111	18	11	114	131	156
Ba	552	914	228	214	464	179	18	1330	947	845
Cr	148	178	159	107	142	137	125	110	125	292
Ni	148	136	134	96	76	68	40	79	187	300
Co	48	51	47	45	39	35	83	43	42	125
Pb	67	85	72	43	58	38	292	43	83	125
Cu	152	268	230	235	98	88	94	149	22	34
Zn	290	178	171	151	176	143	58	147	35	98
Li	---	---	---	---	---	---	69	---	15	15
K/Rb	376	512	326	369	376	383	12	434	327	303
K/Sr	692	313	421	147	292	765	15	316	264	229
K/Ba	79	43	102	90	70	72	9	27	37	42
Rb/Sr	1.84	0.61	1.29	4	0.77	2	1.27	0.73	0.81	0.76
Ba/Rb	4.76	11.87	3.21	4.12	5.4	4.97	1.29	16.02	8.93	7.16
Ba/Sr	8.76	7.25	4.15	16.46	4.18	1.64	9.94	11.67	7.23	5.42

proportion in the first two varieties range from 179-914 and 845-1330, comparable to the (420-1090) range of the Australian shield granulites (Heier, 1968; in Wedepohl, 1969). K/Rb ratios in sillimanite - bearing assemblages range from 326 to 512, while the corresponding value in sillimanite - absent types is 355 (av), similar to the range of K/Rb values of shales (20-663) reported by Heier & Adams (1964). K/Ba mean values are relatively low at 76 and 35, respectively for the two types. Rb/Sr and Ba/Sr ratios average around 1.75 and 7.07 in the former while, in the sillimanite - absent varieties, they attain mean values of 0.77 and 8.11 respectively.

Ba/Rb mean values are 5.72 for the sillimanite - bearing type and 10.70 for the sillimanite - absent type. Corresponding values of K/Rb, K/Ba, Rb/Sr, Ba/Sr and Ba/Rb for the cordierite - bearing assemblages are 12, 9, 1.27, 9.94 and 1.29.

Inter-element plots of FeO, MgO show a well-defined positive correlation with respect to Al₂O₃ while, K₂O and TiO₂ yield rather scattered plots. With respect to silica, these are negatively correlated (Fig.83 a & b). Chromium, cobalt and nickel concentrations show sympathetic variations (see Table.5) but do not correlate with major elements like Mg. Values of Cu and Zn also show significant positive correlation with each other (see Table.5). Strontium increases with increase in CaO (Fig.84a). Rubidium vary

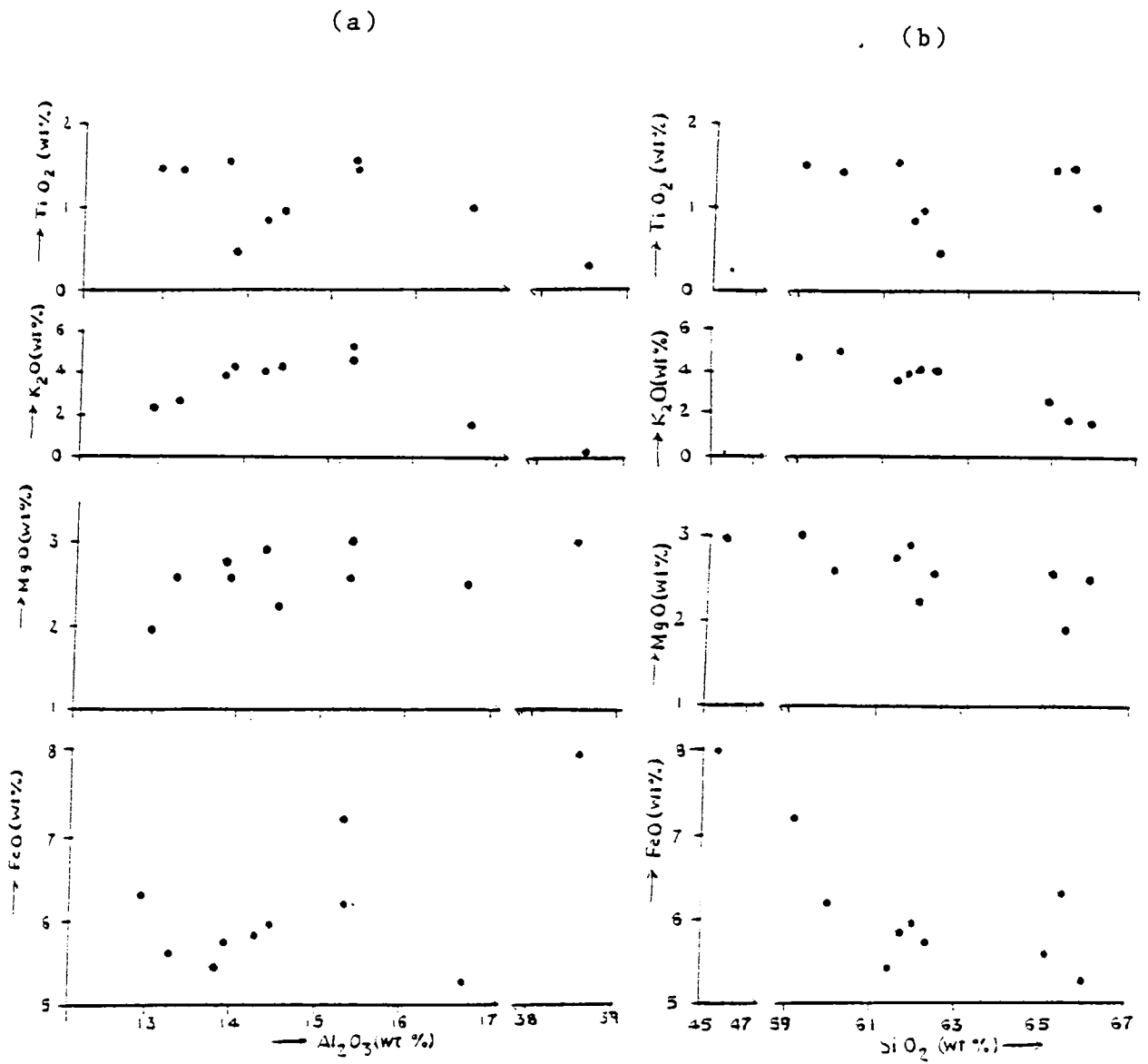


Fig.83 Inter-elemental plots of khondalites with respect to (a) Al₂O₃ and (b) SiO₂.

sympathetically with K wt% while, K/Rb shows almost a linear trend (Fig.84 b & c), contrary to the granulite trend (Sighinolfi, 1969; 1971; Lewis & Spooner, 1973; Field & Clough, 1976).

Relatively low SiO₂, high Al₂O₃ and MgO contents greater than or equal to CaO of some samples, point to a pelitic composition, while higher SiO₂, lower Al₂O₃ and MgO more or less equal to CaO, of the rest of the samples indicate an arenite parentage. In order to provide explanation for the observed wide variations in SiO₂ contents and CaO/MgO ratios of khondalite samples, results have also been represented in the (CaO/MgO) x 100 Vs. SiO₂ diagram of Maccarrone et al (1982). In this diagram (Fig.85), they fall mostly in and around the field comprising shales (from platform and geosynclines), pelagic clays (Wedepohl, 1969); average shales of Pettijohn, (1975); and average pelitic rocks of shaw, (1956). Plots of samples in the (Fe₂O₃^t + MgO) - Na₂O - K₂O ternary diagram (Fig.86) of Blatt et al (1972), are largely spread over the field of exogeosynclinal sediments. MG - denotes average metagreywacke of Fig.Tree Group, GR - average greywacke of Dharwar greenstone belts (Naqvi & Hussain, 1973), G - average greywacke of Pettijohn (1963), A-average arkose of Pettijohn (1963) and the closed area represents the field for greywacke, after Marston (1978). Average lithic arenite is represented as LA.

Graphical representation of bulk composition of the

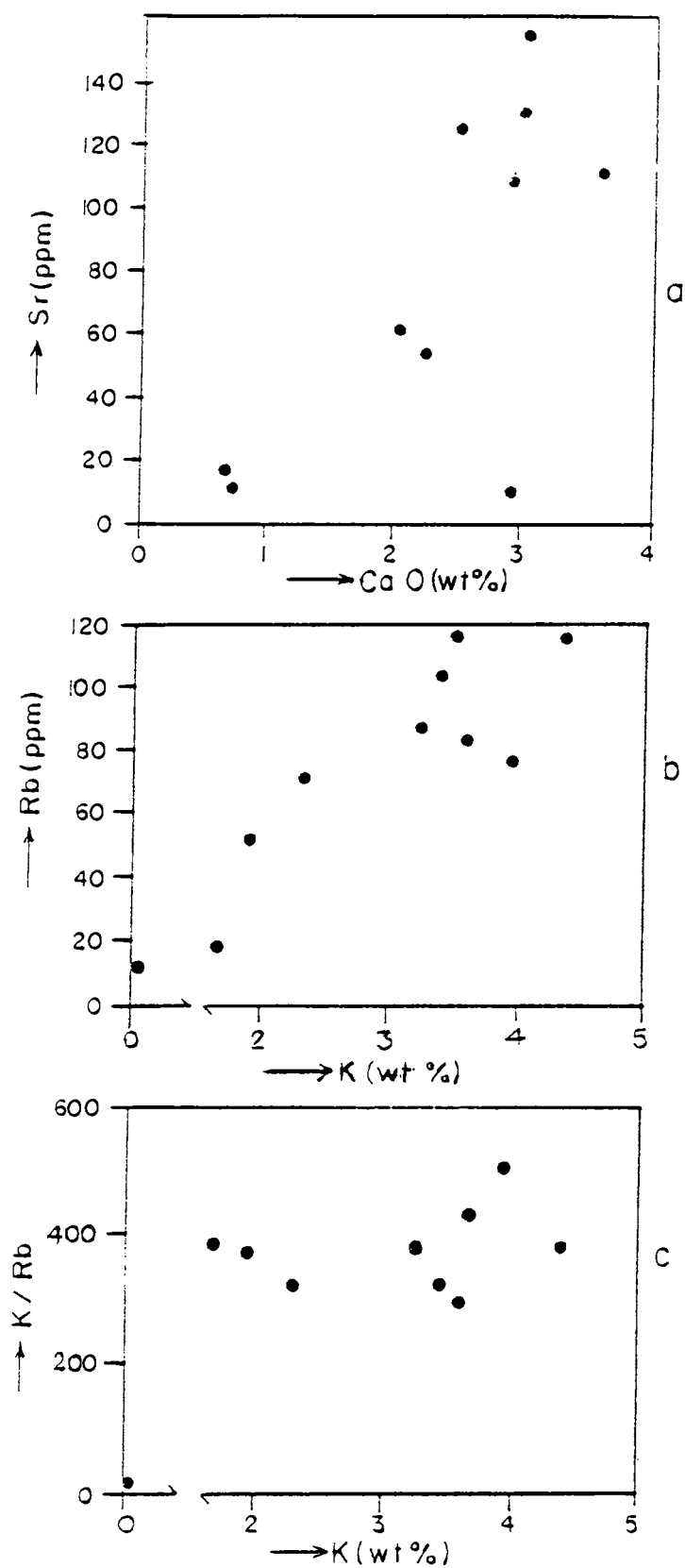


Fig.84 Plots of (a) CaO (wt%) Vs. Sr (ppm) (b) Rb (ppm) Vs. K(wt%) and (c) K/Rb Vs. K(wt%) in khondalites.

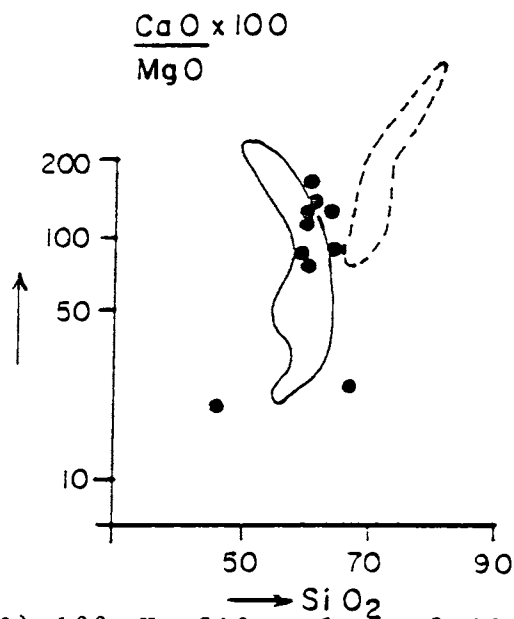


Fig.85 $(\text{CaO}/\text{MgO}) \times 100$ Vs. SiO_2 plot of khondalites & associated gneisses. The dashed line contours the field of greywackes & sandstones. The unbroken line contours the field of shales, pelagic clays & pelitic rocks.

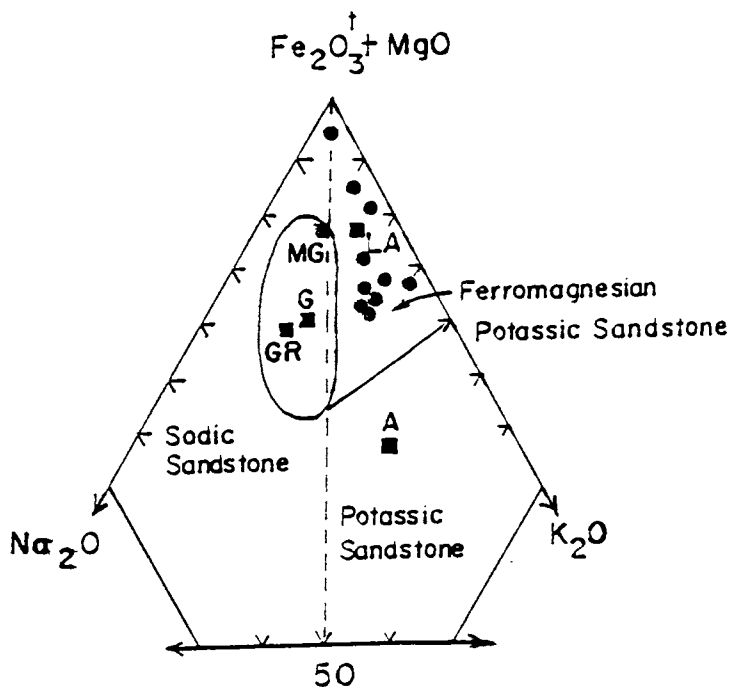


Fig.86 $\text{Na}_2\text{O}-\text{K}_2\text{O}-(\text{Fe}_2\text{O}_3^t + \text{MgO})$ diagram (Blatt et al, 1972) showing plots of khondalites and associated gneisses. For explanation see text.

khondalites in the ACF and A'KF diagrams (Fig.87 a & b), indicates an expected parageneses of Cordierite + Anorthite + Almandine + Sillimanite + Biotite + some Muscovite + Quartz. Sillimanite - absent assemblages plot close to the biotite field in the A'KF diagram while, staurolite makes an additional appearance in the cordierite - bearing assemblages. In the Niggli al-alk-c-fm tetrahedron, most of the plots fall in the field of argillaceous sediments (Fig.88).

IV.1.b PETROGENESIS

Comparison of bulk rock chemical composition of khondalite samples broadly correspond to the average pelitic rock composition of Shaw (1956) and Connemara Pelites of Western Ireland (Senior & Leake, 1978), except for the slightly lower Al_2O_3 and slightly higher CaO contents. Trace element concentration levels of Ba, Cr and Ni in these rocks are also broadly comparable (ref Table.6). Cordierite - bearing sample however, shows no comparison with any of the sedimentary rocks, and is assumed to have experienced chemical changes such as an increase in value of Al_2O_3 (as high as 38 wt%) and a lowering in SiO_2 (as low as 46 wt%) as well as in the alkali contents. High ratios of $Al_2O_3/[3K_2O + Na_2O + CaO + (FeO + MgO)/2]$ indicate an Al - rich petrochemical variety possibly, kaolinitic pelites (Long Kang and Zhendong, 1988). Distinct to indistinct positive correlations of FeO, MgO, K_2O and TiO_2 , with Al_2O_3 and their

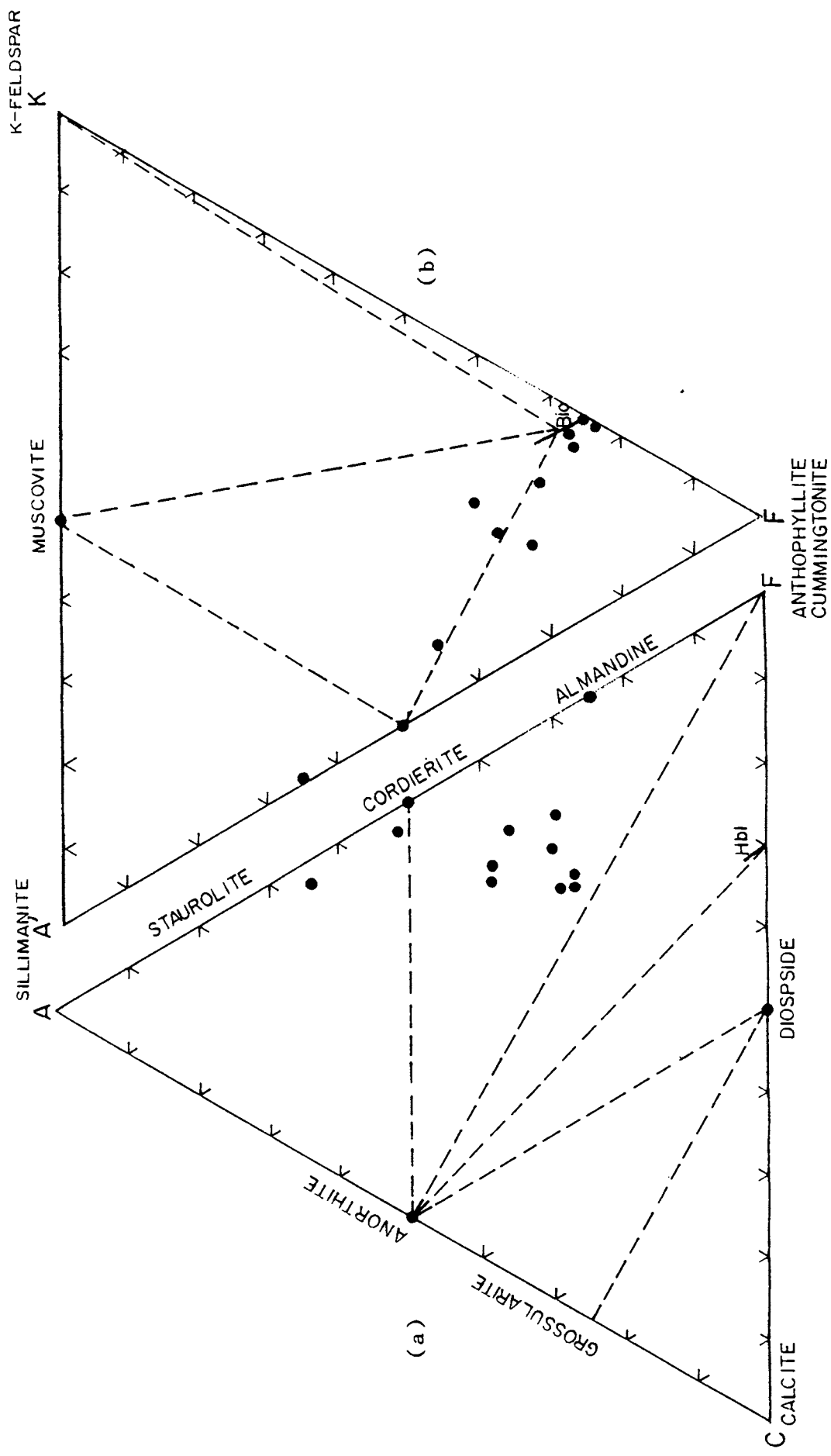


Fig. 87 Chemical compositions of khondalites and associated gneisses plotted in ACF and A'KF diagrams.

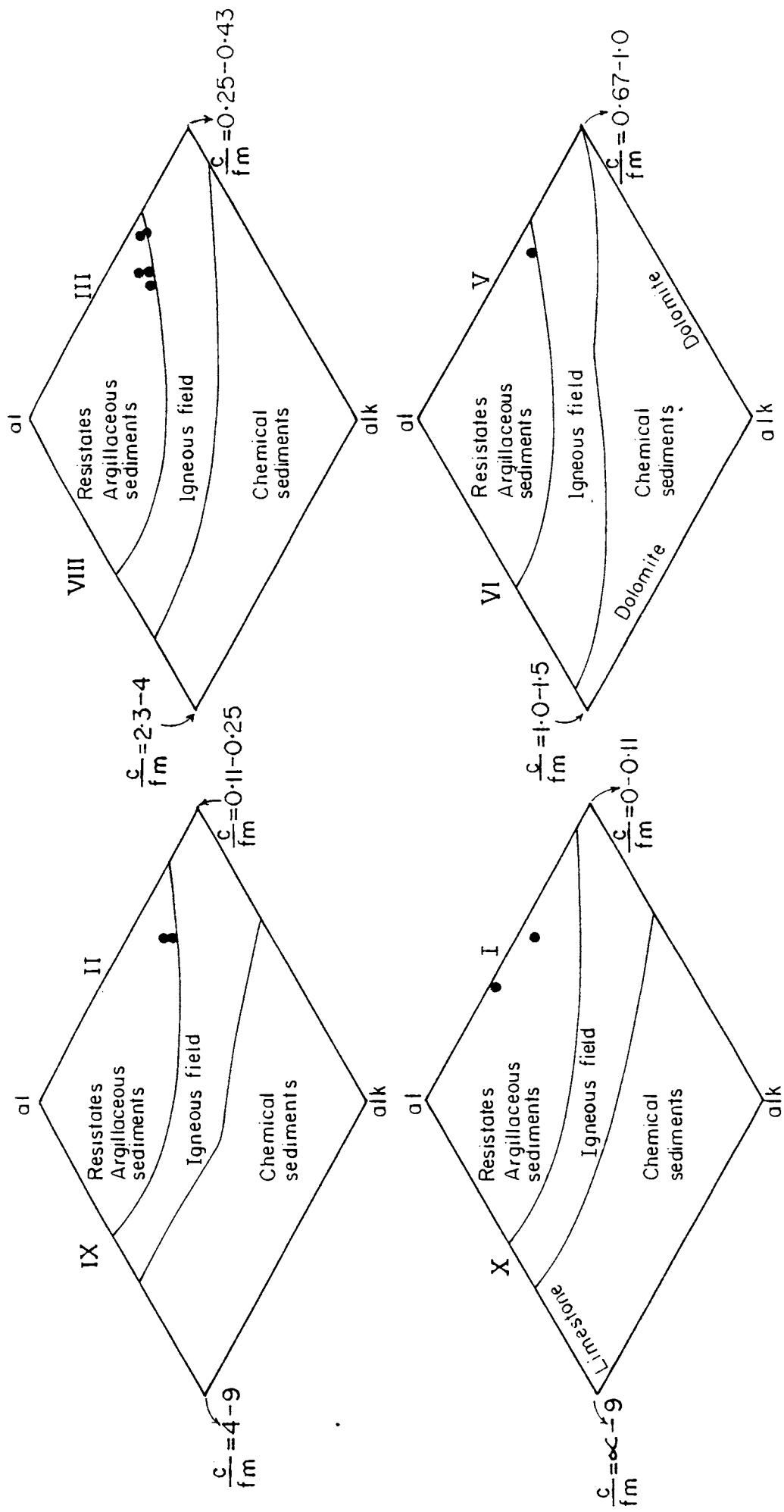


Fig. 88 Plots of khondalites and associated gneisses in the Niggli al-alk-c-fm tetrahedron.

TABLE.6 COMPOSITION OF KHONDALITES (WITH THE EXCEPTION
CORDIERITE-BEARING GNEISS) COMPARED TO
UNMETAMORPHOSED SEDIMENTARY ROCKS.

ELEMENTS	Khondalites av. 9	Graywacke av. 190*	Pelitic rocks av. 155:Shaw, 1956	Pelitic rocks av. 85:Senior & Leake, 1978
SiO ₂	62.67	68.6	61.54	55.39
TiO ₂	1.20	0.7	0.82	1.18
Al ₂ O ₃	14.42	13.4	16.95	20.75
Fe ₂ O ₃	2.87	5.2	2.56	2.69
FeO	5.97	--	3.90	6.52
MnO	0.07	--	--	0.15
MgO	2.67	2.1	2.52	2.90
CaO	2.59	2.0	1.76	1.36
Na ₂ O	1.47	3.0	1.84	1.82
K ₂ O	3.72	2.0	3.45	3.64
P ₂ O ₅	0.27	--	--	0.25
Loi	1.05	--	--	--
Rb	71.67	8.8		160.00
Sr	87.44	145.2		196.00
Ba		114.8		781.00
Cr		30.9		102.00
Ni		25.7		86.00
Co		6.2		31.00

* The mean of trace elements in graywacke is based on 119 samples of Rensselaer graywackes (Data from:Walton, 1955: Ondrick, 1968 Ondrick&Griffiths, 1969:Helmod, 1952:Huchenholz, 1959:Mattiati, 1960:Caporaletti&Pellizzer, 1967:Rivalenti &Sighinoifi, 1969.....in Maccarrone et al 1983.

negative correlations with SiO_2 , are typical of pelitic rocks. Trace element values are also comparable with the reported range for sediments and granulitic rocks. In the $(\text{CaO}/\text{MgO}) \times 100$ Vs. SiO_2 diagram (see Fig.85), plots of khondalites fall inside the shale - pelite field (unbroken line), as well as close to the greywacke + arenite (dashed line) field. Compositional plots in the $(\text{Fe}_2\text{O}_3^t + \text{MgO}) - \text{Na}_2\text{O} - \text{K}_2\text{O}$ diagram of Blatt et al, (1972) fall outside the fields of greywackes and arkose of Pettijohn (1963). They mostly spread out in the fields of ferromagnesian pottassic sandstone and lithic arenites. Chemical compositions plotted in ACF and A'KF diagrams correspond to a composition of clays and shales, either free of carbonate or containing upto 35 percentage carbonate (Winkler, 1979, pp.45). Thus, an argillaceous sedimentary parentage can be suggested for the rocks which is also indicated by the plots in the Niggli al-alk-c-fm tetrahedron where, all the plots fall in the field of resistates. The cordierite - bearing assemblages plot closer to the 'al' corner. The 'muscovite - out' reaction ($\text{Muscovite} + \text{Quartz} = \text{K-feldspar} + \text{Sillimanite} + \text{Water}$) along with the occurrence of widespread K-feldspar and sillimanite with excess quartz, indicate a temperature $> 600^\circ\text{C}$ (Winkler, 1979). Cordierite - almandine - Sillimanite + Quartz assemblage with an average bulk ratio of $\text{FeO}/(\text{FeO} + \text{MgO})$ of 0.68 is indicative of a temperature of 800°C and a pressure range between 4 and 6 Kbars (Winkler, 1979; pp.235). Greyish to yellow colour of sillimanite crystals is also

characteristic of its high - grade metamorphic origin (Rossman et al, 1982). Lack of well-developed pyramidal faces in zircons could be suggestive of a dry environment. Microtextural evidences of sillimanite growth around garnet may speak in favour of an isothermal depression P-T path, while the rimming of garnet by biotite in sillimanite - bearing assemblages could be the result of continuation of retrograde P-T path. The eventual stabilization of biotite - sillimanite with cooling, might suggest a transition from the ITD into an essentially IBC path, associated with a progressive uplift of the relatively dry crustal rocks (see Chapter.VI).

IV.2.a CALC GRANULITE

Whole rock analyses of calc granulite samples (Table.7 a & b) substantiate the petrographic subdivision of calc granulites into two groups namely, type I (K-feldspar + Calcite + Vesuvianite + Scapolite + Diopside + Grossularite + Sphene) and type II (K-feldspar + Calcite + Vesuvianite + Scapolite + Diopside + Sphene).

A predominance of K_2O (2.87 wt%) over Na_2O (1.76 wt%) is prevalent in type I varieties while, the reverse holds true for type II varieties, with Na_2O (2.51 wt%) predominating over K_2O (1.97 wt%). The former also shows slightly higher concentrations (av.wt%) of Fe_2O_3 (5.38), CaO (11.94), TiO_2 (0.79) and MnO (0.28), compared to the corresponding values of average 5.10, 11.79, 0.74 and 0.27

wt % of type II varieties. Oxidation ratios ($2\text{Fe}_2\text{O}_3 \times 100 / (2\text{Fe}_2\text{O}_3 + \text{FeO})$) for type I are higher (av.61.79) than that of type II varieties (av.55.53). Mol. percent Mg values (av.52.41) of type I however, are lower than that of type II varieties (av.58.17). Concentrations of Rb (109 ppm), Ba (1918 ppm), Zn (125 ppm), Cr (149 ppm), Ni (311 ppm), Sr (212 ppm), Co (56 ppm), Pb (45 ppm) and Cu (46 ppm) are also higher in the former, compared to their corresponding values of 47, 1003, 88, 79, 89, 176, 47, 24 and 18 ppm (Table.7) in type II.

Inter-element plots with respect to Al_2O_3 , TiO_2 and the Niggli parameter al-alk (Fig.89 a & b; 90;91) show that, the calc granulites form a distinct cluster away from the marbles. Compared to marbles, they exhibit less distinct trends with Al_2O_3 (Fig.89a). CaO and K_2O show a slight depletion while, $(\text{Na}_2\text{O} + \text{K}_2\text{O})$ shows slight enrichment trends. SiO_2 exhibits almost a linear trend, whereas a marked increase is noticed in TiO_2 and Na_2O values.

With Al_2O_3 , rubidium and chromium show a not-so-well-defined increasing trend; Zn slightly increases, while Ba and Ni show conspicuous positive trends (Fig.89 b). With respect to TiO_2 (Fig.90) and al-alk parameters (Fig.91), similar trends are discerned for both major and trace elements. Values of Sr Vs. CaO (Fig.92 a) as well as Rb and Ba Vs. K_2O (Fig.92b & c), are also plotted to bring out their positive correlation. Compositional plots of calc granulites have

TABLE.7 a MAJOR AND TRACE ELEMENT ANALYSES AND NIGGLI PARAMETERS OF
CALC-GRANULITES.
(a) Major elements

Elements	Type I			Type II		
	Ps.35	Ps.40	Ps.77	Ps.36	Ps.83	Ps.153
SiO ₂	53.04	55.80	56.53	54.44	50.15	53.93
Al ₂ O ₃	12.75	12.75	13.69	14.27	12.00	17.41
Fe ₂ O ₃	5.62	4.88	5.65	4.62	5.02	4.12
FeO _t	3.84	2.69	2.56	3.38	3.54	2.95
FeO	8.89	7.07	7.65	7.53	8.06	6.51
CaO	12.56	12.79	10.48	13.91	13.72	10.97
MgO	2.10	1.77	1.63	1.61	4.65	--
Na ₂ O	2.08	2.01	1.20	2.67	2.12	2.74
K ₂ O	2.54	2.98	3.10	2.46	1.52	1.94
TiO ₂	0.88	0.79	0.70	0.92	0.60	0.94
MnO	0.31	0.27	0.29	0.25	0.19	0.38
P ₂ O ₅	0.06	0.11	0.09	0.12	0.25	0.15
S	--	--	0.04	--	--	--
Oxd. ratio	56.85	62.02	66.51	55.17	55.73	55.69
Mol % Mg	49.61	54.22	53.40	46.16	70.19	--

All concentrations in Wt%.

TABLE.7 (Contd..) b. TRACE ELEMENTS OF CALC GRANULITES.

Elements	Ps.35	Ps.36	Ps.40	Ps.77	Ps.83
Rb	131	44	85	112	50
Ba	1423	905	1555	2777	1100
Zn	130	98	115	130	77
Cr	174	108	205	68	50
Ni	178	108	204	550	70
Sr	223	176	203	210	--
Co	61	47	50	--	--
Pb	58	24	31	--	--
Cu	45	18	47	--	--

All concentrations in ppm.

TABLE.7 (contd...)

c. NIGGLI PARAMETERS						
	Type II	Type I	Type I	Type II	Type I	Type I
	Ps.36	Ps.35	Ps.40	Ps.83	Ps.153	Ps.77
al	23.09	21.18	22.17	18.29	32.25	25.90
alk	11.43	10.26	11.37	7.83	12.25	10.10
fm	24.49	30.56	25.95	35.81	18.48	27.87
c	40.99	38.01	40.51	38.08	37.01	36.12
mg	0.27	0.29	0.30	0.50	---	0.28
k	0.37	0.45	0.49	0.32	0.32	0.63
si	149.75	149.79	164.77	129.74	169.60	181.87
(al-alk)	11.66	10.92	10.80	10.46	20.00	15.80
al	23.09	21.18	22.17	18.29	32.58	25.90
alk	11.43	10.26	11.37	7.83	12.37	10.10
c+fm	64.48	68.57	66.46	73.89	56.05	63.99
c/fm	1.67	1.24	1.56	1.06	2.00	1.30
A	33.23	32.37	33.13	27.71	99.99	99.99
C	48.91	45.34	48.67	42.93	44.66	42.97
FM	17.86	22.39	18.20	29.37	10.56	19.29
Alk	43.28	35.45	42.88	23.17	58.33	38.38
F	25.17	33.80	27.53	23.79	41.67	31.72
M	31.55	30.75	29.59	53.11	---	29.89

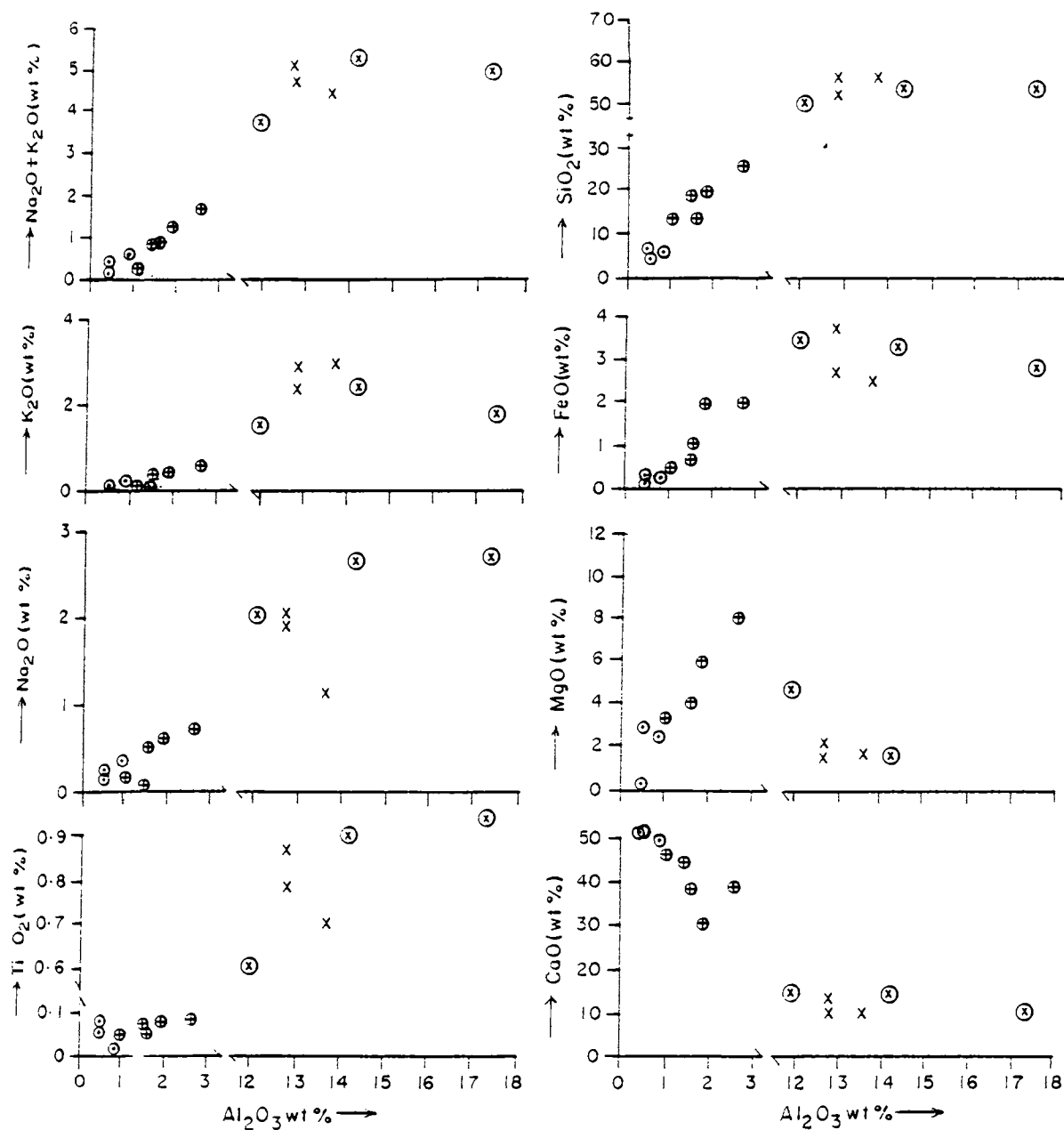


Fig.89 (a)Major element plots of calc-granulites and crystalline limestones Vs. Al_2O_3 . Symbols: x Type I calc-granulite, ⊕ Type II calc-granulite ○ Group I marble and ⊗ group II marble.

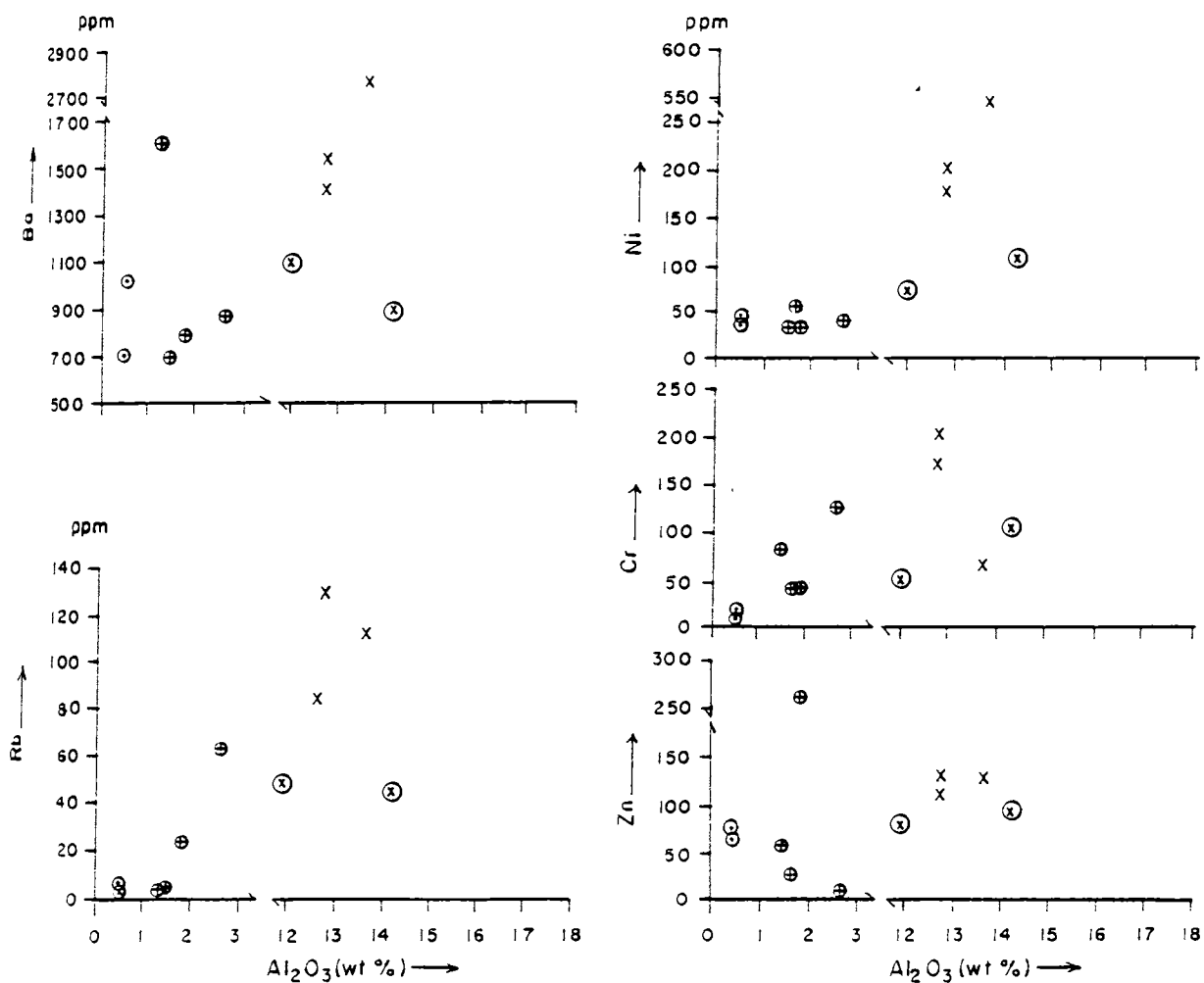


Fig. 89 (b) Trace element plots of calc-granulites and crystalline limestones Vs. Al_2O_3 . Symbols as in Fig. 89 (a).

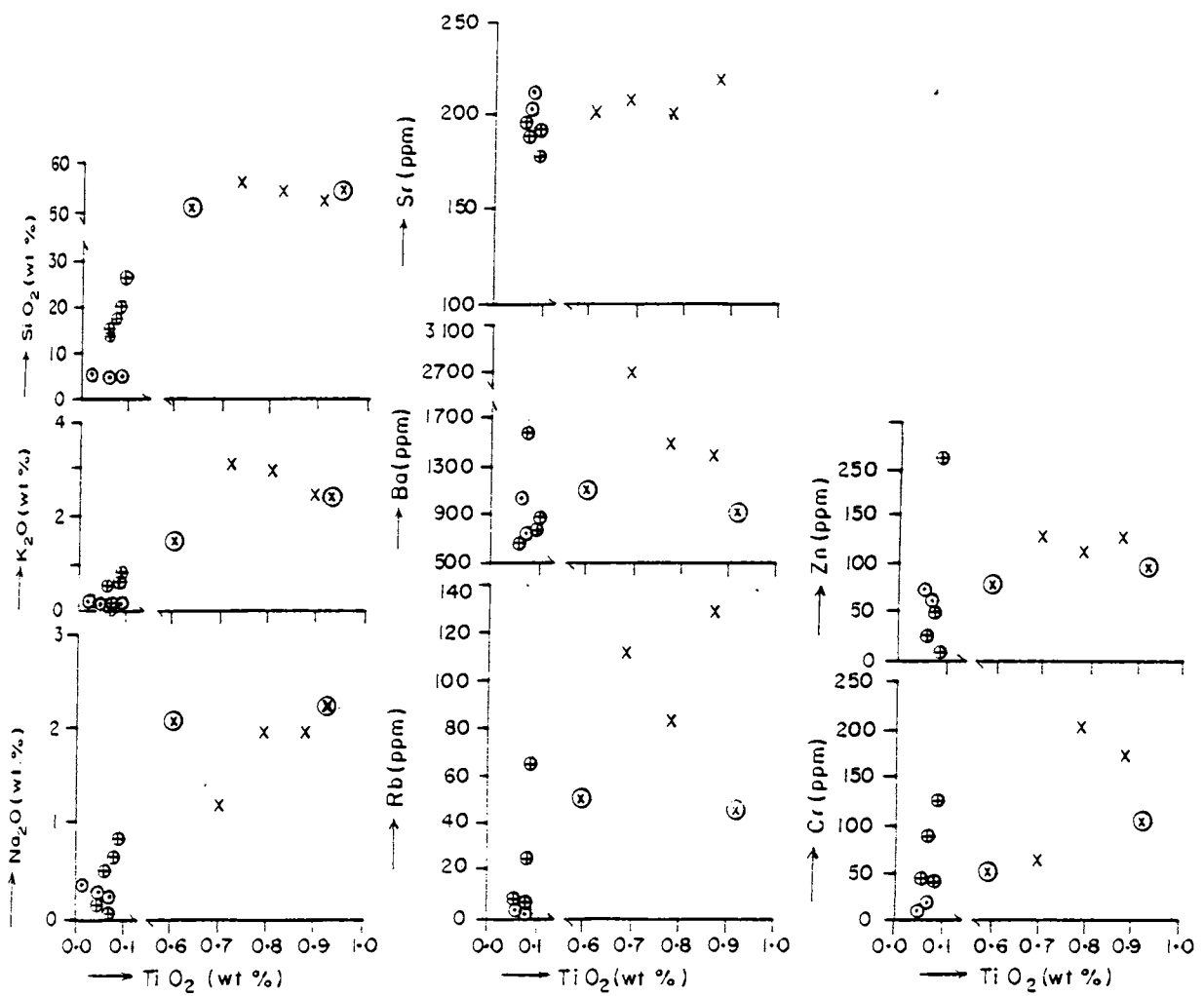


Fig.90 Major and trace element plots of calc-granulites and crystalline limestones Vs. TiO_2 . Symbols as in Fig.89(a).

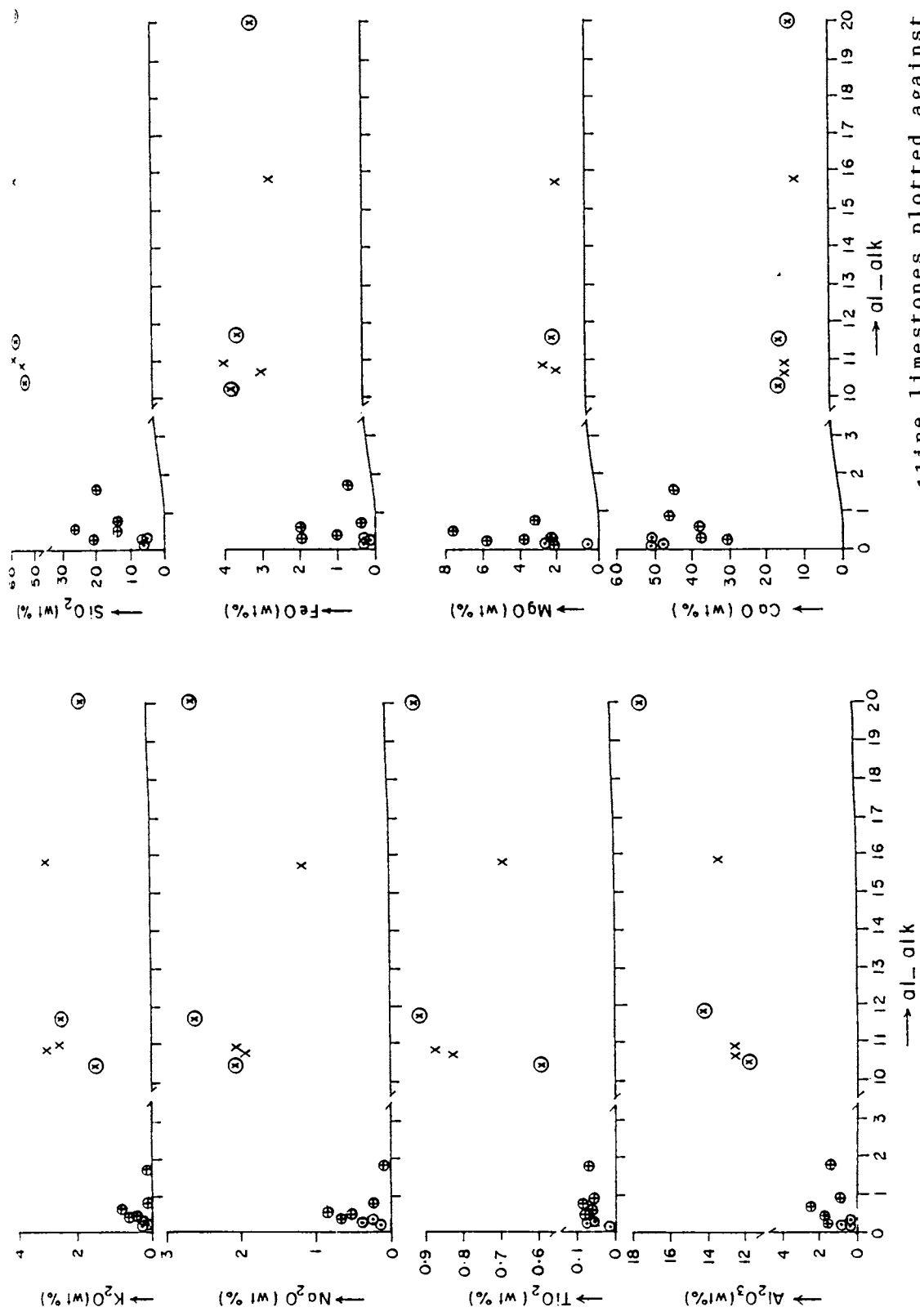


Fig.91 Major elements of calc-granulites and crystalline limestones plotted against Niggli parameter. Symbols as in Fig.89 (a).

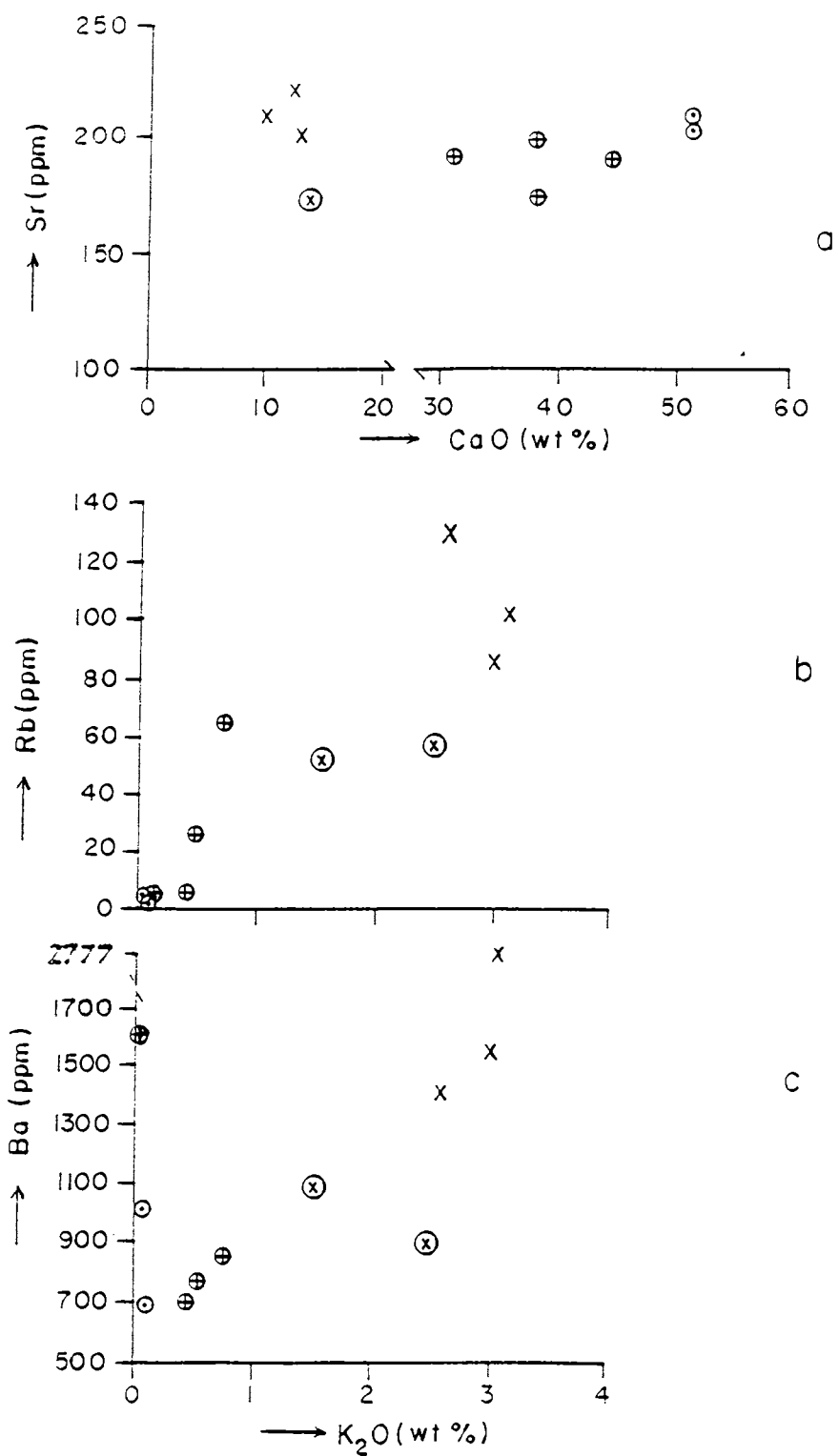


Fig.92 Inter-elemental plots of calc-granulites and crystalline limestones.
(a) Sr (ppm) Vs. CaO (wt%)
(b) Rb (ppm) Vs. K₂O (wt%)
(c) Ba (ppm) Vs. K₂O (wt%)
Symbols as in Fig.89 (a).

also been represented in the ACFM and AlkFM (Fig.93 a & b), al-alk Vs. c diagram (1964), (al-alk) Vs. mg and MgO Vs. CaO diagrams (Fig.94 a,b & c) as well as in Niggli al-fm-c-alk tetrahedron (Fig.95).

IV.2.b PETROGENESIS

Calc granulites are interlayered with khondalites, the overall association reflecting a calcareous sedimentary protolith. Comparison with the compositions of unmetamorphosed sedimentary rocks, as detailed in Table.8, shows that the calc granulites bear a close resemblance to the calcareous shales of Pettijohn (1940), except for the SiO₂ and FeO concentrations. The average wt % of SiO₂ of calc granulites is 53.98, as compared to 48.12 wt % of the calcareous shales. FeO is 7.66 and 4.69, respectively for the two types. Protolith characterisation through the available geochemical data suggests that they have been derived from impure, silica-rich and Fe-poor calcareous sediments similar to the calc granulites of Dharmapuri District (Narayana et al, 1988). Linear arrays obtained by major and trace element plots of calc granulites (Fig.89 to 90) suggests a probable admixture of non-carbonate phases with carbonate, during the deposition of the protolith (Munyanyiwa & Hanson, 1988). Correlation of most of the major and trace elements with Al₂O₃ suggests that an alumina bearing phase, such as clays, detrital micas or feldspars, constituted a major fraction of the material admixed with calcareous sediments. Diffuse to

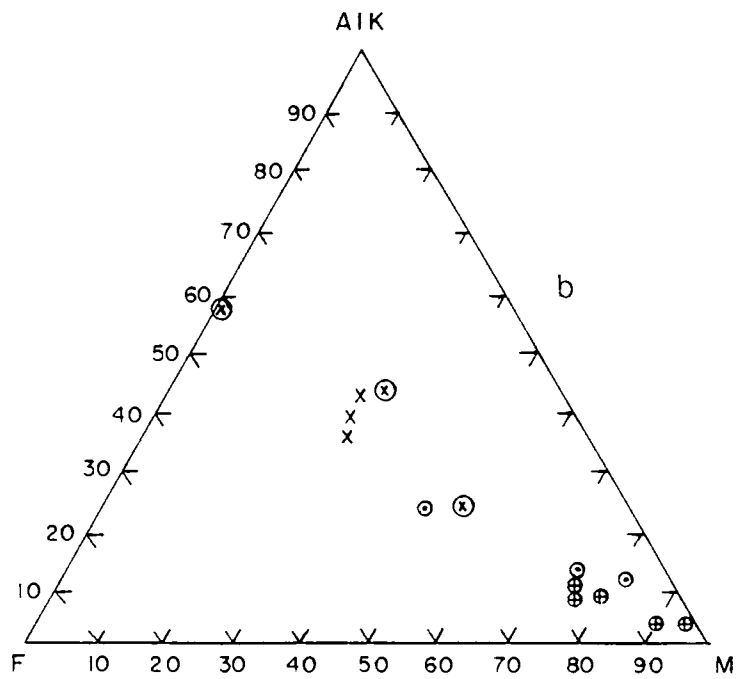
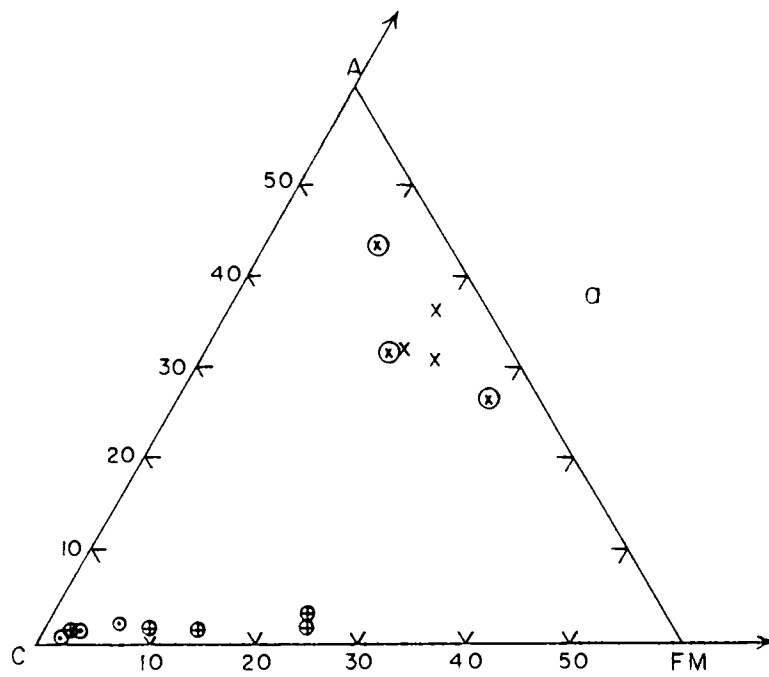


Fig.93 Plots of calc-granulites and crystalline limestones in (a) ACFM and (b) AlkFM diagrams. Symbols as in Fig.89 (a).

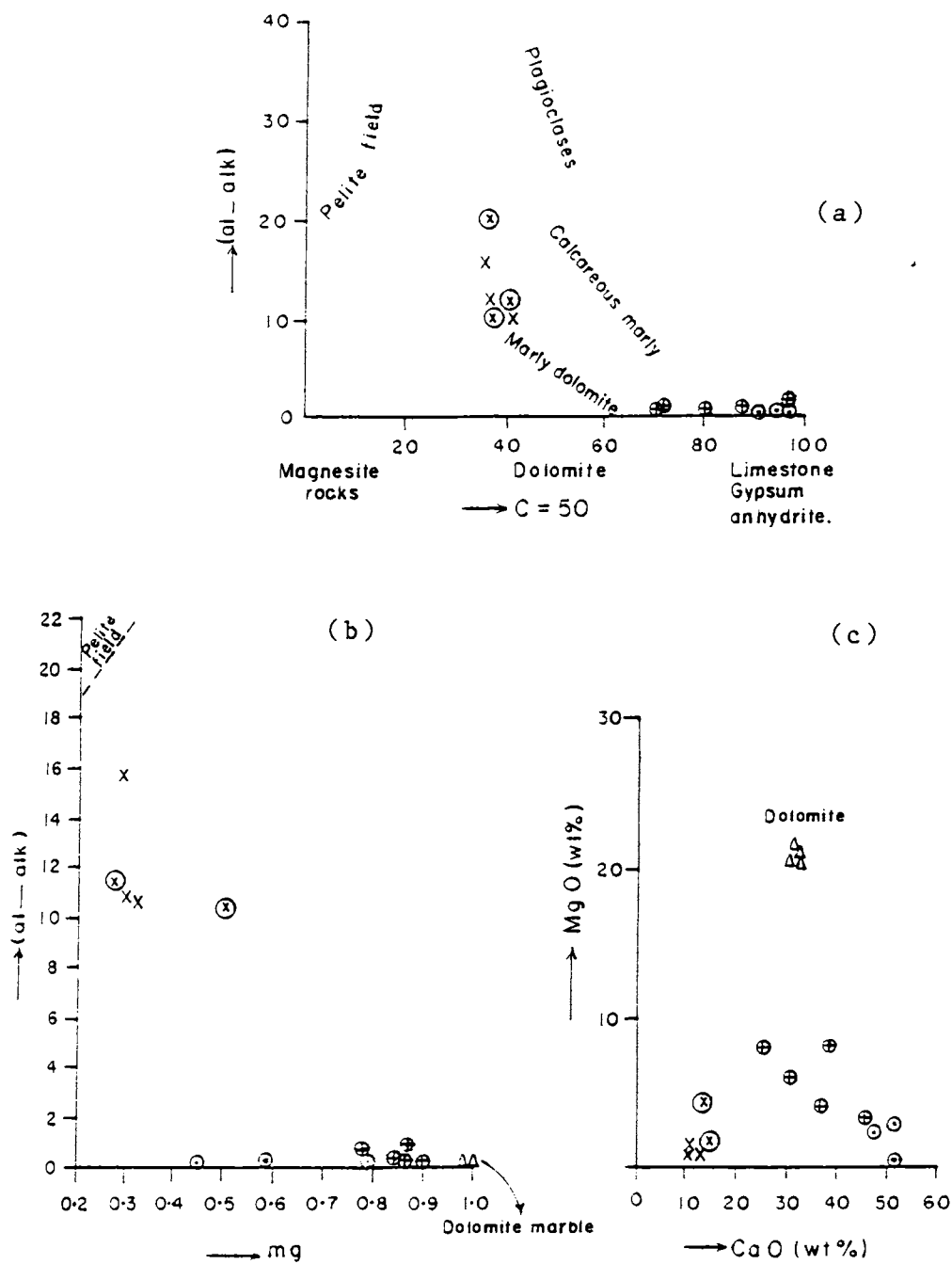


Fig.94 Plots of calc-granulites and crystalline limestones in (a) Niggli (al-alk) Vs. c diagram (Burri,1964) (b) Niggli (al-alk) Vs. mg and (c) MgO Vs. CaO (wt%) diagrams. Pelite field from Van de kamp (1970). Symbols as in Fig.89 (a).

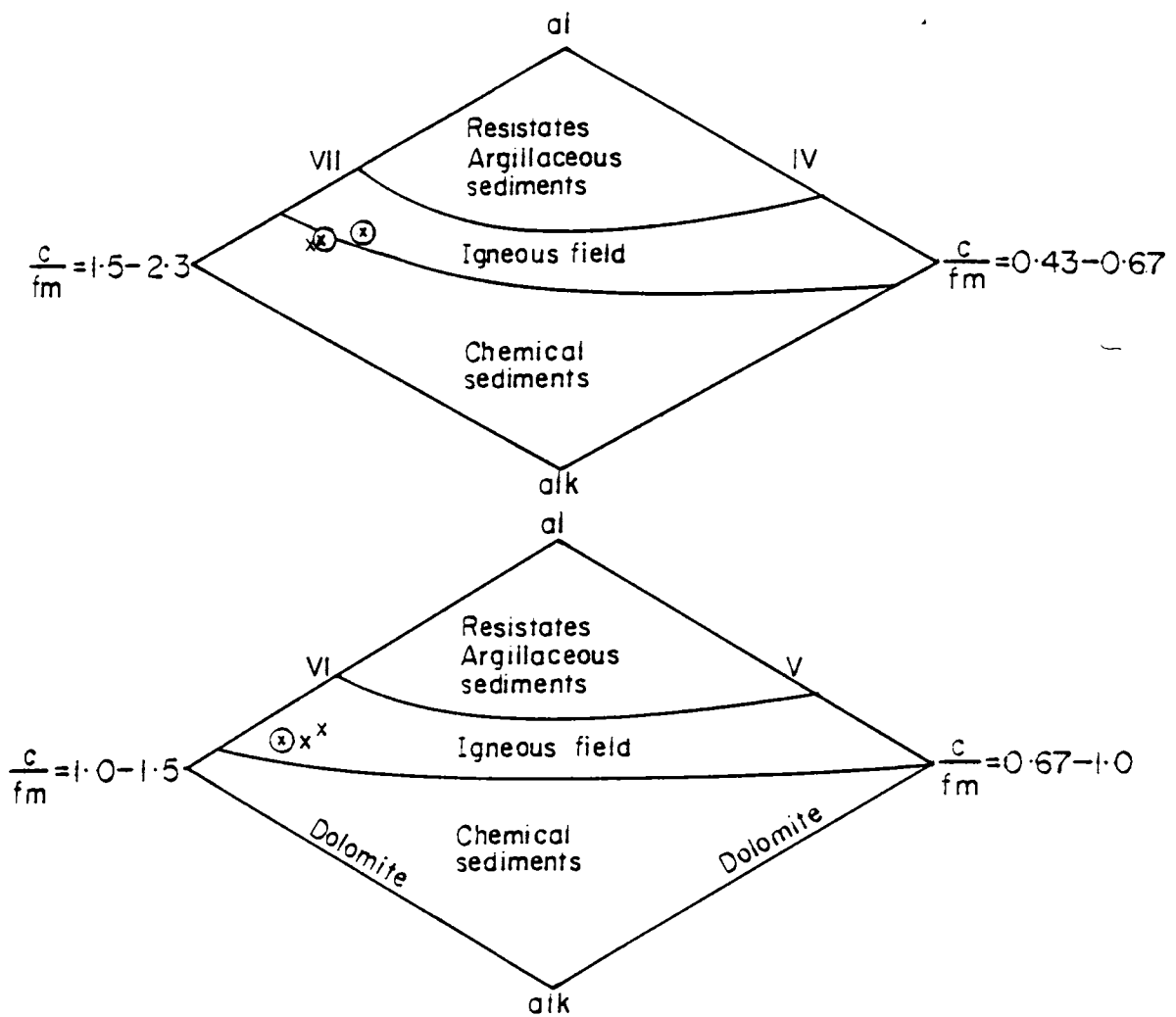


Fig.95 Plots of calc-granulites in the al-alk-c-fm Niggli diagram. Symbols as in Fig.89 (a).

TABLE.8 AVERAGE COMPOSITION OF CALC-GRANULITES AND CRYSTALLINE LIMESTONES COMPARED TO COMPOSITION OF UNMETAMORPHOSED SEDIMENTARY ROCKS

	1	2	3	4	5	6	7	8	9
SiO2	55.12	52.84	5.34	10.50	59.93	1.88	10.61	48.12	
TiO2	0.79	0.74	0.07	0.01	0.85	0.01	0.07	0.78	
Al2O3	13.06	13.32	0.51	0.66	16.62	0.83	4.30	12.80	
FeO*	7.87	7.23	0.94	0.60	5.91	0.26	2.97	4.69	
MnO	0.28	0.27	0.08	0.03	2.63	0.01	0.22	0.09	
MgO	1.83	3.12	0.65	2.80	2.18	2.75	2.01	2.55	
CaO	11.94	11.79	51.15	45.65	1.73	50.89	41.90	10.77	
Na2O	1.76	2.51	0.94	0.02	3.54	0.06	1.38	0.60	
K2O	2.87	2.51	0.06	0.02	-	0.01	0.56	3.60	
P2O5	0.09	0.17	0.1	-	-	0.01	0.21	0.65	
Ba	1294.33			872.50					
Cr	162.33			11.15					
Sr	200.00			208.00					
Rb	86.00			6.55					
Zn	114.33			68.50					
Ni	163.33			42.50					

* Total Fe as FeO; Major elements in wt% and trace elements in ppm
Lst - Limestone.

distinct positive trends of TiO_2 , Zn, Cr and Ni with Al_2O_3 , argues against feldspars being the major aluminium-bearing phase thus, attributing the linear compositional trends to the probable admixture of phyllosilicates and clays. This is well supported by the field relations also. High contents of Ni, Cr, Rb, Ba, Zn, Fe, Ti, Na and K in calc -granulites also substantiate this view, as these elements are typically carried by non-carbonate phases (Sighinolfi, 1974) either as the lattice-forming components of the phyllosilicates or, as in the case of some trace elements, probably absorbed on the clays (Krauskopf, 1979). Compositional plots in the ACFM and AlkFM diagrams show that the calc granulites fall in the intermediate position between A and FM corners of AFM diagram (Fig.93 a) while, in the AlkFM diagram (Fig.93 b), they fall near the high Fe-Mg zones. In the al-alk Vs. c diagram (ref Fig.94 a) of Burri (1964), calc granulites plot close to the pelite field and denote a source of limestone + marly impurities mixture. This view is augmented by the plots of calc granulites in Niggli (al-alk) Vs. mg and MgO Vs. CaO diagrams (Fig.94 b & c). Plots of calc granulites in the al-fm-c-alk tetrahedron of Niggli (see Fig.95) however, fall both in the fields of igneous as well as chemical sediments.

Presence of scapolite, a characteristic mineral of high grade, deep-seated granulite terrains (Knorring & Kennedy, 1958; Lovering & White, 1969) and the reported high temperatures ($800^\circ C$) for the scapolite-plagioclase

assemblages (Goldsmith & Newton, 1977) suggests a high temperature of origin, which is also substantiated by the P-T estimates of the present study (see Chapter.VI). Consistent with the shift of clinopyroxenes to diopsidic-rich compositions, the estimated temperatures drop from 808 to 775°C while, pressures get reduced from 4.39 to 2.20 Kbars. Imprints of this retrogression is manifested in thin sections by the prolific development of post-peak fractures, with attendant mineral alterations. Meionite percentage of 75 in scapolite could also be indicative of a CO₂-rich fluid regime (Srikantappa et al, 1986).

IV.3.a CRYSTALLINE LIMESTONES

Eight whole rock samples of crystalline limestones were analysed for major elements by wet chemical methods. Trace elements were determined by AAS, and cross-checked by XRF method. Results reveal two distinct trends in limestones and accordingly these are designated as Group I and II marbles (Table.9 a & b). The pure marbles (Group I) in general, are silica poor and contain av.6.48 % Al₂O₃ and av.1.90 wt % MgO. Na₂O varies from 0.19 wt % to 0.35 wt % and K₂O, from 0.04 to 0.2 wt % (av.0.11 %). Impure marbles (Group II) have significantly higher quantities of major elements such as SiO₂, Al₂O₃, FeO and MgO (av.19.72, 2.0, 1.68 and 6 wt % resp.,) while, CaO shows a substantial decrease from 47 to 36 wt %. Mol. % of Mg and oxidation ratios averages respectively around 86.55 and 21.56 for Group I while, the

TABLE.9a MAJOR ELEMENTS (WT%) OF CRYSTALLINE LIMESTONE, WALAYAR.

Sample No.	Group I					Group II				
	Ps 27a	Ps 27b	BO	Ps 123b	Ps 152B	Ps.152	W	Ps.133		
Elements										
SiO ₂	5.62	5.06	5.53	20.0	13.02	18.54	13.34	26.14		
Al ₂ O ₃	0.51	0.51	0.90	1.85	1.54	1.46	1.07	2.62		
Fe ₂ O ₃	0.40	1.11	1.25	0.97	0.28	0.12	0.80	0.38		
FeO	0.29	0.22	0.28	2.01	1.01	0.70	0.36	2.03		
FeO	0.65	0.22	1.13	2.88	1.26	0.81	0.72	2.37		
CaO	51.15	51.15	48.16	30.80	37.80	44.44	45.92	38.36		
MgO	0.32	2.97	2.41	6.00	4.00	nd	3.40	8.00		
Na ₂ O	0.19	0.22	0.35	0.63	0.51	0.05	0.20	0.80		
K ₂ O	0.08	0.04	0.20	0.54	0.43	0.03	0.02	0.70		
TiO ₂	0.07	0.06	0.10	0.08	0.06	0.07	0.06	0.09		
MnO	0.08	0.07	0.07	0.17	0.08	0.04	0.02	0.001		
P ₂ O ₅	0.08	0.12	0.02	nd	nd	0.08	nd	nd		
S	nd	nd	nd	nd	nd	0.29	nd	nd		
Oxd.										
ratio 60		82.35	80.06	30.28	19.97	13.37	66.67	14.42		
Mol%										
Mg	66.67	88.89	93.94	84.31	87.70	nd	94.44	87.65		

nd = not detected.

TABLE.9 b. TRACE ELEMENT DATA ON CRYSTALLINE LIMESTONE, MALAYAR.

Sample No.	Group I			Group II		
	Ps-27a	PS-27b	Ps-123b	Ps-152b	PS-152	Ps-133
<u>Minerals</u>						
Rb	2	4	26	6	4	64
Ba	715	1030	780	701	1612	870
Zn	62	75	266	24	54	4
Cr	13	10	42	42	83	125
Ni	45	40	40	50	40	40
Sr	211	205	193	201	190	175
Co	36	31	83	63	31	63
Pb	53	31	83	83	125	83
Cu	45	17	22	19	10	14
Li	--	--	8	2		8

All concentrations in ppm.

corresponding values for Group II are 79.33 and 58.32. Group II marbles have significantly higher amounts of Rb (32 ppm), Zn (98 ppm), Cr (70 ppm), Co (57 ppm) and Pb (83 ppm), compared to values of 3, 69, 13, 33 and 42 ppm of Group I marbles. Sr and Cu occur in lower quantities (184 and 18 ppm resp.,) in Group II marbles while, the values increase to 208 and 31 ppm in Group I marbles.

Inter-element plots with respect to Al_2O_3 (see Fig.89 a), show strong positive correlation for SiO_2 , FeO, MgO and Na_2O ; while CaO exhibits a well defined negative correlation relative to Al_2O_3 . Trace elements like Rb, Ba, Zn, Cr and Ni show only a vague positive trend with respect to Al_2O_3 (see Fig.89 b). Major and trace element data, plotted with respect to TiO_2 (see Fig.90) and al-alk Niggli parameter (Table.9 c), also shows similar trends (see Fig.91). Sr Vs. CaO yields almost a linear trend, whereas Rb and Ba show a positive increase against K_2O (Fig.92 a, b & c).

IV.3.b PETROGENESIS

Comparison of chemical composition of crystalline limestones with that of unmetamorphosed sedimentary rocks (see Table.8) shows that, the Group I and Group II marbles broadly correspond to pure and impure limestones of Pettijohn (1975).

In the ACFM diagram, Group I marbles plot near the 'C' end and the Group II are shifted towards the FM side (see

TABLE.9 (c)

NIGGLI PARAMETERS

Rock Type

CRYSTALLINE LIMESTONES

No:-	Ps.27a	Ps.27b	B03	Ps.95	Ps.152	BC1	W3	Ps.123b	Ps.152b	Ps.133
Parameters										
al	0.53	0.52	0.92	1.17	1.74	2.80	1.12	2.32	1.84	2.66
alk	0.42	0.41	0.82	0.15	0.14	0.25	0.37	2.05	1.50	2.11
fm	1.92	4.26	8.08	1.39	1.44	7.20	10.73	24.78	14.44	24.17
c	97.14	94.81	90.82	97.29	96.68	89.74	87.78	70.84	81.69	71.06
mg	0.44	0.57	0.78	0.25	--	0.78	0.85	0.78	0.84	0.86
k	0.22	0.11	0.27	1.00	0.28	0.34	0.06	0.36	0.35	0.37
si	9.96	8.72	9.67	42.49	37.6	23.93	23.77	42.87	26.40	45.13
al-alk	0.10	0.17	0.11	1.02	1.60	2.55	0.75	0.28	0.34	0.55
c+fm	99.06	99.07	98.27	98.68	98.12	96.94	98.51	95.07	96.66	95.23
c/fm	50.59	22.26	11.24	69.99	67.14	12.46	8.18	2.86	5.66	2.94
A	0.86	1.26	1.77	1.51	1.84	3.62	1.68	3.97	2.09	2.98
C	97.75	95.8	91.69	97.76	96.91	90.68	88.57	72.32	83.65	72.77
FM	1.39	2.94	6.54	0.73	1.26	5.70	9.76	23.72	14.26	24.24
alk	23.14	12.45	11.26	16.76	9.82	4.18	3.67	8.10	9.67	8.19
F	29.56	12.51	1.46	43.84	90.18	0.48	5.63	15.47	11.81	11.35
M	47.30	75.05	87.28	39.4	--	95.35	90.70	76.43	75.52	80.47

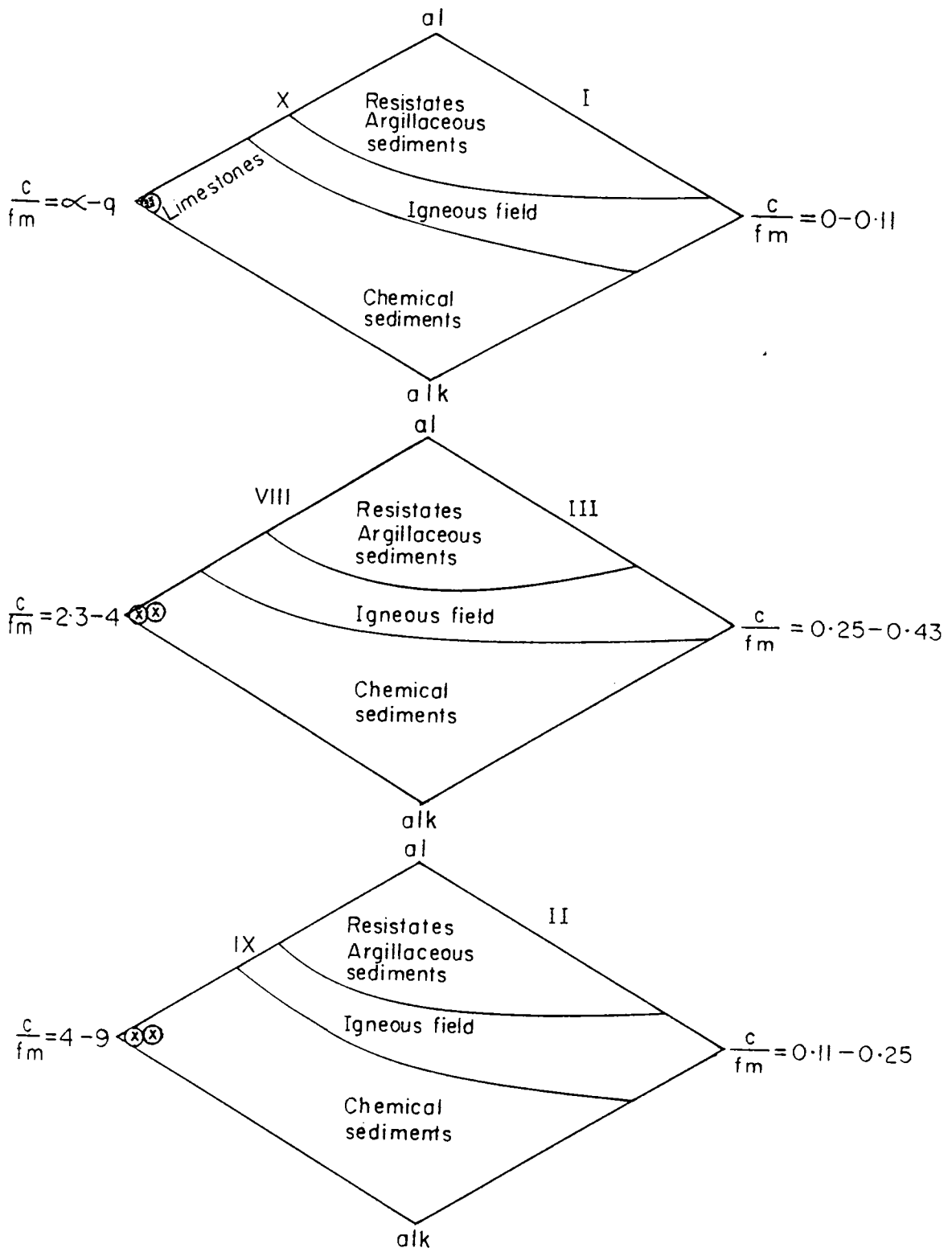


Fig. 96 Plots of crystalline limestones in the al-alk-c-fm Niggli diagram. Symbols as in Fig. 89 (a).

Fig.93 a). In the AlkFM diagram on the other hand, the Group II marbles occupy low alkali and Fe corners (see Fig.93 b). Plots in the al-alk Vs. c diagram (see Fig.94 a) after Burri (1964), implicitly imply an admixture of limestone with variable proportions of marly impurities. Moreover, as evidenced by the Niggli (al-alk) Vs. mg and MgO Vs. CaO diagrams, (see Fig.94 b & c), Group II marbles plot close to ideal dolomite and Group I, away from it. Plots of Group I and Group II marbles in Niggli al-c-fm-alk tetrahedron (see Fig.96) fall invariably in the field of chemical sediments, having implications on the genesis of the limestones.

Thus, based on major and trace elements plotted against Al_2O_3 , TiO_2 and al-alk Niggli parameters and the inter-relationships between elements (see Fig.89 to 92), and as described in the petrogenesis of calc granulites, the crystalline limestone protolith is also assumed to have a substantial alumina-bearing phase. This, as in the case of calc granulites, is suggested to be due to the presence of phyllosilicates admixed with carbonate.

IV.4.a MIGMATITIC GNEISSES

Results of whole rock analyses (Tables.10 a & b) show a spread in SiO_2 values from 54 to 72 wt % while, only a limited variation is exhibited by K_2O (2-5 wt %) and CaO (2-7 wt %). All samples except one (Ps.38c), are characterised by low aluminium (<15% Al_2O_3). Almost all the major

TABLE.10 a RESULTS OF MAJOR AND TRACE ELEMENT ANALYSES OF MIGMATITIC GNEISSES.
(a) Major elements (wt %)

No.	Ps.21	Ps.22	Ps.28	Ps.117	Ps.32	Ps.43	Ps.38c	Ps.131
Elements								
SiO ₂	58.12	61.52	55.90	53.89	71.92	68.76	58.82	63.80
Al ₂ O ₃	14.27	14.27	14.78	15.22	13.26	13.77	15.8	13.89
Fe ₂ O ₃	4.51	3.86	4.26	2.95	1.52	1.68	3.54	3.26
FeO	4.13	3.56	5.35	4.46	0.93	1.65	3.99	3.45
FeO ^t	8.19	7.04	9.19	7.12	2.30	3.16	7.18	6.39
CaO	5.61	4.26	6.73	8.19	2.24	2.92	6.06	3.62
MgO	2.58	2.90	3.71	2.23	0.32	0.64	3.06	2.46
Na ₂ O	4.12	3.84	4.24	3.85	4.07	4.04	4.04	2.42
K ₂ O	4.53	3.73	2.39	3.77	4.55	4.53	2.70	4.08
MnO	0.07	0.05	0.16	0.35	0.02	0.03	0.07	0.09
TiO ₂	1.02	0.73	0.86	0.61	0.29	0.48	0.68	0.70
P ₂ O ₅	0.42	0.20	0.40	0.12	0.05	0.17	0.12	0.28
LOI	0.25	0.35	0.47	2.83	0.25	0.40	0.65	0.54
MOI	0.05	0.07	0.25	0.26	0.10	0.16	0.12	0.16
Na ₂ O/K ₂ O	0.91	1.03	1.77	0.49	0.89	0.89	1.50	0.59

TABLE.10 RESULTS OF MAJOR AND TRACE ELEMENT ANALYSES OF MIGMATITIC GNEISSES
(b) Trace Elements (ppm)

No.	Ps.21	Ps.22	Ps.28	Ps.117	Ps.32	Ps.43	Ps.38c	Ps.131
Elements								
Cu	57	21	140	18	18	20	36	17
Zn	95	67	118	38	25	41	67	25
Rb	85	51	38	52	56	43	49	48
Li	5	6	9	6	11	8	10	5
Pb	47	59	47	55	62	36	54	59
Co	42	40	46	27	22	35	46	45
Ni	94	97	263	63	62	91	73	67
Cr	133	140	322	57	63	94	91	66
Sr	431	396	525	218	160	223	468	193
Ba	918	923	1010	1369	1168	731	863	848
Sr/Ba	0.47	0.43	0.52	0.16	0.14	0.31	0.54	0.23
K/Rb	442	608	521	602	675	874	457	706
Rb/Sr	0.20	0.13	0.07	0.04	0.35	0.19	0.10	0.06
K/Ba	41	34	20	23	32	51	26	40

elements, Al_2O_3 , CaO , FeO^t , TiO_2 and MgO , show depletion trends with SiO_2 with the exception of K_2O , where the trend is markedly positive (Fig.97). Na_2O shows more or less a linear trend. With respect to Al_2O_3 , CaO shows an enrichment trend while, Na_2O maintains almost a linear relationship. K_2O concentrations exhibit a sympathetic variation with alumina (Fig.98). The variable alumina : alkali distribution is also evident from the occurrence of normative corundum in some analyses (Table.10 c). Adopting Harpum (1963) classification based on K_2O and Na_2O abundance, these rocks define a gradation of composition from tonalite to granite (Fig.99 a), which is also distinctly displayed in the normative An-Ab-Or diagram (Fig.99 b) of Barker (1979). In the Ca-Na-K (wt %) diagram after Barker and Arth (1976), a K enrichment trend is discernible (Fig.99 c).

Trace element concentrations of Rb and Ba, exhibits a range from 38 to 85 ppm and 731 to 1369 ppm respectively. Sr abundance level varies from 160 to 525 ppm, with an average value of 32.67 ppm. Sr/Ba ratios correspondingly vary from 0.14 to 0.54. Rb, Sr and Rb/Sr plotted against $(1/3 \text{ Si} + \text{K}) - (\text{Ca} + \text{Mg})$, shows a linear pattern for Rb, decreasing trend for Sr and slight positive trend for Rb/Sr (Fig.100). Ni + Co + Cr together show weak sympathetic relationship with total Fe + Mg wt% content and enrichment in K has resulted in a proportionate increase in Rb. Sr display similar but, somewhat scattered enrichment trend with Ca wt %. (Fig.101

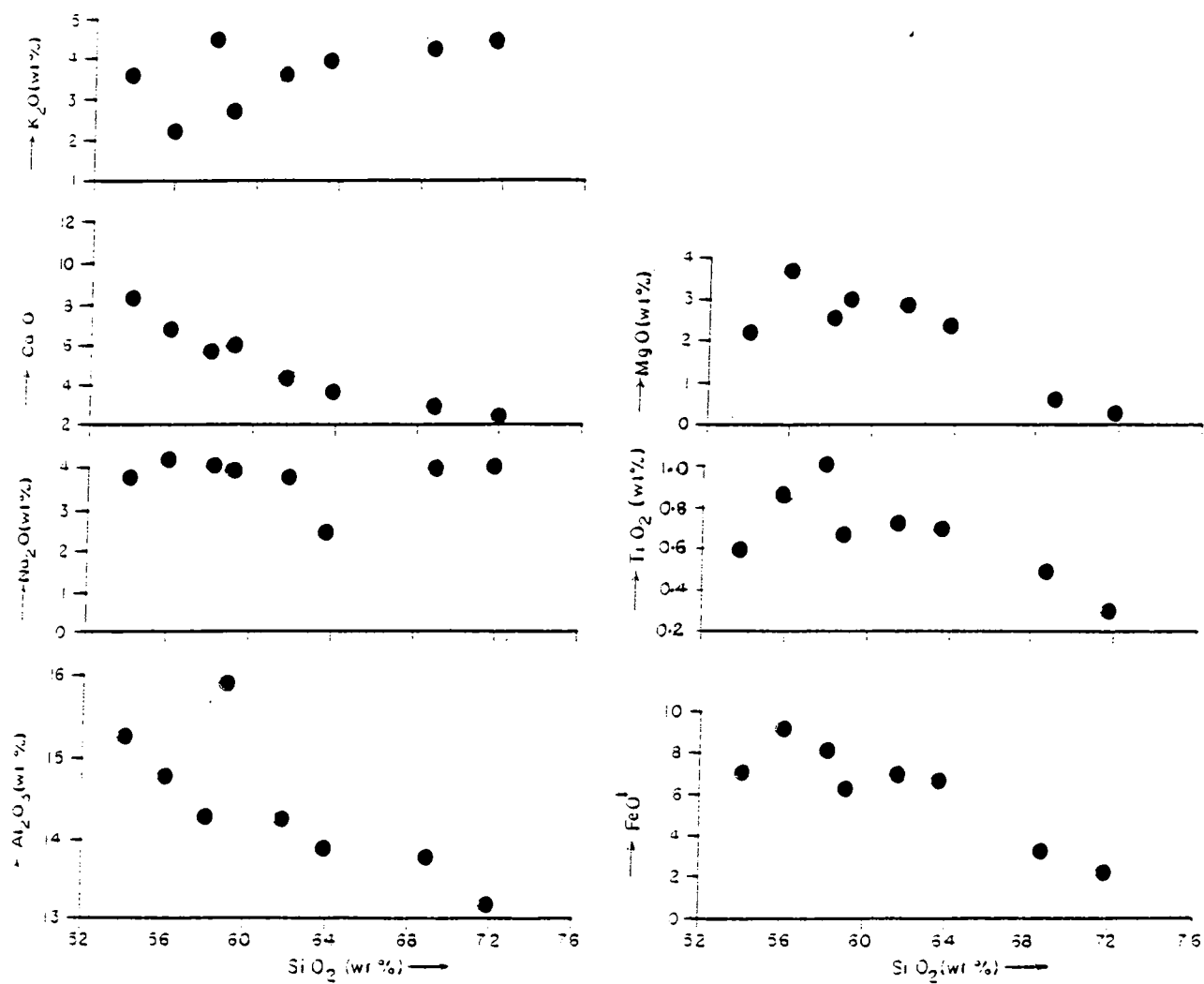


Fig.97 Major element Vs. SiO₂ (wt%) plots of migmatitic gneisses.

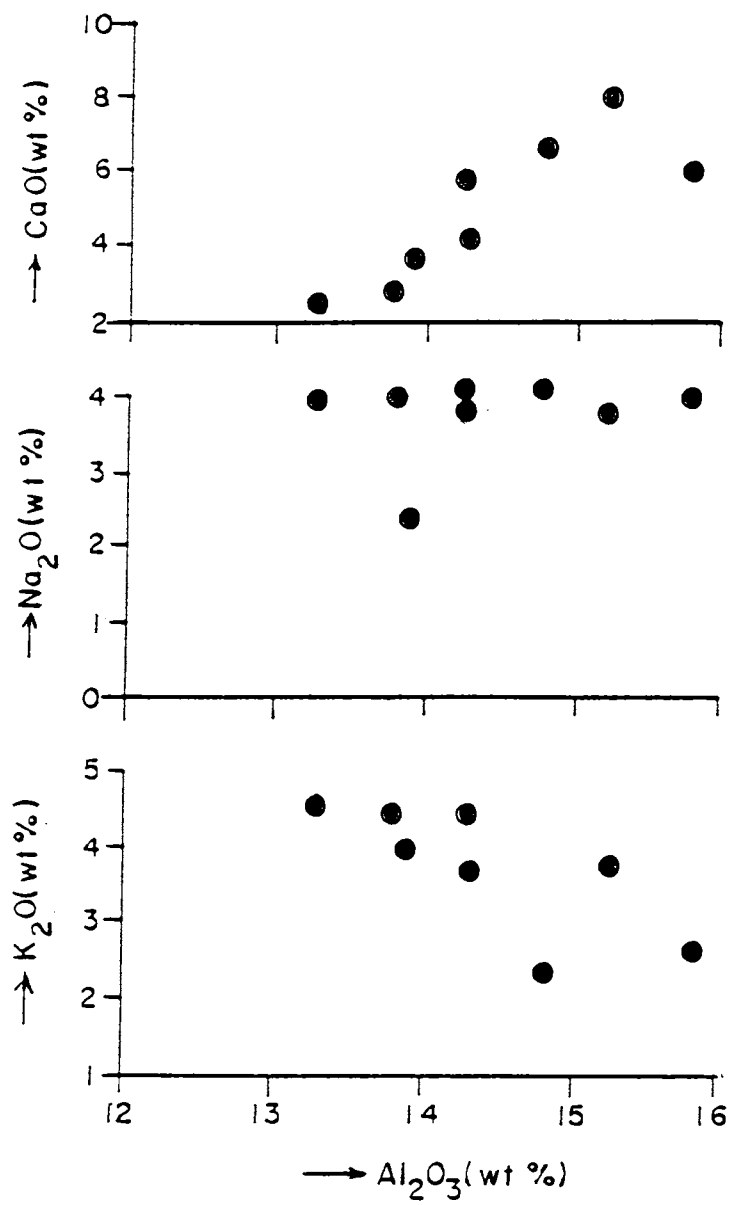


Fig.98 Major element Vs. Al_2O_3 (wt%) plots of migmatitic gneisses.

TABLE.10 (c) NORMATIVE COMPOSITION OF MIGNATITIC GNEISSES.

No.	Q	Or	Ab	An	Diop		Hyp		Mag	Wo	Hem	Ilm	Pyr	Apat	Cor	TOTAL
					Ca	Mg	Fe	Mg								
PS.21	5.64	26.69	34.58	7.23	7.54	5.20	1.72	1.30	0.53	6.50	0.00	1.98	0.00	1.01	0.00	99.92
PS.22	12.72	22.24	32.49	10.56	4.06	2.80	0.92	4.50	1.32	5.57	0.00	1.37	0.00	0.34	0.00	98.69
PS.28	4.74	13.90	35.63	14.46	6.96	4.30	2.24	5.00	2.50	6.26	0.00	1.67	0.00	1.01	0.00	98.67
PS.32	10.92	26.69	34.58	11.12	0.00	0.00	0.00	8.00	1.19	0.00	0.16	0.60	0.00	0.00	6.83	100.09
PS.38c	8.94	16.12	34.06	16.96	5.10	3.30	1.32	4.40	1.85	5.10	0.00	1.37	0.00	0.34	0.00	98.86
PS.43	22.50	26.69	34.06	6.12	0.00	0.00	0.00	1.60	0.79	2.55	3.13	0.91	0.00	0.34	0.00	98.69
PS.117	0.00	22.24	32.49	13.07	11.14	5.60	5.29	0.00	0.00	4.18	0.00	1.22	0.00	0.34	0.00	95.69

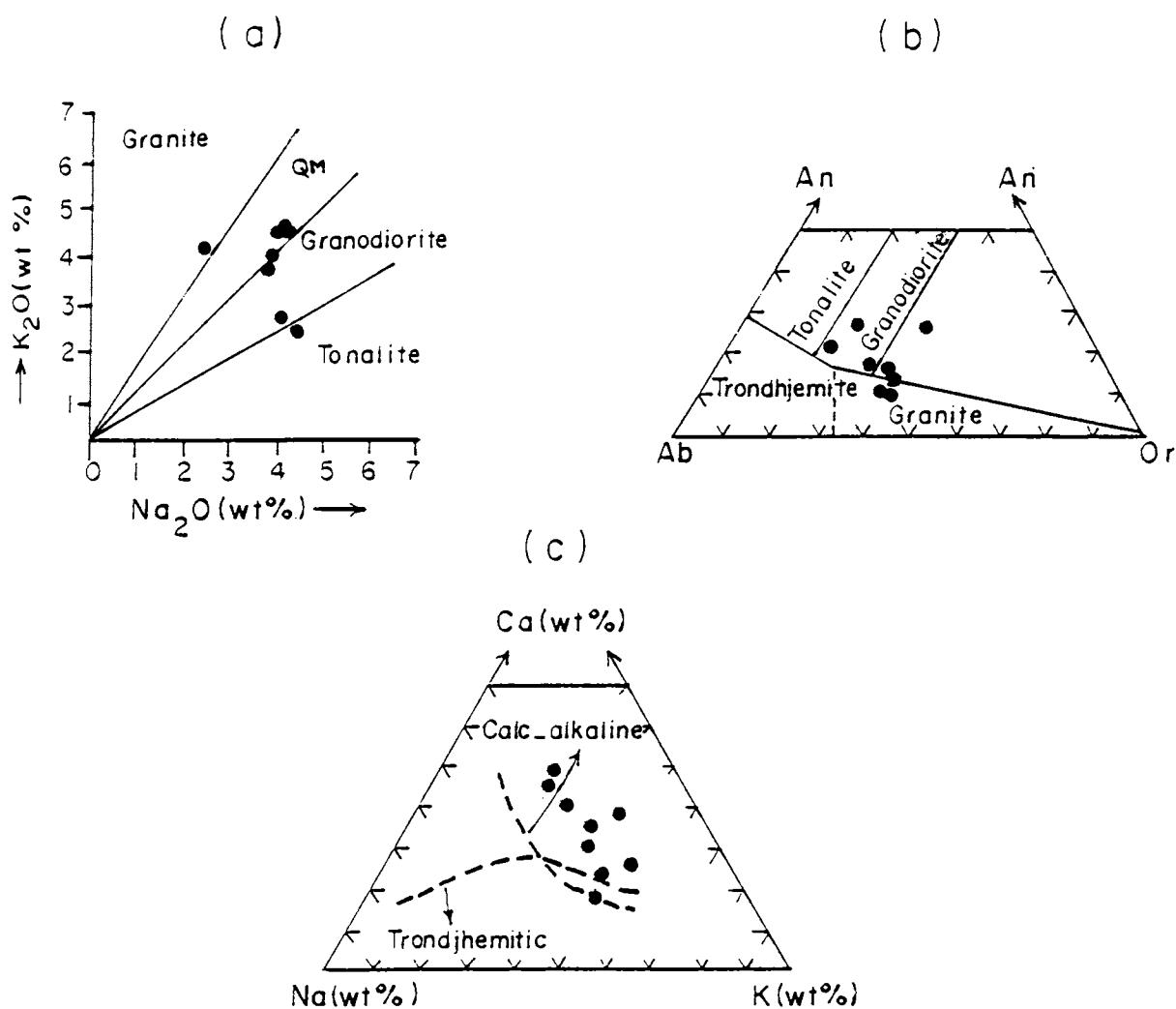


Fig. 99 Plots of migmatitic gneisses in (a) K_2O Vs. Na_2O (wt%) diagram (after Harpum, 1963) (b) normative An-Ab-Or diagram (after O'connor, 1965) and Ca-Na-K (wt%) diagram showing calc-alkaline and trondhjemitic trends (after Barker, 1979).

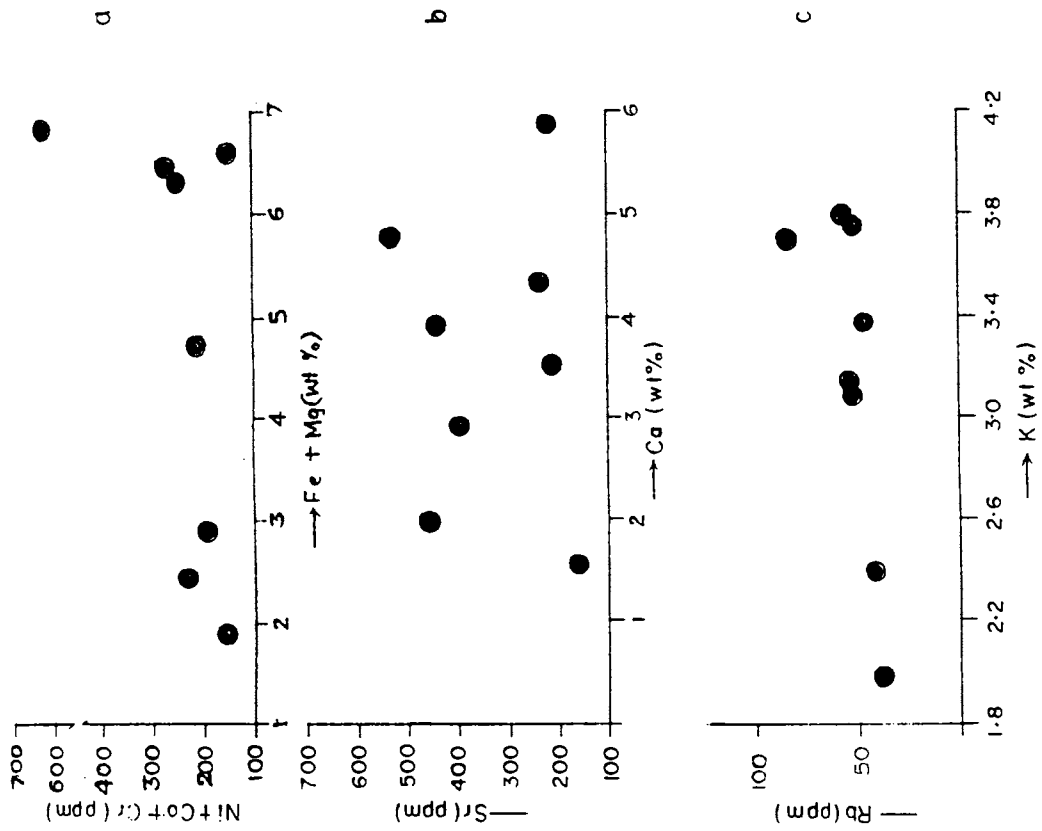


Fig.101 Inter-element plots of migmatitic gneisses.
 (a) (Ni+Co+Cr) Vs. (Fe+Mg) wt%.
 (b) Sr (ppm) Vs. Ca (wt%)
 (c) Rb (ppm) Vs. K (wt%).

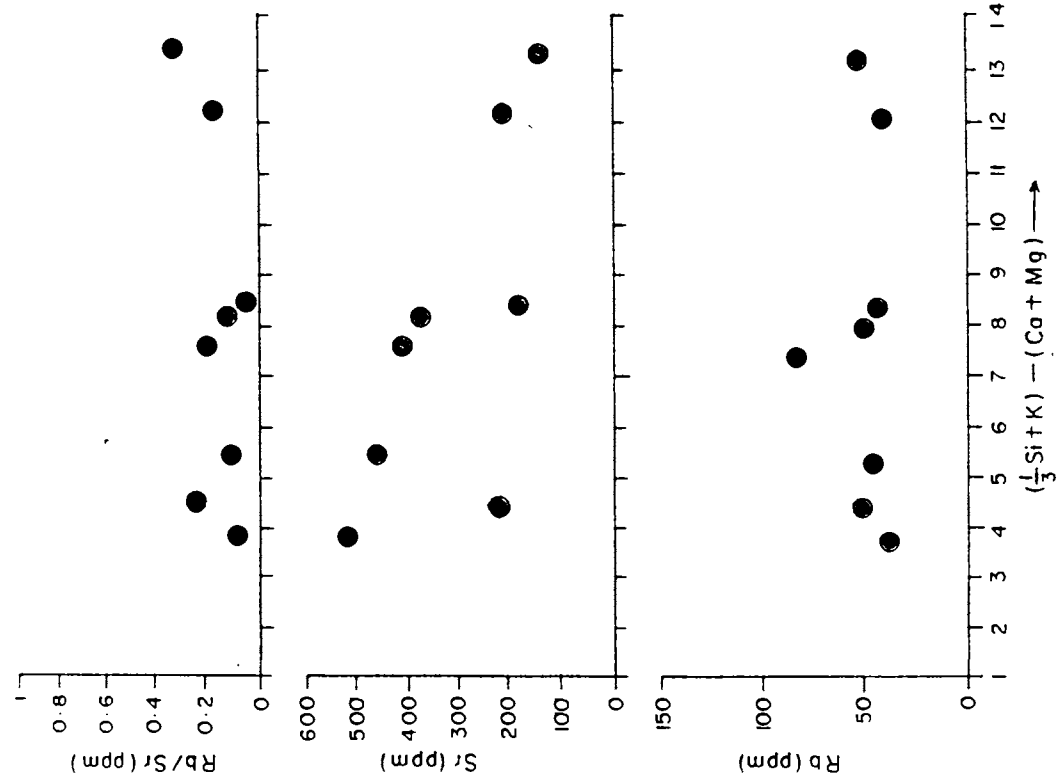


Fig.100 Trace elements of migmatites plotted against $\frac{1}{3}(Si + K) - (Ca + Mg)$.

a, b & c). Average K/Rb values is 611 while, Rb/Sr and K/Ba exhibit a range from 0.06 to 0.35 and 20 to 51 ppm respectively.

Discrimination of the protoliths of the gneisses by plotting the analyses in the AFM [(Na₂O + K₂O), total FeO and MgO] diagram of Irvine & Baragar (1971), shows a calc alkaline trend similar to that of the amphibolites (Fig.102), which is also corroborated by the Ca-Na-K plots of Barker & Arth, (1976) (see Fig.99 c).

IV.4.b PETROGENESIS

Petrogenetic models for migmatitic generation are quite variable (Ashworth, 1985) advocating injection of granitic magmas (Sederholm, 1907, 1913, 1934), metamorphic differentiation at subsolidus temperatures (Ashworth & Mclellan, 1985), metasomatism (Misch, 1968; Olsen, 1985) and anatexis (Winkler, 1961; Mehnert, 1968; Johannes & Gupta, 1982). Though the absence of REE data poses constraints on a geochemical approach of examining their paleotectonic environments, the migmatites, associated amphibolites and granites are examined geologically, petrographically and in part mineralogically, to throw some light on their geotectonic environment.

Na₂O : K₂O (~ 1.01) and Rb:Sr (0.14) ratios of these rock units are lower than the corresponding mean values for Archaean low alumina trondhjemites (2.09 and 0.68

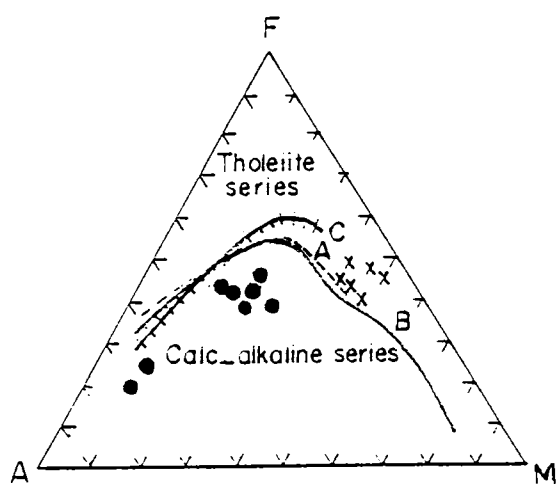


Fig.102 Plots of migmatitic gneisses and amphibolites in the AFM diagram. (A = wt% $\text{Na}_2\text{O} + \text{K}_2\text{O}$, F = total Fe as FeO and M = MgO). A & B = Irvine & Baragar (1971) C = Kuno (1968).
 Symbols : x = amphibolites ● hornblende - migmatitic gneisses.

respectively) reported by Condie, (1981) ; the mean K/Rb (611) however, is higher (216). Compared to the hornblende-biotite gneisses of central Kerala (Rajan et al, 1984), they exhibit lower SiO₂ (av.61.59), Al₂O₃ (14.41), CaO (4.95) and substantially higher Fe₂O₃ (3.36), FeO (3.44) and MgO (2.24). On standard Harker diagram, major element abundance of gneisses display trends generally ascribed to igneous suites; such as a linear decrease of MgO, TiO₂, FeO^t and CaO with SiO₂ content (Fig.97). A gradation in composition from tonalite to granite is also indicated by Na₂O - K₂O (Harpum, 1963) and normative An-Ab-Or (Barker, 1979) plots (Fig.99 a & b).

Decreasing trend of Al₂O₃ and CaO with SiO₂ (see Fig.97) indicate anorthite fractionation, which is augmented by the sympathetic variation of CaO with Al₂O₃ (see Fig.98). MgO, FeO and TiO₂ decrease is consistent with the fractionation of mafic phases (biotite and hornblende). Sympathetic variations of K with Al₂O₃ probably indicates a secondary K-enrichment. The calc-alkaline trend depicted by plots in the Ca-Na-K (wt %) and AFM diagrams is also consistent with the highly differentiated nature of the rocks, as is also evident from the plots of Rb, Sr and Rb/Sr Vs. 1/3 (Si+K) - (Mg+Ca) plots (see Fig.100).

Unlike the migmatitic gneisses of central Kerala which has been assigned a 'two - stage evolution model', involving partial melting of mafic granulites (Rajan et al, 1984), the

Rb depleted and Sr enriched nature of the migmatitic gneisses of the study area supports a fractional crystallization model involving a melt of intermediate (andesine - dacitic) composition and suggest the involvement of crustal rocks with low Rb/Sr values such as amphibolites. Since pure amphibolites contain only very little amounts of 'K', an introduction of the latter, presumably with H₂O, is necessary for the formation of biotite, which also has a 'screening effect' preserving the central part from further action.

Microfabric of the biotite-rich border zone between granitoid neosome and amphibolitic paleosome also envisages the separation of biotite to be a result of quasi-isochemical partial melting (Johannes & Gupta, 1982; Gupta & Johannes, 1982). Their close link with structural events of D₂- and D₃-deformation episodes is also consistent with the findings of Campbell, 1980; Hopgood, 1980; Hopgood et al, 1976) suggesting them to be metatexites of orogenic (introduction from outside) origin (White, 1966). P-T estimates on a migmatitic gneiss sample (Ps.19), located close to a khondalite, gives a temperature range of 520 - 530°C and a pressure of ~ 5 Kbars. Since, migmatization occurred at a temperature and pressure too low for muscovite-dehydration melting and at temperatures too low for biotite-dehydration melting, the melting process might have occurred consequent upon the introduction of differing amounts of externally derived K, H₂O and SiO₂ components, during the waning stages of tectonism.

IV.5.a AMPHIBOLITE

Six samples of amphibolite boudins (core) were analysed for major elements by wet chemical method and were cross-checked by XRF analyses. Results are given in Table (11 a & b).

All the amphibolite samples characteristically possess high Fe, moderate Al and Ti, low MgO, K, Mn, P and Niggli mg values. CaO/Al₂O₃ ratios are less than 0.9 and the calculated oxidation numbers (OX# = FeO/(Fe₂O₃ + FeO)) are variable (0.35-0.97). They contain higher concentrations of Zn (110 ppm) and Co (94 ppm) and lower concentrations of Cu (33 ppm) and Li (20 ppm). Intermediate concentrations are observed for Rb (65 ppm), Pb (69 ppm) and Ni (60 ppm).

Major elements plotted against SiO₂ show a depletion trend for MgO, Fe₂O₃, K₂O, P₂O₅ and TiO₂ while, CaO, Na₂O and Al₂O₃ show an enrichment trend (Fig.103). Geochemical plots of amphibolites have also been represented in the TAS (Irvine & Baragar, 1971), AFM (Miyashiro, 1974), ACF (Orville, 1969), modified Niggli mg-c plot of Leake (1964) and Niggli al-alk-c-fm tetrahedron diagrams (Fig.103 to 106) to bringout their geochemical characteristics and also to draw relevant conclusions about their paragenesis (Fig.103 to 106).

IV.5.b PETROGENESIS

The origin of amphibolites remains a puzzling problem, despite extensive studies and the several models proposed for

TABLE 11.a MAJOR ELEMENT ANALYSES OF AMPHIBOLITES (Wt%)

Elements	Ps.57	Ps.158	Ps.51	Ps.121	Ps.31	Ps.4	Ps.57	Ps.121*
SiO ₂	49.39	51.46	50.57	51.65	44.17	46.83	51.29	49.52
Al ₂ O ₃ T	11.87	14.63	15.17	13.46	12.04	12.63	14.37	12.16
Fe ₂ O ₃	11.85	8.58	9.38	10.46	16.39	10.70	11.35	12.46
CaO	10.68	10.00	11.60	9.72	10.40	7.83	10.10	10.72
MgO	12.25	9.04	7.56	8.63	14.70	8.80	13.35	6.63
Na ₂ O	0.79	2.54	3.01	2.12	0.80	2.20	0.83	2.10
K ₂ O	0.47	0.28	0.54	1.52	0.98	0.28	0.51	0.52
MnO	0.28	0.80	0.17	0.19	0.42	0.18	0.19	0.22
P ₂ O ₅	0.11	0.33	0.61	0.25	0.76	0.55	0.10	0.25
S	0.03	--	--	--	--	--	--	--
TiO ₂	0.28	1.43	1.17	0.98	1.18	2.27	0.22	0.90

Niggli parameter

c	24.34	25.13	28.82	24.62	20.52	21.24
mg	00.67	00.66	00.61	00.62	00.64	00.62

* Data by XRF method, in cross-verification of wet analytical results.

TABLE 11.b TRACE ELEMENTS

Elements	Ps.57	Ps.158	Ps.51
Cu	26	34	39
Zn	110	135	85
Rb	11	66	118
Li	5	39	16
Pb	83	42	83
Co	94	115	73
Ni	20	90	70

All concentrations in ppm.

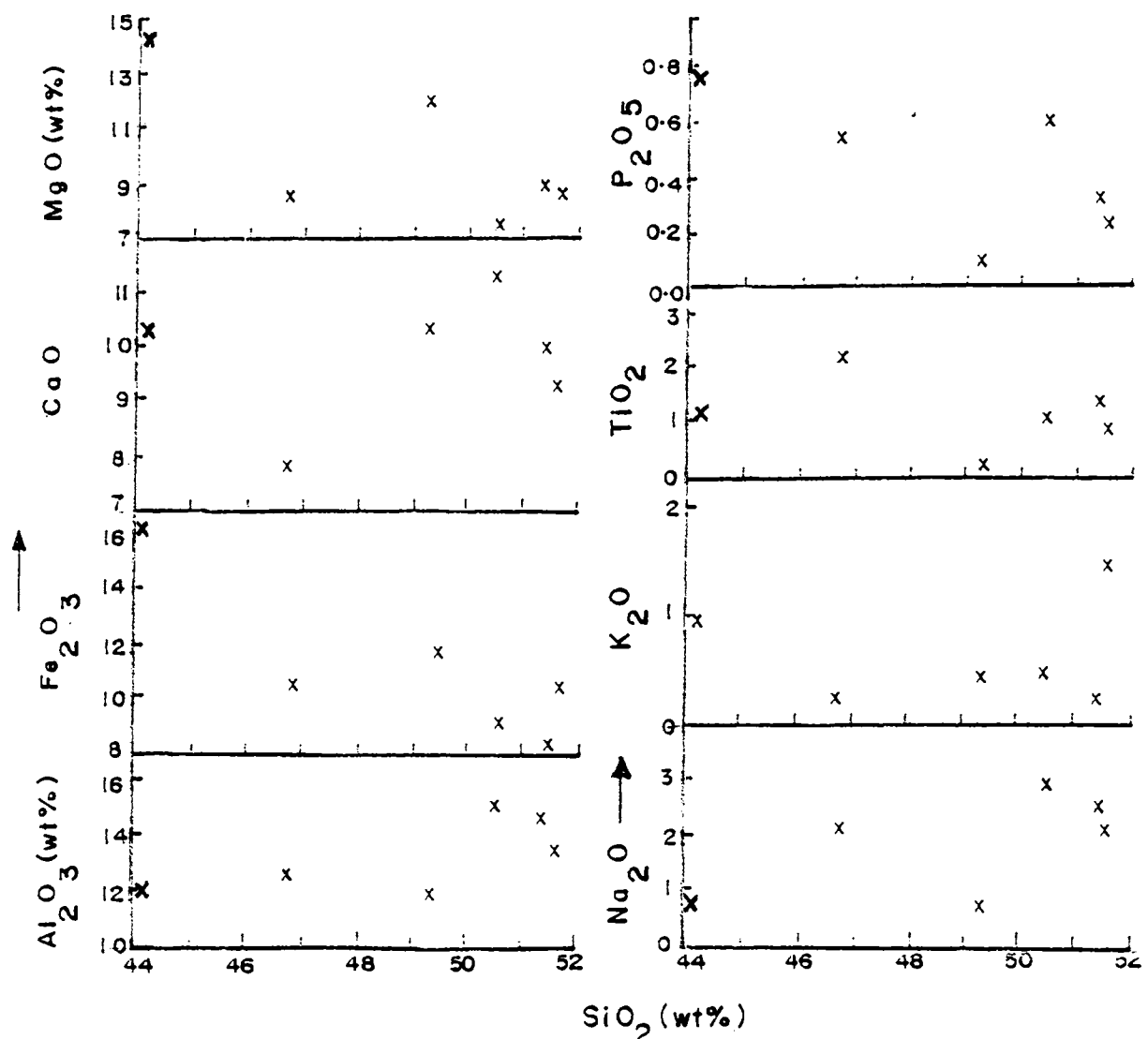


Fig.103. Major elements Vs SiO_2 (Amphibolites)

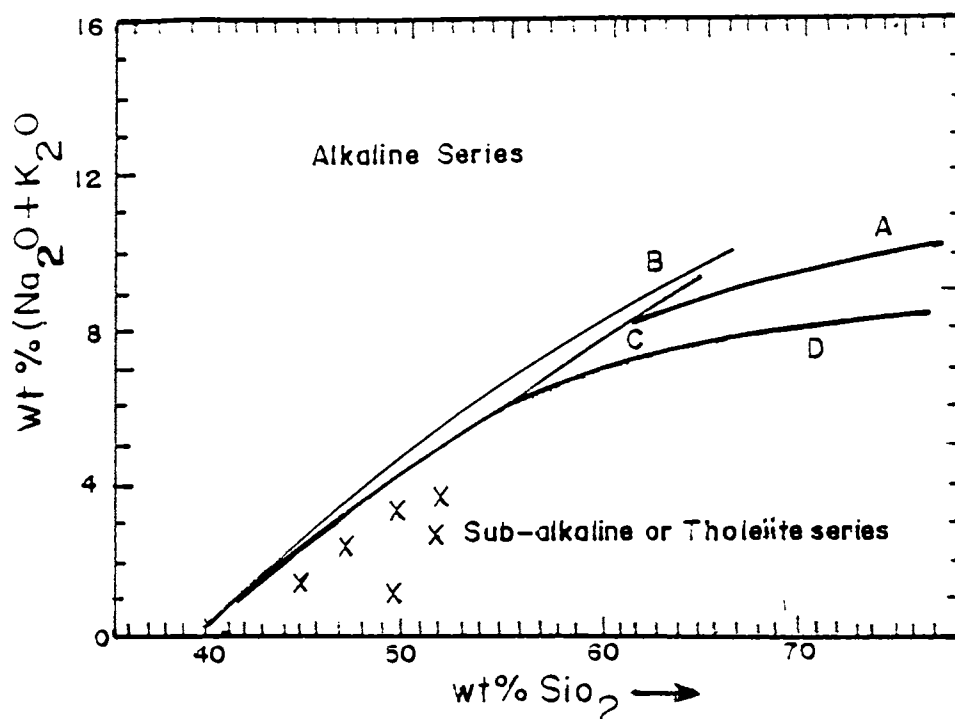


Fig.104 Amphibolite plots in the TAS (Total alkalies Vs. SiO₂) diagram on a H₂O - and CO₂ - free basis (Rickwood, 1989). A & B (Irvine & Baragar, 1971) C = Mac Donald (1968), D = Kuno (1966). Discriminant bands are used in preference to discriminant lines to account for the inter laboratory analytical precision of the empirically derived lines (Rickwood, 1989).

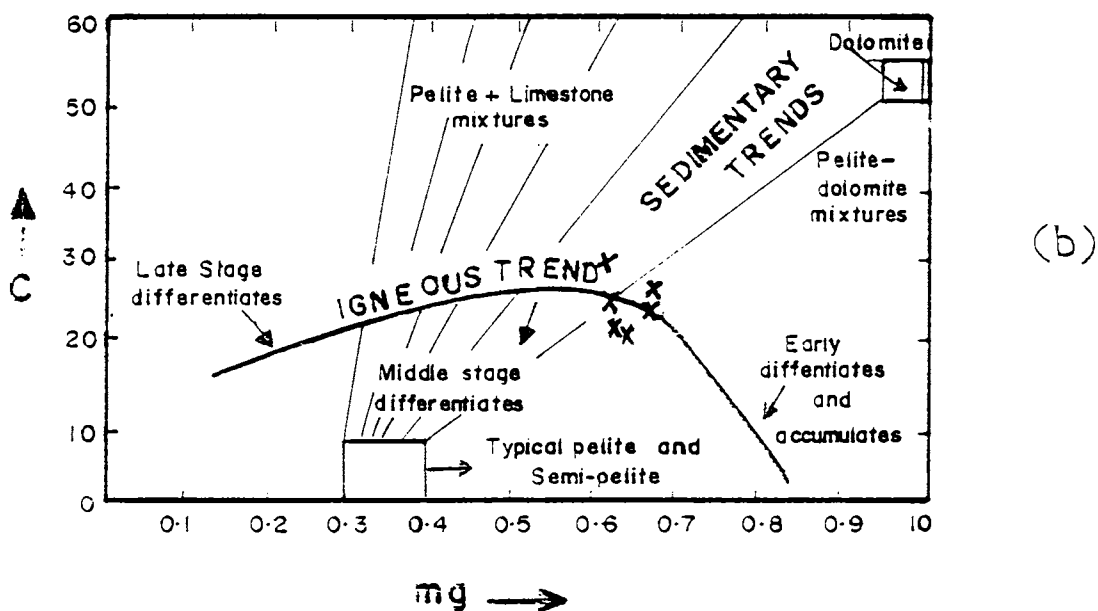
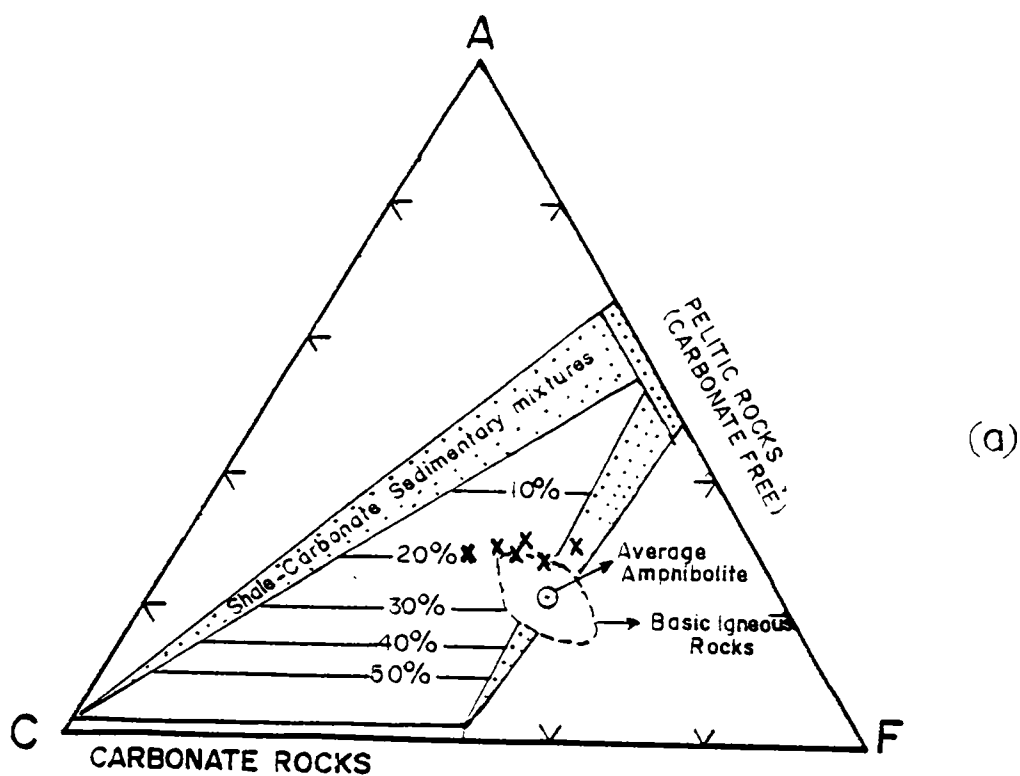


Fig.105 Plots of amphibolite in (a) ACF diagram (Orville, 1969). Mixtures of carbonate - free shale and 10 - 50 wt% of calcite and dolomite are shown. Field of basic igneous rocks is indicated by dashed line. (b) Niggli c - mg diagram (Orville, 1969) modified after Leake (1964). Straight lines indicate various limestone - dolomite mixtures combined with varying amounts of typical pelite.

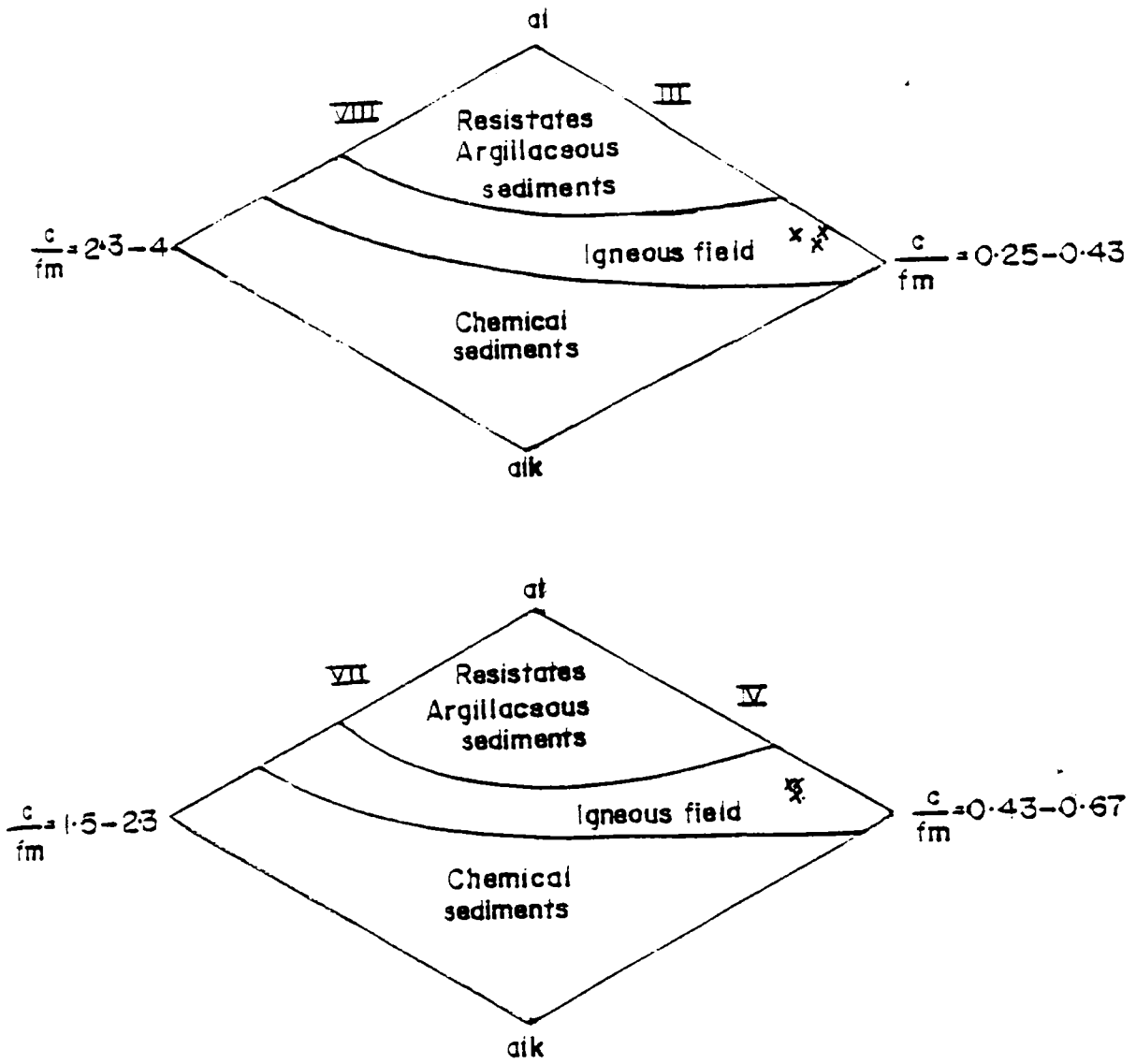


Fig.106 Amphibolite plots in the Niggli al-alk-c-fm tetrahedron.

their genesis. Amphibolites interlayered with rocks of sedimentary origin have commonly been assumed to represent metamorphosed sedimentary rocks such as marly shale. The composition of individual amphibolite layers however, closely resembles the differentiation trend of basic igneous rocks (Leake, 1964; Engel & Engel, 1962; Heier, 1962; Evans & Leake, 1960; Walker et al, 1960; Wilcox & Poldervaart, 1958), rather than that expected for mixtures of shale and carbonate end-members (Leake, 1964; Turner, 1968).

Plots of amphibolites in the TAS diagram (wt % total alkalies ($\text{Na}_2\text{O} + \text{K}_2\text{O}$) vs. SiO_2 on a H_2O and CO_2 -free basis), fall in the tholeiitic field (Fig.104) of Irvine & Baragar (1971). Distinction into calc-alkaline and tholeiitic series has also been confirmed by the AFM (A = wt % $\text{Na}_2\text{O} + \text{K}_2\text{O}$, F = total Fe as FeO and M = MgO) diagram (see Fig.102) of Miyashiro (1974). In the ACF diagram (Fig.105 a) of Orville (1969), most of the amphibolites plot along the boundary of basic igneous rocks, while two plots indicate mixtures of 20% carbonates with pelitic rocks. In the modified Niggli mg-c plot (mg = $\text{Mg}/\text{Mg} + \text{Fe}$ and c = $100 \text{ CaO}/\text{CaO} + \text{MgO} + \text{FeO} + \text{Al}_2\text{O}_3$) of Leake (1964), the samples compare with the trend of Karoo dolerite, with most of the plots falling along the boundary of igneous rocks (Fig.105 b). Plots in the Niggli al-alk-c-fm tetrahedron also fall in the igneous field (Fig.106). Based on the KTP diagram (not shown) of Pearce et al (1975) for the incompatible elements K, Ti and P (in their

oxide wt %), a continental environment of formation is suggested for the amphibolites. The possibility of metasomatic conversion of 'calc-silicate mineral-bearing' marble into hornblende + calcic plagioclase + quartz-bearing amphibolites, through an intervening stage of calc-silicate rocks (Papageorgakis, 1961; p.169; Knup, 1958, p.156), could not be substantiated by field evidences, as no amphibolite layer in contact with calc granulite was observed. The available geochemical data therefore, indicates that the composition of amphibolites could be the result of emplacement and subsequent modification of partial melts from the mantle.

IV.6.a GRANITE

The results of major and trace element analyses, together with the calculated CIPW norms are given in Table.12 a,b and c. Analyses show a spread in SiO_2 values from 55.82 to 73.64 wt %, K_2O from 2.82 to 5.73 wt % and CaO from 1.36 to 8.35 %. MgO content ranges from 1.03 to 3.16 wt %, with one sample showing a substantially higher value of 7.77 wt %. Na_2O averages around 3.60 (wt %) while, Fe_2O_3 and FeO show average values of 2.86 and 1.94 wt % respectively. Trace element analyses show rather high values of Ba (av.963 ppm) while, Sr is lower around 283 ppm, yielding high Ba/Sr ratios (2.57 to 5.13). Copper is low (27 ppm) and Zn averages around 31 ppm. Rubidium and Pb shows a range of values from 44 to 119 and 24 to 51 ppm respectively.

TABLE. 12 a RESULTS OF MAJOR ELEMENTS ANALYSES OF GRANITES.

No. Type	*		*		*		**		**		**	
	Ps. 18 Hb-Bt	Ps. 30 Hb-Bt	Ps. 48 Hb-Bt	Ps. 144 Bt-Hb	Ps. 113 Bt-Hb	Ps. 91 Bt-Hb	Ps. 163 Bt-Hb	Ps. 146 Bt-Hb	Ps. 163 Bt-Hb	Ps. 146 Bt-Hb	Ps. 163 Bt-Hb	Ps. 146 Bt-Hb
<u>Elements</u>												
SiO ₂	64.48	60.66	61.14	72.92	73.64	58.35	56.90	55.82	58.35	56.90	55.82	55.82
Al ₂ O ₃	15.80	15.29	14.78	13.63	13.89	18.63	13.07	13.34	18.63	13.07	13.34	13.34
Fe ₂ O ₃	1.87	2.91	3.03	1.26	1.39	3.37	4.53	4.58	3.37	4.53	4.58	4.58
FeO _t	2.33	3.05	2.87	0.41	0.37	1.41	2.19	2.89	1.41	2.19	2.89	2.89
FeO	4.02	5.67	5.60	1.55	1.62	4.44	6.27	7.02	4.44	6.27	7.02	7.02
CaO	3.36	4.94	5.83	1.36	1.62	4.54	8.35	6.21	4.54	8.35	6.21	6.21
MgO	1.13	1.77	1.61	1.03	--	3.16	2.89	7.77	3.16	2.89	7.77	7.77
Na ₂ O	3.77	4.53	4.72	2.68	2.84	4.18	2.65	3.46	4.18	2.65	3.46	3.46
K ₂ O	5.04	5.13	4.31	4.78	4.43	3.59	5.73	2.82	3.59	5.73	2.82	2.82
TiO ₂	0.54	0.59	0.42	0.16	0.18	0.99	0.65	0.62	0.99	0.65	0.62	0.62
MnO	0.03	0.04	0.03	0.01	0.02	0.02	0.10	0.15	0.02	0.10	0.15	0.15
P ₂ O ₅	0.19	0.17	0.20	0.09	0.10	0.30	0.48	0.29	0.30	0.48	0.29	0.29
LO ₁	0.29	0.38	0.60	0.59	0.62	0.45	0.38	0.47	0.45	0.38	0.47	0.47
MO ₁	0.20	0.32	0.23	0.17	0.20	0.37	0.41	0.42	0.37	0.41	0.42	0.42
S	0.01	0.01	0.01	0.03	0.05	0.01	0.01	0.04	0.01	0.01	0.04	0.04
Na ₂ O+K ₂ O _t	8.81	9.68	9.03	7.46	7.21	7.77	8.35	6.28	7.77	8.35	6.28	6.28
Mg/Mg+Fe	0.18	0.19	0.22	0.34	--	0.36	0.26	0.46	0.36	0.26	0.46	0.46
A	63.00	56.49	55.60	74.30	81.65	50.55	47.78	30.99	50.55	47.78	30.99	30.99
F	28.7	33.18	34.48	15.44	18.35	28.89	35.75	30.65	28.89	35.75	30.65	30.65
M	8.25	10.35	9.91	10.26	--	20.56	16.48	38.35	20.56	16.48	38.35	38.35
Ca	25.60	31.67	37.06	14.03	16.68	34.81	47.03	47.50	34.81	47.03	47.50	47.50
Na	29.77	30.10	31.10	28.66	30.31	33.21	15.47	27.43	33.21	15.47	27.43	27.43
K	44.63	38.23	31.84	57.31	53.01	31.98	37.51	25.07	31.98	37.51	25.07	25.07
A/CNK	1.30	1.05	1.00	1.55	1.56	1.51	.78	1.07	1.51	.78	1.07	1.07
FeO /MgO	3.56	3.20	3.48	1.50	--	1.41	2.17	.90	1.41	2.17	.90	.90
Na ₂ O/CaO	1.12	0.92	0.81	1.97	1.75	0.92	0.32	0.56	0.92	0.32	0.56	0.56
Fe ₂ O ₃ /FeO	0.80	0.95	1.06	3.04	3.76	2.39	2.07	1.58	2.39	2.07	1.58	1.58
Fe ₂ O ₃ /CaO	0.56	0.59	0.52	0.93	0.86	0.74	0.54	0.74	0.74	0.54	0.74	0.74
K ₂ O/CaO	1.50	1.04	0.74	3.51	2.73	0.79	0.69	0.45	0.79	0.69	0.45	0.45
DI	73.00	70.00	75.00	57.00	57.00	77.00	64.00	59.00	77.00	64.00	59.00	59.00
(Q+Or+Ab)												

* - core portions ** rim portions.
All concentrations in wt%.

TABLE.12 b TRACE ELEMENT ANALYSES OF GRANITES (ppm)

Elements Rock type	*	*	*	*	*	**	**	**	**
	Ps.18	Ps.30	Ps.48	Ps.144	Ps.91	Ps.163	Ps.146		
Rb	57	80	44	121	100	83	119		
Sr	203	289	340	375	276	250	250		
Ba	1041	895	915	963	914	1022	993		
Cr	41	94	103	--	87	79	96		
Ni	51	74	103	--	78	68	74		
Co	29	42	38	31	38	29	40		
Pb	35	49	24	42	51	37	46		
Cu	18	31	30	21	27	30	35		
Zn	34	45	43	2	21	41	31		
Li	3	4	2	9	2	3	3		
Ba/Sr	5.13	3.10	2.69	2.57	3.31	4.09	3.97		

* Core portions ** Rim portions.

TABLE. 12 c NORMATIVE COMPOSITION OF HORNBLENDE AND BIOTITE GRANITES.

Sample No. Rock type	Ps. 18	Ps. 30	Ps. 48	Ps. 144	Ps. 113	Ps. 91	Ps. 163	Ps. 146
An	12.51	11.12	6.12	5.84	7.23	20.85	6.67	6.31
Or	16.68	30.02	30.58	28.36	26.13	21.13	33.92	25.58
Ab	29.68	31.96	38.25	22.53	24.10	35.10	22.53	39.82
Apat	0.67	0.34	0.34	0.34	0.34	0.67	1.01	0.36
IPm	1.22	1.06	1.06	0.30	0.30	1.82	1.22	0.76
Mt	6.73	2.78	4.18	0.93	0.46	1.86	5.34	4.41
Ht	---	---	---	0.64	1.12	2.08	0.80	---
Cor	---	---	---	1.94	1.74	0.31	---	---
Mg	13.50	1.60	---	2.60	---	7.90	---	---
Hyp<	---	---	---	---	---	---	---	---
Fe	0.26	2.38	---	---	---	---	---	---
Qz	4.02	14.82	4.44	34.38	36.60	6.80	5.16	6.42
Pyr	---	---	---	---	0.12	---	---	---
Ca	6.96	1.97	7.31	---	---	---	8.35	6.50
Diop<-Mg	5.90	1.20	4.40	---	---	---	7.20	2.11
Fe	0.13	0.66	2.38	---	---	---	---	4.00
Wol	---	---	---	---	---	---	5.10	2.55
Total	97.92	99.91	99.06	97.85	98.26	98.56	97.30	98.82
An	15.07	8.57	8.00	10.53	12.28	27.27	10.94	22.03
Ab	43.84	57.14	50.67	40.35	42.11	45.45	35.94	49.15
Or	41.10	37.14	41.33	49.12	45.61	27.27	53.13	28.81
Q	19.30	6.60	8.64	40.32	42.15	10.85	8.38	8.03
Ab	41.61	52.20	55.44	26.42	27.76	55.65	36.57	58.64
Or	39.09	41.74	35.62	33.26	30.09	33.50	55.05	33.33

Mineralogical peculiarities include a two-feldspar nature with perthites dominating over plagioclase. High ratios of K_2O/CaO (av.1.43) and Fe_2O_3/CaO (av.0.69) are characteristic (Chappel & White, 1974; Taylor, 1977; O'Neil & Chappel, 1977; Beckinsale, 1979; McCulloch & Chappel, 1982). As per the classification of Shand (1927), the granites belong to the peraluminous type with $Al_2O_3/(CaO + Na_2O + K_2O)$ ratios exceeding 1.1 (Chappel & White, 1974; Clemens & Wall, 1984; Fang & He, 1985). In Streckeisen's (1976) diagram (not shown), the analyses plot mostly in the granite field. Since the constituent minerals include alkali and plagioclase feldspars as discrete individuals, it can also be categorised as sub-solvus granite (Tuttle & Bowen, 1958). Based on the K_2O Vs. CaO and K_2O Vs. Na_2O diagram (Harpum, 1963), the rock types show a range between granodiorite and granite (Fig.107 a & b). In the normative An-Ab-Or diagram (O'Conner, 1965) also, the granite plots predominantly in the granitic and granodioritic field (Fig.108 a). The alkali-lime index of ~ 63.2 indicates a calcic field while, a calc-alkaline trend is manifested in the AFM and Ca-Na-K diagrams (Fig.108 b & c).

In the SiO_2 Vs. major elements diagram, Al_2O_3 values show more or less an increasing trend while, MgO , Fe_2O_3 , TiO_2 , Na_2O , MnO and lime exhibit an antipathic relation (Fig.109). K_2O displays a definite positive trend reflecting the increasing peraluminous nature of biotite-hornblende

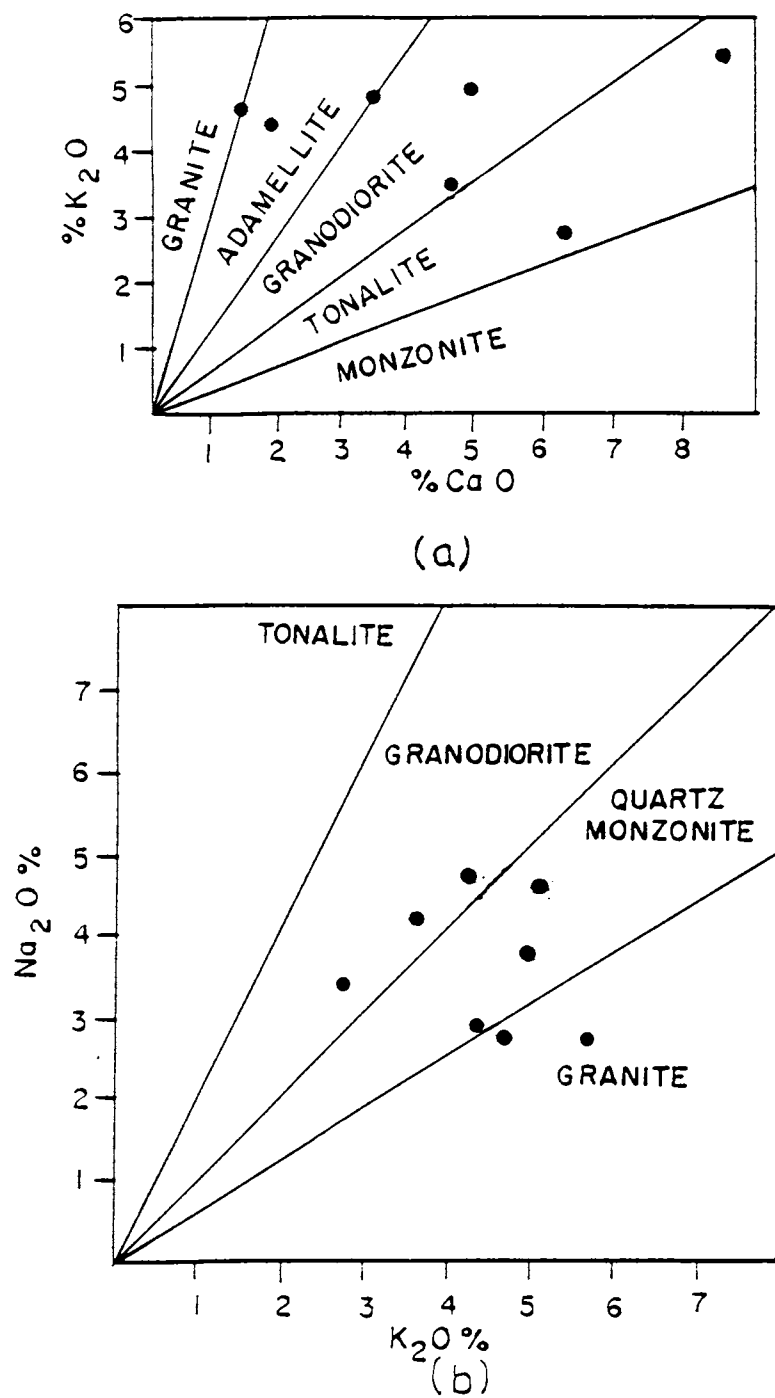
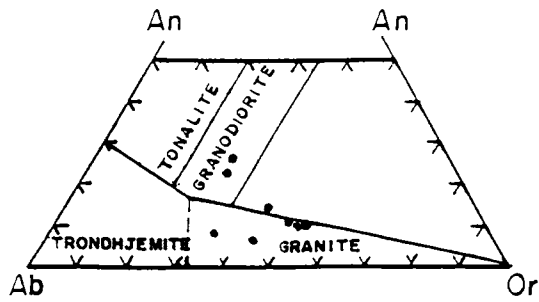
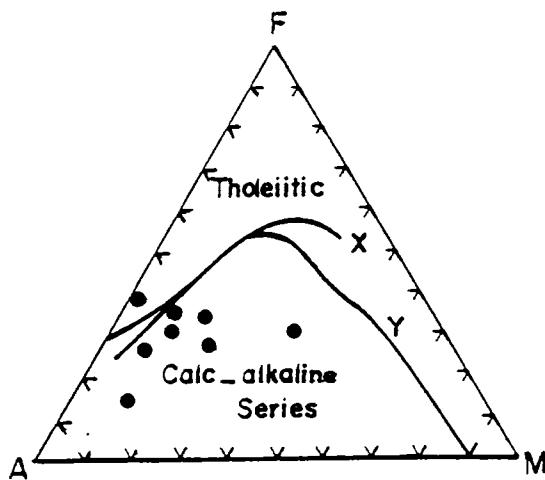


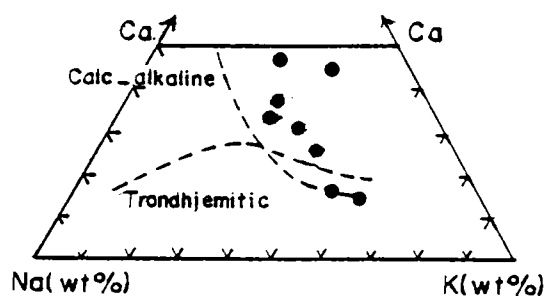
Fig.107 Granite plots (a) K_2O Vs. CaO (wt%) and (b) Na_2O Vs. K_2O (after Harpūm, 1963).



(a)



(b)



(c)

Fig.108 Granite plots in (a) normative An-Ab-Or diagram (after O'connor, 1965), (b) AFM diagram (A = wt% $\text{Na}_2\text{O} + \text{K}_2\text{O}$: F = FeO^T and M = MgO : x = Kuno, 1968 : y = Irvine & Baragar, 1971 and (c) Ca-Na-K (wt%) diagram (after Barker, 1979).

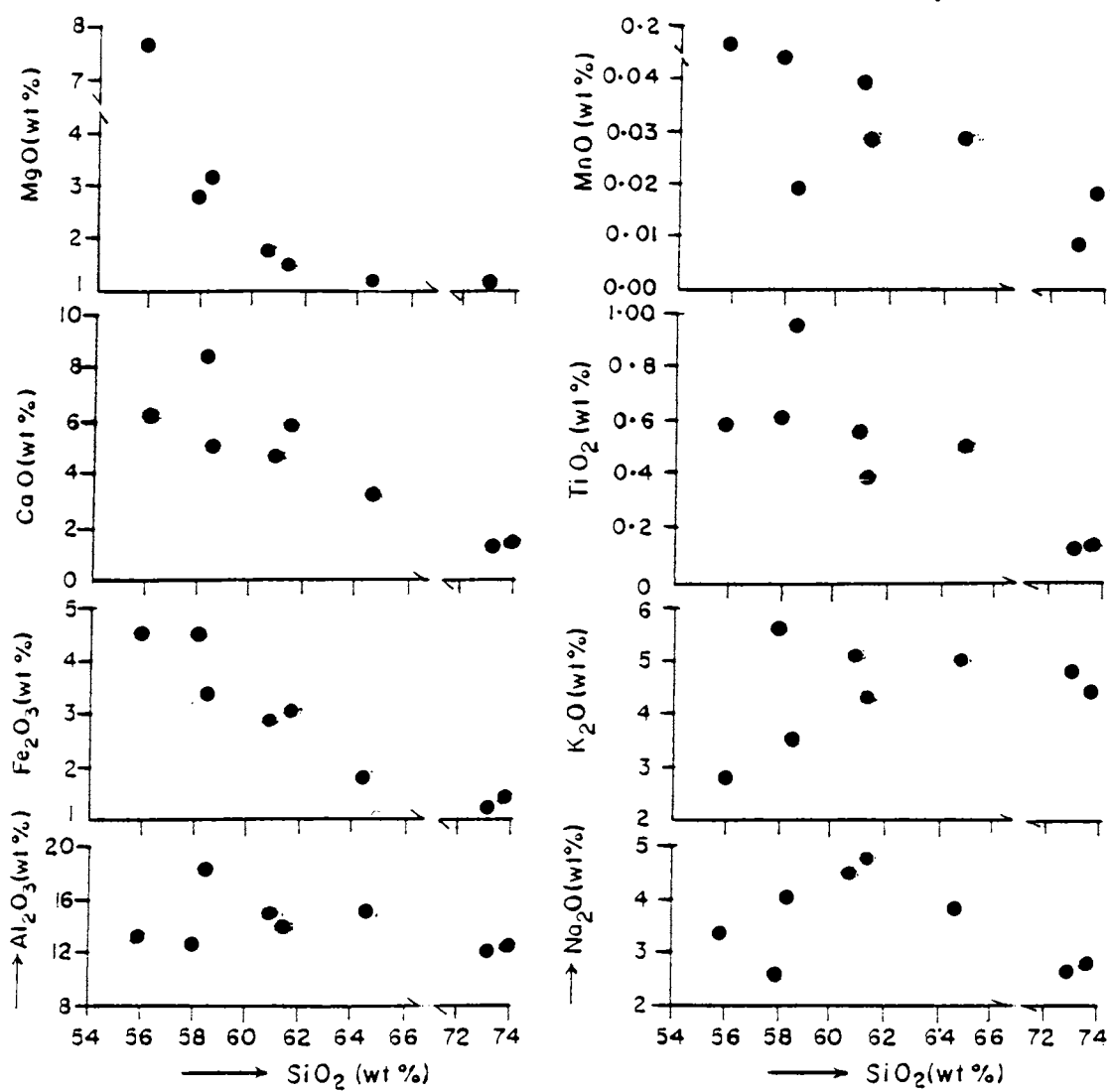


Fig.109 Major elements of granites plotted against SiO_2 (wt%).

granites, compared to hornblende-predominating types. Trace elements plotted against the index of differentiation $Mg/(Mg + Fe^t)$, shows a conspicuous enrichment in Sr and Rb while, Zn shows a depletion (Fig.110). Other elements do not show any definite trend. Increase in SiO_2 as well as the decrease in FeO, MgO and CaO with respect to the normative (Q + Or + Ab) index is also conspicuous (Fig.111). Na_2O increases, while TiO_2 and Sr decrease, consistent with a fractional crystallisation model. Antipathic relationship between Ba and Sr also tally with this model. However, Rb plots are seen scattered.

In the Qz-Ab-Or diagram (Fig.112 a), the granites plot mostly between high temperature isotherms ie, 685°C and 710°C while, in the An-Ab-Or diagram (Fig.112 b), the plots fall near the cotectic line P-E₅, denoting a temperature interval of 640-670°C. In the An-Or-Ab solvus diagram (Fuhrman & Lindsley, 1988), all the plots with the exception of two, fall below 650°C isotherm, close to plots of the garnet-biotite gneisses (Fig.118).

IV.6.b PETROGENESIS

The core zones of the granites showing relatively high Na_2O ($Na_2O > 3.2$ wt %), with a wide range of K_2O/CaO ratios (0.74 to 3.51), are characterised by the presence of hornblende and the general absence of normative corundum. In the peripheral zones on the other hand, Na_2O is relatively

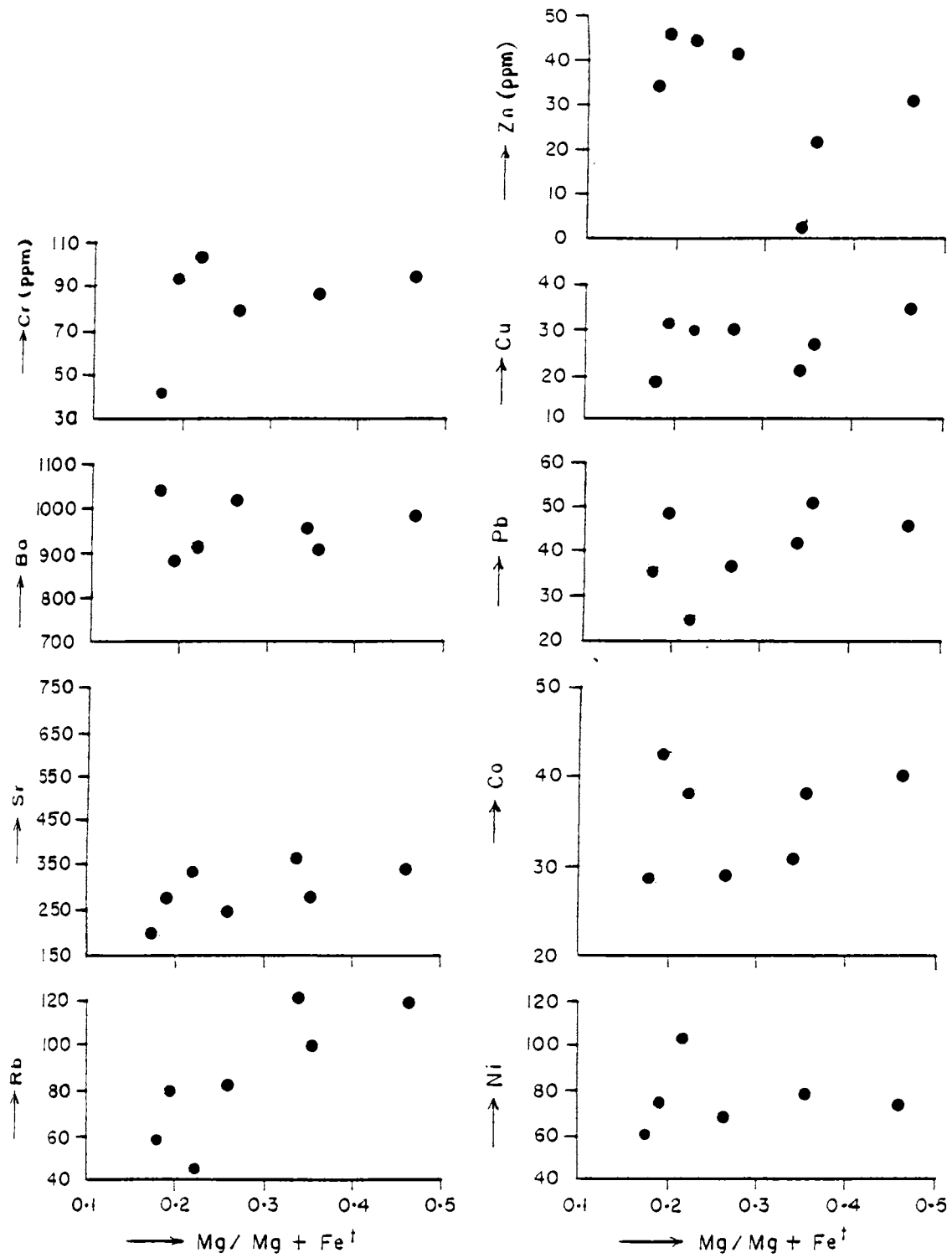


Fig.110 Trace elements of granites plotted against $Mg/(Mg+Fe^t)$.

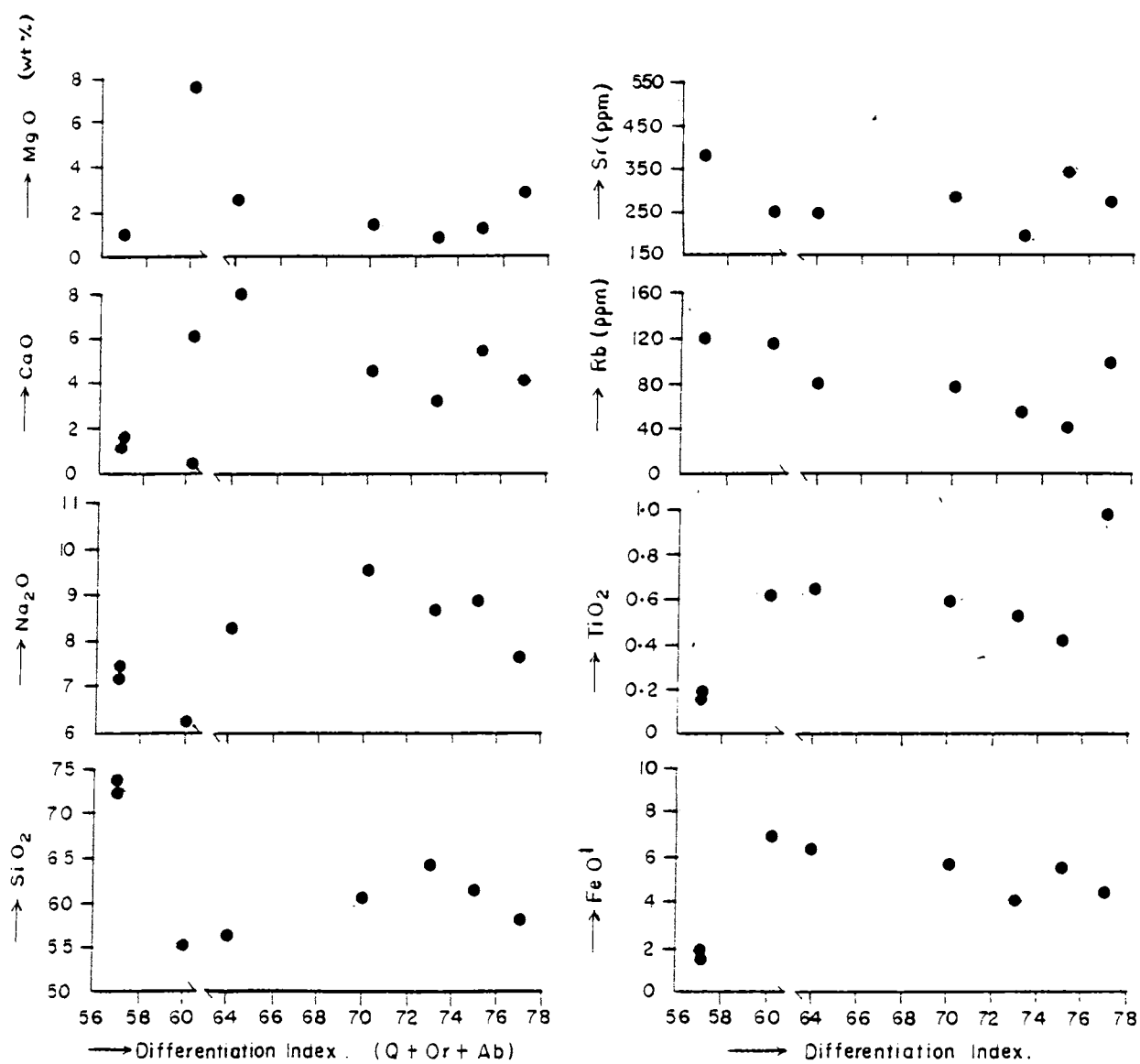


Fig.111 Major and trace elements of granites plotted against differentiation index (Q+Or+Ab).

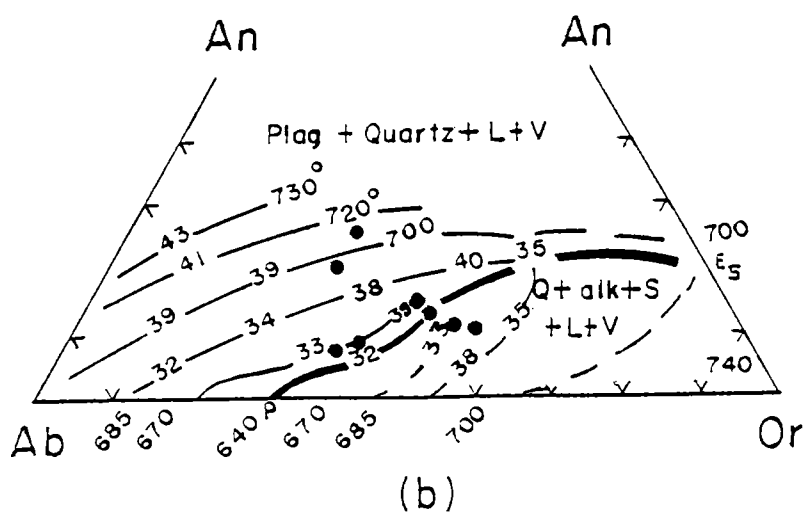
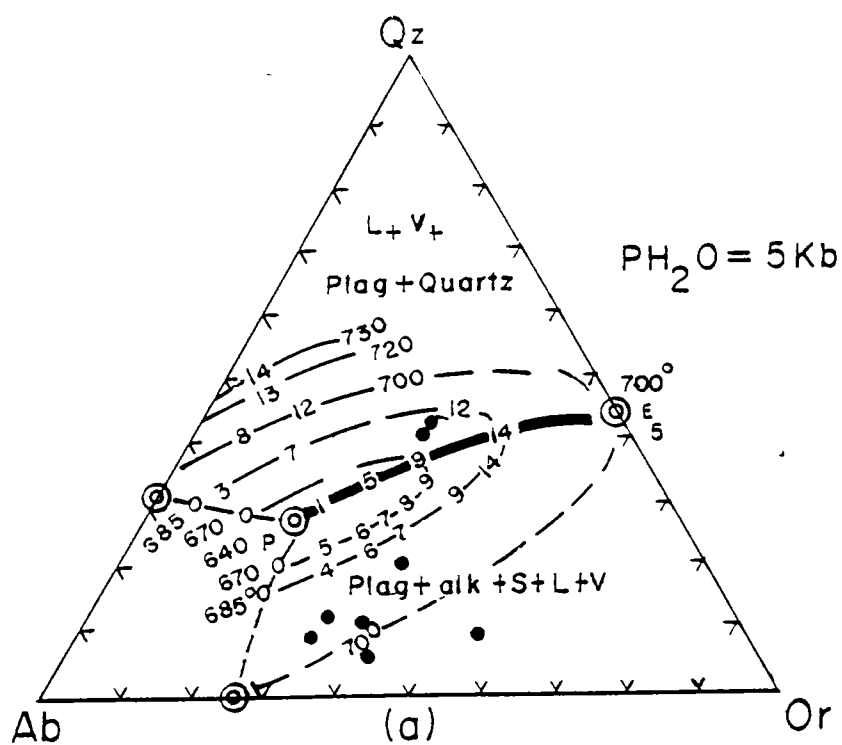


Fig.112 Plots of granite in (a) Qz-Ab-Or and (b) An-Ab-Or diagram showing isobaric cotectic line P-E₅ and isotherms at $P_{H_2O} = 5 \text{ Kbars}$. Numbers in (a) denote An percentage and (b) quartz percentage.

low (< 3.2 wt %), with slightly higher A/CNK ratios. Presence of normative corundum > 1 % and the fairly uniform x_{Ti}^{Bt} (0.486 atoms/O₂₂) values are characteristic of the peripheral zones. However, any peraluminous mineral other than biotite is absent. Magnetite is the major opaque mineral and a few grains of ilmenite have also been reported.

Increase in A/CNK from 1.114 to 1.29 (av) towards the periphery may rather be attributed due to the removal of a metaluminous phase such as hornblende, through fractional crystallisation, leading to the compositional range from hornblende to biotite granites. Exsolution textures, general high potash contents exceeding soda and formation of microcline after plagioclase, argue in favour of a late potash metasomatism.

Sympathetic variations of K₂O and Al₂O₃ with SiO₂ is indicative of substantial feldspar fractionation, which is also supported by the enrichment of Pb (Doe & Tilling, 1967), Rb and Sr (Anderson et al, 1980). Higher values of Ba is explained by the higher content of K. The high TiO₂ and MgO values indicate the presence of mafic components in the source region, possibly an enriched mantle of lower crust at relatively high water pressure. The close field association of granites with the amphibolites and the presence of hornblende, as well as the high Fe₂O₃/CaO values of the granites, support this suggestion.

Plots in the Q-Ab-Or diagram (Fig.112 a) shows a shift towards orthoclase apex while, in the An-Or-Ab diagram (Fig.112 b), they show a shift towards the anorthite apex. These plots moving away from the granite minimum, to higher crystallisation temperatures than normal granites, may suggest their derivation from a minimum partial melt formed during the migmatisation event. Geothermobarometric studies on granites, indicating a temperature of $\sim 530^{\circ}\text{C}$ at a pressure of 4-5 kbars (also see chapter VI), is compatible with the estimated P-T conditions of neomineralisation in khondalite occurring close to a pegmatite at the Pandarettu limestone quarry. This temperature is also near to its plagioclase-amphibole equilibrium. Perthitic equilibrium temperatures are somewhat higher at 584°C , consistent with the findings of Tuttle & Bowen (1958). These temperatures are similar to the average temperatures obtained for garnet (rim)-biotite and two-feldspar assemblages of the khondalites ($\sim 660^{\circ}\text{C}$), suggesting that solidification of alkali feldspar in the granite might have begun at similar P-T conditions.

Discrimination of tectonic environments of granitoids based on the major element chemistry and the proposed discrimination scheme of Maniar & Piccole (1989), points to their classification as the POG group (post orogenic granitoids).

IV.7.a PEGMATITE

Whole rock analyses of pegmatites reveal an average SiO_2 wt % of 72.33 and 14.81 wt % of Al_2O_3 (ref Table.13). Fe_2O_3 ranges between 0.30 and 0.71 while, FeO is almost constant at 0.82 wt % (av.). MgO is virtually absent and Na_2O and K_2O wt % averages around 3.28 and 6.24 respectively. Trace element analyses show rather high values of Co (102-135 ppm), Rb (92-186 ppm) and Zn (97-105 ppm). Cu and Li are low at 41 and 29 ppm (av) respectively.

IV.7.b PETROGENESIS

Mineralogical composition supports a migmatitic derivation of the pegmatitic melts. Field relations suggest that the major phase of pegmatite emplacement belongs to post D_2 -syn D_3 -deformation stage. Lower values of X_{Tl} and X_{Mg} in biotite, as compared to other rock types, are also consistent with their formation during retrograde metamorphism. P-T estimates reveal a peak garnet (core)- biotite (matrix) temperature of 784°C , which is close to the equilibration temperature of second generation biotites in khondalites. Biotite neomineralisation temperature of 547°C (av.) in pegmatite is comparable to the garnet (rim)- secondary biotite temperature (521°C) in khondalites.

TABLE.13 RESULTS OF MAJOR AND TRACE ELEMENT ANALYSES OF PEGMATITES.

Sample No.	Ps.159	Ps.26
<u>Major elements</u>		
SiO ₂	71.80	72.86
Al ₂ O ₃	14.98	14.63
Fe ₂ O ₃	0.30	0.71
FeO	0.80	0.83
CaO	0.84	1.04
MnO	0.02	0.07
Na ₂ O	3.39	3.17
K ₂ O	6.39	6.08
P ₂ O ₅	0.05	0.08
S	0.07	0.04
LOI	0.47	0.37
Total	99.11	99.88
<u>Trace elements</u>		
Cu	43	39
Zn	97	105
Rb	92	186
Li	22	36
Pb	78	83
Co	102	135
Ni	--	40
Cr	--	167

CHAPTER V
MINERAL CHEMISTRY

Mineral analyses were performed on a JEOL- JXA -733 electron microprobe at the National Institute of Polar Research, Tokyo, Japan and at the Geochemical Laboratory of the Hungarian Academy of Sciences, Budapest.. 389 spot analyses were done on samples of garnet-biotite-sillimanite gneiss (khondalite *sensu stricto*), garnet- biotite gneiss, cordierite-bearing khondalite, calc-granulite, hornblende-biotite migmatitic gneiss, granites and pegmatites. A specimen current of 0.012 to 0.013 microampere, at an accelerating voltage of 15 kv was used. In samples showing disequilibrium textures such as myrmekitic intergrowths, an acceleration voltage of 10kv and a sample current of 0.02 μ A were used in the analyses of Ca, Na, K, Si, Fe and Al, so as to check volatilisation of sodium. Perthites have been measured with ϕ 50 μ m electron beam and inclusion compositions are measured with a focussed electron beam.

All the analyses were done using natural and synthesised minerals as standards. For garnet analyses, spessartine was used for Si,Al and Mn, hematite for Fe, olivine for Mg, wollastonite for K and pure oxide for Ti estimations. For other minerals, orthoclase was used for Si, Al, K and artificial glass for Fe, Mg and Ca estimations. For each of these minerals, point analyses were carried out on traverses across several grains in order to detect compositional zoning

or inhomogenities. Selected analytical results of garnet, biotite, feldspars, cordierite, clinopyroxene and amphibole are given in Tables.14 to 20.

V.1. GARNET

Results of 68 spot analyses in garnet-sillimanite-biotite greisses, 50 in garnet-biotite gneisses, 5 in cordierite-bearing samples, 43 in calc-granulites and 20 in pegmatites (Table.14) suggest that the garnets in general, are almandine-rich and constitute essentially solid solutions of almandine, pyrope and grossularite end-members (Fig.113).

In garnet -biotite-sillimanite gneiss, almandine varies from 62-77 mol % and pyrope from 11-26 mol %. Grossular content remains almost a constant except in one of the samples (ps.25a) where a wide variation from 15.1 (core) to 3.8 mol % (rim) is observed.

In garnet-biotite gneiss samples, the bulk chemical composition of garnet rims show higher contents of almandine (76.2 mol %), spessartine (3.5 mol %) and grossular (4.1 mol %), as compared to that of core (70.9, 2.3 and 3.7 mol % respectively). Pyrope decreases from 23.1 to 16.2 mol %. Average composition of garnet core in cordierite-bearing rocks in terms of almandine, grossularite, pyrope and spessartine is 71.9, 2.1, 25.5 and 0.5 mol % respectively.

TABLE 14 MICROPROBE ANALYSES OF GARNET

Rock type with sample No.5	Gar-Bt-Gn Ps.14		Gar-Bt-Sill-Gn Ps.16		Gar-Bt-Sill-Gn Ps.25(a)		Gar-Bt-Sill-Gn Ps.76		Gar-Bt-Sill-Gn Ps.100		Cord-Khondalite Ps.79		Calc- granulite Ps.26 Ps.35		Pegmatite Ps.26					
	Core	Rim	Core	Rim	Core	Rim	Core	Rim	Core	Rim	Core	Rim	Core	Rim						
Elements	Core	Rim	Core	Rim	Core	Rim	Core	Rim	Core	Rim	Core	Rim	Core	Rim	Core	Rim				
			AVI(5Anal)	31 Rim	Core	Rim	Core	Rim	Inside	Rim	Core	Rim	Core	Rim	Core	Rim				
				(AV.6)	(quartz)(biot)(AV.3)	(AV.7)	(AV.5)	(AV.7)	(AV.3)	(biot)	(AV.3)	(biot)	(cord)							
SiO ₂	37.62	37.21	37.56	37.56	37.65	38.53	38.01	37.73	38.09	38.35	37.73	37.64	38.05	38.12	37.59	34.94	37.71	36.53		
TiO ₂	0.00	0.00	0.00	0.00	0.00	0.00	0.04	0.01	0.03	0.04	0.02	0.02	0.03	0.00	0.03	0.65	0.00	0.02		
Al ₂ O ₃	21.15	20.63	20.79	20.39	21.35	20.84	21.85	21.95	21.93	21.85	21.56	21.63	21.83	21.65	21.66	6.97	20.66	20.95		
Cr ₂ O ₅	0.00	0.00	0.00	0.00	0.00	0.00	0.00	0.00	0.00	0.00	0.00	0.00	0.00	0.00	0.00	0.09	0.00	0.00		
Feo	32.31	33.77	31.06	35.19	28.71	32.93	27.84	31.83	32.11	34.14	30.28	32.43	32.73	32.79	33.75	34.82	22.10	33.37		
Mno	1.04	1.52	0.89	1.36	1.74	4.26	1.70	0.94	0.52	0.66	1.51	1.48	1.74	0.21	0.22	0.30	1.91	1.15	3.28	
Mgo	5.91	4.03	6.66	4.11	5.03	3.45	5.30	6.40	6.41	4.78	6.84	6.91	5.22	5.06	6.53	4.88	0.18	5.10	3.54	
CaO	1.30	1.42	1.92	1.31	5.49	1.33	4.80	0.56	0.75	1.05	1.46	1.27	1.15	1.17	0.73	0.69	0.70	28.69	1.55	1.67
Na ₂ O	0.00	0.00	0.00	0.00	0.00	0.00	0.00	0.05	0.02	0.01	0.00	0.00	0.00	0.00	0.01	0.00	0.00	0.00	0.00	
K ₂ O	0.00	0.00	0.00	0.00	0.00	0.00	0.00	0.00	0.00	0.00	0.00	0.00	0.00	0.00	0.00	0.00	0.00	0.00	0.00	
Total	99.33	98.58	99.88	99.92	100.10	99.76	97.84	100.16	99.68	100.34	100.14	99.98	99.79	99.99	100.17	100.05	99.99	95.52	99.26	99.36
ON THE BASIS OF 12 OXYGENS																				
Si	2.995	3.018	2.993	3.019	2.979	2.986	3.024	3.015	2.994	2.986	2.981	2.999	2.995	2.988	2.987	3.009	2.989	3.12	3.020	3.020
Al	1.984	1.972	1.953	1.932	1.984	1.986	1.945	2.015	2.026	2.047	2.023	2.014	2.017	2.024	2.020	2.014	2.030	0.733	1.950	2.004
Ti	0.000	0.000	0.000	0.000	0.000	0.000	0.000	0.000	0.003	0.001	0.002	0.003	0.001	0.001	0.002	0.000	0.002	0.044	0.000	0.001
Cr	0.000	0.000	0.000	0.000	0.000	0.000	0.000	0.000	0.000	0.000	0.000	0.000	0.000	0.000	0.000	0.000	0.000	0.006	0.000	0.000
Fe	2.151	2.291	2.070	2.366	1.893	2.226	1.870	2.083	2.116	2.259	1.982	1.967	2.153	2.173	2.153	2.228	2.316	1.851	2.216	2.265
Mn	0.070	0.104	0.060	0.090	0.116	0.292	0.116	0.037	0.035	0.044	0.100	0.098	0.113	0.117	0.014	0.015	0.020	0.144	0.078	0.225
Mg	0.701	0.487	0.791	0.493	0.591	0.416	0.635	0.747	0.753	0.564	0.798	0.806	0.618	0.599	0.764	0.661	0.579	0.024	0.609	0.428
Ca	0.111	0.123	0.164	0.113	0.464	0.115	0.413	0.079	0.064	0.089	0.123	0.107	0.098	0.100	0.062	0.059	0.060	2.745	0.133	0.145
Na	0.000	0.000	0.000	0.000	0.000	0.000	0.000	0.008	0.003	0.002	0.000	0.000	0.000	0.000	0.000	0.000	0.002	0.000	0.000	0.000
K	0.000	0.000	0.000	0.000	0.000	0.000	0.000	0.000	0.000	0.001	0.000	0.000	0.000	0.000	0.000	0.000	0.000	0.000	0.000	0.000
Alm	0.709	0.762	0.671	0.772	0.618	0.730	0.616	0.707	0.713	0.764	0.660	0.661	0.722	0.727	0.719	0.752	0.779	0.362	0.730	0.739
Spe	0.023	0.035	0.019	0.030	0.038	0.096	0.038	0.013	0.012	0.010	0.033	0.033	0.038	0.039	0.005	0.005	0.007	0.031	0.026	0.074
Pyr	0.231	0.162	0.256	0.161	0.193	0.136	0.209	0.253	0.254	0.191	0.266	0.271	0.207	0.200	0.255	0.223	0.195	0.005	0.201	0.140
Grs	0.037	0.041	0.053	0.037	0.151	0.038	0.136	0.027	0.021	0.030	0.041	0.036	0.033	0.033	0.021	0.019	0.020	0.602	0.044	0.047
Mg/Hg+Fe	0.246	0.175	0.277	0.172	0.238	0.157	0.253	0.284	0.262	0.226	0.287	0.291	0.223	0.216	0.262	0.229	0.200	0.014	0.216	0.159
Fe/Hg+Fe	0.754	0.825	0.723	0.828	0.762	0.843	0.747	0.736	0.738	0.774	0.713	0.710	0.777	0.784	0.738	0.771	0.800	0.986	0.784	0.841

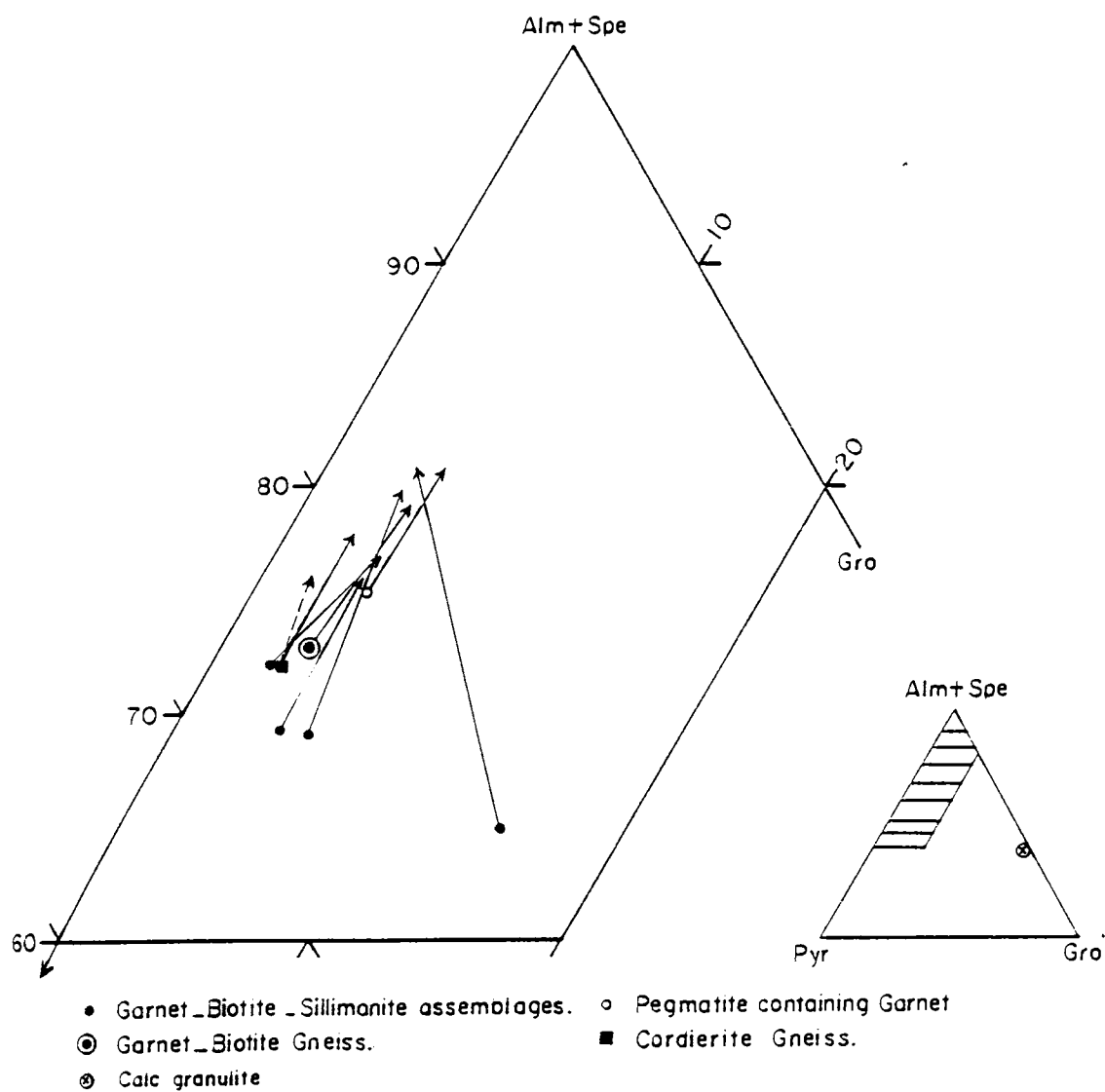


Fig. 113 Plot of garnet composition in terms of end-members. Compositional zoning is indicated by arrows pointing to rim compositions.

Enrichment of almandine towards rim is also expressed in chemical terms by a lower X_{Mg} ratio. In garnet - biotite-sillimanite gneiss sample, it shows a decrease from av.0.27 (core) to av.0.21 (rim). Chemical zoning with respect to Mg in garnet- biotite gneiss, shows a decrease from core (0.701) to rim (0.487 p.f.u)*.

The composition of garnet and its textural relationships with other minerals reflect different stages in the metamorphic evolution of rocks. The high Mg-cores of garnets bear evidence for a pre-metamorphic peak pressure history and the reduced X_{Mg}^{grt} at grain boundaries must be reflective of Fe-Mg diffusion exchange.

Fe/Fe+Mg ratio is greater than 1 in all garnets, with values showing an increase from core to rim. This ratio is in the range of 0.73 (av.core) to 0.79 (av.rim) in garnet-sillimanite- biotite gneisses and from 0.75 (core) to 0.83 (rim) in garnet- biotite gneiss. In cordierite-bearing granulites, Fe/Fe+Mg increases from 0.74 (core) to 0.80 towards rim, adjacent to cordierite.

In terms of Fe, Mg and Mn, all garnets from the granulite rocks are characterised by uniform low Mn contents of cores (0.014 to 0.123 p.f.u), consistent with high temperature diffusion during high-grade metamorphism (Tracy, 1982, Plank, 1987). In sillimanite-bearing granulite, Mn content (p.f.u)

* p.f.u. parts per formula unit.

slightly increases from core (av \sim 0.08) to rim (av 0.12). In garnet- biotite gneiss, garnet has low Mn (0.07 p.f.u) and Ca is 0.11 p.f.u, both showing a marginal increase towards rims (0.104 and 0.123 p.f.u respectively). In cordierite-bearing assemblages, Mn and Ca contents (0.015 and 0.062 p.f.u respectively) are low, compared to garnets of cordierite-free assemblages.

Zoning profiles of garnets from the garnet-biotite - sillimanite gneisses (ps.76 & 100) are shown in Fig.114 & 115. Compositional profiles for FeO, MgO, CaO and MnO across garnet, from a cordierite-bearing sample, is also shown in Fig.116. MgO decreases towards cordierite and quartz. FeO shows a counter-balancing profile. The magnitude of changes in Fe:Mg ratio is smaller in the vicinity of quartz and plagioclase, and greater, beside biotite or cordierite.

In general, these profiles show many characteristics of garnets from granulite terrains, such as a broad, relatively homogeneous core and a thin rim with significant variation in composition.

In calc granulites, no compositional zoning of garnet has been observed. The garnets are characterised by a remarkably high grossular content (59-61 mol %), while almandine is distinctly low at 36-38 mol %. Spessartine exhibits a range in value from 2.8 to 3.6 mol %. The ratio of Mg:(Mg+Fe) ranges from 0.009 to 0.022.

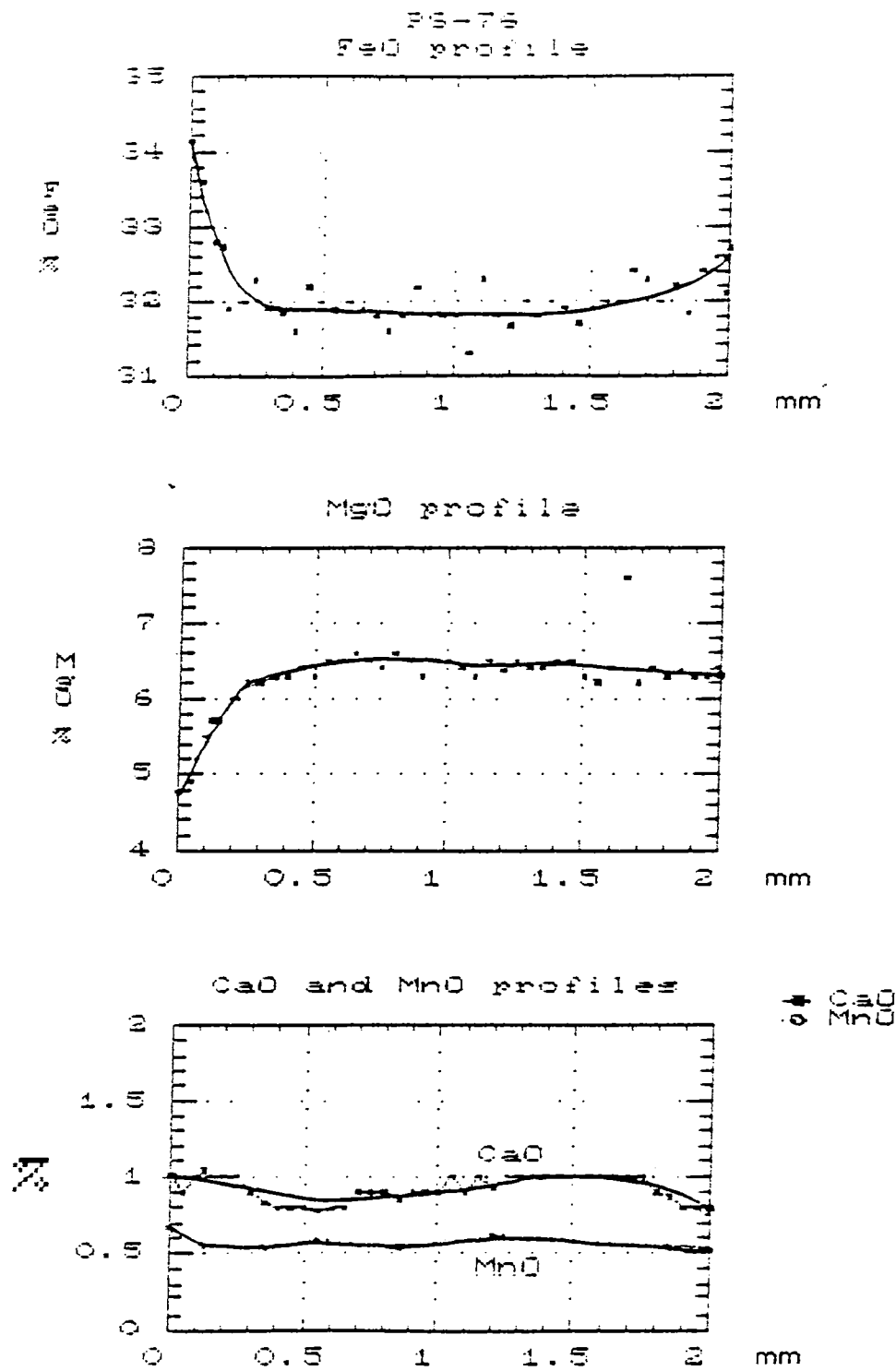


Fig.114 Compositional profiles of garnet from biotite to quartz in garnet-biotite-sillimanite gneiss (Ps.76).

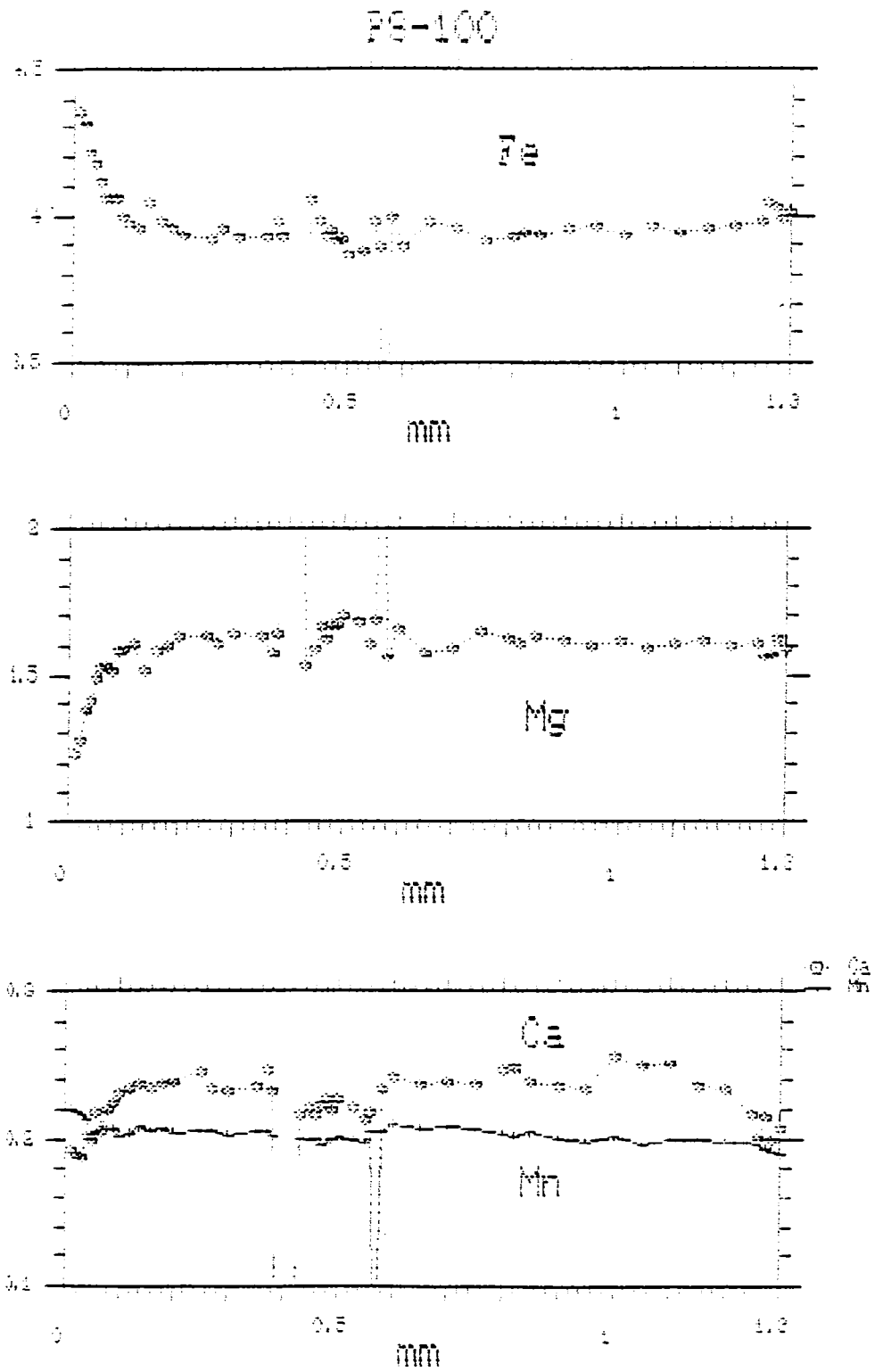


Fig.115 Compositional profiles of garnet from garnet-biotite-sillimanite gneiss (Ps.100).

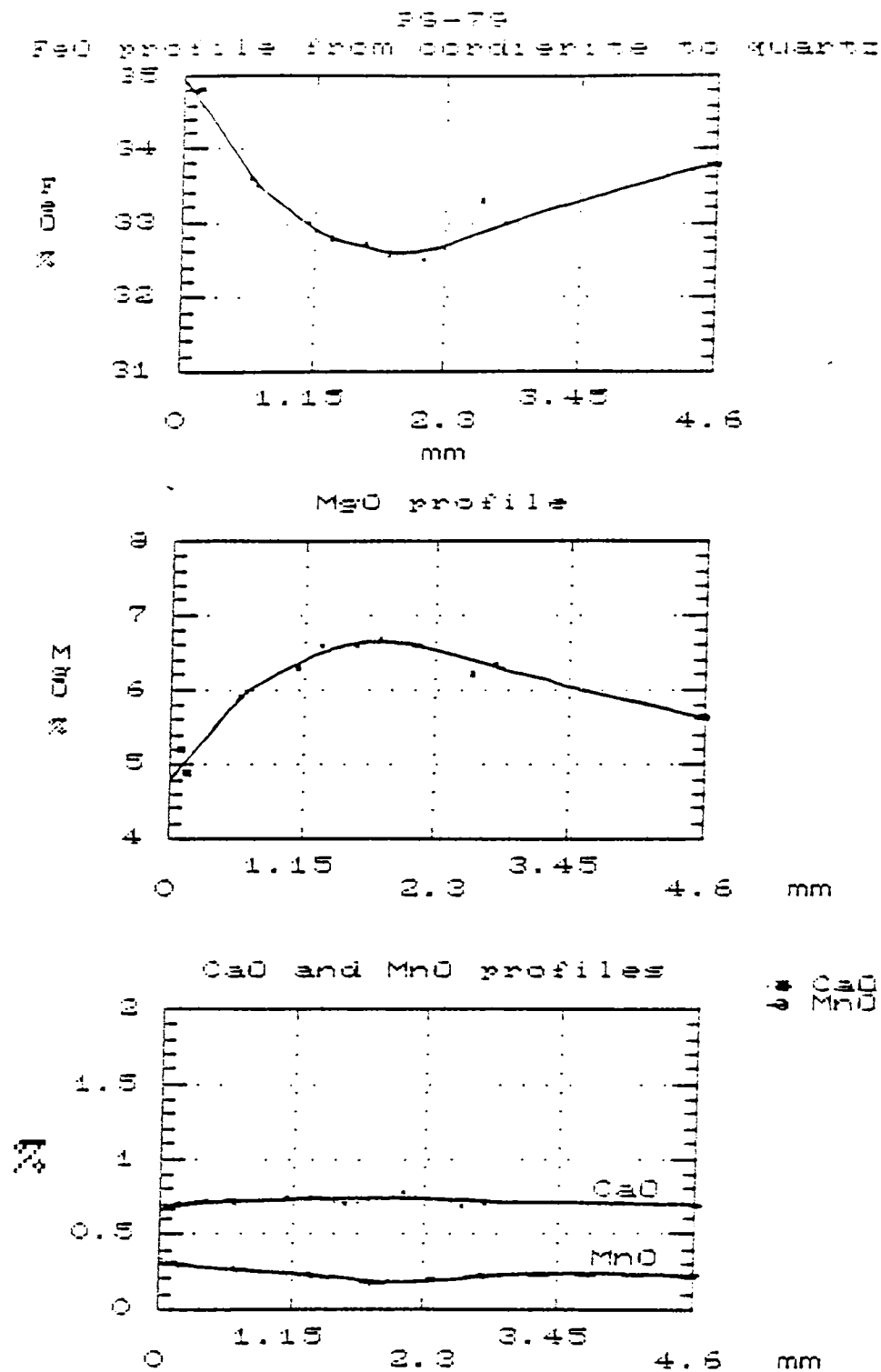


Fig.116 Compositional profiles of garnet from cordierite-bearing khondalite (Ps.79).

In pegmatites, all the end-member components, with the exception of pyrope, increases from core to rim. Almandine (mol %) varies from 73(core) to 74 (rim); spessartine from 2.6 to 7.4 and grossularite from 4.4 to 4.7 mol %. Pyrope shows a depletion from core (20.1) to rim (14 mol %).

On the whole, the almandine enrichment trend in garnet is more striking in the garnet-sillimanite-biotite samples, than in the pegmatites or garnet-biotite gneiss. In one of the garnet-biotite-sillimanite samples (ps.25a), zoning is also with respect to grossular contents (see Fig.113).

Increase in Fe, Ca and Mn and decrease in Mg indicate that the garnets maintained local equilibria during initial retrogression events. Since the garnets isolated from ferromagnesian minerals, such as those in contact with quartz and plagioclase, also show similar compositional variations though of less intensity, the rim compositions are suggested to be representative of their retrograde P-T evolution history and not due to simple Fe-Mg exchange during cooling.

V.2. BIOTITE

78 spot analyses were carried out in garnet-biotite-sillimanite-gneisses, 8 each in garnet-biotite gneisses and pegmatites and 5 each in migmatitic gneisses and granites. In the absence of data on H₂O contents, the structural formulae have been calculated on the basis of 22 oxygens.

(Table.15).

On the basis of their increasing Mg and decreasing Ti and Fe concentrations (atomic proportions), 3 groups of biotites, (biotite-I, II and III) have been distinguished; an assumption which goes well with the petrographic evidences too.

Matrix biotites in sillimanite-bearing samples contain high Ti (0.522 - 0.624 p.f.u) and Fe (1.972 - 2.570 p.f.u). Mg:Fe ratio increases from av.1.032 p.f.u in matrix biotite to av.1.432 towards contact zones with garnets and attains a maximum value in inclusion biotites (av. 2.37 p.f.u). Silica is less than 6 p.f.u and alumina (Al_2O_3) is 10-18 mol %, increasing slightly towards contact zones. Tetrahedral Al^{iv} is less than Al^{vi} , and is limited to 2.652 p.f.u in occupancy. A slight decrease (2.587 p.f.u) is observed towards rims.

In sillimanite-absent assemblages, Fe increases from 0.564 to 0.446 (p.f.u) towards contact with garnet. Weight percentage Al_2O_3 in biotite ranges from 17.89 to 18.38. Partitioning into Al^{vi} is more, compared to Al^{iv} (0.537 p.f.u). Tetrahedral aluminium increases to 2.713 near contacts and Si decreases to 5.287 p.f.u. Magnesium content (X_{Mg}^{Bt}) averages at 0.488.

In migmatitic gneisses, X_{Fe} of biotite is 0.47 and X_{Mg} is 0.53. Al^{iv} occupancy is 2.361 (p.f.u) and Mg is 2.834

(p.f.u). Mg is higher, compared to biotite in granites (2.231 p.f.u), while Fe is lower (2.504 p.f.u). Mn also is low (0.03 p.f.u.).

In granites, X_{Ti} in biotite is fairly uniform (0.486 p.f.u). It has high Al_{Ti} (3.099 p.f.u), Mn and Fe (0.066 and 2.739 p.f.u respectively), compared to the corresponding values of 2.531, 0.03 and 2.504 (p.f.u) in hornblende-biotite migmatitic gneiss sample (ps.19). Average X_{Mg}^{Bt} is 0.53 and Mg:Fe ratio is as high as 1.13 (av).

Matrix biotite in pegmatite has an average Fe value of 2.464 (p.f.u), which is lower (2.105 p.f.u) in inclusions. Titanium shows a positive correlation with Fe and exhibits a striking decrease from 0.419 (in matrix-biotite) to 0.026 p.f.u in inclusions. Values of X_{Mg} , correspondingly increases from 0.463 to 0.556 and Mg:Fe ratio increases from 0.86 to 1.25. Al^{iv} occupancy is lower in inclusion biotite (2.60 p.f.u), compared to matrix biotite.

Plots of Al^{iv} vs $Mg / (Mg+Fe)_{total}$ (Fig.117a) show that the matrix biotite composition corresponds to the Fe-rich varieties (Mg:Fe < 2:1) while, the rims and especially the inclusions, trend towards Mg-rich (Mg:Fe > 2:1) or phlogopite composition. The overall compositional variation of biotite is better described in terms of X_{Mg} vs. Ti plots (Fig.117b). In garnet-biotite gneiss however, the shift is towards siderophyllite.

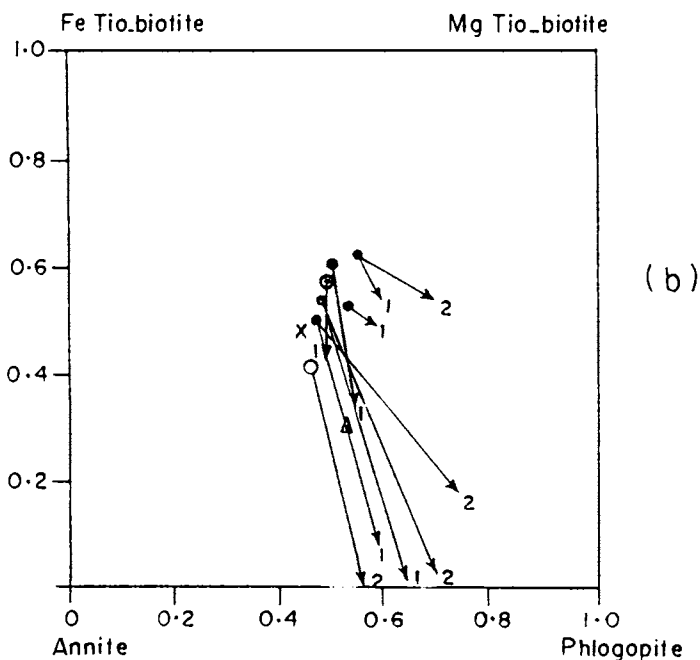
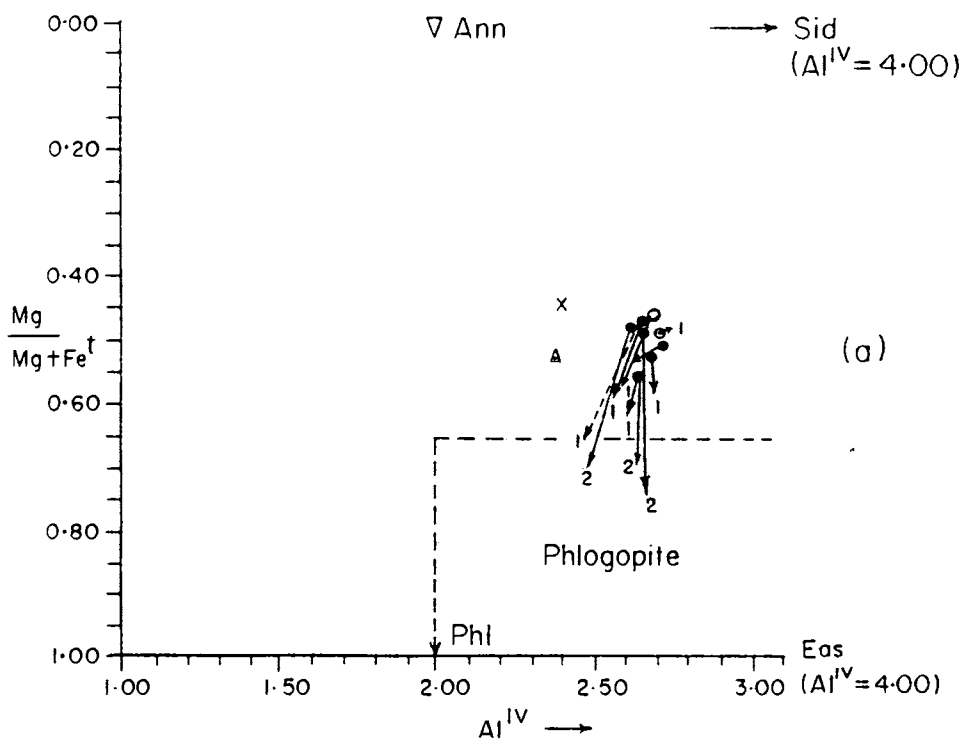


Fig.117 (a) Al_{IV} Vs. $Mg/Mg+Fe^t$ plot of biotites. (b) Plot of biotite composition in terms of XMg and Ti. Arrows indicate compositional variations of biotite from (1) matrix to contact zone and (2) matrix to inclusion. Symbols : x-granite (av.4) and Δ hornblende-biotite migmatitic gneiss (av.5). All the other symbols are the same as in Fig.113.

The general Mg enrichment trend - matrix biotite < biotite adjacent to garnet biotite inclusion, indicates chemical exchange with host garnet. Aluminium, in general is high (10-20 wt %) and is incorporated mainly into the tetrahedral layer. High contents of TiO_2 (~ 4.97 wt %) in matrix biotite of granulitic rocks is consistent with their higher metamorphic grade. The high X_{Fe} ratios (~ 0.4-0.6) may be suggestive of a strongly reducing environment. The clear shift towards phlogopite also shows that the composition of biotite is controlled by metamorphic conditions possibly resulting from re-equilibration with garnet during cooling.

V.3. ALKALI FELDSPAR

A total of 50 spot analyses were carried out (23 in sillimanite-bearing assemblages, 3 in calc granulite, 4 in migmatitic gneisses and 20 in granites (Table.16)).

Albite content of alkali feldspar (matrix) in sillimanite-bearing assemblages ranges between 15.4 and 21.5 mol %. Iron is low (0.002 p.f.u) and Mg is absent. Orthoclase varies between 78 and 84 mol % and anorthite is limited to 0.3 to 0.6 (mol %) range. At plagioclase contacts, 'Or' content (85-91mol %) increases while, Ab (8.9-14.8 mol %) shows a corresponding decrease. In sillimanite-absent assemblages, orthoclase averages around 85 mol % while, Anorthite content is 0.2 mol % and albite is 15.4 mol %.

TABLE 16 MICROPROBE ANALYSIS OF ALKALI FELDSPAR

Rock type Anal.No.	Gar-Bt-Gn PS.14		Gar-Bt-Sill-Gn PS.76		Gar-Bt-Sill-Gn PS.100		Cordierite - khondalite PS.79		Calc- granulite PS.35		Hb-Bt-Gn PS.19		Granite PS.11	
	inside 4	at plag 1	inside 4	at plag 1	inside 4	at plag 1	perth 1	all 6	at plag 3	Av.3	4	perth 4	at plag 3	all 13
SiO ₂	62.99	64.20	63.86	64.09	64.33	65.32	64.47	64.31	63.71	64.37	64.95	63.79	64.35	
TiO ₂	0.06	0.00	0.00	0.00	0.00	0.04	0.03	0.03	0.00	0.03	0.03	0.03	0.04	
Al ₂ O ₃	18.76	19.52	19.06	19.31	19.21	19.73	19.54	19.25	18.11	18.28	18.85	18.86	18.84	
Feo	0.02	0.02	0.03	0.00	0.00	0.05	0.02	0.00	0.12	0.04	0.05	0.03	0.05	
Mno	0.03	0.00	0.00	0.00	0.00	0.00	0.01	0.00	0.00	0.03	0.01	0.01	0.01	
Mgo	0.00	0.00	0.00	0.00	0.00	0.00	0.00	0.00	0.00	0.01	0.00	0.01	0.01	
CaO	0.03	0.13	0.05	0.07	0.03	0.25	0.15	0.04	0.02	0.04	0.17	0.04	0.12	
Na ₂ O	1.61	2.39	1.63	1.73	0.99	5.48	3.07	1.59	0.79	1.39	2.15	1.02	1.66	
K ₂ O	13.45	13.18	14.19	14.31	15.32	8.95	12.43	14.58	14.81	14.72	13.44	15.37	14.30	
Total	96.92	99.44	98.82	99.50	99.87	99.82	99.72	99.8	97.56	98.91	99.66	99.15	99.38	
						BASED ON OI, #0.24								
Si	8.925	8.866	8.904	8.881	8.904	8.861	8.861	8.892	9.006	8.984	8.955	8.908	8.927	
Al	3.132	3.177	3.132	3.154	3.134	3.155	3.165	3.137	3.018	3.007	3.063	3.105	3.081	
Ti	0.003	0.000	0.000	0.000	0.000	0.004	0.003	0.003	0.000	0.003	0.003	0.003	0.004	
Fe	0.003	0.002	0.003	0.000	0.000	0.006	0.002	0.000	0.015	0.005	0.006	0.004	0.006	
Mn	0.003	0.000	0.000	0.000	0.000	0.000	0.001	0.000	0.000	0.004	0.001	0.001	0.001	
Mg	0.000	0.000	0.000	0.000	0.000	0.000	0.000	0.000	0.000	0.002	0.000	0.002	0.002	
Ca	0.006	0.019	0.007	0.010	0.004	0.036	0.022	0.006	0.003	0.006	0.026	0.006	0.018	
Na	0.444	0.640	0.441	0.465	0.266	1.441	0.818	0.426	0.216	0.376	0.576	0.276	0.447	
K	2.430	2.322	2.524	2.530	2.705	1.549	2.180	2.572	2.670	2.621	2.365	2.738	2.531	
An	0.002	0.006	0.003	0.003	0.002	0.012	0.007	0.002	0.001	0.002	0.009	0.002	0.006	
Ab	0.154	0.215	0.148	0.155	0.089	0.476	0.271	0.142	0.075	0.125	0.194	0.091	0.149	
Or	0.845	0.779	0.849	0.842	0.909	0.512	0.722	0.856	0.924	0.873	0.797	0.907	0.852	

* Measured with 50µm electron beam

In cordierite-bearing assemblages, the composition of alkali feldspar is approximated to orthoclase 72.2 mol %, albite, 27.1 mol % and anorthite, 0.7 mol %. Towards plagioclase contacts, orthoclase increases to 85.6 while, albite and anorthite reduces to 14.2 and 0.2 mol % respectively. The Na-less rim of alkali feldspar must have formed at a later stage. Perthites have a lower orthoclase content (51.2 mol %) and higher mol.percentage of albite (47.6 mol %) and anorthite (1.2 mol %).

Average of 3 analyses of alkali feldspar in calc-granulites show an orthoclase value of 92.4 mol %. Iron content is 0.015 p.f.u and is higher compared to all the other rock types. In migmatitic gneisses, average of 4 spot analyses indicate more or less uniform composition. Orthoclase content is 87.3 mol %, albite, 12.5 mol % and anorthite (0.2 mol %). In granites, albite in orthoclase constitutes less than 20 mol %. On contact with plagioclase, Ca is depleted from 0.018 to 0.006 p.f.u while, K is enriched from 2.53, to 2.738 p.f.u. Iron concentration in perthites is slightly higher (~ 0.006 p.f.u), compared to that at plagioclase contacts (~ 0.004 p.f.u). This is also reflected in the higher temperature estimates (Bingen et al, 1990) for the alkali feldspar (perthite) -plagioclase (average) pairs (see Chapter.VI). Slightly higher FeO and CaO contents of alkali feldspar in granites, with respect to that reported in migmatitic gneisses, is also consistent with the higher

temperature of the former. Compositional plots in the An-Or-Ab diagram (Fig.118 a & b) of Fuhrman & Lindsley (1988) fall in a narrow compositional field, below 650°C isotherm (drawn using the experimental data of Seck, (1971, in Fuhrman & Lindsley, 1988) at a pressure of 5 kbars. This temperature is taken only as an approximate indication because of the uncertainties involved in P correction and analytical errors in estimation of calcium concentrations.

In summary, the alkali feldspars are characterised by small Ca (~0.013 p.f.u, average) and Fe (~0.004 p.f.u). Anorthite content of alkali feldspar is largely controlled by the rock chemistry, especially the $\text{Na}_2\text{O} / (\text{Na}_2\text{O} + \text{K}_2\text{O})$ ratio of the host rocks. The 'apparent' low temperatures (<650°C) obtained from the An-Or-Ab ternary plots (Fuhrman & Lindsley, 1988), are distinctly lower than the expected temperature in granulite terrains and might characterise the late metamorphic history of the rocks.

V.4. PLAGIOCLASE

Results of 63 spot analyses of plagioclase are given in Table.17.

The grains are unzoned and exhibits more or less a uniform composition. In sillimanite-bearing metapelitic assemblages, plagioclase has a uniform composition corresponding to oligoclase, maximum compositional variation in terms of anorthite being 22.6 to 31.8 mol %. In one of

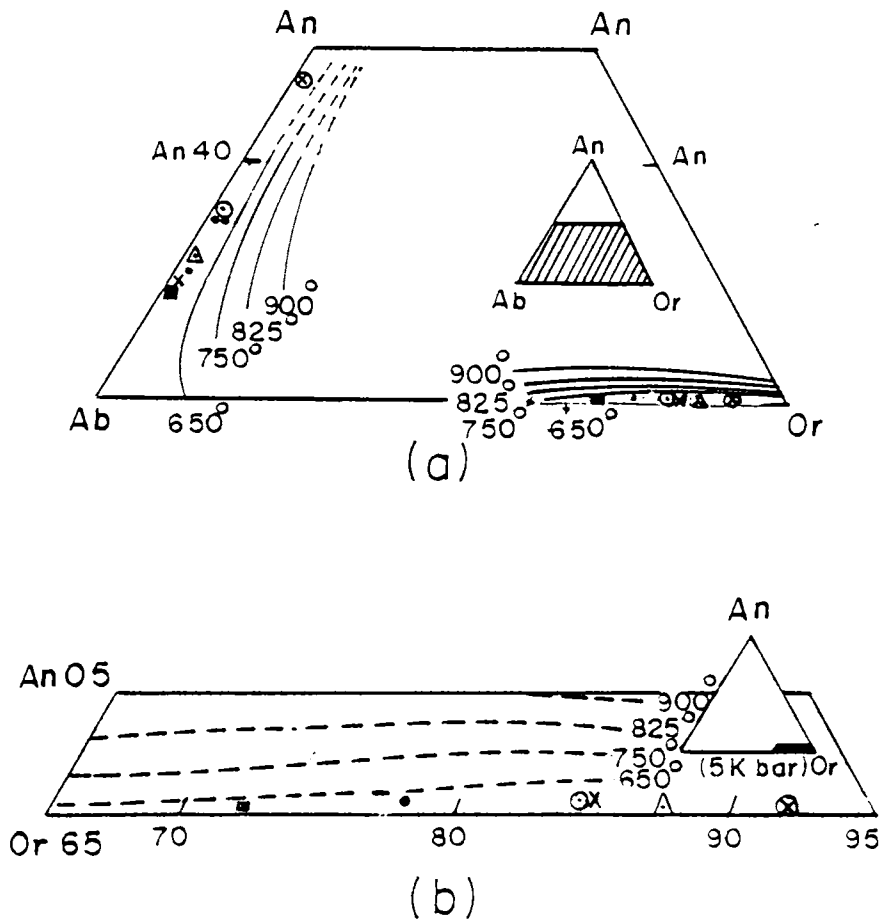


Fig.118 Plots of average composition of alkali feldspar and plagioclase in An-Or-Ab ternary diagram. (b) Enlarged portion of the diagram showing alkali feldspar plots. Isotherms, after Fuhrman & Lindsley (1988) based on experimental data of Seck (1971, in Fuhrman & Lindsley, 1988). Symbols as in Fig.113 & 117.

TABLE 17 MICROPROBE ANALYSES OF PLAGIOCLASE

Anal. No.	Gar-Bt-Gn		Gar-Bt-Sill		Gar-Bt-Sill-Gn		Gar-Bt-Sill-Gn		Gar-Bt-Sill-Gn		Cord- khondalites		Calc-gra- nellites		Hb-Bt-Gn		Granite			
	Ps.14	-Gn	Ps.16	Ps.25(a)	Ps.76	Incl.1	Ps.100	Ps.100	Ps.19	Ps.11	Av(5)	Av(5)	Av(4)	Av(5)	Av(5)	Av(5)	Av(5)	Av(5)		
	58.68	59.47	60.14	62.59	60.34	59.41	63.23	53.00	62.34	63.14										
SiO ₂	0.01	0.00	0.00	0.00	0.00	0.00	0.10	0.08	0.01	0.01										
TiO ₂	25.27	25.10	24.75	23.91	26.00	25.96	23.81	28.54	24.05	23.31										
Al ₂ O ₃	0.05	0.02	0.08	0.04	0.00	0.00	0.02	0.35	0.10	0.09										
FeO	0.01	0.00	0.00	0.01	0.00	0.00	0.01	0.00	0.01	0.00										
MnO	0.01	0.00	0.00	0.01	0.00	0.00	0.00	0.00	0.01	0.00										
MgO	6.93	6.63	6.36	4.69	6.54	7.05	3.85	11.59	5.16	4.08										
CaO	7.50	7.76	8.08	8.71	7.71	7.58	9.39	4.95	8.49	9.26										
Na ₂ O	0.25	0.14	0.20	0.25	0.06	0.22	0.23	0.15	0.25	0.26										
K ₂ O																				
Total	98.7	99.15	99.57	100.21	100.64	100.21	100.64	98.48	100.42	100.14										
				BASED ON OX. NO. 24																
Si	7.950	8.016	8.070	8.293	7.993	7.932	8.333	7.320	8.255	8.368										
Al	4.050	3.987	3.939	3.734	4.060	4.985	3.699	5.400	3.754	3.641										
Ti	0.001	0.000	0.000	0.000	0.000	0.000	0.010	0.003	0.001	0.001										
Fe	0.006	0.003	0.009	0.004	0.000	0.000	0.002	0.042	0.011	0.009										
Mn	0.001	0.000	0.000	0.002	0.000	0.000	0.001	0.000	0.001	0.000										
Mg	0.001	0.000	0.000	0.002	0.000	0.000	0.000	0.000	0.002	0.000										
Ca	1.008	0.957	0.915	0.666	0.929	1.009	0.544	1.713	0.732	0.579										
Na	1.974	2.028	2.103	2.238	1.980	1.962	2.400	1.323	2.180	2.379										
K	0.042	0.029	0.036	0.042	0.010	0.037	0.039	0.021	0.042	0.043										
An	0.333	0.318	0.299	0.226	0.318	0.335	0.182	0.561	0.248	0.193										
Ab	0.652	0.673	0.689	0.759	0.678	0.652	0.805	0.433	0.738	0.793										
Or	0.015	0.009	0.011	0.014	0.003	0.012	0.013	0.006	0.014	0.014										

Measured with focussed electron beam.

the samples (ps.76), pure albite occurs at the plagioclase-alkali feldspar contact zones and orthoclase content in plagioclase inclusion is reduced to 0.3 mol %, as compared to 1.43 mol % of matrix plagioclase.

In garnet-biotite gneiss, the compositional variation of plagioclase in terms of anorthite, is from An₃₀ to An₃₇ (oligoclase). FeO content is low (0.045 wt %) and orthoclase averages around 1.5 mol. percentage.

In cordierite-bearing khondalites, the average composition of plagioclase corresponds to albite, the mol. percentages of anorthite and orthoclase being 18.2 and 1.30 respectively.

In calc granulite, a wide range in composition is observed with an average value of 56 mol % of anorthite (andesine). Potassium content is low at 0.021 p.f.u. In migmatitic gneisses, plagioclase shows a composition corresponding to oligoclase (An_{24.8}). Iron and potassium are low at 0.011 p.f.u and 0.042 p.f.u respectively. In granites also, the plagioclase characteristically possesses low Fe and K⁺ (0.009 and 0.043 p.f.u respectively).

In the An-Or-Ab ternary diagram of Fuhrman & Lindsley (1988), with isotherms drawn for 5 kbars, all the plots of plagioclase fall below the 650°C isotherm (see Fig.118a). Plagioclase of sillimanite-absent assemblages occupy intermediate anorthite positions while, those of the

cordierite-bearing rocks fall close to that of granites.

V.5. CORDIERITE

Results of six spot analyses (Table.18) made across the cordierite grains reveal the absence of any substantial difference in composition between core and rim. These are Mg-rich (8.43 wt % MgO) and contain comparatively high percentages of FeO also (7.84 wt %). Na and K proportions are very low (< 0.03 & 0.001 p.f.u respectively). Manganese is present only in trace amounts (< 0.004 p.f.u). Values of X_{Fe} shows a slight decrease from 0.36 (core) to 0.33 (rim). Decrease in Fe:Mg ratio of cordierite towards rim is expressed by a lowering of temperature also (see Chapter.VI). Microprobe totals are below 98% indicating its hydrous nature. Total amount of cations on the basis of 18 oxygens are close to the theoretical value of 11, suggesting water contents of 2.5-3.5 wt %.

V.6. CLINOPYROXENE

Microprobe analyses (10 points) of the clinopyroxenes from calc granulites (Table.19) show wide compositional variations. They fall into two sets, one set of analyses showing an Fe-rich composition (0.620 p.f.u, av), the other set being relatively Fe-poor (0.376 p.f.u, av). Mg numbers (Mg/Mg+Fe) correspondingly range from 0.382 to 0.632. The Fe-rich set has Al_2O_3 in the range of 2-4 wt % while, in the Fe-poor set it is as low as 0.2 to 1 wt %.

TABLE.18 MICROPROBE ANALYSIS OF CORDIERITE

Rock type	Cordierite - bearing Khondalite (Ps.79)	
Anal. No.	Core (Av.5)	Rim 1
SiO ₂	48.19	48.80
TiO ₂	0.00	0.02
Al ₂ O ₃	32.43	32.54
FeO	8.15	7.53
MgO	8.28	8.59
MnO	0.02	0.03
CaO	0.01	0.01
Na ₂ O	0.16	0.14
K ₂ O	0.00	0.01
Total	97.24	97.24

on the basis of ox no.18

Si	5.012	5.035
Ti	0.000	0.002
Al	3.976	3.958
Fe	0.709	0.650
Mg	1.284	1.321
Mn	0.002	0.003
Ca	0.001	0.001
Na	0.032	0.028
K	0.000	0.001
X _{Fe}	0.356	0.330
X _{Mg}	0.644	0.670
Mg/Mg+Fe	0.640	0.670

The structural formulae of the Fe-poor pyroxenes have been reformulated and cations are distributed to different sites as shown below:-

Si (1.959), Al³⁺ (0.0064) and Fe³⁺ (0.0346), occupy the 'T' site; Ti⁴⁺ (0.0006), Fe³⁺ (0.0384), Mg²⁺ (0.646), Mn²⁺ (0.0116) and Cr²⁺ (0.0004) occupy the M₁-site while, Ca²⁺ (0.968), Na⁺ (0.0312) and Mn²⁺ (0.0284) are allocated to the M₂-site. For the Fe-rich varieties, the ideal site occupancy of cations between T, M₁ and M₂ sites of pyroxenes are as follows:-

'T' site is occupied by Si (1.851) and Al (0.149), M₁-site by Fe³⁺ (0.152), Al³⁺ (0.037), Ti (0.006), Cr (0.001), Mg (0.383) and Fe²⁺ (0.421). M₂-site is allocated to Fe²⁺ (0.047), Mn (0.0312), Ca (0.946) and Na (0.053).

Considering both M₁ and M₂ as a single M-site, in order to avoid the difference between the real and ideal site occupancies, the pyroxene has been plotted in the Q-J diagram (Q = Ca+Mg+Fe²⁺ and J = 2Na) of Morimoto et al (1988). The plots fall in the quadrilateral field Ca-Mg-Fe pyroxenes, limited by the lines representing Q+J = 2 and Q+J = 1.5 (Fig.119). These Ca-Mg-Fe clinopyroxenes defined on the basis of symmetry and relative amounts of Ca₂Si₂O₆ (Wo), Mg₂Si₂O₆ (En) and Fe₂²⁺Si₂O₆ (Fs) (after normalising the composition to Ca+Mg+Fe = 100, where Fe = Fe²⁺ + Fe³⁺ + Mn²⁺), indicate a solid solution between hedenbergite and

TABLE. 19 MICROPROBE ANALYSES OF CLINOPYROXENE

Anal. No.	11	12	15	18	19	32	33	36	37	38
SiO ₂	50.88	51.12	50.61	49.18	48.03	47.78	44.23	45.92	44.1	45.88
TiO ₂	0.00	0.00	0.06	0.03	0.00	0.10	0.24	0.23	0.27	0.20
Al ₂ O ₃	0.20	0.45	1.07	0.57	0.60	2.52	4.52	4.15	4.06	4.09
Cr ₂ O ₃	0.00	0.00	0.00	0.00	0.05	0.00	0.03	0.00	0.05	0.00
Feo	10.98	10.33	12.26	11.90	11.82	17.80	17.66	19.03	18.21	18.43
Mno	1.45	1.11	1.21	1.13	1.17	0.95	0.99	0.79	0.96	0.83
Mgo	11.49	12.01	10.54	10.43	10.82	7.01	6.21	6.03	6.17	6.19
CaO	23.40	23.26	22.86	22.57	23.09	22.07	21.43	21.89	21.63	21.56
Na ₂ O	0.18	0.21	0.37	0.25	0.21	0.55	0.69	0.70	0.68	0.73
K ₂ O	0.00	0.00	0.00	0.00	0.00	0.00	0.00	0.00	0.00	0.00
Total	98.58	98.49	98.98	96.06	95.79	98.78	96.00	98.74	96.13	97.19

ON THE BASIS OF 6 OXYGENS										
Si	1.971	1.971	1.959	1.963	1.932	1.905	1.826	1.846	1.826	1.854
Al	0.009	0.020	0.041	0.027	0.028	0.095	0.174	0.154	0.174	0.146
Al	0.000	0.000	0.007	0.000	0.000	0.028	0.046	0.043	0.024	0.049
Ti	0.000	0.000	0.002	0.001	0.000	0.003	0.007	0.007	0.008	0.006
Cr	0.000	0.000	0.000	0.000	0.002	0.000	0.001	0.000	0.002	0.000
Fe	0.356	0.333	0.397	0.397	0.398	0.594	0.610	0.640	0.631	0.623
Mn	0.048	0.036	0.040	0.038	0.040	0.032	0.035	0.027	0.034	0.028
Mg	0.663	0.690	0.608	0.621	0.649	0.417	0.382	0.361	0.381	0.373
Ca	0.971	0.961	0.948	0.965	0.995	0.943	0.948	0.943	0.960	0.934
Na	0.014	0.016	0.028	0.019	0.016	0.043	0.055	0.055	0.055	0.057
K	0.000	0.000	0.000	0.000	0.000	0.000	0.000	0.000	0.000	0.000
Mg	0.333	0.348	0.311	0.313	0.316	0.218	0.197	0.186	0.193	0.193
Fe	0.179	0.168	0.203	0.200	0.195	0.304	0.314	0.329	0.320	0.323
Ca	0.498	0.484	0.485	0.487	0.487	0.483	0.489	0.485	0.487	0.484
Mg/Fe+Mg	0.651	0.675	0.605	0.610	0.620	0.412	0.385	0.361	0.377	0.374

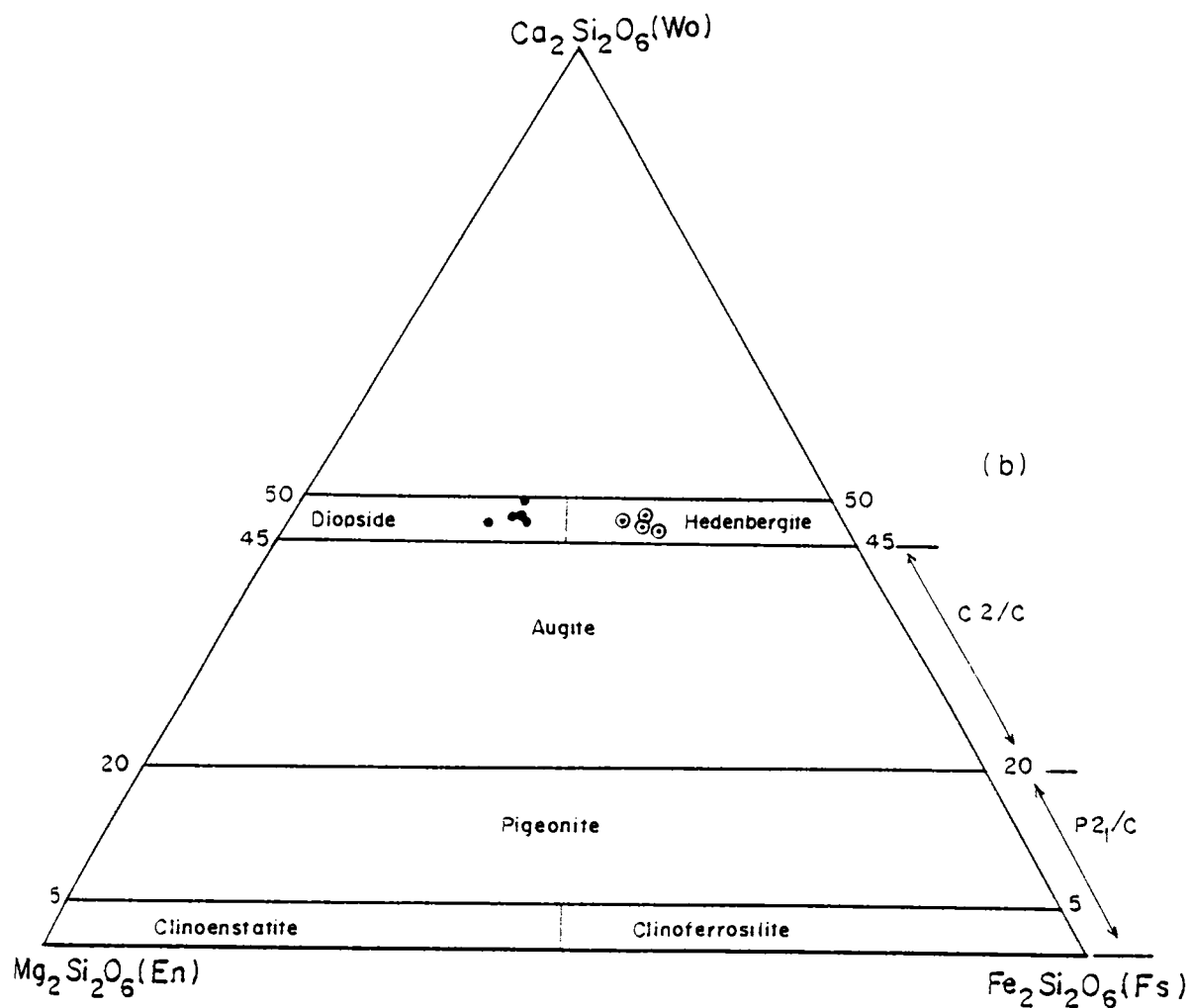


Fig.120 Plots of pyroxenes in the $\text{Ca}_2\text{Si}_2\text{O}_6$ - $\text{Mg}_2\text{Si}_2\text{O}_6$ - $\text{Fe}_2\text{Si}_2\text{O}_6$ (after Morimoto et al, 1988). C2/C and P₂₁/C denote their space groups.

diopside series (Fig.120).

The large variation in Mg/Mg+Fe and Ca/Ca+Fe+Mg of the two sets of clinopyroxenes imply that the mechanism of equilibration was a combination of cation exchange and solution regrowth. More specifically, the change in composition is related to the incomplete re-equilibration during decrease in temperature (see also Chapter.VI).

V.7. AMPHIBOLES

Analyses (Table.20) of amphiboles in calc granulite (based on 23 oxygen), show an atomic proportion of 6.957 p.f.u for silica and 1.043 p.f.u for Al^{iv}, both occupying the T site. Tetrahedral Al (0.271), Ti⁴⁺ (0.019), Cr³⁺ (0.025), Mg²⁺ (2.371), Mn²⁺ (0.120) and total Fe (2.470) occupy the octahedral sites M₁, M₂ and M₃. Eight co-ordinated sites (M₄) are occupied by both Ca²⁺ (1.9765 p.f.u) and Na⁺ (0.0235 p.f.u). A part of Na (0.4355) and K (0.136) are distributed into A-site. No zoning is apparent. Compared to Al_{total} (1.3135 p.f.u), Ti contents are low (0.015 to 0.026 p.f.u), both showing antipathic relationship with respect to Mg/Mg+Fe^t (Fig.121a). Values of X_{Mg} ranges between 0.42 and 0.55 and total Al, between 0.967 and 1.787 p.f.u.

Amphibole in hornblende-biotite migmatitic gneiss (ps.19) has almost a uniform composition. (Table.20) they contain 1.869 p.f.u (av) of Ca and 1.00 p.f.u (av) of Na.

TABLE.20 MICROPROBE ANALYSES OF AMPHIBOLE

Rock type	Calc granulite			Hb-Bt-Gn	
Anal. No.	Ps.35			Ps.19	
	3	4	20	21	Av(6)
Elements					
SiO ₂	46.09	47.43	41.61	44.47	43.65
TiO ₂	0.13	0.13	0.22	0.18	0.94
Al ₂ O ₃	5.27	5.73	9.55	8.11	9.6
Cr ₂ O ₃	0.00	0.00	0.05	0.03	0.00
Feo	16.99	17.87	20.23	19.11	18.18
Mno	0.83	0.93	0.86	1.05	0.36
Mgo	11.60	11.48	8.22	9.79	10.62
CaO	12.04	12.01	11.85	11.69	11.49
Na ₂ O	0.68	0.76	1.20	0.81	1.56
K ₂ O	0.57	0.47	1.03	0.67	1.09
Total	94.20	96.81	94.82	95.91	97.49

ON THE BASIS OF 23 OXYGENS.

Si	7.171	7.180	6.604	6.374	6.624
Al	0.829	0.820	1.396	1.126	1.376
Al	0.138	0.202	0.391	0.352	0.341
Ti	0.015	0.015	0.026	0.021	0.107
Cr	0.000	0.000	0.006	0.004	0.000
Fe	2.211	2.262	2.685	2.471	2.307
Mn	0.109	0.119	0.116	0.137	0.046
Mg	2.691	2.591	1.945	2.256	2.403
Ca	2.007	1.948	2.015	1.936	1.869
Na	0.205	0.223	0.369	0.243	0.459
K	0.113	0.091	0.209	0.132	0.211
Mg/Fe+Mg	0.549	0.534	0.420	0.477	0.510

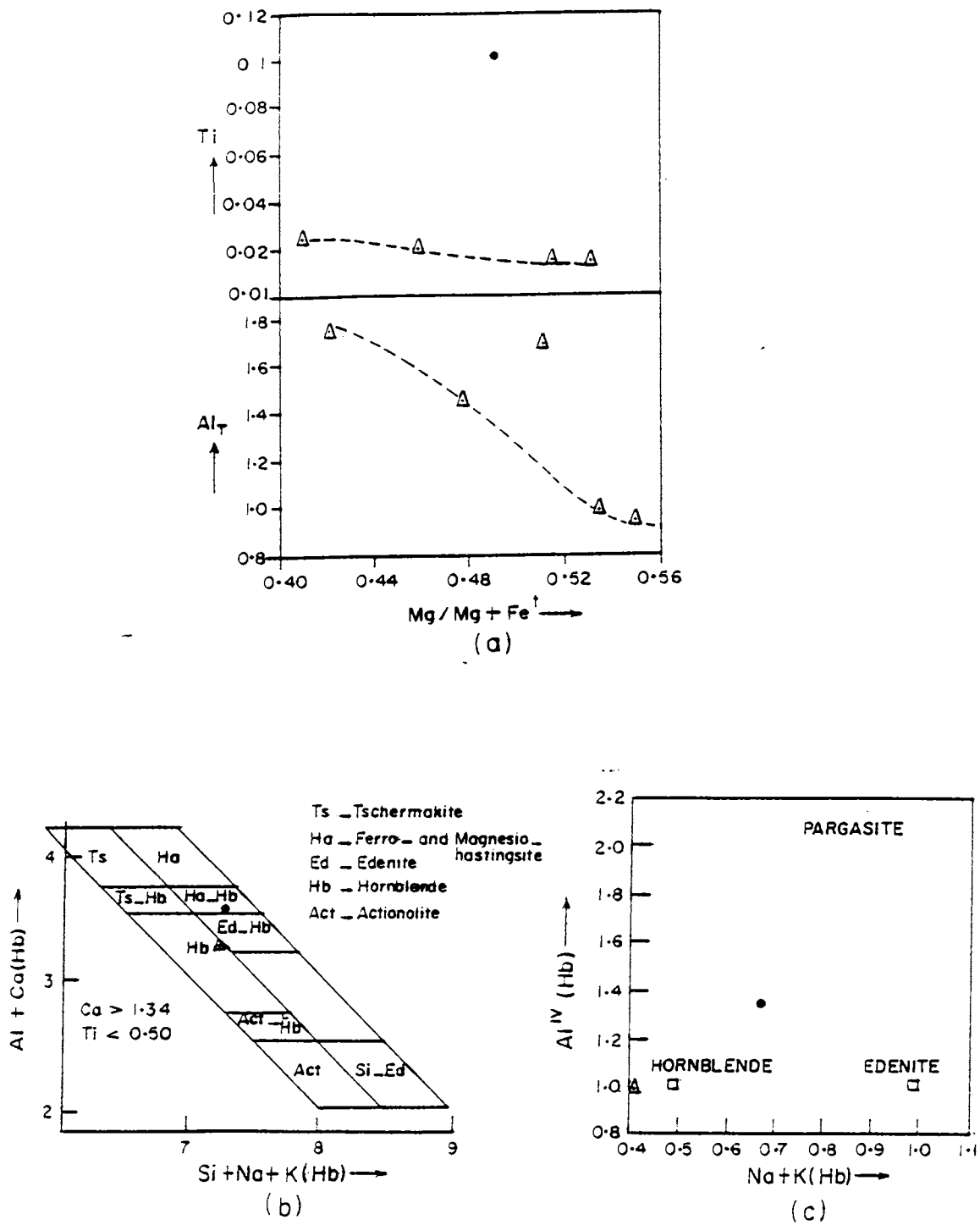


Fig.121 (a) $Mg/Mg+Fe^t$ Vs. Al_{total} and Ti (atoms p.f.u) in amphiboles (b) Plots of amphiboles in (Al+Ca) Vs. (Si+Na+K) diagram (Giret et al, 1980). (c) Plots of Al^{IV} Vs. (Na+K) of amphiboles (Robinson et al, 1971). Filled circles represent av. composition of hornblende-biotite gneiss and small triangles

Distribution of cations between T, M₁, M₂, M₃, M₄ and A sites are as shown below:-

Si ⁴⁺	--	6.624	T site
Al ^{iv}	--	1.376	
Al ^{vi}	--	0.341	M ₁ M ₂ M ₃
Ti ⁴⁺	--	0.104	
Cr ³⁺	--	0.000	
Mg	--	2.403	
Mn ²⁺	--	0.046	
Fe ³⁺ +Fe ²⁺	2.307		
Mn ²⁺	--	0.000	M ₄
Ca ²⁺	--	1.869	
Na ⁺	--	0.131	A
Na	--	0.129	
K	--	0.211	

Iron, silica and Mg/Mg+Fe²⁺ contents of amphibole in calc granulite are lower (2.307, 6.624 and 0.510 respectively) compared to values reported for granulite facies rocks. However, Ti (0.107 p.f.u) and Al_T (1.717 p.f.u) values are higher.

Amphiboles of calc granulites and migmatitic gneisses have a calcium content in the range of 1.9 to 2.0 (p.f.u) which corresponds to calcic types. The Al^{iv} vs (Al^{vi} + Si) plots of Leake (1978) could not be used since, most of the analyses fall outside the range specified.

Based on the classification of Giret et al (1980), mineral analyses of hornblende from the gneisses and granulitic rocks plot respectively in the fields of hornblende and ferro-magnesian-hastingsite (Fig.121b). In the binary plot of (Na+K) vs Al^{iv} (Fig.121c) after Robinson et al (1971), amphiboles from granulites lie close to the hornblende composition while, that from migmatitic gneisses lie towards pargasite field. This may be related to an origin of amphibole in migmatitic gneisses by the retrogressive breakdown of pyroxenes and plagioclase of the host rocks. Total aluminium content of amphiboles in calc-granulites is higher (1.787 p.f.u), compared to that in migmatitic gneiss (1.717 p.f.u), reflecting the higher temperature and increased grade of metamorphism of the former. (Leake; 1962) Kostyuk, 1970; Hietanen, 1974; Graham, 1974; Helz, 1982).

CHAPTER VI

CONDITIONS OF METAMORPHISM

The static process of metamorphism of rocks involving changes in pressure, temperature, mineral and fluid composition, is not directly observable. The equilibrium mineral assemblages in a metamorphic rock often preserves only a partial, favourably preserved record of a continuum of crustal conditions attained in response to major tectonic processes, leaving only the later, post-peak or retrograde segments of the P-T paths to base inferences upon.

Determination of pressure - temperature - time path provides a valuable constraint on the development of tectonic models of regional metamorphism. Geothermobarometers provide quantitative data on specific P-T points and help in retrieving prograde as well as retrograde P-T trajectories of the terrain provided, chemical equilibrium of mineral assemblages is preserved during chemical zoning (Bohlen, 1987; Harley, 1985).

Despite the tremendous momentum gained and attention devoted to the development of various P-T sensors in recent years, their application to petrological problems is fraught with serious shortcomings and limitations. The problem of 'resetting' during cooling

resulting in temperatures lower than 'peak' temperatures had been recognized by Bohlen and Essene (1977, 1978); O'Hara, (1977) O'Hara and Yarwood (1978) and Indares and Martignole (1985). The disquieting realization that the temperature obtained from a geothermometer represents only a point on the cooling curve which need not be the maximum attained by a granulite body (Frost and Chacko, 1989), called into question the reliability and significance of P-T values. Other major drawbacks are the extreme extrapolation of experimental conditions and over sensitivity to compositional variability.

However, modern advances in metamorphic petrology, especially in the fields of (1) chemical analysis of minerals by microanalytical techniques (2) application of reversible and irreversible thermodynamics to petrology and (3) laboratory phase-equilibrium experiments involving metamorphic minerals, allow sophisticated inferences upon the conditions of metamorphism and the factors which control these conditions.

As a part of the present investigations, samples of khondalites, calc-granulites, migmatitic gneisses and garnet-bearing pegmatites were analysed by microprobe, and their geothermobarometric conditions of formation have been calculated. In order to maximise the chances of retrieving peak conditions and to minimise retrograde effects, P-T data for the present study have been confined

to minerals with the largest grain size. This prerequisite had also been necessitated by the reported failure of fine-grained garnets in recording P-T trajectories of large time frame as those of isothermal uplift (Hollister, 1982; St onge, 1987; Frost & Chacko, 1989).

VI.2. GEOTHERMOMETERS

Following the development of Bowen's concept of 'petrogenetic grid' and the better refinement of the facies and grade concepts of metamorphism, the emphasis of imperative metamorphic thermometry was shifted to experimental investigations (Mueller and Saxena, 1977; Helgeson et al., 1978) resulting in more precise characterisation of metamorphic P-T values. Many of the relatively precise geothermometers currently used, deal with chemical equilibria between mineral pairs formed contemporaneously during freezing or metamorphic recrystallization. A great multitude of such calibration methods exists, including isotopic (equilibrium partitioning of light, stable or non-radioactive isotopes; Urey 1947), non-isotopic (inversion, dissociation and eutectic points) exchange, solvus and fluid inclusion thermometry. In the present study, choice has been confined to exchange, solvus and fluid inclusion thermometric methods alone.

Exchange thermometers as a group are characterised by small volume change as compared to large entropy changes and are practically independent of pressure effects. They are based either on the intracrystalline distribution of elements such as Fe, Mg, or Al (Kretz, 1959) between the different sites in one mineral, such as M_1 or M_2 sites in pyroxenes or T_1 and T_2 sites in feldspars (Virgo and Hafner, 1969; Stewart & Ribbe, 1969) or the intercrystalline distribution between sites of two dissimilar phases like clinopyroxene/orthopyroxene and garnet, biotite and garnet, cordierite and garnet etc. The higher activation energy required to redistribute and reset the isovalent cations by diffusion during cooling, render the intercrystalline thermometers better sensors of temperature.

Solvus thermometers on the other hand, are based on the miscibility gap (solvus) between structurally related phases in a temperature - composition (T-X) space, the compositional variability of the co-existing phases being indicative of temperature of equilibration (Essene, 1982)

In addition, several geothermometers based on experimental (Hensen and Green, 1973; Ferry and Spear, 1978), thermodynamic (Saxena, 1979) or combined experimental and thermodynamic (O'Neil and Wood 1979;

Harley, 1984) approaches have also been in use. Methods like the two-pyroxene thermometry (Saxena, 1976), are bedeviled by extensive resetting and re-equilibration of components like Ca, Mg & Fe, except in cases of isolated, exsolved pyroxene grains. (Russ, 1984). The clinopyroxene-garnet exchange thermometers (Pattison and Newton, 1989) on the other hand, are more reliable sensors in granulite terrains because of the large fractionation and slow diffusion rates of Fe and Mg. Other potential geothermometers include exchange of Mg-Tschermak's component between muscovite and biotite (Höisch, 1989), Fe-Mn partitioning between garnet and ilmenite (Pownceby et al., 1987), Fe-Mg exchange between orthopyroxene and biotite (Fonarev and Konilov, 1986; Bhattacharya and Raith, 1987), garnet and orthopyroxene (Wood and Banno, 1973; Harley, 1984; Sen and Bhattacharya, 1984, 1988; Lee and Ganguly, 1988) and between garnet and phengite (Green and Hellman, 1982).

The choice of proper geothermometers for the present study has been constrained by mineral parageneses and the availability of mineral data. Geothermometers used in the study include:

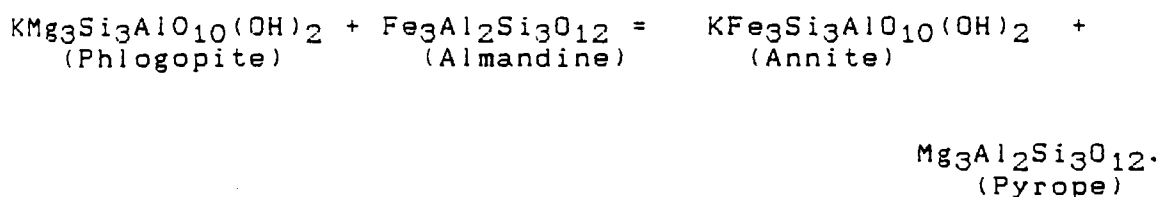
- a. Garnet-Biotite:- Thompson (1976); Ferry and Spear (1978); Holdaway and Lee (1977); Hodges and Spear (1982); Perchuk and Lavrenteva (1983); Indares and Martignole (1985) and Bhattacharya and Raith, (1987).

- b. Garnet-Cordierite:- Holdaway and Lee (1977); Perchuk and Lavrente'va (1983) and Bhattacharya et al. (1988).
- c. Clinopyroxene-Garnet:- Ellis and Green (1979) and
- d. Two-Feldspar:- Green and Uzdansky (1986), based on Na distribution.
- e. Plagioclase - hornblende geothermobarometer: Plyusnina (1982).

VI.2(a) Garnet-biotite thermometers

Since the first attempts of empirical calibrations of K_D as a function of T (Frost, 1962; Perchuk, 1967; Saxena, 1969), experimental (Ferry and Spear, 1978) and empirical calibration (Thompson, 1976; Goldman and Albee, 1977) have been used with improved confidence to evaluate temperatures in medium - to high-grade pelitic rocks. It has potential values as a P-T sensor because of the stability over a broad range of pressure and temperatures, varied chemistry and relatively large volume changes of garnet involved.

Based on the intercrystalline exchange reaction;



the absolute temperature is expressed by the equation:-

$$\overline{\Delta H} - T\Delta S^0 + (P - 1)\overline{\Delta V}^0 + RT \ln K_D + RT \ln K_{\gamma} = 0$$

where K_{γ} is the ratio of activity coefficient, the superscript '0' refer to the hypothetical end-member exchange reactions, H=enthalpy, S=entropy, R=universal gas constant, V=volume change of the reaction (assumed to be negligible) and K_D = the distribution coefficient of chemical components in the concerned phases.

The empirical linear relationship between $\ln K_D$ & $1/T$ proposed by Thompson (1976), is based on the comparison of natural metapelitic assemblages with the independent experimental temperature estimates from various metamorphic reactions. The thermometric expression:-

$$T (^{\circ}\text{K}) = \frac{2740 + 0.0234 \cdot P \text{ (bar)}}{\ln K_D + 1.56} \quad \text{where}$$

$$K_D = \frac{X_{\text{Mg}}^{\text{Bt}}}{X_{\text{Fe}}^{\text{Bt}}} \div \frac{X_{\text{Mg}}^{\text{Gt}}}{X_{\text{Fe}}^{\text{Gt}}}, \quad \text{implicitly}$$

integrates minor element substitutions for Fe and Mg and may be utilised to accurately predict the nature of Fe-Mg variations in prograde metamorphism.

Holdaway and Lee's (1977) thermometric formulations based on experimental calibrations in the divariant Fe-Mg exchange reactions show a positive dependence of K_D on

temperature. Revised form of this equation;

$$T (^{\circ}\text{K}) = \frac{6150 + 0.0246 P (\text{bar})}{R \ln K_D + 3.93}$$

$$\text{Where, } K_D = \frac{X_{\text{Mg}}^{\text{Bt}}}{X_{\text{Fe}}^{\text{Bt}}} \div \frac{X_{\text{Mg}}^{\text{Gt}}}{X_{\text{Fe}}^{\text{Gt}}}$$

has been successfully used by later workers (Ghent et al, 1979; Ferry, 1980; and Novak and Holdaway, 1981).

Ferry and Spear (1978) attempted at an experimental calibration of the thermometer over a restricted compositional range of 0.6 Fe/(Fe+Mg). Their thermometric expression;

$$T (^{\circ}\text{K}) = \frac{12454 + 0.057 P (\text{bar})}{4.662 - 5.9619 \ln K_D}$$

Where, $K_D = (X_{\text{Fe}}/X_{\text{Mg}})^{\text{Bt}} / (X_{\text{Fe}}/X_{\text{Mg}})^{\text{Gt}}$ is consistent with the ideal behaviour of both binary solid solutions.

Subsequent workers (Goldman & Albee, 1977) accounted for the inconsistencies in temperature due to potential effect of bulk compositions of garnet ($X_{\text{Ca,Mn}}^{\text{Gt}}$) and biotite ($X_{\text{Fe,Ti,Al}}^{\text{Bt}}$). They took into consideration the qualitative exchange thermometry corrections of Bohlen & Essene (1980) and temperatures, derived from quartz - magnetite oxygen isotope studies.

Following Ganguly & Kennedy (1974), Hodges & Spear, (1982) presented alternative calibrations assuming non-

ideality only in pyrope - grossular mixing and ideal behaviour for almandine - spessartine and grossular - spessartine binaries. The equilibrium constant K_D for the garnet-biotite geothermometer is reformulated as:-

$$K_D = K_D \frac{(\tau_{py})^3}{(\tau_{al})}$$

where $K_D = (X_{Fe} / X_{Mg})^{Bt} / (X_{Fe} / X_{Mg})^{Gt}$ and

$$\frac{\tau_{py}}{\tau_{al}} = \exp [(3300 - 1.5 (^\circ K)) \frac{(X_{gt}^2 + X_{al} X_{gt} + X_{gt} X_{sp} + X_{py} X_{gt})}{RT (^\circ K)} + \frac{W_{Mg,Mn} (X_{sp}^2 + X_{gt} X_{sp} + X_{al} X_{sp} + X_{py} X_{sp})}{RT (^\circ K)}]$$

Perchuk's (1970) preferential model with negligible effect of Ca, Mn and Fe^{3+} in garnet was later modified (Perchuk, 1981) with a correction introduced for $Mn \rightleftharpoons Mg$ isomorphism, T being subsequently expressed as....

$$T = (3650 / \ln K_D + 2.57) + 252.25 (X_{Mn}^{Gt} - 0.035) \text{ Where}$$

$$X_{Mn} = \frac{Mn}{Mn+Fe+Mg}$$

Perchuk and Lavrenteva's (1983) recent model adopted in the present study takes into account the ideal distribution of Fe & Mg in the system, with $\ln K_D$

showing positive dependence on N_{Al}^{Bt} and N_{Mg}^{Gt} .

Temperature calculations are based on the equation;

$$T (^{\circ}C) = \left[\frac{7843.7 + 0.057 (P - 6000)}{1.987 \ln K_D + 5.699} \right] - 273.15$$

where P is in bars and $K_D = (X_{Mg} / X_{Fe})^{Bt} / (X_{Mg} / X_{Fe})^{Gt}$

Empirical expression of Indares and Martignole (1985) combining both the experimental data of Ferry & Spear (1978) and the data from natural garnet-biotite occurrence, provide an improved calibration. It accounts for the Ti & Al contents in biotite solid solution as well as for the interaction of Ca in Fe-Mg garnet. Temperature estimates are based on the equation:-

$$T (^{\circ}K) = [(12454 + 0.057 P(\text{bar}) + 3(-1590 X_{Al}^{Bt} - 7451 X_{Ti}^{Bt}) - 3(-3000 (X_{Ca}^{Gt} + X_{Mn}^{Gt}))] \div (4.662 - 5.9619 \ln K_D)$$

where $K_D = (X_{Fe} / X_{Mg})^{Bt} / (X_{Fe} / X_{Mg})^{Gt}$

This model yields results which had been rectified for uncertainties in both the K_D -T and K_D -X (composition) correlations of previous models (Goldman & Albee, 1977).

Bhattacharya & Raith's (1987) model takes into account the symmetric mixing parameters for garnet and biotite (Guggenheim, 1967) and assumes a non-ideal Fe-Mg mixing behaviour in biotite phase. The equation used for

thermometric calculations is:-

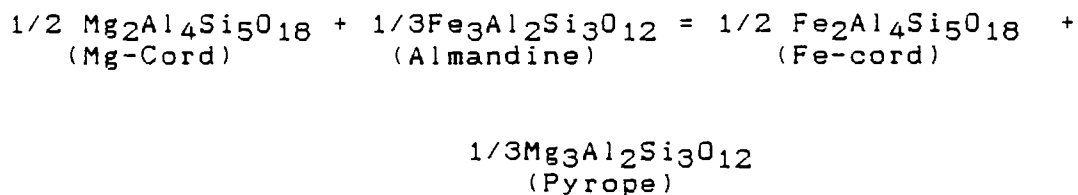
$$T (^{\circ}\text{K}) = [-158 + 2305 (X_{\text{Mg}} - X_{\text{Fe}})^{\text{Bt}} + 583 X_{\text{Al}}^{\text{Gt}} - 2642 (X_{\text{Mg}} - X_{\text{Fe}})^{\text{Gt}} + 3127 X_{\text{Ca}}^{\text{Gt}} + 1749 X_{\text{Ca}}^{\text{Gt}} + 1749 X_{\text{Mn}}] / \ln K_D$$

$$\text{where } K_D = (X_{\text{Mg}} / X_{\text{Fe}})^{\text{Bt}} / (X_{\text{Mg}} / X_{\text{Fe}})^{\text{Gt}}$$

VI.2 (b) Cordierite - garnet geothermometers

The use of cordierite - garnet geothermometer is necessitated due to solubility problems of Al and Ti in biotites (Ferry & Spear, 1978; Ganguly & Saxena, 1984; Indares & Martignole, 1985). Several calibrations exist (Thompson, 1976; Holdaway & Lee, 1977; Currie, 1971; Hensen & Green, 1973; Holdaway, 1976 and Perchuk & Lavrent'e'va, 1983) of which choice for the present study has been confined to models of Holdaway & Lee (1977) and Perchuk & Lavrent'e'va (1983) and Bhattacharya et al (1988).

Holdaway & Lee's (1977) expression based on the relation:



defines T by the equation:

$$T (^{\circ}\text{K}) = \frac{6150 + 30.3 P (\text{Kbar})}{2.69 - 1.987 \ln K_D}$$

where
$$K_D = \frac{(Fe/Mg)^{Crd}}{(Fe/Mg)^{Gt}}$$

Experimental calibrations of the thermometer in the Fe-Mg binary over a restricted compositional range of 600 - 1000 °C (Perchuk and Lavrent'e'va, 1983) for the granulite grade of metamorphism, yield reasonable results since, the pressure effect (0.018 P) is negligible and can be omitted in calculations of temperatures.

$$T (^{\circ}C) = \left(\frac{3020 + 0.018 P \text{ (bar)}}{\ln K_D + 1.287} \right) - 273$$

where, $K_D = (X_{Mg} / 1 - X_{Mg})^{Crd} \times (1 - X_{Mg} / X_{Mg})^{Gt}$

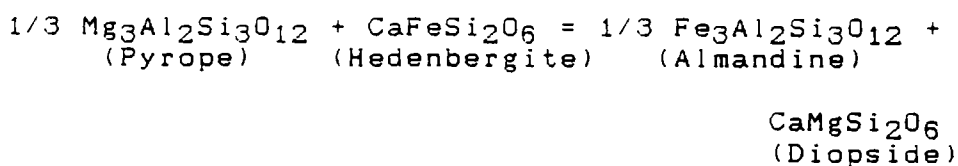
Bhattacharya et al's (1988) formulation based on the chemical data on natural garnet and cordierite samples in the temperature range of 700-850 °C expresses T by the equation:

$$T (^{\circ}K) = [1814 + 0.0152 P \text{ (bars)} + 1122 \frac{(X_{Mg}^{Crd} - X_{Fe}^{Crd})}{X_{Mg}^{Gt} - X_{Fe}^{Gt}} - 1258 (X_{Mg}^{Gt} - X_{Fe}^{Gt}) + 1510 (X_{Ca} + X_{Mn})] \frac{1}{(1.028 - \ln K_D)}$$

where $K_D = (X_{Fe} / X_{Mg})^{Crd} / (X_{Fe} / X_{Mg})^{Gt}$

VI. 2 (c). Clinopyroxene - garnet thermometers

The temperature dependent distribution of Fe and Mg between garnet and clinopyroxene first proposed by Evans (1965) and Banno & Matsui (1965), based on the reaction:



is strongly dependent on temperature and has been repeatedly calibrated as a thermometer.

In addition to published works in more restricted systems by Kushiro et al (1972), Irving (1974), Akella & Boyd (1974), Wood (1976) and Mori & Green (1978), semi-empirical and theoretical studies (Mysen & Heier (1972); Ganguly (1979); Saxena (1979); Dahl; (1980); Oka & Matsumoto (1974) have also been made.

Experimental works of Raheim & Green (1974) in mafic systems indicated and established the temperature sensitive nature of K_D . Its dependence on grossular in garnet and jadeite in pyroxene was demonstrated by Saxena (1979) and subsequently confirmed by later works of Ellis & Green (1979).

$$T \text{ (}^\circ\text{K)} = \frac{3104 X_{\text{Ca}}^{\text{Gt}} + 3030 + 10.86 P \text{ (bar)}}{\ln K_D + 1.9034} \quad \pm 40^\circ\text{C}$$

$$\text{where } K_D = \left(\frac{\text{Fe}^{2+}}{\text{Mg}} \right)^{\text{Gt}} \times \left(\frac{\text{Mg}}{\text{Fe}^{2+}} \right)^{\text{Cpx}}$$

This model attributes all non-ideal effects of K_D to Ca - substitutions in garnet and yield temperatures 50 to 100 °C higher than those obtained from the previous

formulae of Raheim & Green (1974). The distribution of coefficient K_D was showed to be dependent on Mg numbers (Mg / Mg + Fe) of garnet and clinopyroxene at constant temperature, under conditions of ideal solid solutions. The approach adopted by Ellis & Green (1979) correlating K_D with P, T and X_{Ca}^{Gt} is justified because of the sympathetic variations in Di, CaTs components in clinopyroxene and Ca in the coexisting garnets and also due to the shortage of data available on the activity - composition relationships for garnet and clinopyroxene solid solutions. (Hensen et al., 1975; Newton et al., 1977).

Experimental evidence for non-ideality in garnet (Geiger et al., 1987) and in clinopyroxene (Bishop, 1980) argues against the idealities assumed in many of the earlier thermodynamic analyses of silicate systems. The improved version of Pattison & Newton (1989) is characterised by asymmetric, non-ideal mixing in diopside - hedenbergite. However, its application in the present study is constrained since the 'Mg numbers' fall outside the specified range of 0.125 - 0.600.

VI.2(d) Two-feldspar thermometer

The stable equilibrium distribution of end-member components between coexisting plagioclase and alkali feldspar has long been identified to be dependent only on temperature and pressure.

First proposed by Barth (1934), many attempts have been made to evaluate the non-ideality in alkali feldspars and the pressure dependence of $\text{NaAlSi}_3\text{O}_8$ distribution between coexisting alkali and plagioclase feldspars (Stormer, 1975; Whitney & Stormer 1977). Most of the presently used two-feldspar geothermometers are based solely on the distribution of Ab component between plagioclase and alkali feldspars; the equilibrium $\alpha_{\text{Ab}}^{\text{alk}}$ being equal to $\alpha_{\text{An}}^{\text{Plag}}$. With the exception of Powell & Powell (1977) formulation, the effects of minor components like 'Or' in plagioclase and 'An' in alkali feldspars have largely been ignored in most of the "double - binary" formulation based on An-Ab and Ab-Or binary joins (Stormer, 1975; Whitney & Stormer, 1977). Thus they fail to account for the ternary nature of natural feldspar pairs. (Brown & Parsons, 1985). Powell & Powell's (1977) modified version considers the effect of $\text{CaAl}_2\text{Si}_2\text{O}_8$ in alkali feldspar but do not make an equivalent correction for KAlSi_3O_8 in plagioclases. Brown & Parson's (1985) model takes into account the ternary mixing parameters and eliminates arbitrary projection of ternary composition to binaries.

Unlike the previous formulations of Haselton et al (1983), Ghiorso (1984) Price (1985), Green & Uzdansky's (1986) "ternary feldspar thermobarometer", based solely on the

composition of coexisting feldspars, permits estimation of both P & T of equilibration. The dependence of excess Gibbs free energy of mixing functions in the An-Or binary system was semi-empirically estimated using published Margules parameters for the An-Ab (Newton et al., 1980) and Ab-Or binaries (Haselton et al., 1983) and the distribution of Or in the experimental feldspar pairs of Seck (1971a, 1971b). T_{Ab} has been estimated using the following equations:

$$\begin{aligned}
 T_{Ab} \text{ (in Kelvins)} = & [(W_H^{K,Ca} G + W_H^{Ca,K} H + W_H^{K,Na} I + W_H^{Na,K} J \\
 & + W_H^{Ca,Na} K + W_H^{Na,Ca} L + W_V^{K,Ca} G \\
 & + W_V^{Ca,K} H + W_V^{K,Na} I + W_V^{Na,K} J) P] \div \\
 & - 8.3147 [\ln (X_{Ab} (2 - X_{Ab} - X_{Or}) \\
 & (X_{Ab} + X_{Or}))] \\
 & - \ln [X_{Or} (2 - X_{Ab} - X_{Or}) \\
 & (X_{Ab} + X_{Or})] + (W_S^{K,Ca} G + W_S^{Ca,K} H \\
 & + W_S^{K,Na} I + W_S^{Na,K} J)]
 \end{aligned}$$

where constants G to L are defined in terms of mole fractions of albite, anorthite and orthoclase in plagioclase (PF) and alkali feldspar (AF) respectively.

Since the two-feldspar temperatures are lower by about

100-300°C compared to other semi-empirical and theoretical methods, the upper range of temperatures are reported here to yield compatible results on the peak equilibrium conditions. Due to small contents of K in plagioclase and Ca in alkali feldspars and because of the stronger pressure dependence of Na-distribution between coexisting feldspar pairs, compared to garnet-biotite and garnet-cordierite methods, application of the two feldspar thermometer in the present study is restricted to the Ab-distribution.

VI.2(e). Plagioclase - Hornblende geothermometer

The quantitative dependence of Ca:Na ratio of coexisting amphiboles and plagioclase on T (Perchuk, 1970 in Plyusnina, 1982) forms the basis of plagioclase - hornblende geothermometer. Plyusnina's (1982) geothermometer took into consideration the variation of An content in plagioclase and Al content in coexisting Ca-amphiboles over a wide range of temperatures (450-650 °C) and pressures (2-8 Kbars) and has successfully been employed to deduce P-T conditions of metamorphism.

VI.3. Limitations: possible source of errors and precautions:

The accuracy of geothermometers vary considerably, depending upon the thermodynamic model and data used for calibrations. The possibility of continued intraphase diffusion even below the closure temperatures of minerals

such as garnet $(T_c)^{GT}$ may result in temperatures that correspond neither to $(T_c)^{Gt}$ nor to minimum temperature conditions. It has also been suggested that since the effective closure temperatures for exchange equilibria vary with textural setting and reaction mechanism, conventional geothermometers such as the garnet-clinopyroxene (Harley, 1984), garnet-biotite (Thompson, 1976; Perchuk & Laverente'va, 1983) etc., are capable of retrieving only the 'post peak' metamorphic histories of granulitic rocks (Frost & Chacko, 1989).

Absolute temperatures and precision of the various methods of garnet-biotite exchange thermometry, on identical pairs, show large variations in response to inherent uncertainties of individual calibrations.

Thompson's (1976) model, precludes the introduction of any correction factor in terms of minor constituents, from that of the samples used in the calibration and ignores the pressure effect on the equilibrium; while that of Ferry & Spear's (1978) yield unrealistic temperatures, if the Al^{vi} and $Ti / (Al^{vi} + Ti + Mg + Fe^{2+})$ ratios exceed the limit of 0.15, a condition common in many granulite facies biotites.

Assumption of $W_{Mg,Mn} \sim 0$ of Hodges & Spear (1982) yield reasonable temperatures confirming the assumption of ideality of pyrope-spessartine solutions at the

specified P-T conditions. However, because of uncertainties in Margules parameters in garnet solid solutions (esp of Mn) and in the activity-composition relationships for plagioclase, its general applicability outside the aluminium-silicate triple point is doubtful. Since, the calibrated Ti and Al interaction parameters are somewhat dependent on the substitutional model adopted, the application of Indares & Martignole's (1985) empirical expression to upper amphibolite facies rocks has got restricted application.

A critical comparison of the different garnet geothermometers reveal that Ferry & Spear's (1978) and Bhattacharya & Raith's (1987) calibrations yield temperatures that are too high whereas, computed values of Indares & Martignole (1985) give temperatures that are too low. Thompson's (1976) and Holdaway & Lee's (1977) methods have intermediate values while, methods based solely on $\ln K_D$, like that of Perchuk & Lavrent'eva (1983), yield more precise and accurate results to ± 30 °C.

The T-X dependence of Mg-Fe partitioning between coexisting garnet and cordierite had long been a subject of debate; natural samples showing an inverse relationship of $\ln K_D$ with T (Thompson, 1976; Holdaway & Lee, 1977) and hydrothermal runs yielding contradictory results (Currie, 1971, 1974; Hensen & Green, 1973;

Holdaway, 1976 and Perchuk & Lavrente'va 1983).

Holdaway & Lee's (1977) thermometer does not take into account the effect of compositional variations and the $K_{\text{Mg-Fe}}^{\text{Gt-Crd}}$ values are reported to have a pressure dependence of about 51 °C/Kbar. The predicted temperatures of Bhattacharya et al's (1988) thermometer, applicable over a wide compositional range of $0.38 < X_{\text{Mg}} < 0.92$, have an accuracy of about ± 65 °C. Inconsistencies due to regular mixing models of both phases has been rectified and refined in this model and hence, is considered a more dependable geothermometer in meta-aluminous rocks (Bhattacharya et al., 1988).

A serious limitation of Ellis & Green's approach is the cumulative effects of non-ideality in garnet and clinopyroxene, on $\ln K_D$ and the difficulty in isolating non-ideality in garnet from that in clinopyroxene since, the equilibrium involve solid solutions of both phases. The calibrated temperatures have a pressure dependence of about 5.5 °C/ Kbar and the temperature decreases by about 100 °C for every 10 mole percent increase of grossular in garnet.

The use of two-feldspar thermometry provide only minimum estimates due to their lower blocking temperatures as well as due to the exsolution and migration of Na in

alkali feldspar upon cooling. Even with the reintergration of exsolved granular lamellae (Bohlen & Essene, 1977), temperatures above 700 °C are rarely retrieved, except in cases of T_{Ab} . Other important constraints in feldspar thermometry are (1) the negative excess volume in most of the ternary feldspars (2) analytical uncertainties in estimation of Na in alkali feldspars due to volatilization of Na under electron beam (3) variable Al-Si order-disorder in feldspars (4) re-equilibration during cooling (5) extreme dependence of X_{pa} composition of feldspars on pressure (0.5 mol % error in composition resulting in ± 2 Kb variations) (6) analytical difficulties in determining exact feldspar compositions and amount of exsolution (7) problems in identifying the coexisting pairs when one or both phases are zoned and (8) uncertainties in estimation of pressures since the pressure coefficients of the three thermometers T_{Ab} , T_{An} and T_{Or} are different.

Green & Usdansky's (1986) model used in the present study has a pressure dependence of about 12-14 °C/ Kbar and is susceptible to analytical uncertainties in the Or content of plagioclase, An content of alkali feldspars and to any systematic errors in the binary mixing parameters. Other drawbacks inherent in this model are (1) the use of a single equation for both

monoclinic and triclinic feldspars and (2) lack of volume data for ternary feldspars.

The possible reasons for unrealistic temperatures of Green & Uzdansky's (1986) model are suggested to be related to the assumption of a negative entropy term (W_S) for one of the An - Or terms, based on a suspiciously low experimental value of An content of Seck (1971). The strongly negative values for W_H (An - Or) and W_S (An - Or), erroneously predict decreasing solubility of An in Or, with increasing temperatures (Fuhrman & Lindsley, 1989). However, results are expected to get seriously impaired only where there is more than a minimal solution of An in alkali feldspars. Almost all the alkali feldspars used for the present study have anorthite mol% in the range of 0.001-0.066 only, and the uncertainties in analytical estimations have also been reduced by using a 50 μm electron beam for alkali feldspar and a focussed electron beam for plagioclase. This model is, therefore expected to yield compatible results.

Application of the Pl-Hb geothermometer (Plyusnina, 1982) is limited to calciferous and subcalciferous amphiboles and the standard deviation in temperature estimate is $\pm 10-15$ °C for an accuracy of ± 1.0 mol% Al in amphibole and Ca in plagioclase.

VI.4. GEOBAROMETRY

Reconstruction of prograde P-T paths which are obliterated by metamorphic processes is greatly dependent on the availability of well-calibrated geobarometers. Early methods of semi-quantitative pressure estimations, based on simple invariant equilibrium and continuous variations of mineral composition, faced potential complications because of metastable persistence of one mineral into the stability field of another. The net transfer reactions involving breakdown of silica tetrahedron are characterised by a large volume and entropy change and have an added advantage over other barometers because of their stability over a broad range of P-T conditions. Geobarometers since proposed include, those based on assemblages of garnet-plagioclase-aluminium silicate - quartz (Aranovich & Podlesski, 1980), chlorite-biotite-muscovite (Nurminen, 1987), garnet-clinopyroxene-quartz-orthopyroxene (Paria et al, 1988) etc, the more widely used formulations being based on clinopyroxene / orthopyroxene - garnet - plagioclase - quartz assemblages (Perkins & Newton, 1981; Newton & Perkins, 1982; Bohlen et al, 1983; Perkins & Chipera; 1985). Other barometric formulations based on ilmenite-sillimanite-quartz-garnet-rutile (Bohlen et al, 1983) and ilmenite-plagioclase-quartz-garnet-rutile (Bohlen & Liotta, 1986) parageneses are also in use.

Geobarometers used in the present study include :

(i) Garnet-Plagioclase-Aluminiumsilicate-Quartz

- a) Ghent (1976)
- b) Newton & Haselton (1981)
- c) Hodges & Spear (1982)
- d) Koziol & Newton (1988)
- e) Mckenna & Hodges (1988)
- f) Koziol & Newton (1989)

(ii) Clinopyroxene-Garnet-Plagioclase

- a) Perkins & Newton (1981)
- b) Moecher et al (1988)

(iii) Cordierite-Garnet-Geobarometer

- a) Bhattacharya & Sen (1985)
- b) Bhattacharya (1986)

(iv) Hornblende-Plagioclase Geobarometer

- 1) Plyusnina (1982)
- 2) Hammarstrom & Zen (1986)
- 3) Hollister et al (1987)

VI.4.(i).Garnet-Plagioclase-Aluminium silicate-Quartz

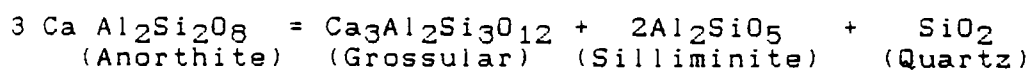
Geobarometer

The association of garnet, plagioclase, aluminium silicate and quartz in high grade pelitic rocks forms the basis of a widely used geobarometer, the calibration of which is based mainly on experimental phase equilibria (Goldsmith, 1980) and measured thermodynamic properties of garnet and plagioclase (Newton & Haselton, 1981)

The possibility of using the products of breakdown of anorthite as a potential geobarometer was first recognised by Kretz (1959) and was further elaborated by various workers

(Ghent, 1976; Boyd & England, 1961).

Ghent's barometric model based on the multivariant reaction:



took into account the aluminum silicate diagram of Holdaway (1971) and made provisions for the activity of grossular solid solution in garnet and activity of anorthite solid solution in plagioclase. The barometric expression makes use of the relation:-

$$\Delta G_A^\circ + RT \ln \left(\frac{\alpha_{Gt}}{\alpha_{An}} \right)^3 + P \overline{\Delta V} \cong 0$$

where ΔG_A° is the 1-bar Gibbs energy change, P° is the pressure of end-member equilibrium at T and $\overline{\Delta V}^\circ$, the partial molal volume change at 1-bar. For the present study, Ghent's (1976) formula as extended by Hodges & Spear (1982) has been utilised:-

$$0 = 11675 - 32.815 T (\text{°K}) + 1.301 [P(\text{bars})-1] + RT (\text{°K}) \ln K_D$$

where, $K_D = (K_1) (K_2)$, K_1 and K_2 representing the ideal and non-ideal components respectively.

Several modifications of the GPAQ model has been proposed by Newton & Haselton (1981), Perkins et al (1982), Ganguly & Saxena, (1984), and Koziol & Newton (1988).

Newton & Haselton (1981) pointed out that Ghent's (1976)

approximation of the activities of $\text{CaAl}_{2/3}\text{SiO}_4$ and $\text{CaAl}_2\text{Si}_2\text{O}_8$ as equivalent to their mole fractions, lead to serious underestimations of pressure. They presented a modified version, adopting more recent solution calorimetry and phase equilibrium data on garnet and plagioclase solid solutions. Their expression, corrected for the error in the sillimanite containing end-member reaction (Froese, 1988):-

$$P(\text{Kbar}) = -1.17 + 0.023 T(^{\circ}\text{C})$$

has been utilised for the purpose of this study.

Following the views of earlier workers (Hays, 1967; Hariya & Kennedy, 1968; Schmid et al 1978; Goldsmith 1980; Gasparik, 1984; Hodges & Mckenna, 1987), Koziol & Newton (1988) explored the sources of uncertainties in pressure estimations. Major causes of uncertainties were concluded to be the result of (1) long extrapolation of the experimental anorthite breakdown equilibria to crustal conditions (2) wide bracketing uncertainties and (3) limited P-T ranges of experiments. They constrained the equilibrium curve to $P(\text{Kbars}) - 22.80 T(^{\circ}\text{C}) - 1093$, in the restricted experimental range of 900-1250°C and 19-28 Kbar and obtained the relation:-

$$P_{\text{sill}} (\text{bars}) = -0.001872 T^2 + 23.41 T - 25.$$

The high quality measured heat capacity data provided for all the phases involved in the barometric formulations allow an improved calculation of the thermodynamic

properties.

Mckenna & Hodges (1988), stressing the importance of P-T control of experiments and the tightness of the experimental bracketing runs over the precision of the geobarometer, suggested the expression:-

$P = (2.20 \pm 0.15)T - [6.2 (\pm 3.0) \times 10^2]$ where P is in megapascals and T in Kelvins, which serves as a unique indicator of pressure.

Koziol & Newton's (1989) reversed displaced equilibrium experiments in ternary garnets of varying compositions of high grade parageneses, at restricted P-T conditions of 900-1000°C and 8-17 Kbar, predicted near-ideal mixing of grossular in garnet at 30 mol % grossular, and positive deviations from ideality at lower grossular contents. The grossular activity coefficient is expressed in terms of X_{Grs} , W_{FM} and W_{Ca} as :-

$$RT \ln \gamma_{Grs} = (1 - X_{Grs})^2 [W_{Ca} + 2X_{Grs} \cdot (W_{FM} - W_{Ca})]$$

where,

$$W_{Ca}(J) = -2060 + 3.57 \times 10^4 (Mg\#) - 4.95 \times 10^4 (Mg\#)^2$$

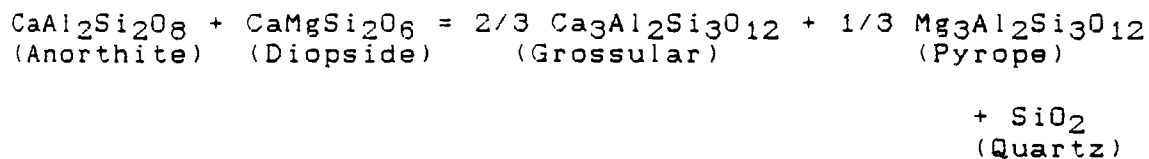
$$W_{FM}(J) = 3390 - 3.71 \times 10^4 (Mg\#) + 6.49 \times 10^4 (Mg\#)^2$$

and Mg#, is the magnesium number.

VI.4.(ii). Clinopyroxene-Garnet-Plagioclase Geobarometer

The composition of garnet, coexisting with clinopyroxene, quartz and plagioclase, is controlled by the strongly

pressure-dependent equilibria:



Barometric formulations of these assemblages by Hensen & Green (1973), Wood (1975), and Wells (1979) are all based on experimental syntheses of the four phases in simple systems (Kushiro & Yoder, 1966; Hensen, 1976) and are all hampered by the insufficient data, non-reversals of compositions of the phases and long extrapolation from experimental temperatures.

Perkins and Newton's (1981) geobarometric calibration expresses pressure by the equation:-

$$P(\text{bars}) = 1425 + 17.929 T + 3.5962 T \ln K_D \pm 1.7 \text{ Kbar}$$

$$\text{where, } K_D = \frac{(\alpha_{\text{Ca}}^{\text{Gt}} \times \alpha_{\text{Mg}}^{\text{Gt}})}{\alpha_{\text{Ca}}^{\text{Pl}} \alpha_{\text{Mg}}^{\text{Cpx}}}$$

Expressions for the pyroxene activity terms are based on the ideal two-site model of Wood & Banno (1973) and Wells (1977). $\alpha^{\text{Diop}} = X_{\text{Ca}}^{\text{M}_2} \cdot X_{\text{Mg}}^{\text{M}_1}$ where Ca, Mn, Na and Fe^{2+} are allotted to M_2 and Mg, Fe^{3+} , Ti, Al^{vi} and the remaining Fe^{2+} are allotted to M_1 -sites. $X_{\text{Ca}} = \text{Ca}$ and $X_{\text{Mg}} = \text{Mg}$, based on a 4-cation pyroxene formula.

Adopting the activity terms of Perkins and Newton (1981) for garnet and plagioclase, the following expressions are obtained for the equilibrium constants (Raith, 1982).

$$\ln K_D = \ln \frac{(X_{Ca} \cdot X_{Mg})^{Gt}}{(X_{Mg} \cdot X_{Ca})^{Cpx} \cdot [X_{An} (1+X_{An})^2]} + \frac{2(3300-1.5T)(X_{Mg} + (X_{Mg} \cdot X_{Fe})^{Gt})}{1.987 T} + \frac{(3300 - 1.5 T)(X_{Ca} + (X_{Ca} \cdot X_{Fe})^{Gt})}{1.987 T} - \frac{(1-X_{An})^2 (2075 + 9318 X_{An})}{1.987 T}$$

More recent geobarometric calibration by Moecher et al (1988), is based on measured thermodynamic data and experimental equilibria. It has been shown that the strongly pressure dependent reactions:-

Diopside + Anorthite = Grossular + Pyrope + Quartz and
Hedenbergite + Anorthite = Grossular + Almandine + Quartz
provides two potential barometers; the DI and HD barometers respectively.

Plagioclase activity model of Newton et al (1980) and the quaternary mixing model of Ganguly & Saxena (1984) are used, with modified values for Ca-Fe mixing parameters. Ideal $CaFeSi_2O_6$ and $CaMgSi_2O_6$ activities are approximated by the relationship:-

$$\alpha_{CaFeSi_2O_6}^{Cpx} = (X_{Ca})^{M_2} (X_{Fe^{2+}})^{M_1}$$

Cpx
 and $\alpha_{\text{CaMgSi}_2\text{O}_6} = (X_{\text{Ca}})^{M_2} (X_{\text{Mg}})^{M_1}$ based on a 4-cation
 pyroxene formula.

Log₁₀ K_D values are represented by the relation:-

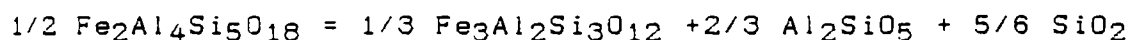
$$\log_{10} K_D = (\alpha_{\text{gr}} \alpha_{\text{alm}})^2 / (\alpha_{\text{an}} \alpha_{\text{hd}})^3$$

for HD barometer and $(\alpha_{\text{gr}} \alpha_{\text{py}})^2 / (\alpha_{\text{an}} \alpha_{\text{di}})^3$ for DI barometer.

The application of Moecher's (1988) geobarometer to the calc granulite sample of the present study area is limited because of the extensive variations between the Mg-rich (diopsidic) and Fe-rich (hedenbergitic) compositions obtained from spot analyses of pyroxene grains (See Table 19, Chapter V).

VI.4.(iii).Cordierite-garnet geobarometer

The bivariant cordierite-garnet geobarometer based on the equilibrium between cordierite, sillimanite and quartz:-



is a potential tool in metamorphic petrology and serves as a unique indicator of pressure-temperature and water fugacity.

Several conflicting calibrations have been attempted at, notable among which, are the experimental calibrations by Currie (1971), Hensen and Green (1973), Weisbrod (1973 a & b) Hutcheon et al (1974), semi-empirical calibrations by Perchuk et al (1981), Thompson (1976), Holdaway & Lee (1977), Newton

& Wood (1979), Martignole & Sisi (1981), Lonker (1981) and Bhattacharya and Sen (1985).

The existing calibrations disagree with each other regarding P-T location, dP/dT slopes of the end-member reactions and activity-composition of Fe-Mg phases. Holdaway & Lee's (1971) experiments in the pure Fe and Fe-rich systems (under $P_{H_2O} = P_{total}$) predict negative slopes for the end-member reactions with K_D increasing with temperature while, a positive dP/dT slope is proposed by Hutcheon et al (1974) and Newton & Wood (1979). Inconsistencies also exist in the experimentally determined phase equilibria (Newton, 1972) and established phase relations (Lonker, 1981).

The contradicting thermodynamic, experimental and theoretical representations of the garnet-cordierite equilibria had been attributed to the poorly known effect of molecular H_2O in the cordierite structure (Newton & Wood, 1979) and the incompatibility in the input thermodynamic data. Early models of Holdaway & Lee (1977), Newton & Wood (1979), Martignole & Sisi (1981), and Lonker (1981), assumed no volume change upon hydration and hence, yield correct pressures only for intermediate values of water pressures. The effect of variability in $X_{H_2O}^{Crd}$ on the computed pressures had also been ignored by Hutcheon et al (1974) and Harris (1981).

Bhattacharya & Sen (1985) provides a theoretical tool for water barometry, assuming an ideal one-site model in the $Mg_2Al_4Si_5O_{18} - Mg_2Al_4Si_5O_{18} \cdot H_2O$ system and incorporated experimental data as well as the refined activity composition relationships of hydrated cordierites (Lee & Holdaway, 1977), leading to the expression :-

$$x_{H_2O}^{Crd} = \frac{\int_{H_2O}^{P,T}}{[\exp(-1/RT [64,775 - 32.26T + G_{H_2O}^{1,T} - P(9 \times 10^{-4}T - 0.5142)]) + \int_{H_2O}^{P,T}]}$$

This expression for ideal solution model of garnet and cordierite, relating pressure, temperature and fugacity of water in the coexisting fluid to the water content of cordierites, is contradictory to the assumption of non-ideality in multicomponent garnet solid solutions of Dahl (1980), Ganguly (1979) and Ganguly & Saxena (1984). The above equation is valid only for $P_{H_2O} = P_{total}$ conditions.

Adopting the internally consistent data base and activity composition relations constrained from natural and experimental data, Bhattacharya (1986) reformulated the geobarometric expression of cordierite in the $FeO-Al_2O_3-SiO_2 \pm H_2O$ system. This model is capable of setting limits on

pressure values in response to varying H₂O. The activity of almandine component in multi component garnet solid solutions is computed from the relation:-

$$\ln \alpha_{alm}^{Gt} = X_{Ca}^2 (1.52 - 5.17X_{Fe}) + X_{Mg}^2 (0.10 + 2.26X_{Fe}) \\ + X_{Ca} \cdot X_{Mg} (3.01 - 6.67X_{Fe} + 1.50X_{Ca} - 1.50 X_{Mg})$$

as suggested by Perkins & Chipera (1984). The barometric expression:-

$$3460 - 2.23T - 0.6101P + RT \ln \left(\frac{\alpha_{alm}^{Gt}}{\alpha_{Fe-Crd}} \right)^{1/3} \\ - 0.994 T \ln (1 - X_{H_2O}) = 0$$

provides an improved theoretical modelling of hydration of cordierites at available P-T- α H₂O conditions.

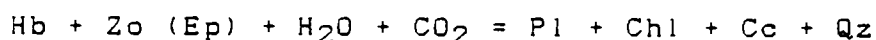
VI.4.(iv). Hornblende - Plagioclase Geobarometer

Evidences presented in favour of increasing Al content of Ca-amphiboles with increasing grade of metamorphism (Leake, 1962; Kostyuk, 1970; Hietanen, 1974 and Graham, 1974) has been employed in the pressure determination of albite - epidote-amphibolites and the amphibolite facies metabasite. In the present study, this method has been applied for the hornblende - biotite migmatitic gneiss from the Gap proper.

Dependence of Al content in calcium amphiboles and Ca content in coexisting plagioclase, on pressure - temperature

conditions of their crystallization, over a wide range of temperatures (450 - 650°C) and pressures (2-8 Kbar), is utilised in plyusnina's (1982) experimental geothermobarometer. It depends on the three interacting effects of pressure, temperature and activity of water, which in turn, control the Al^{iv} and Al^{vi} contents of amphibole.

The continuous transition from tremolite (actinolite) to Al-rich hornblende is fixed along the equilibrium curve of the reaction:-



Pressure of formation is directly determined by plotting the coexisting Ca-Amphibole and Pl composition in the Pl_{An} vs Hb_{Ca} diagram, with isobars based on the variation of Al in Ca-Amphibole and isotherms, based on X_{Ca} .

Hammarstrom & Zen (1983; 1985; 1986) proposed an empirical linear correlation between the estimated pressure of crystallization of calc-alkaline plutons and the total Al content of hornblende and expressed the relation as $P (\pm 3 \text{ Kbar}) = -3.92 + 5.03 Al_T$, where Al_T is the sum of tetrahedral and octahedral Al, per 23 oxygens.

Hollister et al (1987) reviewed the linear relation between Al_T and P and suggested their extension in predicting metamorphic pressures of solidifications. Their equation :

$$P (\pm 1 \text{ Kbar}) = -4.76 + 5.64 Al_T$$

is valid for intermediate pressures of 4 to 6 Kbars.

The consistency of Hammarstrom & Zen (1986) & Hollister et al's (1987) geobarometers was confirmed by Rutter et al (1989), by providing data on newly crystallised, near solidus amphiboles in partly melted, vapour absent garnet-tonalite, at 10 kbar.

1.4.5. Accuracy and precision

The application of geobarometers is beset with insurmountable uncertainties and unresolved experimental difficulties. Ambiguities also result from the differential closure temperatures of barometers with respect to thermometers (Frost & Chacko; 1989), lack of tightly reversed experiments and extrapolation to lower and higher temperatures, especially in the absence of quantitative data on partial molar volume (Goldsmith, 1980; John & Essene, 1982). An accurate insight into these problems of accuracy, precision and validity of pressure estimations is therefore, an essential prerequisite to successful geobarometry.

Major advances in the accuracy and precision of geobarometers have been made in the last decade with the help of experimental reversal of pressure dependent equilibria (Bohlen et al, 1980; 1983; Koziol & Newton, 1988), more precision thermodynamic data (Haselton & Newton, 1980 in Newton & Haselton, 1981; Robie et al, 1987) and more accurate

modelling of activity composition relations for mineral phases (Newton & Haselton, 1981; Anovitz & Essene, 1987).

The solution properties of garnet are the greatest obstacle to accurate geobarometry, even small error in the activity coefficient of a garnet component being converted into sizable errors in calculated values of pressures.

Ghent's (1976) assumption of simple binary solution for garnets and ideal solution for plagioclase led to serious over estimates of pressure. It also suffered from analytical uncertainty introduced by the kyanite-sillimanite transition, being at variance with the experimental transition. However, reasonable pressures are obtained for middle and high-grade parageneses.

Major drawbacks of the apparently successful model of Newton & Haselton (1981) are (1) the strong dependence of computed pressures on the solid solution models for garnet and the assumed temperature (50°C difference resulting in 1.2 Kb variation) (2) uncertainty regarding ΔV_s , at P-T required, to calculate the large shift in P from the end-member garnet (3) relatively large errors inherent in analysing minor components and the associated large uncertainties involved in the activity coefficient data for such garnets below 600°C and (5) the occurrence of end-member grossular at pressures approximately 10-15 Kbar above those of granulite terrains, in which the barometer applies.

Newton and Haselton's (1981) expression, modified and corrected by Froese (1988) for the error in the sillimanite containing end-member reaction has much steeper P-T line (15-17 bar/degree) and agree well with the Al_2SiO_5 stability field constraints.

Mckenna & Hodges (1988) formulations reduces the uncertainty of calculated pressures by a factor of 2, over previous calibrations. The precision of Koziol and Newton (1988) is small (± 0.6 Kbar) but, better results are obtained from Mckenna & Hodge's (1988) calibration with ± 2.5 Kbar accuracy.

Koziol and Newton's (1989) method with an uncertainty of about 15%, is valid only over the compositional range of 3-40% grossular content and Mg number in the range of 0 to 0.6.

Newton and Perkin's (1982) version yeilds consistent and reasonable results for the entire range of crustal pressures and serves to bracket equilibrium pressures within reasonable limits. The unknown mixing properties of Mn in garnets, restricts their application to garnets with $\text{Mn} < \text{Mg}/3$. The calculated pressure is dependent on the mineralogical determination of T with its inherent uncertainties. This barometer involves an uncertainty of about 1700 bars at a given temperature. The uncertainties regarding the high

structural state of plagioclase and Al-Si ordering is at its minimum, at temperatures above 700°C and $X_{An} \leq 0.25$.

The thermodynamic, temperature and compositional dependence of Moecher et al's (1988) thermodynamically based barometer and the inherently less precise nature of these experiments, compared to reversed experiments, warrant caution in its application to natural assemblages. Accurate results are not obtained at extreme garnet compositions as well as in garnet with large amounts of andradite components.

Garnet - cordierite - sillimanite - quartz geobarometer is limited by a relatively narrow pressure range of application and also by the conflicting calibrations. Ambiguities also results from the poorly understood mixing relations of Mg & Fe and the role of H₂O in cordierite. The main drawback of cordierite - bearing pressure sensors is the dependence of estimated pressures on the $\frac{P_{H_2O}}{2}$ ratio of the coexisting fluid. Its geobarometric use is limited to cases where the actual hydration of cordierite has been proved to have inherited from high grade metamorphic conditions. Other sources of ambiguities arise out of (1) the order - disorder transition above 1450°C in cordierite (Putnis & Bisch, 1983) (2) absence of high-pressure phase experiments, (3) the assumption of ideal Fe-Mg mixing in cordierite and other phases and the presence of different types of water (type I

with H-H Vector of H₂O parallel to c - axis of crystal and type II, with H-H Vector parallel to b-axis of crystal) and (5) changes of chemistry of water content of cordierite during depressurization and uplift. Geobarometers involving cordierite are therefore, best suited for bracketing the equilibrium pressures rather than obtaining unique values.

The dispersion in the computed values of Bhattacharya's (1986) geobarometer is within ± 1.2 Kbar. Errors in the order of $\pm 50^\circ\text{C}$ in temperature estimations, introduces discrepancies of about 100 bar.

Application of the hornblende - plagioclase geobarometer is limited to calciferous and subcalciferous amphiboles containing more than 1.50 Ca and less than 1.00 Na. Resolution of plyusnina's (1982) geothermometer depends on the analytical uncertainty in the composition of anorthite and plagioclase. Taking into account the experimental uncertainties, the standard deviation in pressure estimates is reported to be ± 1 Kb for an accuracy of ± 1.0 mole percent of Al in amphibole and Ca in plagioclase.

Hollister et al's (1987) barometer reduces the error in pressure estimations from ± 3 Kbar, proposed by Hammarstrom & Zen (1986) to ± 1 Kbar. Its reliability is dependent on the syngenetic crystallization of quartz + plagioclase + orthoclase + biotite + hornblende + titanite + magnetite +

sphene ± epidote.

VI.6. RESULTS

Temperature estimates for the various units of the study area have been made using a variety of exchange and solvus thermometers and the results, for assumed pressures from 4 to 10 Kbars, have been compiled in Table.21a,b,c. Microprobe data used in P-T estimates are given in Tables.14 to 20 (see Chapter.V).

An approach of 'centre to centre' compositions has been used for estimating peak P-T parameters of equilibrium assemblages and 'rim to rim' compositions of contacting grains of cordierite, garnet, biotite etc., for evaluating the re-equilibration (retrogressive) conditions. This has been based on the assumption that the cores of minerals, coexisting in isolation from each other, preserve their high-grade composition and the composition of rim areas, in mutual contact with each other, preserve some retrogressive stage during cooling (Indares, 1982).

A comparison of average temperature, calculated at peak pressures of ~8 Kbars (Table.22), reveal that the khondalites and associated gneisses have experienced peak garnet (core) - biotite (matrix) temperatures of 938 °C by Ferry & Spear (1978), 949 °C by Hodges & Spear (1982) and 1000 °C by Bhattacharya & Raith (1987) methods. Estimates by Indares &

TABLE.21 Model temperature estimates for assumed pressures of 4 to 10 khars from the microprobe data given in Table.14 to 20.

(a) GARNET - BIOTITE TEMPERATURES

GH = Ghent (1976), TH = Thompson (1976),
 HOL = Holdaway & Lee (1977),
 FER = Ferry & Spear (1978), HOD = Hodges &
 Spear (1982), PER = Perchuk & Lavrente'va (1983),
 IND = Indares & Martignole (1985),
 GRE = Green & Usdansky (1986) based on Na,
 BHA = Bhattacharya & Raith (1987).

GAR.CORE-MATRIX BT							
Ps.14	4000	5000	6000	7000	8000	9000	10000
Gar(10)							
Bt (17)							
GH	654	745	818	891	963	1036	1109
TH	796	805	814	823	831	840	849
HOL	752	756	760	764	768	772	776
FER	863	868	873	878	883	889	894
HOD	868	873	879	885	888	895	899
PER	709	717	724	731	738	746	753
IND	667	672	678	683	688	693	698
GRE	603	620	635	648	662	676	690
BHA	-----		905	-----			

Ps.16.							
Gar.26							
Bt 39							
GH	541	621	685	749	813	877	941
TH	835	844	854	863	872	881	890
HOL	784	788	792	797	801	805	809
FER	923	928	934	939	944	950	955
HOD	930	935	941	946	951	957	962
PER	734	741	748	755	763	770	778
IND	725	730	735	741	746	752	757
BHA	-----		943	-----			

	4000	5000	6000	7000	8000	9000	10000

PS (25a)							
Gr 36							
Bt(11&12)							
GH	342	402	450	499	547	596	644
TH	858	867	876	886	895	905	914
HOL	803	807	811	815	820	824	828
FER	963	970	975	981	986	992	997
HOD	983	990	996	1001	1007	1012	1018
PER	747	754	762	770	777	785	792
IND	848	854	859	865	870	876	881
BHA	-----		1152	-----			

TABLE.21 contd...

	4000	5000	6000	7000	8000	9000	10000

GAR CORE-BT(2)							
PS 25(a)							
Bt-2 Anal:							
21,42,43,44							
45,53&55							
TH	763	772	780	789	797	806	814
HOL	725	728	732	736	740	744	748
FER	813	819	823	829	834	839	844
HOD	835	841	846	851	855	860	865
PER	689	696	703	711	718	725	732
IND	729	734	738	743	748	753	758
BHA	-----		1069	-----			

GAR.CORE-MATRIX BT

Ps 26 Gr

Bt (Av 11, 12, 13, 14&16)

TH	776	785	793	802	811	819	828
HOL	735	743	747	751	755	759	763
FER	835	841	846	851	856	861	866
HOD	842	848	853	858	862	867	872
PER	697	704	711	719	726	733	740
IND	675	680	685	690	695	700	705
BHA	-----		909	-----			

	4000	5000	6000	7000	8000	9000	10000

GAR(RIM)-BT							
Ps. 14							
GAR(44), Bt(45)							
GH	620	708	778	848	919	989	1059
TH	658	666	673	681	689	696	704
HOL	635	639	643	646	650	653	657
FER	666	670	674	679	683	687	691
HOD	670	676	680	684	689	693	697
PER	621	627	634	641	647	654	660
IND	549	553	558	562	566	570	574
BHA	-----		817	-----			

TABLE.21 contd....

	4000	5000	6000	7000	8000	9000	10000
Ps. 16. GAR-10							
Bt(Av. 31&32)							
GH	639	728	800	871	943	1014	1086
TH	585	592	599	607	614	621	628
HOL	572	576	579	582	586	589	592
FER	569	574	578	582	585	589	593
HOD	574	579	583	587	590	594	598
PER	571	577	583	590	596	602	608
IND	469	472	476	480	484	587	491
BHA	-----		792	-----			
GAR RIM-BT(II)							
Ps. 25(a)							
Gr. (Av. 1, 2, 3, 4&26)							
Bt(Av. 15, 16, 17&19)							
GH	614	701	771	840	910	979	1049
TH	520	527	533	540	546	553	559
HOL	515	518	521	524	527	530	534
FER	490	494	497	501	504	508	511
HOD	494	498	502	505	509	512	516
PER	559	565	571	577	583	589	595
IND	443	447	450	453	457	460	464
BHA	-----		772	-----			
	4000	5000	6000	7000	8000	9000	10000
GAR-BT(INCL)							
Ps. 25(a). Gr. 31							
Bt-32							
GH	357	419	468	518	567	617	666
TH	508	514	520	527	533	540	546
HOL	498	501	504	507	510	513	516
FER	822	828	833	838	842	847	852
HOD	841	847	852	857	861	866	871
PER	510	516	522	527	533	539	545
IND	456	459	462	465	469	472	475
BHA	-----		864	-----			
GAR(RIM)-BT(III)							
Ps. 26							
Gr. 20							
Bt-10							
TH	548	555	562	569	575	582	589
HOL	540	543	546	550	553	556	559
FER	523	527	531	534	538	541	545
HOD	529	533	537	540	544	547	551
PER	545	551	557	563	569	575	581
IND	490	493	497	500	504	507	511
BHA	-----		795	-----			

TABLE.21 (b) GARNET-CORDIERITE TEMPERATURES

HOL = Holdaway & Lee (1977), PER = Perchuk & Lavrente'va (1983), BHA = Bhattacharya et al (1988).

	4000	5000	6000	7000	8000	9000	10000
Ps.79.							
Gar.3 (core)							
Cord.5 (core)							
HOL	794	798	803	808	813	818	824
PER	778	784	790	796	802	808	815
BHA	788	794	800	805	811	817	822
Ps.79.							
Gar 1b (rim)							
Cord.1 (rim)							
HOL	741	745	750	754	758	763	767
PER	640	645	650	656	661	676	672
BHA	659	703	707	712	717	722	727

TABLE.21 (c) GARNET-CLINOPYROXENE TEMPERATURES

ELL = Ellis & Green (1979)

PS.35							
Gar (Av)							
Cpx-Mg-rich (32,33,36 37 & 38, Av)	768	770	771	773	775	777	779
Gar (Av)							
Cpx-Fe-rich (11,12,15 18 & 19, Av)	800	802	804	806	808	810	812

TABLE.22 Model temperature (°C) obtained from core, rim and inclusion compositions for mean pressure estimates (~8 Kbar) from the data given in Table.21

Rock type, sample No & description	Gar-Bt thermometer					Gar-Crd thermometer					Two-Fs thermometers		Pl-Hb
	GH	TH	HOL	FER	HOD	PER	IND	HOL	PER	BHA	ELL	GRE	
Gar-bt-Gn													
PS.14 Gar(core)-bt(matrix)	963	831	768	883	888	738	688						662
Gar-bt-Sill-Gn													
PS.16. *	a: 878	872	801	944	951	763	746						
PS.25a *	a: 729	895	820	986	1007	777	870						
Gar(core)-Bt(Secondary)		797	740	834	855	718	748						
Gar(Core)-Bt(incl)	800	533	510	842	861	533	469						
PS.79(Cord-bearing).													
Gar(core)-Cord								813	802	811			
Calc. granulite													
PS.35.Gar(core)-cpx(av)											av. 792		
Pegmatite													
PS.26 Gar(core)-matrix biotite		811	755	856	862	726	695						
Ps.14.Gar(rim)-Bt	919	689	650	683	689	647	566						
PS.16 *		614	586	585	590	596	484						
PS.79 Gar (rim)-cord								758	661	717			
PS.25a Gar(rim)-Bt(II)		546	527	504	509	583	457						
PS.26 Gar(rim)-Bt(III)*		575	553	538	544	589	504						
Hb-Bt-Gn													
PS.19 plag-alk.Fs (av)												520	530
Granite													
PS.11													527

a: average, Pl :-Plyusnina (1982). * Neomineralization. Other abbreviations as in Table.21

Martignole (1985) method record an average value of 768 °C, which is comparable to that obtained by the method of Perchuk & Lavrent'e'va (1983), with a value of 759 °C (average). Ghent (1976), Thompson (1976) and Holdaway & Lee (1977) methods yield intermediate values of 857, 866 and 796 °C respectively.

The correction factors arising out of Fe^{3+}/Fe^{2+} ratios and the solubility of Ti and Cr in cordierites are significantly less and hence, the garnet - cordierite 'pressure-independent' thermometers have been used to cross-check the garnet - biotite temperatures. Accordingly, temperature estimates ranging from 813°C (Holdaway & Lee 1977), through 811°C (Bhattacharya et al, 1988) to 802°C (Perchuk & Lavrent'e'va (1983) have been obtained for garnet (core) - cordierite pairs in the cordierite - bearing khondalite samples. A comparison of perthitic alkali feldspar - plagioclase (average) temperatures (Green & Usdansky, 1986) and garnet - cordierite temperatures, at 5 kbars (Table.23) show that. the former gives higher (828 °C) temperatures than the corresponding garnet - cordierite temperatures (792 °C, av.) but, are comparable to that obtained by the garnet - biotite methods (816°C).

Temperature estimates obtained for the Khondalites are also conformable to the garnet-clinopyroxene temperatures of the calc-granulites, estimated by Ellis & Green (1979)

TABLE.23 Garnet-biotite, Two-feldspar, garnet-cordierite and garnet-clinopyroxene temperatures calculated for p = 5 Kbars

Garnet-biotite	Two-feldspar	Garnet-cordierite	Garnet-clino pyroxene
Sample, Anal No & description	Temp (°C)		
PS.14.Gar(core)			
Bt (matrix)	757		
PS.16 *	798		
PS.25a *	806		
PS.Gar(core)-Bt(II)	765		
PS.26.Gar(core)- Bt(matrix)	767		
PS.76 *	868		
PS.100 *	849		
PS.79 *	*944 Plag(av)-alk.Fs (perthitic)	828 Gar((core)-cord	792
PS.35 Gar(core)- cpx(av)			786(AV)
PS.14.Gar (rim)-Bt	648 Plag-alk.Fs(av)	620	
PS.16 *	585 *		
PS.25a *	536		
PS.76 *	610 *	637	
PS.100 *	611 *	619	
PS.79 *	556 *	663	
PS.25(a) Gar(core)- Bt(incl)..	583		
PS.100 *	605		
Ps.79.Gar(core)- Bt(III)	538		
PS.26 *	534		
PS.19	Plag-alk.Fs(av)	520	
PS.11	*	527	
'	Plag-alk.Fs (perthitic)	584	

*Anomalous temperature

method, which are considered to be pressure independent temperature sensors in granulite terrain. The results indicate a peak temperature of 792°C on an average.

Garnet (core) - matrix biotite pair in one of the samples (Ps.25a), have equilibrated at an average temperature of 869°C while, the second generation biotite (Bt.II) gives a lower average temperature of 782°C. This is closer to the garnet-matrix biotite temperatures of pegmatites, which yield an average temperature of 784°C by different methods (See Table.22).

Garnet (core) - biotite (inclusion) temperatures in the same sample (PS 25 a), indicates 861°C by Hodges and Spear (1982) method, at 8 kb pressure. Locationwise, PS.25a sample is in contact with a pegmatite.

Since, the granulitic rocks of the study area have been affected by retrogression, the re-equilibration conditions were also estimated using garnet (rim) - adjacent biotite compositions of khondalites and associated gneisses. Corresponding to mean pressure estimates, the temperature values estimated by the various methods range from 794 °C (Bhattacharya & Raith, 1987) through 652°C (Thompson, 1976), 622°C (Perchuk & Lavrenteva', 1983), 640°C (Hodges & Spear, 1982), 634°C (Ferry, Spear, 1978) and 618°C (Holdaway & Lee, 1977) to 525°C (Indares and Martignole, 1985) etc., with an average value of 638°C (see Table.22). Plagioclase (av) -

alkali feldspar temperature of khondalites and associated gneisses, calculated at 5 kbar, averages around 625°C (see Table.23), which are higher than the corresponding average temperatures estimated by the garnet - biotite temperature sensors (616°C). Garnet (rim) - adjacent cordierite temperatures estimated for the cordierite - bearing assemblages at 8 kbars, are 758°C (Holdaway & Lee, 1977), 661°C (Perchuk & Lavrenteva (1983) and 717°C (Bhattacharya et al, 1988), which broadly correspond to the estimated re-equilibration temperatures. Average alkali feldspar - plagioclase temperatures of the cordierite-bearing khondalites calculated at 5 kb, are also around 663°C (see Table.23).

Garnet (rim) - secondary biotite temperatures of Khondalites are lower at 521°C, comparable to the garnet rim - biotite (III)* temperatures of pegmatite samples (547°C, average). Plagioclase - amphibole equilibrium temperature estimated by amphibole Al_T content (Plyusnina, 1982), for one of the hornblende-biotite migmatitic gneiss samples close to a granite occurrence, is 530°C (see Table.22). Alkali feldspar (av)-plagioclase (av) temperature of 527°C obtained for one of the granites (FS.11) at 5 kbars (see Table.23), is also close to the plagioclase-amphibole equilibration temperature of the gneiss. All these values correspond to the neomineralisation temperature of the pegmatite sample.

* Neomineralization

It is, therefore concluded that the granulitic rocks including the khondalites, associated gneisses and cal-granulites, experienced (1) a peak metamorphic temperature of 834°C (2) a retrogressive or reequilibration event at 652°C and (3) a neomineralisation episode associated with migmatisation and granitic emplacement at 532°C (av).

Because of the susceptibility of geothermometers to re-equilibration, the peak as well as rim temperatures obtained from ion-exchange geothermometers had also been confirmed by the use of intersecting barometers (Perkins et al, 1982) of differing dP/dT slopes. Crossings of GPAQ P-T lines with garnet-biotite and two-feldspar thermometers, are shown in Table 24 a & b.

GEOBAROMETRIC calculations based on the methods of Ghent (1976), Newton & Haselton (1981), Mckenna & Hodges (1988) and Koziol & Newton (1988 and 1989), for various temperatures ranging from 500 to 1100°C, have been compiled in Table.25. Pressure estimations by garnet - cordierite geobarometers of Bhattacharya & Sen, (1985) and Bhattacharya, (1986) and the Cpx - Gar - Pl - Qz geobarometric estimations, based on Perkins & Newton (1981), are compiled in Table.26 & 27.

Core pressures estimated for the khondalites and associated gneisses using Ghent (1976), Newton & Haselton, (1981), Mckenna & Hodges, (1988) and Koziol & Newton (1988

TABLE. 24 b CROSSINGS OF GPAQ P-T LINES WITH BIOTITE - GARNET AND TWO-FELDSPAR THERMOMETERS FOR RIM COMPOSITIONS.

Rock type No Description	Ps.14	Ps.16	Ps.25a Gar (rim) -Bt	Ps.76	Ps.79	Ps.100
	P(Kbar)	T(°C)	P(Kbar)	T(°C)	P(Kbar)	T(°C)
					Bt	Gar
					Gar	T(°C)
GPAQ(GHENT)						
GR-BI(F-S)	4.43	668	2.73	566	1.88	483
(NE-HA) "	4.46	668	2.48	565	1.19	480
(KO-NE) "	5.30	672	3.37	568	2.14	484
(H-S)	4.52	674	2.80	571	1.95	488
(H-S)	4.57	674	2.57	570	1.29	486
(H-S)	5.40	678	3.46	573	2.22	489
(GHENT)-2fsp.						
(Gr-Us)	3.43	598				
(NE-HA) "	3.23	595				
(KE-NE) "	4.29	610				

INDEX:-GPAQ:-Garnet-Plagioclase-Al-sil-Quartz; NE-HA- (Newton & Haselton, 1981) KO-NE (Koziol and Newton, 1988) F-S (Ferry & Spear, 1978); H-S (Hodges & Spear, 1982); Gr-Us (Green & Usdansky 1986).

and 1989) barometers, yield pressures of 7.58, 8.87, 8.19, 8.99 and 9.99 Kbars respectively. Cordierite-bearing gneisses show peak pressures (Kbars) of 5.7 (Ghent, 1976), 7.48 (Newton & Haselton, 1981), 6.96 (Mckenna & Hodges, 1988), 7.98 (Kozioł & Newton, 1988) and 8.15 (Kozioł & Newton, 1989). Pressure estimation by garnet-cordierite geobarometers Bhattacharya & Sen (1985) and Bhattacharya (1986), generally serve to bracket equilibrium pressures, within reasonable limits and the obtained values range from 9.07 to 10.38 kbars for $P_{H_2O} = P_{total}$ conditions (Table. 28).

Geobarometric calculations based on clinopyroxene - garnet-plagioclase-quartz method (Perkins & Newton, 1981), of a calc-granulite sample close to the Gap proper, yields a mean pressure value of 3.3 kbars. Since, this geobarometer registers pressures 1000 to 1500 bars lower than that obtained from independent methods, the values reported here are considered to be the minimum estimations. Extensive application of Moetcher et al (1988) method for the present study has been restricted due to compositional constraints of the clinopyroxenes (see Chapter.V). Pressure estimates however, has been made for one of the calc-granulite samples, which yield low pressure values (4.5-4.8 kbars) by the DI barometer and unrealistically high (10.8 kbars) values by the HD barometer. The low pressure values obtained by DI barometers may be related to the high content of X_{Ca} (0.602)

TABLE.25 Model pressures(Kb) of the rocks estimated for temperature in the range of 500-1100°C

(a) GPAQ BAROMETERS

(GH=Ghent(1976), NE & HA = Newton & Haselton (1981),

MC & HOD = Mc Kenna & Hodges (1988),

KO & NE = Koziol and Newton (1988 and 1989)

	Temperature (°C)				
	500	700	800	900	1100

PS.14. Gar core(10)					
Plag (AV)					
GH (1976)	1.63	4.38	5.76	7.13	9.88
NE & HA (1981)	1.55	4.80	6.42	8.04	11.29
MC & HOD (1988)	1.77	4.71	6.19	7.66	10.60
KO & NE (1988)	2.43	5.56	7.12	8.67	11.77
" (1989)	2.52	5.63	7.19	8.75	11.86

PS.14. Gar rim (44)					
-Plag (AV)					
GH (1976)	2.03	4.88	6.31	7.74	10.60
NE & HA (1981)	1.61	5.00	6.73	8.39	11.39
MC & HOD (1988)	1.85	4.97	6.53	8.10	11.22
KO & NE (1988)	2.49	5.76	7.39	9.02	12.26
KO & NE (1989)	3.53	6.70	7.23	8.86	12.10

PS.16. Gar. core(26)					
Plag (AV)					
GH (1976)	3.11	6.24	7.80	9.36	12.49
NE & HA (1981)	2.11	6.79	8.63	10.48	14.16
MC & HOD (1988)	3.30	6.67	8.35	10.03	13.39
KO & NE (1988)	4.01	7.57	9.34	11.11	14.64
KO & NE (1989)	3.98	7.51	9.27	11.04	14.56

TABLE.25 (contd...)

Temperature (°C)

	500	700	800	900	1100

PS.16.Gar rim(10)					
Plag (AV)					
NE & HA (1981)	1.39	4.75	6.44	8.12	11.48
MC & HDD (1988)	1.64	4.73	6.27	7.81	10.90
KO & NE (1988)	2.27	5.51	7.12	8.74	11.95
KO & NE (1989)	2.03	5.23	6.84	8.44	11.64

PS.25a.Gar.core(36)					
Plag (AV)					
GH (1981)	7.01	11.15	13.22	15.29	19.42
NE & HA (1981)	7.21	12.47	15.10	17.73	22.96
MC & HOD (1988)	6.89	11.35	13.59	15.82	20.29
KO & NE (1988)	8.18	13.32	15.89	18.43	23.50
KO & NE (1989)	6.92	11.50	13.79	16.09	20.67

Ps.25a.Gar.rim(Av.5)					
Plag (AV)					
GH (1976)	2.12	4.99	6.42	7.86	10.73
NE & HA (1981)	1.53	5.02	6.77	8.51	12.00
MC & HOD (1988)	2.08	5.35	6.98	8.61	11.88
KO & NE (1988)	2.42	5.79	7.47	9.14	12.48
KO & NE (1989)	2.54	5.91	7.59	9.27	12.64

PS.76a.Gar(core)					
Plag (AV)					
NE & HA (1981)	1.48	4.81	6.47	8.14	11.47
MC & HOD (1988)	1.49	4.46	5.95	7.44	10.41
KO & NE (1988)	2.23	5.39	6.97	8.55	11.71
KO & NE (1989)	2.35	5.50	7.08	8.66	11.09

PS.76.Gar(rim)					
Plag (Av)					
NE & HA (1981)	0.68	3.79	5.36	6.93	10.06
MC & HOD (1988)	0.66	3.46	4.84	6.23	9.00
KO & NE (1988)	1.42	4.38	5.86	7.34	10.30
KO & NE (1989)	1.59	4.89	6.54	8.19	11.49

TABLE.25 (contd..)

Temperature (°C)

	500	700	800	900	1100

PS.76 Gar(core)					
Plag (incl)					
NE & HA (1981)	0.92	3.98	5.53	7.07	10.16
MC & HOD (1988)	0.89	3.64	5.01	6.37	9.10
KO & NE (1988)	1.65	4.57	6.03	7.48	10.40
KO & NE (1989)	1.77	4.68	6.14	7.59	10.50

PS.79 Gar (core)					
Plag (Av)					

NE & HA (1981)	2.17	5.71	7.48	9.25	12.80
MC & HOD (1988)	2.16	5.36	6.96	8.56	11.76
KO & NE (1988)	2.91	6.29	7.98	9.67	13.05
KO & NE (1989)	3.08	6.46	8.15	9.84	13.22

PS.79.Gar(rim)					
Plag (Av)					
NE & HA (1981)	-0.58	4.16	6.53	8.91	13.66
MC & HOD (1988)	-0.57	3.82	6.02	8.21	12.60
KO & NE (1988)	-0.63	3.19	5.10	7.01	10.80
KO & NE (1989)	2.64	5.95	7.60	9.26	10.91

PS.100 Gar(core)					
Plag (Av)					
NE & HA (1981)	2.56	5.79	7.40	9.10	12.32
MC & HOD (1988)	2.32	5.36	6.88	8.40	11.44
KO & NE (1988)	3.06	6.29	7.90	9.51	12.73
KO & NE (1989)	3.09	6.31	7.91	9.52	12.74

PS.100 Gar(rim)					
Plag (Av)					
NE & HA (1981)	1.28	4.53	6.15	7.77	11.02
MC & HOD (1988)	1.30	4.19	5.63	7.07	9.96
KO & NE (1988)	2.04	5.11	6.65	8.18	11.26
KO & NE (1989)	3.57	5.09	6.60	8.12	11.14

TABLE.26 RELEVANT COMPOSITIONAL PARAMETERS, PRESSURE, TEMPERATURE AND WATER CONTENT IN CORDIERITE OF KHONDALITE SAMPLE (Ps.79).

Pressure(bars)	T°C	H ₂ O	GH ₂ O	X ^{crd}	Bhattacharya H ₂ O & Sen (1985)	Bhattacharya (1986)	P1	P2	Min.P	Max.P
<u>Gar-Bt</u>										
5000	944(core) 556(rim) 538(incl)	5303.0 2591.6 2424.9	-43119.5 48255.0 -48488.5	0.8892 0.9520 0.9541	3.66 4.15 4.17	7.65 7.89 7.80	4.52 4.78 4.80	8.88 8.88 8.87		
5000 (GH, 1976)		5544.0	-45050.1	0.9401	3.84	8.34	2.84	9.58		
6900(NE&HA, 1981)	800	7646.0	-45050.1	0.9648	3.84	9.19	2.84	10.51		
7600(KO&NE, 1988)		9140.0	-45050.1	0.9741	3.84	9.68	2.84	11.04		
<u>Gar(rim)- Plag (Av)</u>										
2200(GH, 1976)	545	941.5	-48397.7	0.7801	4.54	6.38	4.79	6.81		
2600(NE&HA, 1981)	547	1107.5	-48371.7	0.8242	4.54	6.66	4.79	7.11		
3500(KO&NE, 1988)	550	1549.5	-48332.9	0.8916	4.53	7.26	4.78	7.76		
3600	646	-2157.6	-47084.9	0.8787	4.46	7.34	4.68	7.84		
4500	657	-2967.1	-46940.5	0.9213	4.45	7.97	4.67	8.52		
5400	669	-4004.1	-46783.2	0.9484	4.44	8.60	4.65	9.20		

TABLE.27 MODEL PRESSURE ESTIMATED FOR CALC-GRANULITES
FOR TEMPERATURES FROM 500-1100°C.

	TEMPERATURE (°C)				
	500	700	800	900	1100
No. & Description					
Ps.35 Gar-Cpx					
(Fe-rich)	3.89	4.22	4.39	4.55	4.88
(Mg-rich)	1.81	2.07	2.20	2.33	2.59

TABLE.28 Model pressure estimates (Kb) from core, rim and inclusion compositions for peak temperatures derived from the data given in Table.25 & 26
 dp/dT (bar/°C) calculated for selected samples are shown in brackets.

METHODS	Gar-plag-sill-qz geobarometer		Gar-cord geobarometer		Pl-Hb geobarometer	
	Gar-plag-cpx- qz geobarometer	Gar-plag-cpx- qz geobarometer	Gar-cord geobarometer	Gar-plag-cpx- qz geobarometer	Pl-Hb geobarometer	Pl-Hb geobarometer
Sample No, Rock type & description	Ghent(1976) Newton & Haselton(1981) Hodges(1988) Newton(1988) Newton(1989) & Sen (1985) (1986)	Kozioł & Kozioł & Bhattacharya Bhattacharya Perkins & Newton (1981)	Bhattacharya Bhattacharya Perkins & Newton (1981)	a.Plyusnina(1982) b.Hammarstrom & Zen(1985) c.Hollister et al.,(1987)		
Gar-Bt-Gn						
PS.14.Gar(core)-Plag(av)	5.76	6.42	6.19	7.12	7.19	
Gar-Bt-sill-Gn						
PS.16 *	7.8	8.63	8.35	9.34	9.27	
PS.25(a) *	13.22	15.1	13.59	15.89	13.49	
PS.76 *	5.9	6.8	5.95	7.5	7.08	
PS.100 *	5.2	7.4	6.88	7.9	7.91	
	(13.2)	(15.7)		(15.0)		
PS.79(cord bearing Khondalite)						
	5.7	7.48	6.96	7.98	8.15	9.07 10.36
	(13.7)	(17.0)		(16.2)		(PH 0 = P total)
PS.14.Gar(rim)-Plag(av)						
PS.16 *	6.31	6.73	6.53	7.39	7.23	
PS.25a *	6.42	6.44	6.27	7.12	6.84	
PS.76 *		6.77	6.98	7.47	7.57	
PS.100 *		5.36	4.84	5.86	6.54	
PS.79 *		6.15	5.63	6.65	6.60	
		6.53	6.02	5.10	7.60	
PS.25a gar(core)-plag(incl)						
	4.4	5.53	5.01	6.03	6.14	
	(12.5)	(14.9)		(14.3)		
PS.79						3.84 2.84
						(PH 0 = 0)
Calc granulite						
PS.35.						3.3
Hb-Bt-Gn						4.66(a)
PS.19						4.72(b)
						4.92(c)

while, the high pressure values of HD barometers might be due to their tendency to overestimate pressures in Fe-rich systems.

Rim pressures corresponding to peak temperatures calculated for the Khondalites and associated gneisses, show a general decrease from 9.16 Kbars (average) to 6.49 Kbars (average), with the exception of Ps.14 (garnet-biotite gneiss), which shows rim pressures higher by 0.302 Kbars than the core pressures. One of the garnet-biotite-sillimanite - gneiss samples (Ps.25a) shows a pressure reduction of greater magnitude (6-7 kbars). The rim pressure obtained by the various models for the Khondalites and associated gneisses are 6.37 (Ghent, 1976), 6.29 (Newton and Haselton, 1981), 6.05 (Mckenna & Hodges, 1982), 6.90 (Koziol & Newton, 1988) and 6.96 (Koziol & Newton 1989). Average rim pressure of cordierite-bearing khondalites is 6.31, which is lower by 0.94 Kbars, compared to their corresponding core values.

Pressures estimated by plagioclase - hornblende geobarometer of Plyusnina (1982), for one of the migmatitic samples (Ps.19) close to a granite occurrence, is 4.66 Kbars at a temperature of 530°C. Barometers of Hammarstrom & Zen (1986) and Hollister et al (1987), yield closely corresponding values of 4.72 & 4.92 Kbars respectively. Equilibration pressures of plagioclase inclusions, calculated

for one of the Khondalite samples (Ps.25a), show values of 4.4 (Ghent, 1976), 5.53 (Newton & Haselton 1981), 5.01 (Mckenna & Hodges, 1988), 6.03 (Koziol & Newton, 1988) and 6.14 Kbars (Koziol & Newton, 1989). Pressures estimated by the cordierite - garnet geobarometer (Bhattacharya & Sen, 1985; Bhattacharya (1986) for $P_{H_2O} = 0$ conditions (3.84 and 2.84 Kbars resp.,) approximates to the average neomineralization pressures of pegmatites.

The peak equilibration pressures of the granulite rocks of the study area are therefore, concluded to be around 8.4 Kbars while, the retrogressive pressures are lower at 6.50 Kbars. Neomineralisation with attendant granitic emplacement and migmatization is fixed at a still lower pressure of 4.97 Kbars.

VI.7 FLUID INCLUSION STUDIES

Background :

Fluid inclusions represent microgeochemical systems containing remnants of mineral forming fluids. During the crystallization history of minerals, small portions of mineral forming media get entrapped within tiny cavities in the growing crystal faces and along crystal growth faces. The first category known as "primary inclusions", which yield information on the early growth history of the mineral and the second category, known as "pseudosecondary inclusions",

which yield data on the processes that operated during crystal growth, are generally studied during the course of fluid inclusion investigations of granulitic rocks. Post crystallisation inclusions trapped in the minerals, termed 'secondary inclusions', yield information on the nature of post crystallisation fluids, which are not very valuable in granulite petrogenesis.

Study of fluid inclusions in granulites assumes special importance in the light of the 'carbonic metamorphism' model for the granulite petrogenesis, propounded on the basis of fluid inclusion data, and the suggested role of CO₂ streaming in the evolution of south Indian granulites by various workers (Newton & Hansen, 1986; Hansen et al, 1984; Santosh, 1984, 1986; Srikantappa, 1987).

Although several assumptions are involved, together with a number of limitations, this technique has been widely applied in elucidating a variety of problems in igneous, metamorphic and hydrothermal processes (Hollister & Crawford, 1981; Roedder, 1984) and the study of these true 'petrologic fossils' is increasingly being applied in investigating the nature and role of fluids involved in granulite petrogenesis.

Methodology :

Trapped fluid phases were examined in doubly polished, 0.2 to 0.8 mm thick, quartz, feldspar and garnet plates from the khondalite rocks. Inclusion petrographic studies were carried out using a petrologic microscope under varying magnifications. Heating-freezing experiments for microthermometric observations were carried out using a temperature calibrated CHAIXMECA microthermometry apparatus with a precision of $\pm 0.5^{\circ}\text{C}$.

Inclusion petrography :

Fluid inclusions occur in quartz, garnet and feldspars of the khondalite assemblage. Size ranges from less than 10 microns to about 60 microns and show a variety of cavity shapes, ranging from negative or diamond (Fig.122), polygonal, ovoidal, tabular to irregular shapes. Inclusions in garnet are attributed to a single generation, while those in quartz belong to more than one generation, as indicated by cross-cutting arrays. Inclusions in feldspars are ill-preserved and hence, are not used for microthermometric measurements.

The most dominant type is characterised by inclusions which are completely filled at room temperature, containing a dense dark fluid phase (Fig.123). These are the pure CO_2 inclusions, as indicated by freezing data. These include

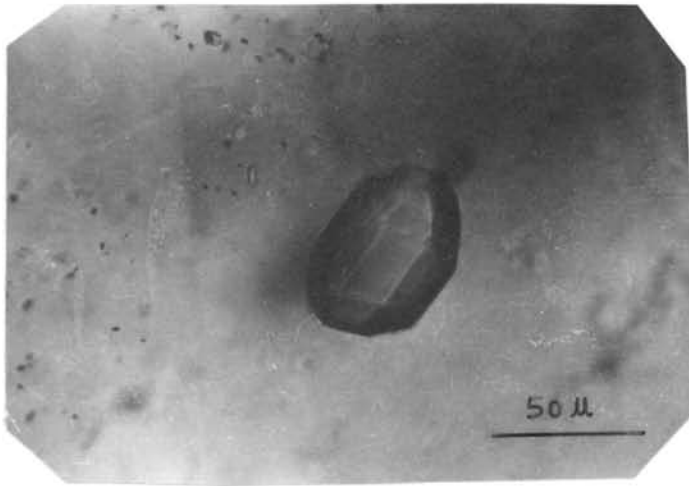


Fig.122 Photomicrograph of negative-crystal or diamond shaped cavity in khondalite.
Scale : 2 cm = 50 μ.

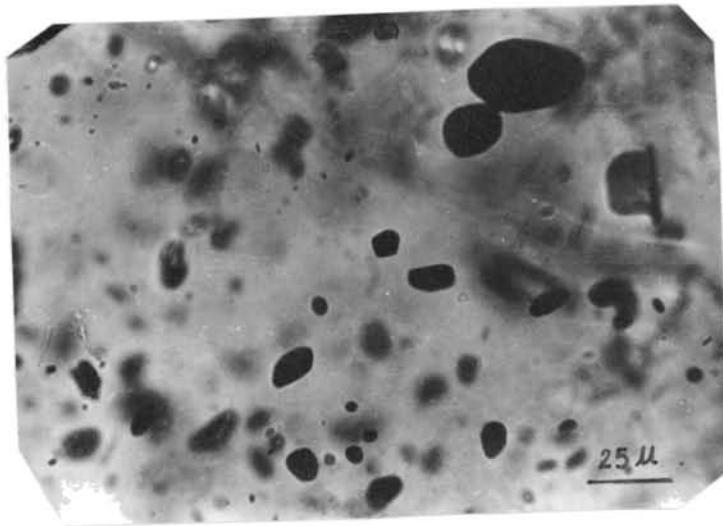


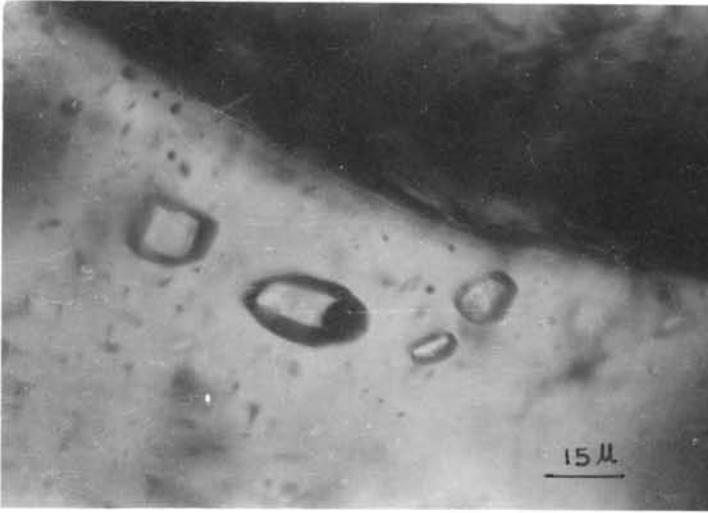
Fig.123 CO₂ inclusions in khondalites.
Scale : 1.1 cm = 25 μ.

isolated and azonal clusters and arrays of inclusions in quartz.

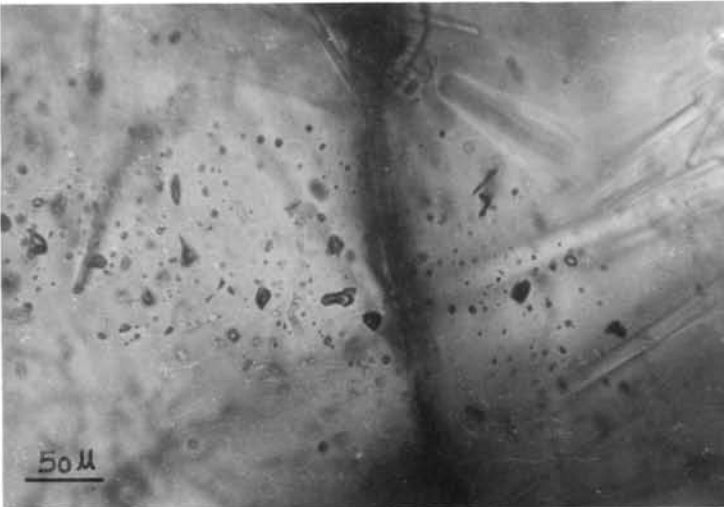
The second variety of inclusions is constituted by carbonic inclusions which are bi-phase (mixed carbonic-aqueous) at room temperature and develop a third phase on cooling, yielding a composition corresponding to CO_2 (liquid) + CO_2 (gas) + H_2O (liquid).

The third category consists of H_2O -rich inclusions which lack any daughter crystals at room temperature, indicating their low salinities (Fig.124a). Mostly occurring as polygonal or elongate cavities of small dimensions (5-25 microns), they are concentrated along healed fractures and are also seen transecting growth lines (Fig.124b), obviously post dating the carbonic inclusions. Necking effect is frequently exhibited with varying vapour liquid ratios in adjacent inclusions, which speaks of a post- deformation episode related to retromorphosis. The various inclusion types in the khondalites are schematically summarised in Fig.125 a & b. Of all the inclusion types described, carbonic inclusions constitute the dominant category.

Inclusion petrography enables to conclude that fluid evolution in khondalites is characterised by an early pure carbonic regime, followed by an intermediate mixed type (carbonic-aqueous) and a late aqueous phase.



(a)



(b)

Fig.124 H_2O -rich inclusions (a) concentrated along healed fractures. Scale : 2cm = 30 μ . and (b) transecting growth lines. Scale : 1 cm = 50 μ .

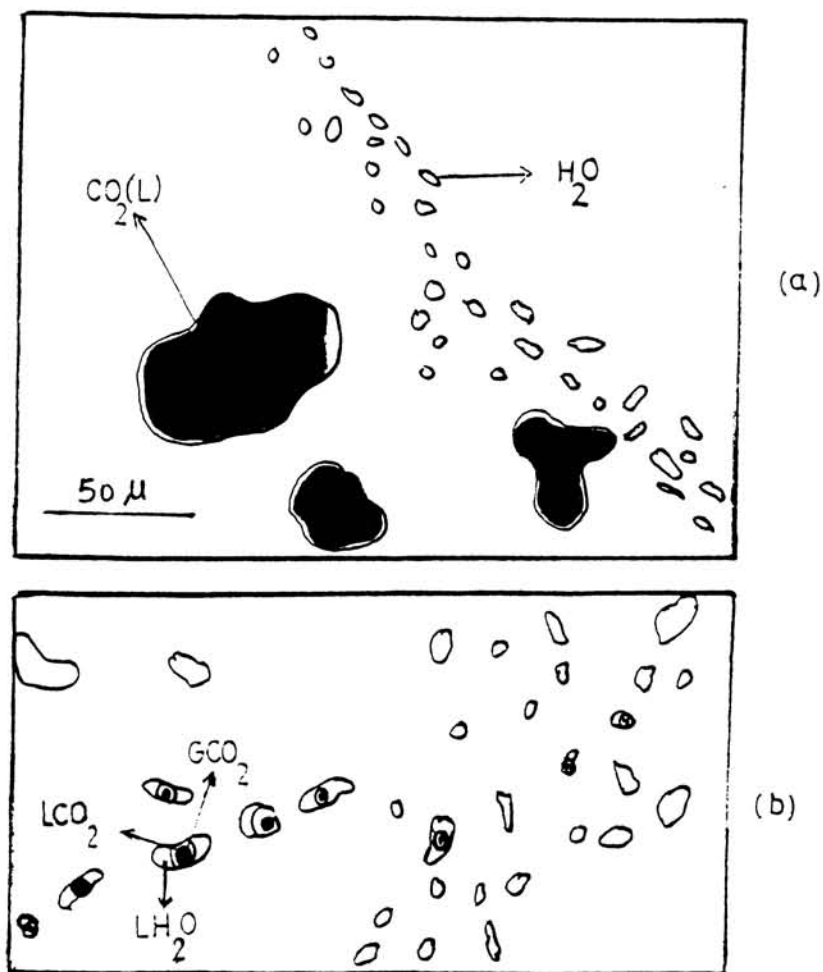


Fig.125 Sketch of inclusion types observed in khondalites (a) CO_2 -rich inclusions transected by aqueous inclusions. (b) Biphasic ($\text{H}_2\text{O}+\text{CO}_2$) and aqueous inclusions.

Freezing-heating experiments :- Microthermometric runs were carried out to determine the compositions and densities of the carbonic inclusions by observing the phase changes. Only those inclusions which do not show any evidence of leakage or necking down and occurring away from healed fractures were chosen. The inclusions were deep-cooled upto -80°C and on slow heating, the first melting (T_m) occurred around -56.6°C (Fig.126a). Since this temperature corresponds to the triple point for pure CO_2 , it is concluded that the entrapped fluids in these inclusions are pure CO_2 .

On further warming, the vapour carbondioxide phase in carbonic inclusions homogenised into liquid, within a temperature range of 3 to 16°C , with a peak around 6°C . Histograms of homogenisation temperatures of CO_2 ($T_{h\text{CO}_2}$) for carbonic inclusions in the investigated samples are depicted in Fig.126 b.

These values indicate a pure CO_2 composition and the corresponding densities, as deduced from CO_2 isochores, indicate moderate to high values ranging from 0.8 to 0.9 g/cm^3 .

Pressure estimates :

Considering the peak metamorphic temperature of 800°C (mean) deduced from mineral thermometry, the obtained

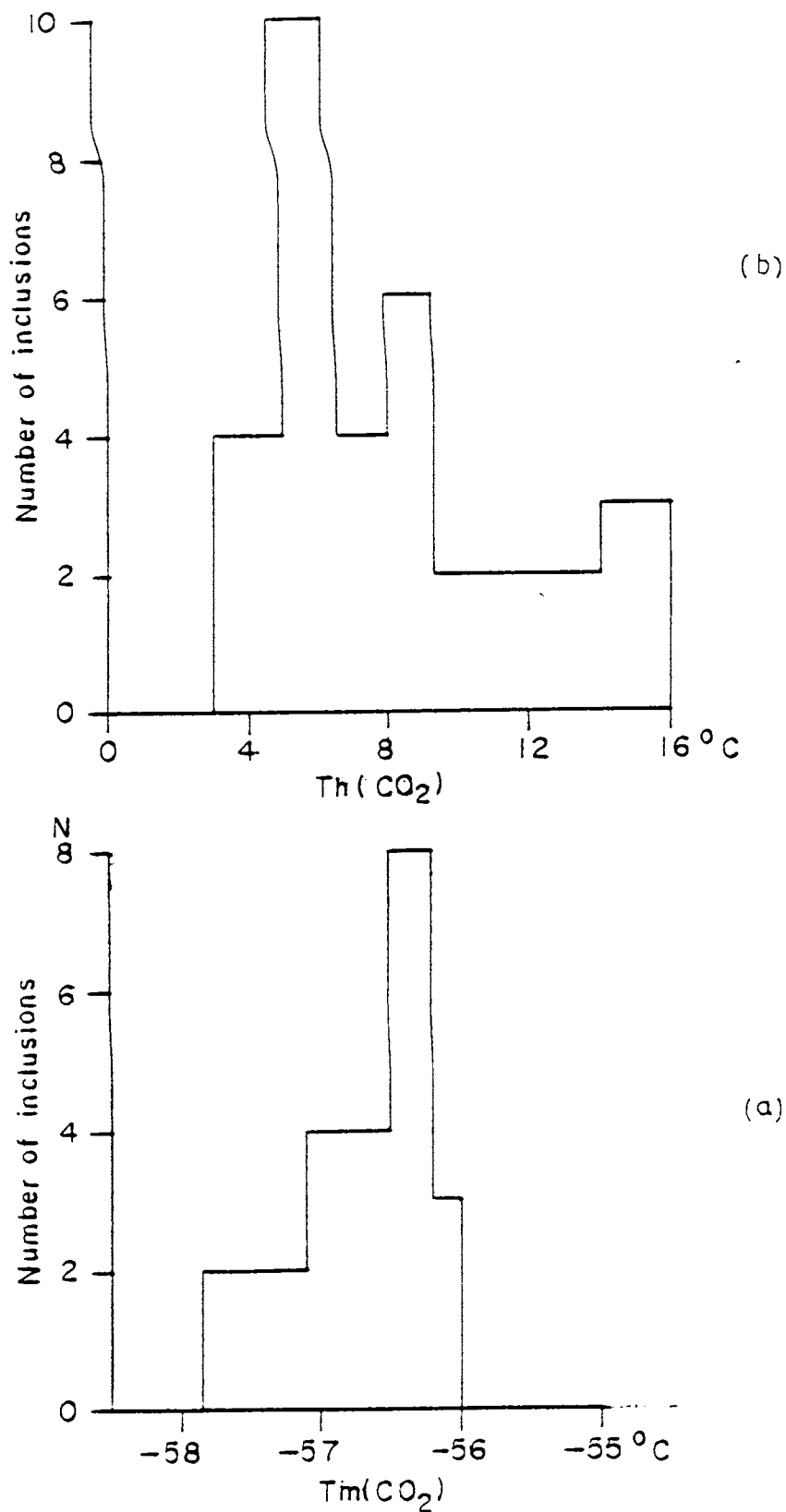


Fig.126 (a) Histogram of first melting temperatures of CO₂ inclusions from khondalites. (b) Histogram of homogenisation temperatures (Th) of CO₂ inclusions from khondalites.

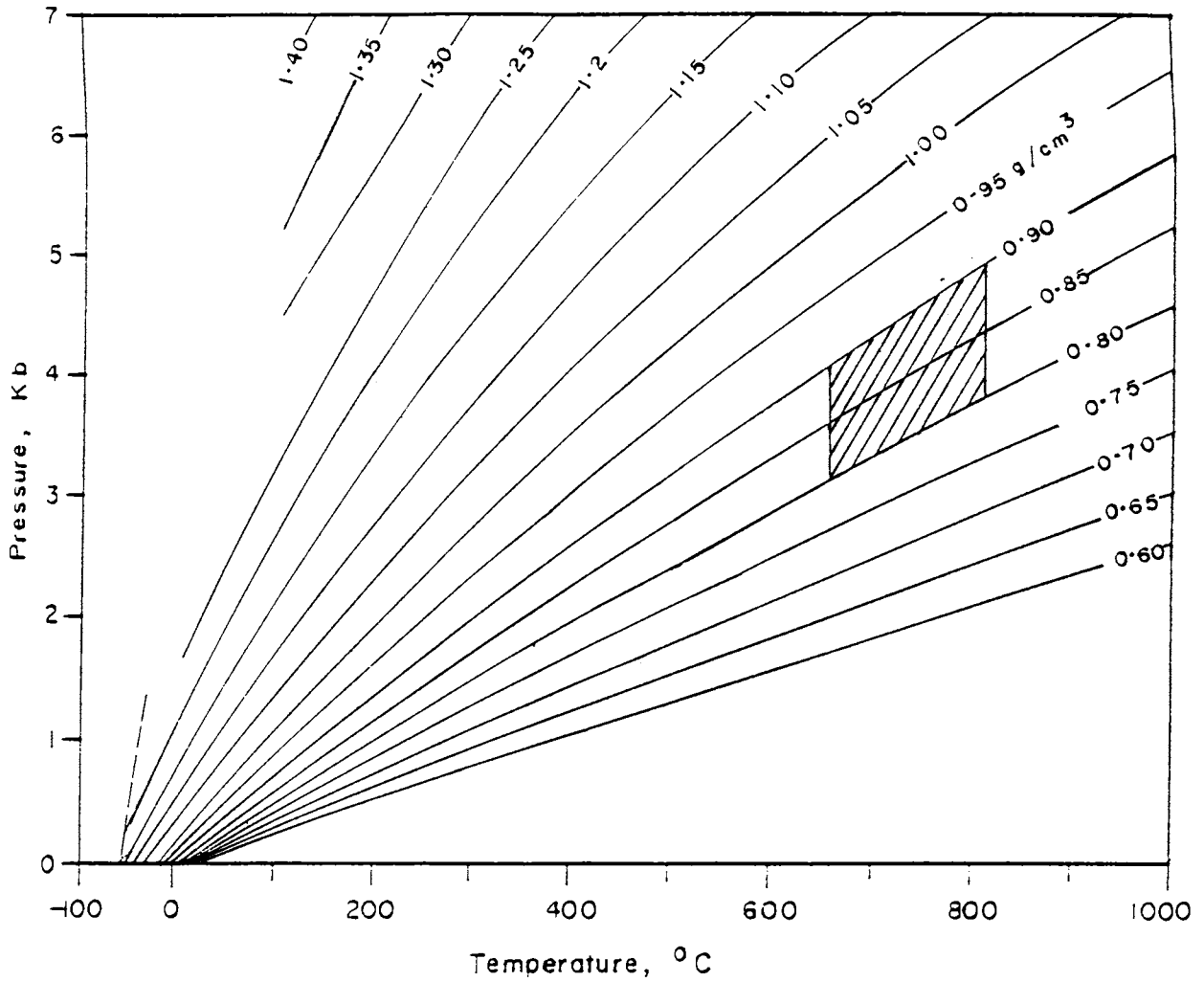


Fig.127 CO₂-isochores (labeled with density in g/cm³)
showing P-T regime demarcated by hatched area.

carbonic inclusion densities set an upper fluid inclusion pressure limit of 4.9 Kbar and a pressure of 4.1 Kbar, corresponding to the retrograde temperature of 650 °C (Fig.127).

VI.8 DISCUSSION AND CONCLUSIONS

Temperature estimates by garnet-biotite thermometers indicate an average metamorphic temperature of 848°C for the granulites of the Palghat Gap area. The more pressure independent garnet-cordierite (Perchuk and Lavrent'eva, 1983) and clinopyroxene-garnet (Ellis & Green, 1979) thermometers also yield closely similar results (av. 809 & 792 °C). This, together with the absence of lines of evidence for anatexis affecting the granulites and P-T constraints introduced by the various phase equilibria assemblages, such as the coexistence of plagioclase, calcite and scapolite in calc granulites, the latter with X_{Mg} in the range of 74-79, limits the peak temperature to 800-820°C (Newton, 1972; Goldsmith & Newton, 1977). The ubiquitous presence of sillimanite in the granulites and its stability relations (Althaus, 1967, 1969; Richardson et al, 1968, 1969)* limits the pressure maxima to less than 11 Kbar (curve 3; Fig.128). P-T fields of cordierite + almandine + sillimanite + quartz for a FeO/FeO + MgO ratio of 0.7273, also fixes the pressure and temperature within the 4-8 Kbar and 750-800°C range (Fig.129, after Winkler, 1979). Peak pressures estimated by

* Ref. Winkler (1979)

different GPAQ barometers for the peak temperature (800°C) convincingly suggests an average pressure of ~ 8.4 Kbars (see Table.28).

Results obtained from the garnet -biotite thermometers indicate a pressure dependence of 3.6 to 5.4°C/Kbar. It is 5.1°C/Kbar for garnet-cordierite and 12-14°C/Kbar for two-feldspar thermometers. Uncertainties in equilibrium temperature values are believed not to exceed $\pm 60^\circ\text{C}$ for most of the rocks. All high temperature indications of the garnet-biotite pairs have been correlated with a correspondingly high Ti values (4-6 wt %; Ref. Table.15, Chapter IV) in biotites (Stellan Ahlin, 1988), though the application of Ferry and Spear's calibrations is limited to biotites low in Ti. The possibility of garnet-biotite thermometers giving erratic results, due to erroneous assumption of all Fe as Fe^{2+} (Ghent et al, 1983), has been shown to be negligible in the present study by the comparable results obtained from other thermometers which do not involve exchange of Fe.

Temperature estimates (828°C), based on plagioclase (av)-alkali feldspar (perthitic) pairs in cordierite-bearing khondalites, at 5 Kbar (see Table.23) and garnet-cordierite temperature values (~ 809°C, av), reflect similar conditions of formation for the alkali feldspar-plagioclase and garnet-cordierite assemblages.

Temperatures based on rim compositions, corresponding to peak pressure estimates, are lower by about $\sim 180^{\circ}\text{C}$ with respect to their cores and support resetting during retromorphosis. The garnet (rim)-biotite and plagioclase-alkali feldspar assemblages have equilibrated in the pressure range of 2.3-4.2 Kbar and temperature range of $540-650^{\circ}\text{C}$, similar to the solidification conditions of alkali feldspar in granulites, indicating the close link between retromorphosis and granite emplacement phase. This is also substantiated by the temperature values obtained for the average composition of alkali feldspar in granite.

Ghent's (1976) pressure results, with a dependence of 12.5 to 14 bar/degree and that of Koziol and Newton (1989), with a pressure dependence of 14.5 to 16.5 bar/degree, sets respectively the minimum and maximum limits of estimated GPAQ pressures. One of the sillimanite-absent garnet-biotite gneiss sample (Ps.14), shows a higher rim pressure (0.2 to 0.5 Kbar) than the core pressure value. Any relation with loading during cooling, as suggested by Sharma (1988) for the granulite facies suite, exposed at Sand Mata, Udaipur district, Rajasthan in NW Indian shield however, is ruled out in this case since, all the other rocks show the expected normal behaviour of pressure reduction (~ 2 Kbars) towards rims. One of the garnet-biotite-sillimanite gneisses (Ps.25a), shows a pressure reduction of much higher magnitude

(6-7 Kbars), towards rims.

The estimated lower pressure (1000 to 1500 bars) by the clinopyroxene geobarometer (Perkins & Newton, 1981) is consistent with the amphibole-hypersthene reaction isograd (see Fig.128, curve 2) and may be related to preferential clinopyroxene reequilibration at lower temperatures. Low pressures obtained at near peak 'T' might also be reflective of a decompression related to uplift or extensional tectonism.

The upper P-T range of cordierite gneiss (av. temperature of 809 °C and av. ~7.25 Kbars, by GPAQ methods; see Tables.22 & 28), though consistent with the P-T fields of cordierite + sillimanite + quartz paragenesis, is higher than the values reported for the cordierite-bearing granulites (~ 5.34 Kbar) of Bangalore terrain (Harris & Jayaram, 1982) and the estimated values (~ 5.0 Kbars) for the cordierite-bearing granulites of Kodaikanal (Harris et al, 1982). Existence of cordierite, a 'low pressure' mineral, in high pressure regimes of 8 Kbars can be explained as due to the presence of high Mg (9 wt %) and water contents (av.0.9741, see Table.26) of cordierites of the study area.

The reported values of peak temperatures (average from all the methods) of metamorphism at 834°C and metamorphic pressures of 8.4 Kbars, are comparable to the P-T conditions

of granulites world over and falls in Bohlen's (1987) best fit P-T box of 7.5 ± 1 Kbar and $800 \pm 50^\circ\text{C}$ for granulites. Since, P-T estimates of granulites are minimum estimations of the actual metamorphic conditions (Frost & Chacko, 1989), the presently estimated values of ~ 8.4 Kbars and $\sim 800^\circ\text{C}$ can be suggested as the lower limit of the P-T maxima attained by the granulites of the study area. This is possibly amplified also by the high P-T values (9.5 Kbar, 950°C) reported for the pyroxenites and gabbroic units of the Nilgiri Hills (Srikantappa et al, 1986).

The overall P-T array defined by the estimated maximum and minimum pressure-temperature limits of the granulites of the study area, also suggest a cooling curve corresponding to isothermal depression (ITD) paths (see Fig.128). This is further corroborated by the crossings of the P-T data corresponding to core and rim compositions (Fig.130). Higher pressure values obtained for one of the garnet-biotite-sillimanite samples (Ps.25a), may be related to its proximity to an intrusive pegmatite. P-T values estimated for migmatitic gneiss, granites and pegmatites cluster at ~ 4.5 to 5 Kbars and 500 to 550°C range, suggesting an IBC component towards the last stages of the ITD path (see Fig 128). Termination of these ITD paths in a phase of IBC, around 800°C (see Fig.128), similar to the ITD path described by England and Thompson (1986) also illustrates a

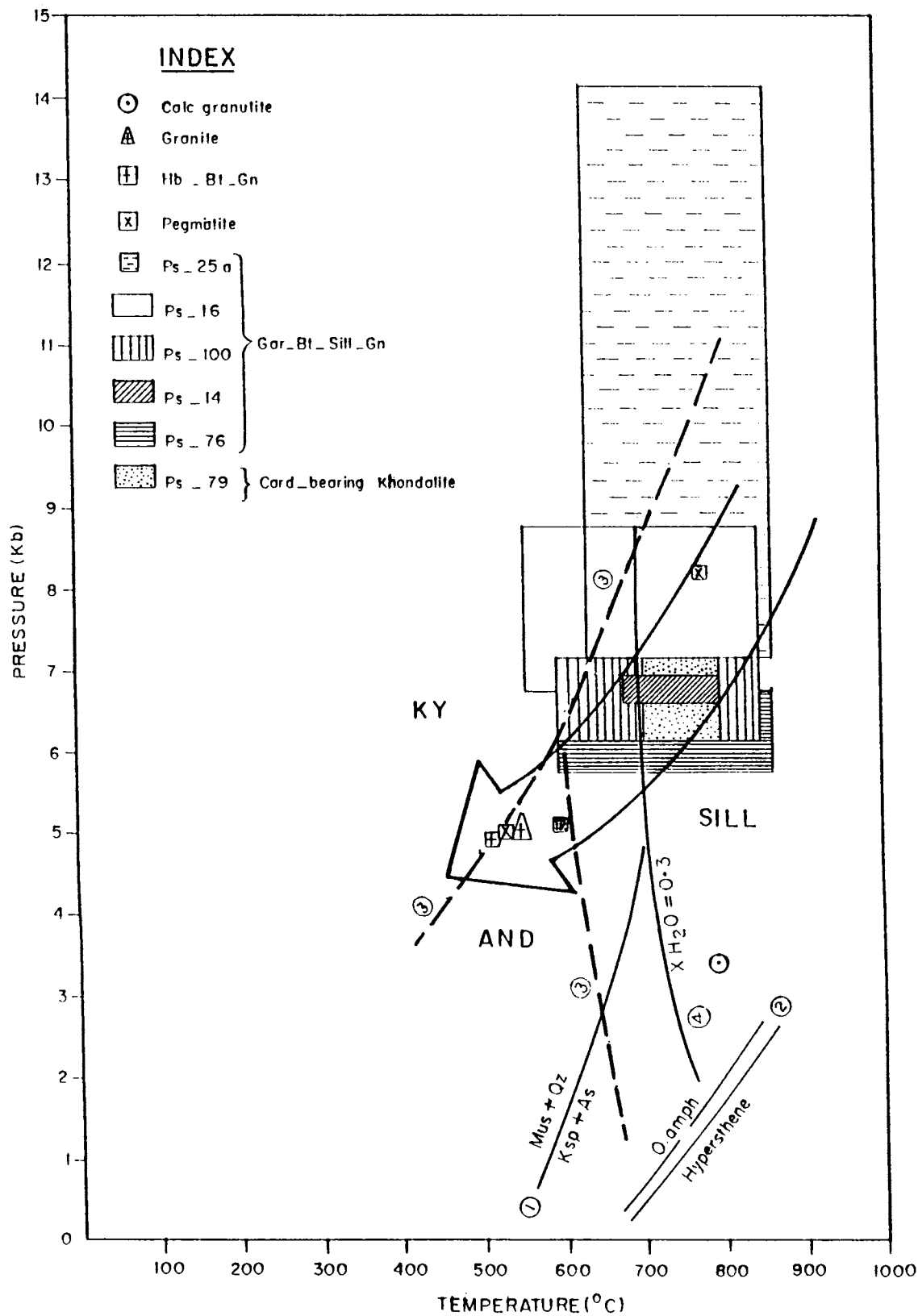


Fig.128 P-T fields derived by geothermobarometry of granulites of the study area. Arrow indicates an ITD P-T evolution path tending towards an IBC path. Curve (1) is after Althaus et al, 1970; curve (2) from Winkler, 1979 and curve (3) the approximate stability fields of Al-silicate representing intermediate positions given by Althaus (1967, 1969a & b) and Richardson et al, (1968,1969) minimum melting curve of granite (curve.4) is after Lee & Holdaway (1977).

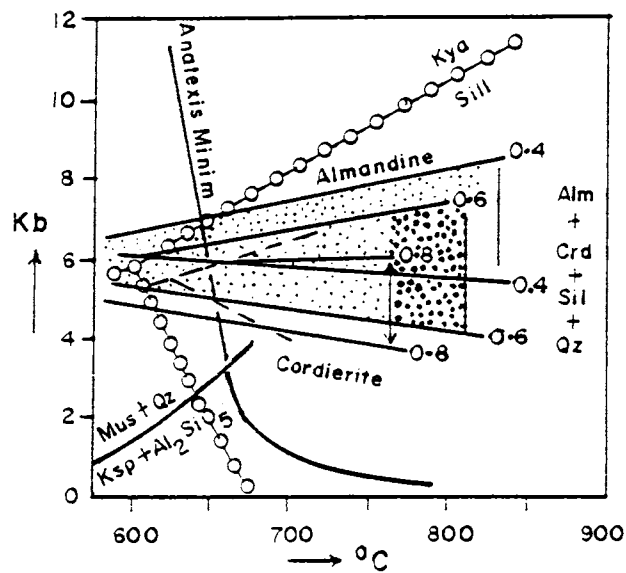


Fig.129 Bulk FeO/FeO+MgO ratio of cordierite field (dark stippled) in P-T diagram of coexisting Crd-Alm-Sill-Qz for various FeO/FeO+MgO ratios of the bulk compositions (after Winkler, 1979). Reactions define the boundary between medium and high grade metamorphism and the approximate phase boundaries of Al₂SiO₅ phases.

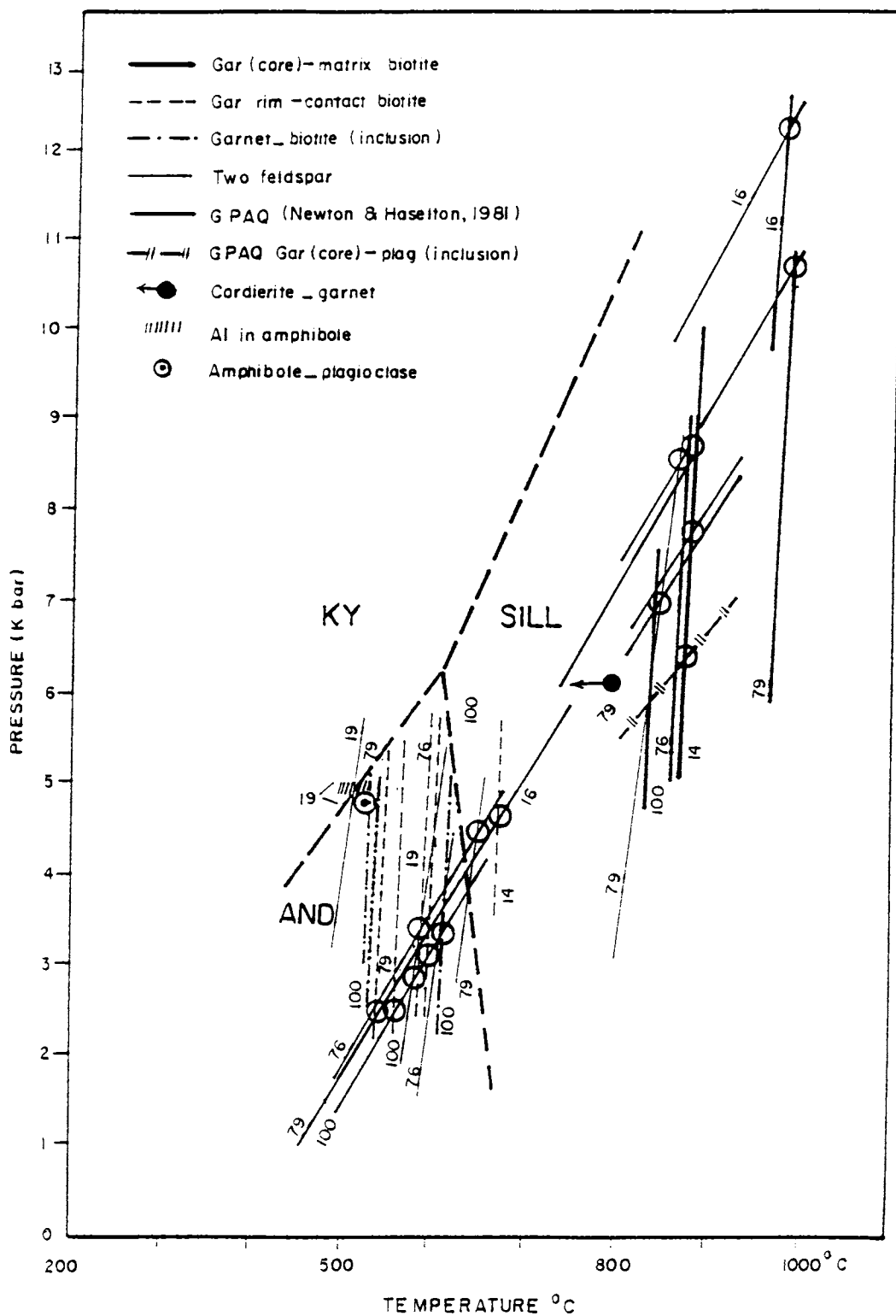


Fig.130 Crossings of GPAQ barometers with two-feldspar and garnet-biotite thermometers showing an evolution path comparable to the ITD path shown in Fig.128.

possible link between ITD and IBC granulite paths.

Decompressional ITD pressure-temperature paths of the granulites also show cooling through $\sim 180^{\circ}\text{C}$, corresponding to a decompression interval of ~ 2 Kbars, concomitant with the typical P-T paths exhibited by the south Indian khondalites (Lal et al, 1984; Hensen, 1984) and Kerala khondalites (Chacko et al, 1987). In pelitic rocks the observed reaction textures such as plagioclase around garnet and sillimanite rimming or enclosing garnet (see Fig.39, Chapter III), also demonstrate ITD histories.

Decompressional P-T path (ITD) has conveniently been ascribed to the net result of tectonic thickening, combined with the vertical redistribution of heat through syn-to post-thickening magmatism, followed by erosion of the crustal piles or to extensional settings. P-T paths which involve significant static isothermal decompression therefore, may be expected in areas of continental collision (England & Thompson, 1984). Comparison of the geometry of the ITD granulite path of the present study with the model paths for erosion (England & Thompson, 1984) show that the latter has much shallower dP/dT slopes, indicating that erosion alone could not have resulted in the obtained configuration. Conformity of the estimated P-T path of the rocks of the study area with the model exhumation paths for faster rates of tectonic stripping (Harley, 1989), signify an increased

rate of exposure and uplift through some mechanism of tectonic thinning process, other than erosion. Although, vertical movement of crustal segments is possible through melt enhanced deformation or surges (Hollister & Crawford, 1986), the most effective tectonic thinning process on a regional scale is extension of the previously thickened crust (Van Reenan et al, 1987 in Harley, 1989). Steep ITD paths followed by an IBC component towards the reequilibration-granite emplacement stage, as the one obtained for the study area could also be produced in a collision-extension regime (Harley, 1989). The rapid extensional setting and attendant decompression of the previously thickened crust (Van Reenan et al, 1987 & Sonder et al, 1987 in Harley, 1989), illustrated by path 2 in Fig.131, has been recognised in broad orogenic belts (England, 1987) and is facilitated by topographic contrasts, if the lithosphere strength is sufficiently low. England (1987) & Sonder et al (1987) proposed a process of detachment of thermal boundary layer (TBL) comprising the lower portion of a thickened sub-continental lithosphere with attendant magmatism, to explain the P-T evolution history of path .2 (Fig.131), which closely simulates the estimated P-T path of evolution of the study area.

The estimated fluid inclusion pressures of 4.9 and 4.1 Kbars, corresponding to peak (800°C) and retrograde

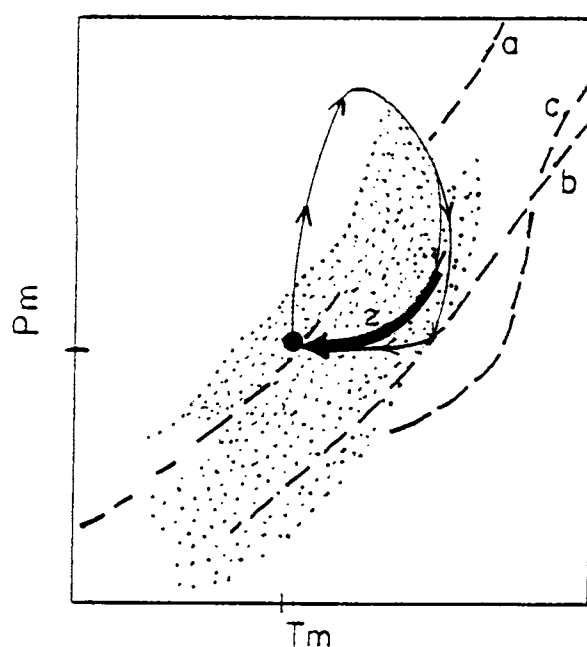


Fig.131 Model path for extension after thickening (path.2) based on Sonder et al (1987). a : Initial geotherm. b : Late extension geotherm and c : Late extension + TBL - detachment - triggered magmatism. Path.2 is similar to the P-T path of England & Thompson (1986). Stippled area represents generalised ITD path P-T regime. For description see text.

temperatures (650°C), are far too low compared to the corresponding mineralogic barometry. Possibility of post-peak entrapment of inclusions, giving pressure estimates lower than that obtained from independent estimates cannot be ruled out (Tuttle, 1949; Lamb 1988). Lowering of estimated pressures by 0.5 to 2 Kbars due to the effect of undetected H₂O in peak metamorphic inclusions has also been proposed by various authors (Brown & Lamb, 1986; Lamb et al, 1987). The reported fluid densities (0.80 to 0.90 g/cm³) are also too low than the expected values of 1.05-1.125 g/cm³, corresponding to peak P-T conditions estimated by the various geothermobarometers. Fluid inclusion density values reported for the south Indian granulite terrains are also higher (Hansen et al, 1984; Santosh, 1986). Probability of obtaining fluid densities considerably less than the peak conditions, especially in the case of fluid inclusions in the 3-50 μm size range, because of their incapability to maintain internal overpressures greater than 1.0 - 1.5 Kbar over geological time in terrains where rapid uplift has resulted in isothermal decompression (ITD), has also been brought to light by several authors (Crawford, 1979; Hollister et al, 1979; Sterner & Bodnar, 1989).

Dense CO₂-rich fluid inclusions in Nilgiri Hills, reported by various authors (Srikantappa, 1987), suggest that the fluids were dominantly carbonic during metamorphism of the charnockitic terrains. However, spacial association of

low density CO₂ rich fluids in rift settings also has been recorded by various workers (Konnerup-Madsen et al, 1981; Konnerup-Madsen & Rose-Hansen, 1982). This is in conformity with the similar observations made in retrogressed areas of Moyar shear zone (Srikantappa & Narasimha, 1988) and Bhavani shear zone (Srikantappa et al, 1988). Since the P-T data of fluid inclusions reported in this study are more akin to the P-T estimates of retrograde-reequilibration event, these inclusions may well represent the P-T-X regime prevailing during that event. Since the CO₂ inclusions in garnet were fully leaked, no attempt to trace the evolution of CO₂ inclusions in garnet could be attempted. Since, most of the CO₂-rich fluid inclusions examined in this study probably relate to post-metamorphic fluid conditions, these are also expected to represent a change in fluid regime, coinciding with the retromorphosis.

The overall P-T array suggested by the various geothermobarometers and the lower fluid inclusion pressures, compared to the values predicted from the mineral assemblages of the rocks, suggest an uplift faster than their cooling rates. Extension/tectonic thinning subsequent to collisional thickening seems to be the most likely mechanism for producing the ITD path obtained for the present study. Towards reequilibration related to granite emplacement, this path shows an isobaric cooling component.

CHAPTER VII

AGE

Published geochronological data for the Precambrians of Kerala region are far too meagre for coming to any reliable conclusions regarding their chronostratigraphy. The available age data on the rocks of Kerala region suggests that there were several episodes of metamorphism and associated igneous activity in this region (Holmes, 1955; Venkatasubramanian & Krishnan, 1961; Vinogradov and Tugarinov, 1964 and Crawford, 1969). Apart from the occurrence of rocks of over 3000 m.y., there are also evidences of 2700, 2100, 1600, 1000, 700 and 500 m.y. events (Soman, 1980).

The oldest ages obtained for rocks from the Kerala region include the whole rock Rb-Sr ages reported (Crawford, 1969) for charnockite and khondalite samples from Ayoor & Pandaplavu, Trivandrum district (2155 and 3070 m.y. respectively). U-Pb zircon dating of garnet-biotite gneiss and charnockites of Nedumannur by Odom (1982) has yielded ages of 2838 ± 40 and 2930 ± 50 m.y. respectively. Recent zircon studies on Ponmudi charnockites have revealed a late proterzoic event (1930 m.y), with a U-Pb zircon age of the principal granulite facies metamorphism fixed around 540 m.y. (Srikantappa et al, 1985). Chacko (1987) indicated a poorly defined Rb-Sr isochron age of 2100 Ma for the khondalite samples from Kallar, South Kerala. Rb-Sr dating of

cordierite gneisses and charnockites from Achankovil yielded ages of 670 ± 8 m.y and 660 ± 45 m.y respectively (Iyer & Santosh, 1987), implying a thermal overprint of Pan African activity in South Kerala (Hansen et al, 1985). A late Precambrian- Early Palaeozoic age for the magmatic phase has been suggested, based on Rb-Sr age of the Ezhimala pluton (Nair and Vidyadharan, 1982). Other age determinations include K-Ar age data on the Kalpatta, Ambalavayal and Thaluru granitic plutons (512 ± 20 , 560 ± 30 , 710 ± 20 m.y respectively) from the northern part of Kerala (Nair et al, 1985) as well as the age data on Chengannur granite (Soman et al, 1983).

As part of the present study, an attempt was made to date a few geologically controlled samples of pegmatites from the Gap area. The new geochronological data reported here represent a small, but significant contribution to the overall picture and are examined in the background of the merits and limitations of various geochronological methods. Though, geochronological methods of isotopic dating in polymetamorphic granulite terrains are fraught with insurmountable uncertainties, each age determination method, U-Pb, Pb-Pb, Rb-Sr, K-Ar or Sm-Nd, furnishes its own specific information. Despite the uncertainties involved, these methods based on the spontaneous disintegration of heavy atoms to lower energy states, through alpha or beta particle emission or capturing of an electron, serves as a tool in

resolving the discrepancies and incongruities of various other chronometers.

U-Pb Method :- Radioactive decay of U^{238} to Pb^{206} , U^{235} to Pb^{207} and Th^{232} to Pb^{208} is effected through a series of intermediate nuclides that themselves are radioactive. The apparent direct parent-daughter relation is often upset by the loss or addition of U, Th or Pb or one of the intermediate members of the radioactive series, resulting in discordant ages (Wickman, 1942 in York & Farquhar, 1972). Under normal circumstances, the U-Pb concordia, which represents the locus of all points having equal U^{235}/Pb^{207} and U^{238}/Pb^{206} ages, would define the time of critical crystallisation and the time of later lead loss is given by the intercepts in the U-Pb concordia, by a straight line defined by the plots of radiogenic lead Vs uranium. In addition to the selective lead loss in response to heat and stress, an added problem can arise due to the presence of common lead in radioactive minerals. The major limitation of the decay process of Th^{232} to Pb^{208} , is the scarcity of Th-bearing mineral and complications arising out of the easy removal of Th by chemical processes.

The single beta decay of Rb^{87} to Sr^{87} (Hahn & Walling, 1938), is a useful method in mica, potash feldspar and pyroxenes but, necessitates a sufficiently high Rb/Sr ratio of the rock. The Rb/Sr whole rock isochron technique has been extended in its utility towards understanding the

stratigraphic sequences, the success in dating being dependent on the assumption of complete homogenisation of 'Sr' isotopes. This method, supposedly yields better results than the K-Ar method since, Sr is easily mobilised and the $\text{Sr}^{87}/\text{Sr}^{86}$ ratio is easily homogenised in the rock body during metamorphism. In minerals, strontium becomes stabilized quickly and at much higher temperatures than does argon gas. However, correction for initial strontium and decay constants results in uncertainty. The extra analytical step to determine the original $\text{Sr}^{87} / \text{Sr}^{86}$ ratio, introduces extra analytical errors which may be huge, if the samples are young (Eicher, 1976). This method works best for rocks that are geologically old. Alteration of radiogenic $\text{Sr}^{87}/\text{Rb}^{87}$ in biotites, due to base exchange phenomena at lower temperatures, also hamper the results.

The choice for the present study has been confined to the decay scheme of K^{40} to Ar^{40} , with a half life period of 1.3 billion years. The major limitations are the accuracy with which exceedingly small amounts of radiogenic argon can be estimated and leakage of argon. The effectiveness of K-Ar dating depends on the system being closed to any loss or addition of radiogenic Ar^{40} and the correction applied for the presence of atmospheric Ar^{40} .

Comparison of the resetting effects of K-Ar and Rb-Sr clocks reveal that the general impression of K-Ar ages being "minimum ages" (Aldrich et al, 1965 in York & Farquhar, 1972),

does not always hold good especially, if base exchange effect due to circulating ground water is considered. Such exchange removes K^{40} and Ar^{40} equally effectively, causing no change in the K-Ar ages. Added proof has also been provided by the concordant Rb-Sr and K-Ar dates of mica samples, reported from pegmatites and associated Dharwar rocks of Kolar (Venkatasubramanian et al 1967).

For the present study, samples of micas have been retrieved from both the concordant and discordant pegmatites localised within the metasedimentary sequence and the migmatites. (Fig.132 shows the location of pegmatite samples chosen for the determination). Dating has been restricted to muscovite and biotite samples, because of their relatively high content of potassium. They also have less pronounced tendencies to incorporate excess radiogenic argon, along crystal imperfections and low angle grain boundaries, at the time of crystallisation (Amirkhanoff et al, 1961; Dalrymple & Lanphere, 1969). Field observations fix the major emplacement of pegmatites within post D₂ Syn D₃ deformation episode (ref.Chapter II). The impact of D₃ deformation has resulted in only slight manifestations of pinch and swell structures and is considered to be less intense. Since, pegmatite emplacement is known to be associated with the closing stages of tectonomagmatic cycles, it has been reasonably assumed that the reported ages of biotites and muscovites from pegmatites belonging to this specific

deformation stage, would represent the closing stage of a tectono-magmatic event.

RESULTS

Biotite and muscovite from 5 pegmatites (see Fig.132), representing the concordant and cross-cutting varieties were dated by K-Ar method, in the laboratory of IGEM, USSR Academy of Sciences. The samples were fused in an all metal fusion system with an internal molybdenum coil of 1 mm diameter. Purification of radiogenic argon was carried out in a metallic device AU-4M, designed and fabricated in the IGEM. Content of radiogenic argon was determined on the mass spectrophotometer model M1-1201, by isotope dilution method, using Ar³⁸ as tracer. Potassium was determined by flame spectrophotometry. These extremely sensitive methods of potassium and argon determination reduces the possibility of analytical error to a minimum.

Large flakes of the samples were investigated in detail. Central and peripheral zones of large crystals of the samples (Ps.92), were subjected to analysis. A schematic sketch of the sample showing portions separately analysed, is shown in Fig.133. The age is calculated using decay constants recommended by the IGC, Australia, 1976 as follows:

$$\lambda_e = 0.581 \times 10^{-10} \text{ A}^{-1}, \quad B = 4.962 \times 10^{-10} \text{ A}^{-1}$$

$$40_k = 0.01167 \text{ (atom \%)}$$

$$T \text{ (in } 10^6 \text{ years)} = 1885 \ln [1.910 \text{Ar}^{40} / \text{K}^{40}]$$

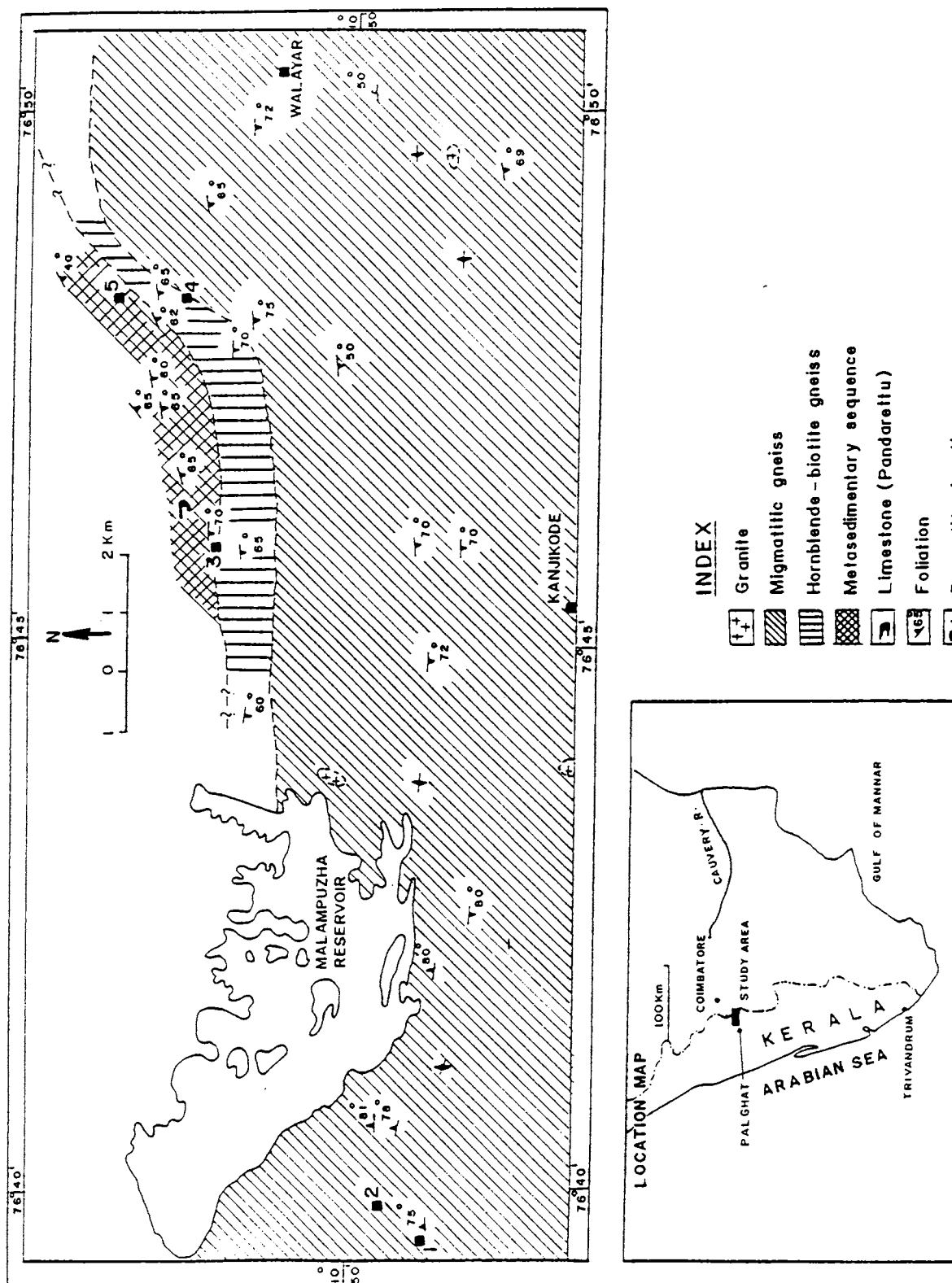


Fig. 132 Location map of the dated pegmatites.

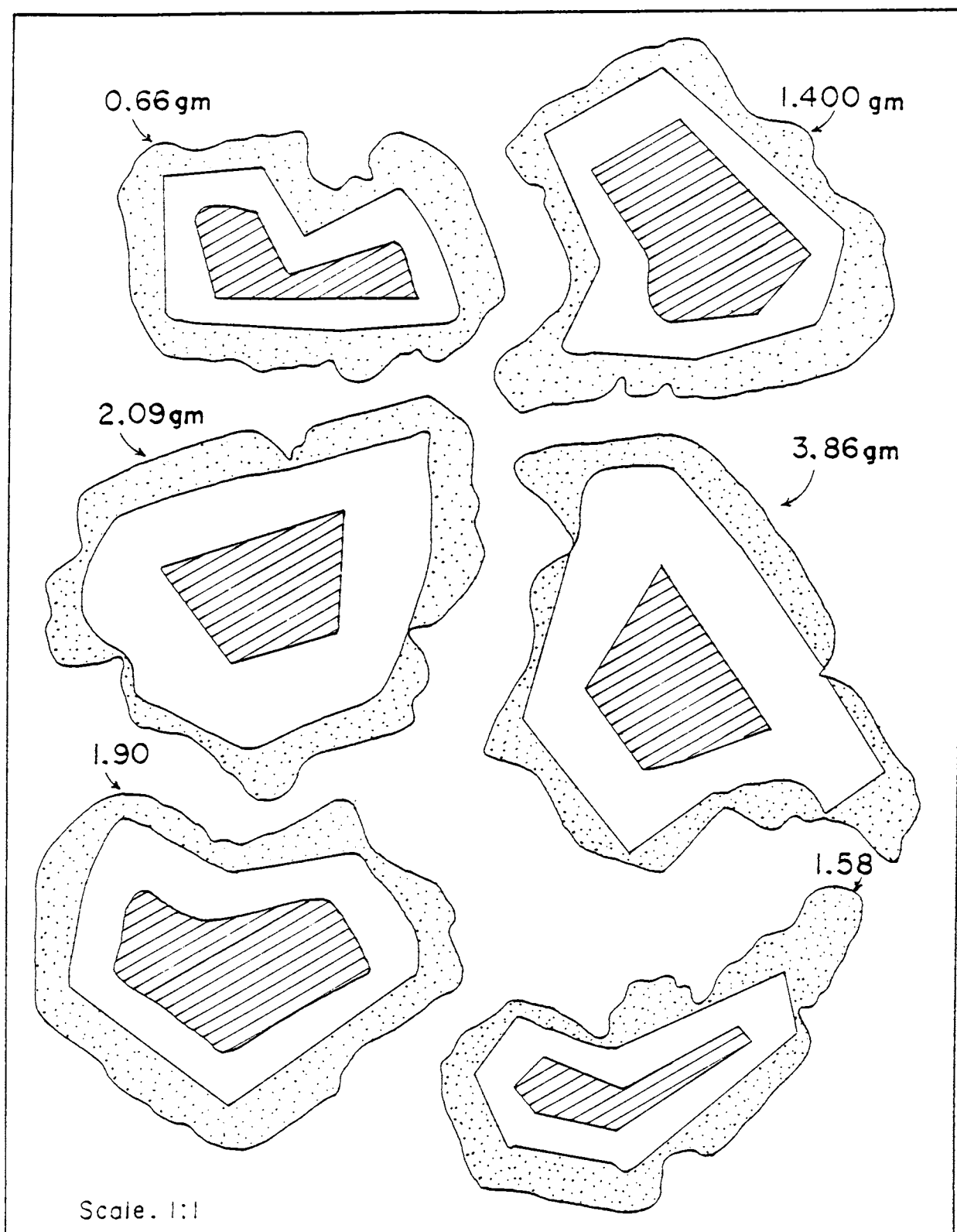


Fig.133 Sketch of mica sample (Ps.92) analysed for dating. Stripes indicate central portion and dots, the peripheral zones. Sample weights and scale are shown in figure.

The 1.60 σ probable error on age is calculated, based on the standard error in the determination of radiogenic argon and potassium. Results are given in Table.29.

DISCUSSION

The results obtained from micas occurring in both the concordant and discordant pegmatites of the present study show a range from 484 to 512 m.y. The close corresponding age results, obtained from the central and peripheral portions of large mica flakes (Table.29), suggests that these did not undergo any major and intense change after their crystallisation, since any later metamorphic event would have fully reset the K-Ar clock by the removal of the earlier accumulated radiogenic argon. The chances of such an event in the given geologic setting is far too meagre. Field observations of the pegmatites under study, reveal no indications of later metamorphic or thermal events or alteration by aqueous fluids. Concordance of ages determined for two different minerals such as muscovite and biotite, having different "blocking temperatures", from the same rock, also provide powerful argument in favour of the absence of substantial thermal changes after their emplacement.

Close clustering of the ages of biotite and muscovite from pegmatites, around 490-510 m.y indicates a major geologic event during this period. As pegmatite emplacement is known to be associated with the closing stages of tectono-

TABLE. 29 K-Ar AGES OF MICAS FROM PEGMATITES, PALGHAT GAP AREA IN KERALA

Locality/ Samples No.	Long	Lat.	Mineral	Content		⁴⁰ Ar Rad.		Age m.y
				K%	Rad. argon [ng/g]	⁴⁰ Ar General	⁴⁰ Ar General	
1/PS-52	76°39'27"	10°49'19"	Biotite	7.28±0.07	289±5	61 : 64		498±15
2/PS-53	76°39'48"	10°49'44"	Biotite	7.67±0.07	303±5	53 : 58		496±15
3/PS-92			Central part	7.88±0.08	324±5	63 : 70		512±15
			Periphery	7.66±0.08	313±6	53 : 65		509±15
4/PS-85	76°48'11"	10°51'31"	Biotite	7.40±0.07	284±5	67 : 72		484±14
5/PS-97	76°48'25"	10°52'13"	Muscovite	8.43±0.08	330±5	77 : 78		491±14

1. E-W trending 1.5m thick pegmatite [Q+F+Bi] in migmatite
 2. 140°-320° trending 0.07m thick pegmatite [Q+F+Bi+Ilb] in migmatite
 3. 35°-215° trending 8.0m thick pegmatite [Q+F+Bi+Ca ± graphite] in khondalite
 4. 70°-250° trending 2.5m thick pegmatite [Q+F+Bi] in Ilb-Bi gneiss
 5. 35°-215° trending pegmatite [K+F+Bi+Mu] in khondalite
- Q - quartz, F - feldspars, Bi - biotite, Mu - Muscovite,
Ca - garnet, Ilb - hornblende

Analyses - I GEM, ANSSR, Moscow.

magmatic cycles, it is reasonable to suggest, that the 490-510 m.y. time interval represent the closing stages of a tectono-magmatic event in the Palghat Gap region. Since, this post dates the granulite metamorphism of the meta sedimentary sequence, the pegmatitic emplacement may be related to the closing stage of a retrogressive metamorphic event, associated with crustal uplift in the Palghat Gap region. This event must have laid the tectonic frame work for the formation of the Gap later.

The reported ages also coincide with the available age determination of granite (475 m.y) from the southern foothills of the Nilgiris (Venkata Rao & Subramanian, 1979) and are consistent with the reported regional thermo-tectonic metamorphic event in South India around 500 m.y (Aswathanarayana, 1965; Grasty & Leelanandam, 1965; Crawford, 1969; Soman et al, 1982; 1983). The reported evidences of younger orogenic metamorphic events of granitic (<780 m.y) and pegmatitic activities (upto c.450 m.y) which affected the whole of south west India (Sarkar, 1969), are correlatable with that of adjacent parts of Gondwana land (Kennedy, 1964)* Africa & Madagascar (Cahen & Snelling, 1966), Antarctica (Nicolaysen et al, 1961) and Australia (Wilson et al, 1960).

Imprints of taphrogenic 'Pan African Magmatism' (750-550 m.y) in the form of alkali granites and syenites, have also been reported in Kerala (Nair & Vidyadharan, 1982; Nair et al, 1985; Santosh & Thara, 1984; Santosh et al, 1988). The

* Ref.Sarkar (1968)

K-Ar age determinations of 550 Ma of the post D₂ - syn D₃ pegmatite from the study area therefore, must be a reflection of Pan-African reworking that reactivated the Gap.

The ages reported in the present study indicates that the pegmatites of the Palghat Gap are marginally older than the south Kerala pegmatites, with a mean 460 m.y (Soman et al, 1982) and younger than the Wynad pegmatites with a U-Pb zircon age of 730 ± 20 m.y (Odom, 1982) and Rb-Sr muscovite age of 680 m.y. (Soman, personal communication). This in turn, may imply that the tectono-magmatic events in the Kerala region were younger towards south, affecting different crustal segments at different times.

Field relations preclude the possibility of radiogenic argon loss due to later metamorphic processes. The reported K-Ar ages (484-512 m.y) of biotite and muscovite from the Palghat Gap region, corresponds to the prominent Late Precambrian - Early Paleozoic acid magmatic emplacement phase in Kerala and elsewhere in South India. The confinement of all the other pegmatites and granites to the shear zones, might imply that this region also must have underwent repeated reactivation or mobility along the existing shear zones and the reported ages are likely to be representative of a cooling stage, presumably related to uplift.

CHAPTER VIII

CONCLUSIONS

Though geophysical investigations were supporting a tectonic origin of the Palghat Gap (Bose & Kartha, 1977; Rao, 1978; Reddy et al, 1988), geologists have held various views about the origin of the Gap. This was mostly due to the similarity of structural patterns in rocks of the Gap proper and the flanks (Jacob & Narayana Swamy, 1954; Nair, 1990). The present investigations, involving geological mapping (1:25,000 scale) of a segment of Palghat Gap including a part of its northern flank, bring out a conspicuous difference in lithology of the Gap proper and its northern flank though, only limited variations could be discerned in the structural style of the rocks of the two domains. The Gap proper is characterised by the presence of fissile rocks comprising the migmatitic suite, showing concordant enclaves of amphibolites with associated granites and pegmatites. The northern flank on the other hand, consists of a meta-sedimentary sequence of khondalites, calc granulites and associated crystalline limestones. Transition between the two units is gradational with the appearance of a sequence of hornblende-biotite gneiss, possibly in tectonic contact with the calc granulites.

Field investigations indicate the presence of an early compositional layering (S_1), which is identified as the

earliest recognisable planar structure of the area. The rootless isoclinal folds observed in migmatitic gneisses are suggested as folds of an earlier generation (F_1). Small scale symmetrical to isoclinal folds in calc granulites and migmatites, defined by S_1 constitute the F_2 folds belonging to the second deformation phase (D_2). The third deformation episode is marked by the presence of N-S open or gentle folds, with associated ENE-WSW and N-S fracture systems.

Occurrence of open mesofolds with an E-W axial plane, associated with fracturing in calc granulites, is observed in the northern flank. Equal area lower hemisphere plot of joints reveal two major sets trending ENE-WSW and N-S in the flank area while, the Gap proper shows the presence of NW-SE trending joints also. These are in fact succinct, but distinct differences in the structural patterns of the two domains. Slickensides with steep mineral lineation and intense fracturing in rocks of the flank close to the Gap, sillimanite augens, together with the presence of scarp faces as well as the steep and deep valleys in the flank running parallel to the Gap direction, are other possible evidences in support of a 'tectonic framework' in the formation of the Palghat Gap. Prolific development of fractures and locally pronounced granulation effects with attendant mineral alterations etc., observed in thin sections of various rock types of the study area, are results of the late brittle response of D_3 -deformation in the area.

Granulite facies metamorphism is presumed to have preceded all deformational episodes and since, the amphibolite boudins display effects of F_2 -folding, boudinage is attributed to D_1 -deformation phase. The migmatisation event is suggested to be continuous and coeval with both D_1 and D_2 deformation phases. Emplacement of granites and related pegmatites, closely linked to the migmatisation event, has been suggested to belong to the waning stages of D_2 -deformation or event syngenetic with respect to D_3 -deformation phase.

Presence of clinozoisite in calc granulite, a characteristic mineral of high temperature but, low grade metamorphic zone and development of hornblende after clinopyroxene, also speak in favour of a retrogressive metamorphic event in the region. Pertinent proof for retrogression has also been offered by the zoning in garnet. The apparent low temperatures of $< 650^\circ\text{C}$, obtained from the An-Or-Ab ternary plots (Fuhrman & Lindsley, 1988) of plagioclase and alkali feldspar composition of granulitic rocks, distinctly lower than the expected temperature in granulite terrains also characterises the late metamorphic history of the rocks, probably coinciding with an uplift. More specific indications has also been provided by the rather flat compositional gradients of cordierite (indicating partial homogenisation by volume diffusion at high temperature). The slight increase in Fe:Mg ratios towards

rims is consistent with a reduction in temperature. Shift towards diopsidic composition of clinopyroxene in calc granulites and a change from hornblende towards pargasitic composition in amphiboles of migmatitic gneisses, as compared to amphibole from granulites, also may be related to the incomplete re-equilibration during decrease in temperature.

Geochemical investigations suggest a sedimentary parentage of the rocks occurring in the flanks, while an igneous protolith is favoured for the rocks exposed in the Gap proper. Protolith characterisation suggests a pelitic to semi-pelitic argillaceous sedimentary parentage for the khondalites with widely varying SiO_2 (46-65 %) and Al_2O_3 (13-39 %) contents. This is substantiated also by petrographic observations. Geochemical data on calc granulites indicate their derivation from impure, silica-rich and Fe-poor calcareous sediments. Limestone + marly impurities admixture has been suggested as the protolith for the marbles. A major control of dolomites over the petrogenesis of Group II marble (impure variety) has also been established (Thara, 1992). Pertinent proof for the ortho character of the migmatitic gneisses is offered by the typical igneous trend patterns and the geochemical evidences suggesting involvement of a melt and crustal rocks (with low Rb/Sr values), such as the amphibolites. Geochemical characteristics of amphibolite enclaves occurring within migmatitic gneisses depict a conspicuous tholeiitic trend and indicate that the

composition of amphibolites could be the result of an emplacement and subsequent modifications of partial melts from the mantle. The observed mineralogical variations from core to periphery of granites has been explained as due to the removal of hornblende through fractional crystallisation.

Geothermobarometric studies indicate peak thermo-barometric conditions of 800°C and ~ 8.4 Kbars for the granulite metamorphism while, the conditions of retrogressive metamorphism has been fixed at 652°C and 6.5 Kbars. Neomineralization associated with migmatization and attendant granitic emplacement has been fixed at a still lower P-T condition of 532°C and 4.97 Kbars (Thara, 1989; Soman et al, 1992). Possibility of the obtained P-T estimates of granulites to be the lower limit of P-T maxima attained, is accentuated by the arguments of Frost & Chacko (1989) as well as by the high P-T values reported for the pyroxenites and gabbroic units of the Nilgiri massif (Srikantappa et al, 1986). Possibility of a higher pressure pre-peak metamorphic history is also suggested by the high Mg-cores of garnets. The high TiO₂ contents (4.97 wt %) of matrix biotite and higher Al_T of amphiboles in calc granulites (Leake, 1962; Kostyuk, 1970; Hietanen, 1974; Graham, 1974; Helz, 1982) are also consistent with a possible higher grade metamorphism.

The suggested peak temperature of 800°C is also well substantiated by the mineral equilibria constraints such as:

(1) the presence of scapolite, a characteristic mineral of high grade, deep seated granulitic terrain (Knorring & Kennedy, 1958; Lovering & White, 1969), (2) the coexistence of scapolite-plagioclase-calcite assemblages in calc granulites (Goldsmith & Newton, 1977), (3) X_{Mei} range of 74 to 79 in scapolite, (4) stability relations of aluminium silicate phases, (5) $FeO/(FeO + MgO)$ bulk chemical ratio of 0.7273 of cordierite in cordierite-bearing granulites and (6) absence of indications in favour of anatexis in granulites.

Close link between granite emplacement and retrogression is well supported by the similar temperatures obtained for garnet (rim) - secondary biotite and alkali feldspar-plagioclase assemblages in khondalite and the solidification conditions of alkali feldspar in granite. CO_2 -rich inclusions, probably related to post metamorphic fluid conditions are expected to represent a change in fluid regime coinciding with retrogression.

Formation of biotite-rich border zone separating the K-depleted amphibolites and granitic neosomes, requiring introduction of K and SiO_2 may speak of a late potash metamorphism. The general predominance of K_2O over Na_2O , presence of exsolution textures, formation of microcline after plagioclase and the transition of hornblende to biotite observed in thin sections of granites further support this view. Addition of externally derived K, presumably with water during the waning stages of tectonism is also necessary

to effect the quasi-isochemical partial melting of amphibolites into migmatitic gneisses since, the temperature and pressure reported for the latter are too low to cause biotite-or muscovite-dehydration melting. Relative hydrous nature of the system during retromorphosis is also indicated by the micro textural evidences such as the partial or complete replacement of clinopyroxene by hornblende, formation of cordierite from a prograde reaction involving increase in the activity of H_2O . Fluid inclusion petrography also suggests a fluid evolution characterised by an early carbonic regime followed by an intermediate mixed (carbonic-aqueous) and a late aqueous phase. An early CO_2 -rich phase is also indicated by the Meionite percentage of 75 in scapolite of calc granulites (Srikantappa et al, 1986) and by the assemblage of diopside + dolomite observed in impure marbles.

The overall P-T array defined by the estimated maximum and minimum pressure limits of the granulites, suggest an isothermal depression (ITD), followed by a small component of isobaric cooling history (IBC). This is also indicated by the crossings of the mineralogic GPAQ barometers with the garnet-biotite and two-feldspar thermometers. Microtextural evidences of fibrolitic sillimanite growing around garnet is typical of ITD histories while, the continuation of P-T path, as indicated by the rimming of garnet by biotite in sillimanite-bearing assemblages, concurs well with the

transition from ITD into an essentially IBC path. Close clustering of P-T estimates on granites, migmatitic gneisses and pegmatites towards the closing stages of the P-T evolution path, further substantiate this line of argument.

Decompressional P-T paths (ITD) have conveniently been ascribed to the net result of tectonic thickening combined with the vertical redistribution of heat through syn-to post-thickening magmatism followed by erosion of the crustal piles, or to extensional settings. P-T paths which involve significant static isothermal decompression therefore, are expected in areas of continental collision (England & Thompson, 1984). Comparison of the geometry of the ITD granulite path of the study area with the model paths for erosion (England & Thompson, 1984) shows that the latter has much shallower dP/dT slopes indicating that erosion alone could not have resulted in the obtained configuration. Conformity of the estimated P-T path of the rocks of the study area, with the model exhumation paths for faster rates of tectonic stripping (Harley, 1989) also signifies an increased rate of exposure and uplift through some mechanism of tectonic thinning, other than erosion. Moreover, although vertical movement of crustal segment is possible through melt enhanced deformation or surges (Hollister & Crawford, 1986), the most effective tectonic thinning process on a regional scale has been suggested to be extension or lateral spreading of the previously thickened crust (Van Reenan et al, 1987 in Harley, 1989).

The rapid extension of continental crust subsequent to collisional thickening, as illustrated by path.2 in Fig.132 has been recognised in broad orogenic belts (England, 1987) and is facilitated by topographic contrasts, if the lithospheric strength is sufficiently low. England (1987) and Sonder et al (1987) proposed a process of detachment of thermal boundary layer (TBL), comprising the lower portion of a thickened sub-continental lithosphere with attendant magmatism, to explain the P-T evolution history of path.2 (Fig.132), which closely simulates the estimated P-T path of evolution of the study area.

Low pressure at near peak temperature obtained for calc granulites might also be reflective of a decompression, related to uplift or extensional tectonism. Increase in 'T' accompanying the uplift in areas of lower metamorphic grade, by emplacement of granites, has also been suggested by some (Martinez & Gilbarguchi, 1982), while the role of underplating of magmas in heating up of the crust before and during loading, such that thermal maxima is attained before the P maxima, has been cited by others (Wells, 1980; Subramanian, 1956). Discrimination of tectonic environment of the granites of the present study also typifies them as POG (Post Orogenic Granitoids) types of Maniar & Piccole (1989).

The spatial association of migmatites and the granites

along with the microtextural evidences of mylonites and occurrence of augen gneisses also indicate a major shear control in their generation. It conforms well with the established relationships between shear zones, major faults and lineaments and igneous activity (Murthy & Venkataraman, 1964; Bowden, 1974; Jayananda & Mahabaleswar, 1991; Santosh & Thara, 1984) which can also explain the extensive occurrence of concordant igneous bodies present in the Gap.

Recent investigations pointing to the lack of correspondence between P-T data on rocks lying south and north of the Palghat-Cauvery shear zone (Harris et al, 1982; Janardhan et al, 1982; Raith et al, 1983; Chacko et al, 1987) has facilitated arguments in favour of its being a tectonic boundary between two distinct terrains, within the southern Indian shield (Drury et al, 1984; Ramakrishnan, 1988). The basement highs located beneath Nilgiris and the basement low located in the Palghat Gap, also speak in favour of uplift or down fault of distinct blocks against each other, along deep crustal breaks (Reddi et al, 1988). Presence of a thick crust south of Palghat-Tiruchi region, in the high grade terrains of south India, as shown by higher bouger anomaly indications of 30-40 mgls (Mishra, 1988) as compared to the magnetic lows on either sides of the Gap has also been explained as a result of crustal accretion or as due to underplating along a shear zone, which is substantiated by the electrical conductivity measurements carried out across

Palghat Gap (Raval, 1988).

The lower pressure estimates (4.1 - 4.9 Kbars) corresponding to 0.8-0.9 g/cm³ density of fluid obtained by fluid inclusion data, which are more akin to the retrograde-reequilibration conditions, also bear evidences in favour of an uplift faster than their cooling rate, ending in an IBC path towards the reequilibration event.

Age determination of pegmatite minerals by K-Ar method indicates an emplacement age of 484-512 Ma (Soman et al, 1990). Field relations, indicate that it is later to the granulite metamorphic event of the meta-sedimentary sequence there. Since, pegmatite emplacement is associated with the closing stages of tectono-magmatic cycles, it is reasonable to suggest that the pegmatite were emplaced towards the closing stage of a tectono-magmatic cycle associated with retrogressive metamorphism, which is further substantiated by petrographic data, mineral chemistry data on garnet zoning, as well as the geothermobarometric estimations for various rock units. The available data also permit to conclude that this event coincided with crustal uplift in the region, around ca. 490-510 Ma ago, laying the tectonic frame work for the formation of the Gap.

Origin of the Palghat Gap :-

Field observations such as (1) the conspicuous difference in lithology of the Gap proper and its northern

flanks (2) development of fissile migmatitic gneisses in the Gap proper (3) structural features such as the presence of slickensides with steep mineral lineation and intense fracturing and presence of open mesofolds in the rocks of the flank region, (4) micro textural evidences of mylonitisation and neomineralisation and (5) mineral chemistry data on garnet zoning and shift of clinopyroxene towards diopsidic composition further substantiate the role of lithologic and tectonic factors controlling the formation of the Gap.

However, the present day configuration of the Gap is a result of erosional cycles, belonging to post Indian cycle (King, 1950) corresponding to late Tertiary-Recent age, though Jacob & Narayanaswami (1954) advocated a geomorphological age not later than lower Miocene coinciding with the west coast faulting. Tectonically active nature of the areas surrounding the Palghat Gap region is also brought out by the evidences such as (1) presence of pseudotachylites in areas adjacent to Nilgiri granulite terrain (Radhakrishnan, 1988; Narayanaswamy, 1975) and (2) the occurrence of a major earthquake at Coimbatore (1900) in the northern side and the earth tremors around Mangalam and Sarkarpathi in the southern part of the Gap.

APPENDIX

1.1 OUTLINE OF THE PROCEDURE FOLLOWED FOR THE CHEMICAL ANALYSIS OF SAMPLES FROM THE STUDY AREA.

Sample preparation and part geochemical analyses of 30 samples, by wet chemical methods, were done at the chemical Laboratory of Centre for Earth Science studies, Trivandrum and a few trace element determinations were carried out by Atomic Absorption Spectrophotometer (Perkin Elmer 4000) at the chemical Laboratory of Kerala Minerals Exploration Development project, Trivandrum. Na and K analyses were carried out at the Regional Research Laboratory, Pappanamkode, Trivandrum. Analysis of about twenty samples were done by X-ray fluorescence (XRF) methods at the geochemical laboratories of the National Geophysical Research Institute, Hyderabad and Geological survey of India, Bangalore).

1.1.a Analytical procedure for wet chemical analysis

Fresh rock samples are pulverized in a ball mill to -230 mesh size and are coned and quartered for the analyses.

Estimation of SiO₂

A weighed quantity (0.5gms) of the powdered sample is ignited and fused with anhydrous sodium carbonate in a platinum crucible. To the melt obtained, some water and a few drops of ethyl alcohol are added. It is then extracted with 50ml of 1:1 Hcl and evaporated to dryness, by placing over a water bath. After baking at 110°C for one hour, it is

extracted with Hydrochloric acid and filtered through whatman No.42 filter paper. The residue is heated at 950°C for 15 to 20 minutes. It is allowed to cool in a desiccator and weighed (A). After moistening with water, some drops of 1:1 H₂SO₄ (to convert all the contaminating bases to sulphates and to prevent loss of titanium or zirconium as fluorides) and 10ml of Hydrofluoric acid are added and evaporated on a steam bath. The sulphuric acid is expelled and the residue is ignited at 1000°C for 1 or 2 minutes. After cooling, the weight is again determined (B). The weight difference gives the weight of silica.

The residue left behind in the crucible is melted, after adding a little potassium pyrosulphate and the fused mass is dissolved in water. This is added to the main filtrate and made up to 250ml solution. This solution is utilised for estimation of Fe₂O₃, Al₂O₃, CaO and MgO.

Estimation of Fe₂O₃

The stock solution is reduced with stannous chloride and the ferrous iron is titrated with potassium dichromate.

Procedure:- A known quantity of the stock solution (25ml) is diluted and brought to boiling after adding concentrated HCl. Stannous chloride is added dropwise till the solution becomes colourless (reduction of Fe³⁺ to Fe²⁺). Mercuric chloride is added (to remove excess of SnCl₂) along with 1:1 H₂SO₄ and orthophosphoric acid. Titration is carried out against

standard (0.01N) $K_2Cr_2O_7$, using Barium diphenylamine indicator. End point is indicated by the colour change from green to purple.

Estimation of FeO

A weighed quantity (0.25gms) of the powdered rock sample is taken in a conical flask and 10ml of con: H_2SO_4 and 5ml of con:HF are added and the contents put to heating in an atmosphere of carbon dioxide. 10ml boric acid (15%) is added and the flask is placed on an ice bath. After adding 1:1 H_2SO_4 (2ml) and 10ml of orthophosphoric acid, titration is carried out against 0.01N $K_2Cr_2O_7$, using barium diphenylamine indicator (End point :- change from blue to vine red).

Estimation of Al_2O_3

A known quantity (25ml) of the stock solution is taken and 20% NaOH and a few drops of phenolphthalein are added. It is heated and filtered through whatman 42. The residue is washed well with hot dilute NaOH and the PH is adjusted by adding very dil.HCl. 5ml of 20% ammonium acetate and 25ml of standard EDTA (0.1M) are added and the solution is cooled on an ice bath. Titration is carried out against 0.1M Zn^{2+} solution, after adding xylenol orange indicator and glacial acetic acid. End point:- colour change from yellow to orange. Procedure is repeated for blank solution also.

Estimation of CaO and MgO

Twenty millilitre of the stock solution is taken and NH_4Cl and NH_4OH are added. It is boiled for five minutes and filtered. Eriochrome Black T indicator and ammonia solution buffer are added and titration is carried out against 0.01M EDTA. The titration value corresponds to total Ca and Mg. End point is indicated by a change from vine red to blue.

Measured quantity of the filtrate is titrated against standard EDTA after adding sodium hydroxide (20%) buffer and murexide indicator. The titre value gives an estimation of Ca. (End point:- change from violet to salmon pink).

Estimation of alkalies

Solution for the estimation of Na, K and trace elements is prepared by taking a weighed quantity (0.5gms) of the powdered sample in a platinum crucible and adding a few drops of H_2SO_4 along with 25ml of HF. This is evaporated to dryness and 30ml of 1:1 HCl is added. The solution is made up to 100ml after boiling. Na_2O and K_2O are determined by flame photometer and trace elements, by atomic spectrophotometer.

Moisture and Loss-on ignition contents

The powdered rock sample (1gm) is heated in an oven at 105°C - 110°C for about 1 hour and the moisture content is determined from the difference in weight of the sample before

and after heating. Loss on ignition is estimated by weighing the sample after heating it in a muffle furnace at 1000°C for about half an hour.

Estimation of P₂O₅

Measured quantity of the powdered sample (0.5gm) is fused with 2gms of potassium pyrosulphate and cooled. Added 10ml of 1:1 HNO₃ and boiled in a water bath. It is filtered and collected in a 50ml standard flask. A suitable volume of the solution is taken and 5ml of vanado-molybdate reagent is added. The colour developed is compared with a standard phosphorous solution using a spectrophotometer at a wavelength between 460 and 480 nm.

For all determinations of major and trace elements by AAS, synthetic multi-element standards were used.

1.1.b Analytical procedure for XRF analysis

Sample Powdering:

All the samples are finely powdered to -300 mesh by 'HERZOG' swing-grinding mill, using hard chrome steel grinding tool.

Sample Preparation:

For the analysis of the trace constituents, sample pellets are prepared by pressing the rock powder with the backing of boric acid in collapsible aluminium cups at 20 tonnes of pressure, employing a 'HERZOG' hydraulic press

model TP 2d. to give pellets of 40 mm diameter.

For the determination of major elements, samples are fused with lithium tetraborate-metaborate flux, after adding lithium carbonate to bring down the melting point of the flux. Samples are fused in 5% gold-platinum crucibles using 'HERZOG'-automatic fusion machine with 12 positions. Sample to flux ratio is kept at 1:10, with a total weight of 10 g having the following recipe:

Wt of the sample	---	1.0 g
Wt of the flux	---	7.5 g
Wt of Li_2CO_3	---	1.5 g

A tilting device is used in the fusion machine to shake the melt of the sample + flux, to have homogeneous solution.

Instrumentation

Philips PW 1400 microprocessor controlled, sequential X-ray fluorescence spectrometer, with 100 KVA X-ray generator and 72 position automatic sample changer (to load and unload the samples in the spectrometer) is used to measure different peaks and background counts for elements. Philips P 851 on line, dedicated computer is used to do the regression analysis to prepare calibration curves [using USGS II and III Series, Canadian Sy-2, Sy-3 and French CRPG and ANRT series standards and the data published by Flanagan (1973,1976) and Abbey (1977,1980)].

A spinner is used to spin the sample inside the

spectrometer while measuring the counts, to have uniform counts and to remove heterogeneity effect from the pressed sample. A 32 mm primary beam aperture mask is used to restrict the X-ray beam only to the sample surface. Flow and scintillation detectors are used to count the X-ray photons. Pulse height discriminator and fine collimator are used for greater sensitivity for most of the trace and minor elements. Instrumental parameters and operating conditions are reported in Table.30 below.

Table.30.Operating conditions for XRF analysis X-ray tube: multipurpose Rh target 3000 W except mentioned otherwise.

Element X-ray line	Colli- mator	Crystal	Detector	Peak 20° angle	Background 20° angle
Si K α	F	PE	F	109.19	111.19
Al "	C	TIAP	F	37.86	39.86
Ti "(Cr tube)	C	LIF 200	F	86.18	85.18
Ca "	C	"	F	113.13	115.14
Mg "	C	ADP	F	136.83	138.83
Na "	C	TLAP	F	55.06	57.06
K "	F	LIF 200	F	136.77	138.77
Mn "(Cr tube)	C	LIF 220	F	95.26	96.26
P "(" ")	C	Ge	F	141.06	143.06
Fe "	C	LIF 220	F	85.79	87.79
Zr "	F	"	FS	32.09	32.79
Y "	F	"	FS	33.92	34.52
Sr "	F	"	FS	35.84	36.54
Rb "	F	"	FS	37.98	38.78
Ba L α	F	LIF 200	FS	87.25	89.25
V K α	F	LIF 220	F	123.28	124.78
CR "	F	"	F	107.19	108.19
Ni "	F	"	F	71.31	72.31
Co "	F	"	F	77.95	79.95
Cu "	F	LIF 200	F	45.07	46.07
Zn "	F	"	F	41.83	42.83

Collimator F=Fine; C=Coarse
Detector F=Flow; FS=Scintillation.

Accuracy and precision

In general, reproducibility of the data obtained is reported to be within the range of $\pm 1.0\%$ for major and minor elements, 5% for the trace elements and ± 10 to 15% for the trace elements, at concentration level below 10 ppm.

1.2 Thin section staining technique for carbonates

The uncovered thin sections are stained by a method after Dickson (1965). First, the sections are etched with 1.5% HCl for 10-15 seconds, which affects only the calcite grains. The sections are further stained with a mixture of 0.2 M Alizarin red, dissolved in 100 cc of 1.5% HCl (ARS) and 2 gms of potassium ferricyanide dissolved in 100 cc of 1.5 HCl acid (PF) (mixed in the ratio ARS:PF = 3:2), for 30-45 seconds. Calcites are stained pale pink (basal sections) to red (prismatic). Dolomites take no stain. The sections are again stained with ARS solution for 10-15 seconds, which imparts a permanent pale pink colour to calcites.

1. Abbey, S.(1977) Studies in 'Standard samples for use in the general analysis of silicate rocks and minerals'. Geol. Surv. Canada, Paper. 77-34.
2. " (1980) Studies in 'Standard samples for use in the general analysis of silicate rocks and minerals. Part 6, 1979 edition of 'Usable values'. Geol. Surv. Canada, Paper. 80-14
3. Ahmed, F.(1966) Post Gondwana faulting in peninsular India and its bearing on the tectonics of the sub continent. Annals Geol. Aligarh Muslim Univ.,V. 11; 40p.
4. Akella, J.and Boyd F.R. (1974). Petrogenetic grid for garnet peridotites. Carnegie Inst. Washington Year Book.,V.73; pp. 263-273.
5. Amirkhanoff, K.I., Brandt, S.B. and Bartinsky, E.N. (1961) Radiogenic argon in minerals and its migration. Annals. N.Y. Acad. Sci., V. 91; pp. 235-275.
6. Anovitz,L.M.and Essene, E.J. (1987) Compatibility of geobarometers in the system CaO-FeO-Al₂O₃-SiO₂-TiO₂: implications for garnet mixing models. Jour. Geol.,V.95; pp. 633-645.
7. Aranovich, L.Y. and Podlesskii, K.K. (1980) Garnet-plagioclase barometer. Dokl Akad nauk USSR.,V. 251; pp. 1216-1219.
8. Arogyaswamy, R.N.P. (1958). A note on the examination of the excavations for the Kundhapalam, Emerald and Avalanche dams, Kundah Hydro-electric scheme, Nilgiri district, Madras (Unpublished Report, G.S.I.).
9. Arogyaswamy, R.N.P. (1962). The origin of the Palaghat Gap. Records of the Geol. surv. India., V. 93; Part 2, pp. 129-134.
10. Ashworth, J.R. (1985) Migmatites, Ashworth, J.R. (ed): Blackie, Edinburgh, Scotland. 302p.
11. Ashworth, J.R. and Mclellan, E.L. (1985) Textures, In: Migmatites. Ashworth J.R (ed): Blackie, Scotland, pp. 180-203.
12. Aswathanarayana, U. (1965) Isotopic ages from the Eastern Ghats and Cuddapahs of India. Jour. Geophys. Res., V.69; pp. 3479-3486.

13. Balasundaram, M.S. (1953). Inspection note on the Mangalam and Walayar damsites. (Unpublished Report, G.S.I).
14. Balasundaram, M.S. (1954) A short geological note on the foundation rock exposed in the Mangalam damsites; Malabar district. (Unpublished Report, G.S.I)
15. Barker, F. (1989) Trondhjemite; Definition, environment and hypotheses of origin. In: Trondhjemites, Dacites and Related Rocks. F. Barker (ed), Elsevier, Amsterdam, pp. 1-12.
16. Barker, F. and Arth, J.G. (1976) Generation of trondhjemitic - tonalitic liquids and Archean bimodal trondhjemitic basalt suites. *Geology*, V.4; pp. 596-600.
17. Barth, T.F.W. (1934) Polymorphic phenomena and crystal structure. *Am.Jour. Sci.*, V.232; pp. 273-313.
18. Beckinsale, R.D. (1979) Granite magmatism in the tin belt of south east Asia. In: Origin of Granite Batholiths - Geochemical Evidence. M.P. Atherton and J. Tarney (eds), Shiva Publ. Ltd.
19. Bhattacharya, A. (1986). Some geobarometers involving cordierite in the $\text{FeO-Al}_2\text{O}_3\text{-SiO}_2$ ($\pm\text{H}_2\text{O}$) system: refinements, thermodynamic calibration and applicability in granulite facies rocks *contrib. Mineral. Petrol.*, V.94; pp. 387-394.
20. Bhattacharya A., Mazumdar, A.C. and Sen, S. K. (1988) Fe-Mg mixing in cordierite: constraints from natural data and implications for cordierite - garnet geothermometer in granulites. *Am. Mineral.*, V. 73; pp. 338-344.
21. Bhattacharya, A. and Raith, M. (1987) an updated calibration of Mg-Fe partitioning between garnet - biotite and orthopyroxene- biotite based on natural assemblages. *Fortschritte der Mineralogie Band 65; Beiheft -1, Stuttgart.*
22. Bhattacharya, A. and Sen, S.K. (1985) Energetics of hydration of cordierite and water barometry in cordierite granulites. *Contrib. Mineral Petrol.*, V.89; pp. 370-378.

23. Bingen, B., Demaiffe, D. and Hertogen, J. (1990) Evolution of feldspars at the amphibolite-granulite - facies transition in augen gneisses (SW Norway): geochemistry and Sr isotopes. *Contrib. Mineral. Petrol.*, V.105: pp. 275-288.
24. Bishop, F.C. (1980) The distribution of Fe²⁺ and Mg between coexisting ilmenite and pyroxene with applications to geothermometry. *Am. Jour. Sci.*, V.280; pp. 46-77.
25. Blatt, H., Middleton, G. and Murray, H. (1972) *Origin of sedimentary Rocks*, Prentice Hall, 634 p.
26. Bohlen, S.R. (1987) Pressure-temperature-time paths and a tectonic model for the evolution of granulites. *Jour. Geol.*, V. 95; pp. 617-632.
27. Bohlen, S.R. and Essene, E.J. (1977) Feldspar and oxide thermometry of granulites in the Adirondack Highlands: *Contrib. Mineral. Petrol.*, V.65; pp. 153-169.
28. " (1978). Igneous pyroxenes from metamorphic anorthosite massifs. *Contrib. Mineral. Petrol.*, v. 65; pp. 433-442.
29. " (1980). Evaluation of co-existing garnet-biotite, garnet-clino pyroxene and other Mg-Fe exchange thermometers in Adirondack granulites. *Geol. Soc. Am. Bull.*, V.91; pp. 685-719.
30. Bohlen, S.R., Liotta, J.J (1986) A new barometer for garnet amphibolites and garnet granulites. *Jour. Petrol.*, V.27; pp. 1025-1034.
31. Bohlen, S.R., Wall, V.J., Boettcher, A.L. (1983) Geobarometry in granulites In: *Advances in Physical Chemistry*, Saxena S.K. (ed.) ; Springer. Berlin. Heidelberg, New York, pp. 141-171.
32. Bose. R.N. and Kartha, T.D.G. (1977) Geophysical studies in parts of west coast (Kerala) of India. *Ind. Jour. Earth. Sci.* (S. Ray volume)., pp. 251-266.
33. Bowden, P. (1974) Oversaturated alkaline rocks, granites, Pantellerites and commendites. In : *The Alkaline Rocks*, John, Wiley, New York, Sorensen, H (ed). pp. 109 - 123.

34. Boyd, F.R. and England, J.L. (1961) melting of silicates at high pressure. Carnegie Institution of Washington Year Book, V.60; pp. 113-125.
35. Brown, P.E. and Lamb, W.M. (1986). Mixing of H₂O - CO₂ in fluid inclusions; Geobarometry and Archean gold deposits. Geochim. Cosmochim. Acta., V.50; pp. 847-852.
36. Brown, W.L. and Parsons, I. (1985) Calorimetric and phase diagram approaches to two feldspar geothermometry: a critique. Am. Mineral., V.70; pp. 356-361.
37. Burrie, C. (1964) Petrochemical Calculations. Jerusalem. Israel Programme for scientific transactions, 304p.
38. Cahen, L. and Snelling, N.L. (1966). The Geochronology of Equatorial Africa, pp.150-161.
39. Cameron, M. and Papike, J.J. (1981) structural and chemical variations in pyroxenes. Am. Mineral., V. 66; pp.1-50.
40. Campbell, D.S. (1980) Structural and metamorphic development of migmatites in the Svecokareliides near Tampere, Finland, Trans. Roy. Soc. Edin (Earth Sciences)., 71; pp. 185-200.
41. Chacko, T. (1987) Petrologic, geochemical and isotopic studies in the charnockite-khondalite terrain of southern Kerala, India: The deposition and granulite facies metamorphism of a Pre-cambrian sedimentary sequence. Unpublished ph.D thesis, Univ of North Carolina., pp.191.
42. Chacko, T., Ravindra Kumar, G.R. and Newton, R.C. (1987) Metamorphic P-T conditions of the Kerala (south India) Khondalite belt, a granulite facies supracrustal terrain. Jour. Geol., V. 95; pp: 343-358.
43. Chappel, B.W. and White, A.J.R. (1974) Two contrasting granite types. Pacific Geology., V. 8; pp 173-197.
44. Clemens, J.D. and Wall. V.J. (1984) origin and evolution of a peraluminous silicic ignimbrite suite: the Violet Town Volcanics. Contrib. Mineral. Petrol., V.88, pp 354-371.

45. Condie, K.C. (1981) Archean Greenstone Belts. Amsterdam : Elsevier ., 434 p.
46. Crawford, A.R. (1969) India, Ceylon and Pakistan: New age data and comparisons with Australia. Nature., V.223; pp.380-384.
47. " (1979) Aqueous fluids. In: Fluid Inclusions. Roedder. E (ed), 644p.
48. Currie, K.L. (1971) the reaction, 3 cordierite = 2 garnet + 4 sillimanite + 5 quartz as a geological thermometer in the Opinicon Lake Region, Ontario. Contrib. Mineral. Petrol.,V. 33; pp. 215-226.
49. " (1974). A note on the calibration of the garnet - cordierite geothermometer and geobarometer. Contrib. Mineral . Petrol.,V. 44; pp. 35-44.
50. Dahl, P.S., (1980) the thermal - compositional dependence of Fe²⁺ -Mg distribution between co-existing garnet and pyroxene : applications to geothermometry. Am. Mineral.,V. 65; pp.852-866.
51. Dalrymple, G.B. and Lanphere, M.A. (1969). Potassium Argon Dating, principles, techniques and applications to geochronology. W.H. Freeman and company; Sanfrancisco.
52. Decaprarriis, P. (1974) Stress-induced viscosity changes and the existence of dominant wavelengths in folds. Tectonophysics., 23; pp.139-148.
53. Deer, W.A., Howie, R.A. and Zussman J. (1966). An introduction to the rock-forming minerals. Longman Group Ltd., 528 P.
54. " (1978) Rock-forming minerals. Vol.2A. Single-chain Silicates (2nd edition) Long man. U.K. and Wiley. New York.
55. Demongeot, J. (1975) Recherches geomorphologiques en Indes. Z. Geomorph., N.F., V.19 (3); pp.229-272.
56. Dickson, J.A.D. (1965) A modified staining technique for carbonates in thin section. Nature., 205; No.497, pp.587.

57. Dietz, R.S. and Holden J.C. (1970). Southern Pangea, breakup and dispersion of continents, permian to present. Jour. Geophys. Res., V.75; No.26, pp.4939-4956.
58. Doe, D.R. and Tilling, R.I. (1967) The distribution of lead between coexisting k-feldspar and plagioclase. Am. Mineral., 52; pp. 805-816.
59. Drury, S.A (1973) The geochemistry of Precambrian granulite facies rocks from the Lewisian complex of Tiree, Inner Hebrides, Scotland. Chem. Geol., pp. 11-167.
60. Drury, S.A., Harris, N.B.W; Holt, R.W., Reeves smith, G.J. and Wightman, R.J. (1984) Precambrian geotectonics and crustal evolution in southern India. Jour. Geol., V.92; pp. 3-20.
61. Drury, S.A. and Holt, R.W. (1980) The tectonic framework of the south Indian craton, a reconnaissance involving Landsat Imagery. Tectonophysics., V.65; pp. T1-T15.
62. Eicher, D.L. (1976) Geologic Time, 2nd edition. The Prentice Hall Foundation of Earth Science series.
63. Ellis. D.J. and Green D.H. (1979) An experimental study, of the effect of Ca upon garnet - clinopyroxene Fe-Mg exchange equilibria. Contib. Mineral. Petrol., V. 71; pp.13-22.
64. Engel, A.E.J. and Engel, C.G. (1962) Progressive metamorphism of amphibolites, northwest Adirondack mountains, New York: Geol. Soc. Am., Buddington volume, pp. 37-82.
65. England, P. C. (1987) Diffuse continental deformation : length scale, rates and metamorphic evolution. In : Tectonic Settings of Regional Metamorphisms. E.R. Oxburgh, B.W.D. Yardley and P.C. England (eds), Roy. Soc.Lond. Cambridge. Univ. Peress., pp . 3-22.
66. England. P.C. and Thompson, A.B. (1984) Pressure - Temperature - time paths of regional metamorphisms. 1. Heat transfer during the evolution of regions of thickened continental crust. Jour. Petrol., V . 25; pp . 894-928.

67. England, P.C. and Thompson, A.B. (1986) Some Thermal and Tectonic models for crustal melting in continental collision zones. In: Collisional Tectonics. M.P. Coward and A.C. Ries (eds), Geol. Soc. Lond. spl. publ., No. 19, pp. 83-94.
68. Essene, E.J. (1982) Geologic thermometry and barometry. In: Reviews of Mineralogy. J.M. Ferry (ed.), Mineralogical Soc. of America., V. 10; Washington.
69. Evans, B.W. (1965) Pyrope garnet - barometer or thermometer. Geol. Soc. Am. Bull., V.76; pp. 1265-1330.
70. Evans, B.W. and Leake, B.E. (1960). The composition and origin of the striped amphibolites of Connemara, Ireland: Jour. Petrol., V.1; pp. 337-363.
71. Fang, Q. and He, S. (1985) Application of cordierite - garnet geothermo-barometer to Darongshan s-type granite. In: The Crust - the Significance of Granites, Gneisses, Wu. L., Yand, T., Yuan, K., Didier, J., Greenberg, J.K., Lowelle, G.R., Xia, H., Yu. S. and Augustithis, S.S., (eds) The Lithosphere, Theophrastus, Athens, pp. 462-478.
72. Ferry, J.M. (1980) A comparative study of geothermometers and geobarometers in pelitic schists from south - central Maine. Am. Mineral., V.63; pp. 113-117.
73. " and Spear. (1978). Experimental calibration of the partitioning of Fe and Mg between biotite and garnet. Contrib. Mineral. Petrol., V. 66; pp. 113-117
74. Field, D. and Clough, P.W. (1976). K/Rb ratios and metasomatism in metabasites from a Precambrian amphibolite - granulite transition zone. J. Geol. Soc. Lond., V.132; pp.277-288.
75. Flanagan, F.G. (1973) 1972 values for international geochemical reference samples. Geochem. Cosmochim. Acta. V.37: pp. 1189-1200.
76. " (1976) Description and analysis of eight New USGS rocks standards. U.S. Geol. Surv. Prof. Paper. 840p.

77. Fonarev, V.I. and Konilov, A.N. (1986) Experimental study of Fe - Mg distribution between biotite and ortho pyroxene at P = 490 Mpa. *Contrib. Mineral. Petrol.*, V.93; No. 2, pp. 227 - 235.
78. Froese, E. (1988) Metamorphic P-T conditions of the Kerala (south India) Khondalite belt, a granulite facies supracrustal terrian: a disussion. *Jour. Geol.*, V. 96; pp. 386-384.
79. Frost, M.J. (1962). Metamorphic grade and iron - magnesium distribution between co-existing garnet - biotite and garnet hornblende. *Geological Magazine.*, V.99; pp. 427-438.
80. Frost, B.R. and Chacko, T. (1989). The granulite uncert- ainity principle : limitations on thermobarometry in granulites. *Jour. Geol.*, V. 97; pp. 435-450.
81. Fuhrman, M.L. and Lindsley, D.H. (1988) Ternary feldspar modeling and thermometry, *Am. Mineral.*, V.73; pp. 201-215.
82. Ganguly J. (1979). Garnet and clinopyroxene solid solutions and geothermometry based on Fe-Mg distribution coefficient. *Geochim. Cosmochim. Acta.*, V.43; pp. 1021-1029.
83. Ganguly, J. and Kennedy, G.C. (1974). The energetics of natural garnet solid solution: 1. Mixing of the alumino silicate end members. *Contrib. Mineral. Petrol.*, V. 48; pp. 141-148.
84. Ganguly, J. and Saxena, S.K. (1984). Mixing properties of aluminosilicate garnets: constraints from natural and experimental data, and applications to geothermobarometry: clarifications. *Am. Mineral.*, V. 69; pp. 88-97.
85. Gasparik, T. (1984) Experimental study of subsolidus phase relations and mixing properties of pyroxene in the system CaO - Al₂O₃ - SiO₂. *Geoch. Cosmo. Acta.*, V.48; pp.2237-2545.
86. Gebauer, D. and Grunfelder, M. (1974) Rb-Sr whole - rock dating of late diagenetic to anchi-metamorphic Paleozoic sediments in southern France (Montagne Noire). *Contrib. Mineral. Petrol.*, V. 47; pp. 113.

87. Geiger, C.A. Newton R.C., Kleppa O.J. (1987) Enthalpy of unmixing of synthetic almandine-grossular and almandine-pyrope garnets from high temperature solution calorimetry. *Geochim. Cosmochim. Acta.*, V. 51; pp. 1755-1763.
88. Ghent, E.D. (1976) Plagioclase - garnet - silicate - quartz: a potential geobarometer - geothermometer. *Am. Mineral.*, V. 61; No.7 and 8, pp. 710-714.
89. Ghent, E.D., Robbins, D.B. and Stout, M.Z. (1979). Geothermometry, geobarometry, and fluid compositions of metamorphosed calc-silicates and pelites, Mica Creek, British Columbia. *Am. Mineral.*, V. 64; pp. 874-885.
90. Ghent, E.D., Stout, M.Z. and Raeside, R.P. (1983) Plagioclase - clinopyroxene garnet - quartz equilibria and the geobarometry and geothermometry of garnet amphibolites from Mica Creek, British Columbia. *Canad. Jour. Earth. Sci.* V. 20 : pp. 699-706.
91. Ghiorso, M.S. (1984) Activity composition relations in the ternary feldspars. *Contrib. Mineral. Petrol.*, V.87; pp. 282-296.
92. Giret, A., Bernard, B. and Leger, J.M. (1980) Amphibole compositional trends in over-saturated alkaline plutonic ring complexes. *Can. Mineral.*, V.75; pp. 481-495.
93. Goldman, D.S. and Albee A.L. (1977) Correlation of Mg / Fe partitioning between garnet and biotite with O^{18} / O^{16} partitioning between quartz and magnetite. *Am. Jour. Sci.*, V. 277.; pp. 750-767.
94. Goldsmith, J.R. (1980). Melting and breakdown reactions of anorthite at high pressure and temperatures. *Am. Mineral.*, V. 65; pp. 272-284.
95. " and Newton, R.C., (1977) Scapolite - plagioclase stability reactions at high pressures and temperatures in the system $NaAlSi_3O_8 - CaAl_2Si_2O_8 - CaCO_3 - CaSO_4$. *Am. Mineral.*, V. 62; pp. 1063 - 1081.
96. Gopalakrishnan, K. (1979) Geology of parts of Anaimalai Hills, Coimbatore District, Tamil Nadu. *Geol. Surv. India* (unpublished report)., 10p.

97. " (1981) Report on the traverses taken across Coimbatore and Nilgiri District, Tamil Nadu. Geol. Surv. India. (Unpublished report)., 7p.
98. Graham, C.M. (1974) Metabasic amphiboles of the Scottish Dalradian. *Contrib. Mineral. Petrol.*, V. 47; pp. 163-185.
99. Grasty, R.L. and Leelanandam, C. (1965). Isotopic ages of the basic charnockite and khondalites from Kondapalli, Andhrapradesh, India, *Mineral. Mag.*, V. 35; pp. 529-535.
100. Green, T.H. and Hellman, P.L., 1982. Fe - Mg Partitining between coexisting garnet and phengite at high pressure, and comments on a garnet-phengite geothermometer. *lithos.*, V. 15; pp. 253-266.
101. Green N.L. and Usdansky, S.I. (1986) Ternary feldspar mixing relations and thermobarometry. *Amer. Mineral.*, V. 7; pp. 1100-1108.
102. Guggenheim, E.A. (1967) *Thermodynamics* Amsterdam, North Holland Publ. co. 390p.
103. Gupta, L.N. and Johannes, W. (1982) Petrogenenesis of stromatic migmatite (Nelaug, southern Norway). *Jour. Petrol.*, V.23; pp. 548-567.
104. Hahn, O. and Walling, E. (1938) Uber die Moglichkeif geologischer Alterbestimmungen rubidium haltiger Mineralen and Gesteine. *Z. Anorg. Allgem. Chem.*, V. 236; pp. 78-82.
105. Hammarstrom, J.M. (1985) An empirical equation for igneous calic amphibola geobarometry *Geol. Soc. Am.*, Abstr. with programs., V. 17; pp.602.
106. " and Zen, E-an. (1983) possible use of Al. content in hornblende as a geobarometer for plutonic rocks. *Geol. Soc. of Am. Abstr.* with progrms., 15; pp. 590.
107. " and Zen, E-an. (1986). Aluminium in hornblende: an empirical igneous geobarometer. *Am. Mineral.*, V. 71; pp.1297-1313.
108. Hansen, E.C., Hickman, M.H., Grant, N.K. and Newton, R.C. (1985) Pan- African age of 'Peninsular Gneiss' near Madurai, south India. *EOS.*, V.66; pp.419-420

109. Hansen, E.C., Newton, R.C. and Janardhan, A.S., (1984) Fluid inclusions in rocks from the amphibolite - facies gneiss to charnockite progression in southern Karnataka, India: direct evidence concerning the fluids of granite metamorphism. *J. Metamorph. Geol.*, V. 2; pp. 249-264.
110. Hariya, Y. and Kennedy, G.C.C. (1968) Equilibrium study of anorthite under high pressure and high temperature. *Am. Jour. of science.*, V. 266; pp. 193-203.
111. Harley, S.L. (1984) An experimental study of the partitioning of Fe and Mg between garnet and orthopyroxene. *Contrib. Mineral. Petrol.*, V. 86; pp. 359-373.
112. " (1985) Garnet - orthopyroxene bearing granulites from Enderby Land, Antarctica: metamorphic pressure - temperature - time evolution of the Archean Napier Complex. *Jour. Petrol.*, V. 26; pp. 819-856.
113. " (1989) The origin of granulites: a metamorphic perspective. *Geol. Mag.*, V. 126 (3); pp. 215 - 247.
114. Harpum, J.R. (1963) Petrographic classification of granite rocks in Tanganyika by partial chemical analysis. *Rec. Geol. Surv. Tanganyika.*, V. 10; pp. 80-88.
115. Harris, N.B.W. (1981). The application of spinel bearing metapelites to P/T determinations: an example for south India. *contrib. Mineral. Petrol.*, V. 76; pp.229-233.
116. Harris, N.B.W., Holt, R.W. and Drury, S.A. (1982) Geobarometry, Geothermometry and late Archaean geotherms from the granulite facies terrane of South India. *Jour. Geol.*, V. 90; pp.509-527.
117. Harris, N.B.W. and Jayaram, S. (1982) Metamorphism of cordierite gneiss from the Bangalore region of the Indian Archean. *lithos.*, V. 15; pp.89 - 98.
118. Haselton, H.T., Jr., Hovis, G.L., Hemingway, B.S. and Robie, R.A. (1983). calorimetric investigation of the excess entropy of mixing in analbite - sanidine solid solutions: Lack of evidence for Na, K, short-range order and implications for two-feldspar thermometry. *Am. Min.*, V. 68; pp.398-413.

119. Heier, K.S. (1962) The possible origins of amphibolites in an area of high metamorphic grade: *Norsk. Geol. Tidsskr.*, V. 42; pp. 157-165.
120. " and Adams, J.A.S. (1964) the geochemistry and genesis of the alkali metals. *Phys. Chem. Earth*; V. 5; pp.253-381.
121. Helgeson, H.C., Delany, J.M., Nesbitt, H.W. and Bird, D.K. (1978) Summary and critique of the thermodynamic properties of rock-forming minerals. *Am. J. Sci.*, V. 278; pp.229.
122. Helz, R.T. (1982) Phase relations and compositions of amphiboles produced in studies of the melting behaviour of rocks. *Reviews in Mineralogy. Mineral. Soc. of Am.*, V.9B; pp.279 -346.
123. Hensen, B.J. (1976). The stability of pyrope - grossular garnet with excess silica. *Contrib. Mineral. petrol.*, V. 55; pp.279-292.
124. " (1987) P-T grids for silica undersaturated granulites in the system MAS (n+4) and FMAS (n+3) - tools for the derivation of P-T paths of metamorphism. *Jour. Metamorph. Geol.*, V.5 ; pp.255 - 271.
125. " and Green, D.H. (1973). Experimental study of the stability of cordierite and garnet in pelitic compositions at high pressures and temperatures. II synthesis of experimental data and geological applications. *Contrib. Mineral. petrol.*, V. 38; pp.151-166.
126. Hensen, B.J, Schmid, R, Wood, B.J. (1975) Activity - composition relationships for pyrope - grossular garnet. *Contrib. Mineral. Petrol.*, V. 51; pp.161-166.
127. Hietanen, A. (1974) Amphibole pairs, epidote minerals, chlorite and plagioclase in metamorphic rocks. northern Sierra Nevada, California. *Am. Mineral.*, V. 59; pp.22 -29.
128. Hodges, K.V. and Mckenna, L.W. (1987) Realistic propagation of uncertainties in geologic thermobarometry. *Am.Mineral.* V.72; pp.671-680.
129. Hodges, K.V. and Spear, F.S. (1982). Geothermometry, geobarometry and the Al_2SiO_5 triple point at Mt. Moosilauke, New Hampshire. *Am. Mineral.*, V.67; pp.1118-1132.

130. Hoisch, D.T. (1989), A muscovite - biotite geothermometer. *Am. Mineral.*, V. 74: pp.565-572.
131. Holdaway, M.J. (1971). Stability of andalusite and aluminium silicate phase diagram. *Am.Jour.Sci.*, V. 271; pp.97-131.
132. Holdway, M.J. and Lee, S.M. (1977). Fe-Mg cordierite stability in high-grade pelitic rocks based on experimental, theoretical and natural observations. *Contrib. Mineral. Petrol.*, V. 63; pp.175-198.
133. Hollister, L.S (1982) Metamorphic evidence for rapid (2mm/yr) uplift of a portion of the central Gneiss complex, Coast Mountains, B.C. *Can. Mineral.*, V.20; pp.319-332.
134. Hollister, L.S., Burruss, R.C., Henry, D.L. and Hendel, E.M. (1979) Physical conditions during uplift of metamorphic terranes, as recorded by fluid inclusions. *Bull. Mineral.*, V. 102; pp.555-561.
135. Hollister, L.S. and Crawford, M.L. (1986) Melt-enhanced deformation: a major tectonic process. *Geology.*, V. 14; pp. 558 - 561.
136. Hollister, L.S. Grissom G.C., Peters, E.K., Stowell, H.H. and Sisson, V.B. (1987) confirmation of the empirical calibration of Al in hornblende with pressure of solidification of calc-alkali plutons. *Amer. Miner.*, V. 72; pp.231-239.
137. Holmes, A. (1955) Dating the precambrians of peninsular India and Ceylon. *Proc. Geol. Assn. Canada.*, V. 7(2); pp.81-106.
138. Holmquist, P.J. (1920), Om pegmatit palingeneses och ptymatisk veckning. *Geol. Foren. Stockholm Forh*; V. 42; pp.191-213.
139. Hopgood, A.M. (1980) Polyphase fold analysis of gneisses and migmatites. *Trans. Royal. Soc. Edinburgh (Earth sciences).*, V. 71; pp.55-68.
140. Hopgood, A.M., Bowes, D.R. and Addison, J. (1976) Structural development of migmatites near Skaldo, southwest Finland. *Bull. Geol. Soc. Finland.*, V. 48; pp. 43-62.

141. Hutcheon, I., Froese, E., Gordon T.M. (1974) the assemblage quartz - sillimanite - garnet - cordierite as an indicator of metamorphic conditions in the Daly Bay complex, N.W.T. *Contrib. Mineral. Petrol.*, V. 44; pp.29-34.
142. Indares, A. and Martignole, J. (1985) Biotite - garnet geothermometry in the granulite facies : the influence of Ti and Al in biotite. *Am. mineral.*, V.70; pp.272-278
143. Irvine, T.N. and Baragar, W.R.A. (1971) A guide to the chemical classification of the common volcanic rocks. *Can. J. earth. Sci.*, V. 8; pp. 523-548.
144. Irving, A.J. (1974) Geochemical and high pressure experimental studies of garnet pyroxenite and pyroxene granulite xenoliths from the Delegate Basaltic Pipes, Australia. *Jour. Petrol.*, V. 15; pp.1-40.
145. Iyer, S.S. and Santosh, M. (1987). Upper proterozoic Rb-Sr ages from the cordierite gneiss - charnockite terrain in kerala, south india. (Manuscript).
146. Jacob, S.C. (1962) Geology of the Western Ghats around Nagercoil, Kanyakumari District, Madras State. *Indian. Mineral.*, V. 3; pp.1-45.
147. Jacob, K. and Narayanaswamy, S. (1954) the structural and drainage patterns of the western Ghats in the vicinity of the Palghat Gap. *Proc. Nat. Inst. Sci. India.*, V. 20; No.1, pp.101-118.
148. Janardhan, A.S., Newton, R.C. and Smith, J.V. (1982) The transformation of amphibolite facies gneiss to charnockite in southern Karnataka and northern Tamil Nadu. *Contrib. Mineral. Petrol.*, V. 79; pp.130-149.
149. Jayananda, M. and Mahabaleswar, B. (1991) The generation and emplacement of closepet granite during Late Archaean granulite metamorphism in south eastern Karnataka. *Jour.Geol.Soc. India.*, V. 38 (4); pp. 418 - 426.
150. Johannes, W. and Gupta, L.N. (1982) Origin and evolution of a migmatite. *Contrib. Min. Petrol.*, V.79; pp.114-123.

151. Johnson, C.A., Essene E.J. (1982). The formation of garnet in olivine bearing metagabros from the Adirondacks, *Contrib. Mineral. Petrol.*, V. 81; pp. 240-251.
152. King, L.C. (1950) The study of the World's plain lands: A new approach in geomorphology, *Quart. Jour. Geol. Soc. Lond.* V. 106; pp. 101 - 131.
153. " (1962) The morphology of the Earth. Oliver and Boyd, Edinburgh and London, 638 p.
154. Knorring, O.V. and Kennedy, W.Q. (1958) The mineral parageneses and metamorphic status of garnet - hornblende - pyroxene - scapolite gnoisses from Ghana (Gold Coast). *Mineral. Mag.*, V.31; pp. 846-859.
155. Knup, P. (1958) Geologie Und Petrographie des Gebietes Zwischen Centoyalle - Valle Vigezzo und Onsernone. *Schweizerische Chem. Mineralog. Petrog. Mit.*, V. 38; pp. 83-235.
156. Konnerup - Madsen, J. and Rose-Hanson, J (1982) Volatiles associated with alkaline igneous rift activity: fluid inclusions in the Illimaussaq intrusion and the Gardar granitic complex (south Greenland). *Chem. Geol.*, V. 37; pp. 79-93.
157. Konnerup - Madsen, J., Rose - Hansen, J. and Larsen, E (1981) Hydrocarbon gases associated with alkaline igneous activity evidence from composition of fluid inclusions. *Bull. Grond, Geol. Unders.*, V. 103; pp. 99-108.
158. Kostyuk, E.A. (1970) Statistical analyses and paragenetic type of the metamorphic amphibolas. Nauke, Moscow. (in Russian).
159. Koziol, A.M. and Newton R.C. (1988) Redetermination of the An breakdown reaction and improvement of the plagioclase- quartz- Al_2SiO_5 -quartz geobarometer. *Am. mineral.*, V. 73; pp. 216-223
160. Koziol A.M. and Newton R.C. (1989) Grossular activity composition relationships in ternary garnets determined by reversed displaced- equilibrium experiments. *contrib. Mineral. Petrol.*, V. 103; pp. 423-433
161. Krauskopf, K.B (1955) sedimentary deposits of rare metals. *Econ. Geol (50th Anniversary Volume)*., pp. 411.

162. Krauskopf, K.B. (1979) Introduction to Geochemistry (2nd edition). McGraw - Hill, Newyork, 617 p.
163. Kretz, R. (1959) chemical study of garnet, biotite, and hornblende for gneisses of S.W. Quebec, with emphasis on distribution of elements in co-existing minerals. Jour. Geol., V. 67: pp. 371-402.
164. Krishnan, M.S. (1953) The structural and tectonic history of India. Mem. Geol. Surv. India., V. 81; 137p.
165. Kuno, H. (1966) Lateral variation of basalt magma type across continental margins and island arcs. bull. volcanol., V. 29; pp. 195-222.
166. " (1968) Differentiation of basalt magmas In: The Poldervaart Treatise on Rocks of Basaltic Composition: H.H. Hess. and A. Poldervaart (eds.), Interscience, Newyork, N.Y, V. 2; pp. 623-688.
167. Kushiro, I, Shimizu. N. and Nakamura Y.(1972) compositions of coexisting liquid and solid phases formed upon melting of natural quartz and spinel Iherzolites at high pressures: a preliminary report. Earth - Planet. Sci. Lett., V. 14; pp. 19-25.
168. Kushiro, I. and Yoder. H.S. (1966) Anorthite - forsterite and anorthite - enstatite reactions and their bearing on the basalt - eclogite transformation. Jour. Petrol., V. 7; pp. 337-362.
169. Lake, P. (1890) The geology of south Malabar. Mem. Geol. Surv. India., V. 24(3); pp. 201-246.
170. Lal, R.K. Ackermant, D., Raith, P., Raase, P. and Seifert, F. (1984) Sapphirine - bearing assemblages from Kiranur, southern India : a study of chemographic relationships in the $\text{Na}_2\text{O} - \text{FeO} - \text{MgO} - \text{Al}_2\text{O}_3 - \text{SiO}_2 - \text{H}_2\text{O}$ system. Neues Jahrb. Mineral. Montashefte. V. 150; pp. 121 - 152.
171. Lamb, W.M. (1988) CO_2 - rich inclusions in granulites: evidence for entrapment after the peak of metamorphism. Geol. Sos. India. Mem. No.11, pp.101-115.

172. Lamb, W.M., Valley, J.W and Brown, P.E. (1987) Post - metamorphic CO₂ rich fluid inclusions in granulites. *Contrib. Mineral. Petrol.* V. 96, pp.485-495.
173. Leake, B.E (1962) on the non-existence of a vacant area in the Hallimond calciferous amphibole diagram. *Japan, Jour. Geol. Geophys.*, V. 33; pp. 1-13.
174. " (1964). The chemical distinction between ortho and para-amphibolites. *Jour. Petrol.*, V. 5; pp. 238-254.
175. " (1978) Nomenclature of amphiboles. *Am. Mineral.*, V. 63; pp. 1025-1052.
178. Leake, B.E., Tanner, P.W.G. and Senior, A. (1975) The composition and origin of the Connemara dolomitic marbles and ophiolites, Ireland. *Jour. Petrol.*, V. 16; pp. 237-277.
179. Lee, S.M. and Holdaway, M. (1977) Significance of Fe-Mg cordierite stability relations on temperature, pressure and water pressure in cordierite granulites. In: *The Earths Crust*. Heacock, J.G (ed) AGU, Washington, *Geophys. Monogr. Series*; V. 20; pp. 79-94.
180. Lewis, J.D. and Spooner, C.M. (1973) K/Rb ratios of Precambrian granulite terrains. *Geochim. Cosmochim. Acta.*, V. 37; pp. 1111-1118.
181. Longkang, S. and Zhendong, Y. (1988) The metamorphic petrology of the Susong Group and the origin of the Susong Phosphorite deposits, Anhui Province. *Precamb. Res.*, V. 39; pp. 65-76.
182. Lonker, S.W. (1981) The P-T-X relations of the cordierite-sillimanite-quartz equilibrium. *Am. Jour. Sci.*, V. 281; pp. 1056-1090.
183. Lovering, J.F. and White, A.J.R. (1969) Granulitic and eclogitic inclusions from basic pipes at Delegate, Australia. *Contrib. Mineral. Petrol.*, V. 21; pp. 9-52.
184. Maccarrone, E., Paglionico, A., Piccarreta, G. and Rottura, A. (1982) Granulite - amphibolite facies meta sediments from the serre (Calabria, southern Italy): their protoliths and the processes controlling their chemistry. *Lithos.*, V. 16; pp. 95-111.

185. MacDonald, G.A. (1968) Composition and origin of Hawaiian lavas. In: Studies in Volcanology: A memoir in Honour of Howel Williams: R.R. Coats, R.L. Hay and C.A. Anderson (eds), Geol. Soc. Am. Mem., V. 116; pp.477-522.
186. Mahadevan, T.M. (1964) The origin of charnockite suite of rocks from the Western Ghats in Kerala, India. Inter. Geol. Cong., V. 79; pp. 130-149
187. Mani, G (1975) Report on the structural mapping of Palaghat gap in Coimbatore District, Tamil Nadu. Geol. Surv. India (unpublished report)., 18 p.
188. Maniar, P.D. and Piccoli, P.M. (1989) Tectonic discrimination of granitoids, Geol. Soc. Am. Bull., V. 101; pp. 635-643.
189. Marmo, V. (1971) Granite petrology and the granite problem. Elsevier, Amsterdam, 244 P.
190. Marston, R.J. (1978) The geochemistry of Archean clastic metasediments in relation to crustal evolution, northeast Yilgarn block, west Australia. Precamb. Res., V. 6; pp. 157-175.
191. Martignole, J. and Sisi, J.C (1981) cordierite - garnet - H₂O equilibrium: A geological thermometer, barometer and water fugacity indicator. Contrib. Mineral Petrol., V. 77; pp. 38-46.
192. Mart'inez, F.J. and Gilibarguchi, J.I. (1982) El metamorfismo en el Macizo Iberico. Libro. Jub J.M. Rios (in press).
193. McCulloch, M.T. and Chappell, B.W. (1982) Nd - isotopic characteristics of S and I - type granite. Earth. Planet. Sci. Lett., V. 58; pp. 51-64.
194. McLellan, E.L. (1984) Deformational behaviour of migmatites and problems of structural analysis in migmatite terrains. Geol. Mag., V. 121(4); pp. 339-345.
195. Medlicott, H.B. and Blanord, W.T. (1893) A manual of Geology of India. (2nd ed) Revised by R.D. Oldham, Calcutta, 495 p.
196. Mehnert, K.R. (1968) Migmatites and the origin of granitic rocks (Amsterdam: Elsevier), 405 p.

197. Misch, P. (1968) Plagioclase compositions and non-anatectic origin of migmatitic greisses in northern Cascade Mountains of Washington state. *Contrib. Mineral. Petrol.*, V. 17; pp. 1-70.
198. Mishra, D.C (1988) Geophysical evidence for a thick crust south of Palghat - Tiruchi gap in the high grade terranes of south India. *Jour. Geol. Soc. India.*, V. 31; pp. 79-81.
199. Miyashiro, A. (1974) Volcanic rock series in Island Arcs and active continental margins, *Am. Jour. Sci.*, V. 274; pp. 321-355.
200. Moecher, D.P., Essene, E.J. and Anovitz, L.M. (1988) Calculation and application of clinopyroxene - garnet - Plagioclase - quartz geobarometers. *Contrib. Mineral. petrol.*, V. 100; pp. 92-106.
201. Mori, T, Green D.H. (1978). Laboratory application of phase equilibria observed in natural garnet Iherzolite. *Jour., Geol.*, V.86; pp. 83-97.
202. Morimoto, N., Fabries, J.J, Ferguson, A.K., Ginzburg, I.V., Ross, M., Seifert, F.A., zursman, J., Aoki, K. and Gottardi, G. (1988). Nomenclature of pyroxenes. *Am. Mineral.*, V. 73; pp. 1123 - 1133.
203. Mueller, R.F. and saxena, S.K (1977) *Chemical Petrology*. Springer - Verlag, New York.
204. Mukhopadhyay, D (1986) Structural pattern in the Dharwar craton. *Jour. Geol.*, V. 94; pp. 167-186.
205. Munyanyiwa, H. and Hanson, R.E. (1988) Geochemistry of marbles and calc silicate rocks in the Pan-African Zambezi belt, Zambia. *Precambrian Research.*, V. 38; pp. 177-200.
206. Murthy, M.V.N. and Venkataraman, P.K. (1964) Petrogenetic significance of certain platform peralkaline granites of the world. In: *The Upper Mantle (symp)*, New Delhi. Smith, C.H. and Sorgenfrei, T (eds), pp. 127 - 149.
207. Mysen, B.O. and Heier, K.S. (1972) Petrogenesis of eclogites in high grade metamorphic gneisses exemplified by the Hareidland Eclogite., western Norway. *Contrib Mineral. Petrol.*, V. 36; pp. 73-94.

208. Nageswara Rao, J. and Srinivasan, R. (1980) some aspects of geomorphology, structure and sedimentation in Palaghat Gap area. Geol. Surv. India, spec. Publ., No. 5, pp. 39-43.
209. Naha, K. (1990) Structural relations of Charnockites of South India: In: Granulites of south India: B.P. Radhakrishna, M. Ramakrishnan and B. Mahabaleswar (eds.) Geol. Soc. India., Pichamuthum volume, pp. 196.
210. Nair, M.M. (1990) structural trendline patterns and lineaments of the Western Ghats, South of 13° latitude. Jour. Geol. Soc. India., V. 35; pp. 99-105.
211. Nair, N.G.K., Soman, K., Santosh, M., Arakelyants, M.M. and Golubyer, V.N. (1985) K- Ar. ages of three granite plutons from north Kerala. Jour. Geol. Soc. India., V. 26; pp.674-676.
212. Nair, M.M. and Vidyadharan, K.T., (1982) Rapakivi granite of Ezhimala complex and its significance. Jour. Geol. Soc. India., V. 23; No. 1, pp. 46-51.
213. Naqvi, S.M. and Hussain, S.M. (1973) Geochemistry of Dharwar meta-volcanics and composition of the primeval crust of peninsular India. Geochim. Cosmochim. Acta., V. 37; pp.159-164.
214. Narayana, B.L., Natarajan, R. and Govil, P.K. (1988). Petrology and physical conditions of metamorphism of calc silicate rocks from low to high-grade transition area, Dharmapuri Dist., Tamil Nadu. In: Deep continental crust of S. India (Abstr), Mem. 4; pp. 127-128.
215. Narayanaswamy, S. (1975) Proposal for a charnockite - khondalite system in the Archaean shield of Peninsular India. Geol. Surv. India. Misc. Publ., V. 23; pp. 1 - 16.
216. Narayanaswamy, S. and Lekshmi, P. (1967) Charnockite rocks of Tennevelly District, Madras. J. Geol. Soc. India., V. 8; pp. 38-50.
217. Newton, R. C. (1972) An experimental investigation of the high- pressure stability limits of magnesian cordierite under wet and dry conditions. Jour. Geol., V. 80; pp. 398 - 420.

218. Newton, R.C., Charlu, T.V. and Kleppa, O.J. (1977). Thermochemistry of high pressure garnets and clino pyroxenes in the system $\text{CaO} - \text{MgO} - \text{Al}_2\text{O}_3 - \text{SiO}_2$. *Geochim. Cosmochim. Acta*; V. 41; pp. 369-377.
219. " (1980) Thermochemistry of the high structural state plagioclases. *Geochim. Cosmochim. Acta.*, V. 44; pp. 933-941.
220. Newton, R.C. and Hansen, E.C. (1986) The south India - Srilanka high grade terraiion as a possible deep - crust section. *Jour. Geol. Soc. Lond. spec. publ.*, V. 25; pp. 297 - 309.
221. Newton, R.C., Haselton, H.J. (1981) Thermodynamics of the garnet Plagioclase - Al_2SiO_5 - quartz geobarometer. In: *Thermodynamics of Minerals and melts* Newton R.C., Navrotsky, A, Wood B.J (eds), Springer, Berlin, Heidelberg, Newyork, pp. 131-147.
222. Newton, R.C. and Wood B.J. (1979) Thermodynamics of water in cordierite and some petrologic connnsequences of cordierite as a hydrous phase. *Contrib. Mineral Petrol*, V. 68; pp. 391-405.
223. Nicolaysen, L.O., Buerger, A.J., Tatsumi, T. and Ahrens, L.H. (1961). Age measurements on pegmatites and basic charnockite lens occuring near Lutzow Holm Bay Antarctica. *Geochim. Cosmochim. Acta.*, V. 22; pp. 94-98.
224. Nockolds, S.R. (1954) Average chemical composition of some igneous rocks *Geol. Soc. Am. Bull.*, V. 65; pp. 1007-1032.
225. Novak, J.M and Holdaway, M.J. (1981) Metamorphic petrology, Mineral equilibria and polymetamorphism in the Augusta quadrangle, south-central Maine. *Am. Mineral.*, V. 66; pp. 51-69.
226. Nurminen, K.B. (1987) A recalibration of the chlorite biotite - muscovite geobarometer. *Contrib. Mineral. Petrol.*, V. 96; pp. 519-522.
227. O'conner, J.T. (1965) A classification for quartz rich igneous rocks based on feldspar ratios. *U.S. Geol. Surv. Prof. pap.*, pp. 525-B.

228. Odom, A.L. (1982) Isotopic age determinations of rock and mineral samples from the Kerala district of India. Final report, U.N. Case No. 81 - 10084 (unpub.) 10 p.
229. O'Hara, M.J. (1977) Thermal history of excavation of Archean gneisses from the base of the continental crust. Geol. Soc. London., V. 134; pp.185-200.
230. O'Hara, M.J. and Yarwood, G. (1978) High Pressure - temperature point on an Archean geotherm, implied magma genesis by crustal anatexis, and consequences for garnet - pyroxene thermometry and barometry. Phil. Trans. Royal. Soc. (London)., V. 288; pp. 441-456.
231. Oka, Y. and Matsumoto, T. (1974) Study on the compositional dependence of the apparent partition coefficient of iron and magnesium between co-existing garnet and clinopyroxene solid solution. Contrib. Mineral. Petrol., V. 47; pp. 115-121.
232. Olsen, S.N. (1985) Mass balance in migmatites In: Migmatites. Ashworth J.R. (ed), Blackie, Scotland, pp. 145-179.
233. O'Neil, J.R. and Chapell, B.W. (1977) Oxygen and hydrogen isotope relations in the Berridale batholith. Jour. Geol. Soc., V. 133; 6,pp. 559-571.
234. O'Neil, H. St. C. and Wood, B.J. (1979) an experimental study of Fe - Mg partitioning between garnet and olivine and its calibration as a geothermometer. Contrib. Mineral. Petrol., V. 70; pp. 59-70.
235. Orville, M.P. (1969) A model for metamorphic differentiation origin of thin layered amphibolites. Am. Jour. sci., V. 267; pp. 64-86.
236. Papageorgakis, J. (1961) Marmore und kalsilikatfelse de zone Ivrea-verbeno Zwischen Ascona und Candoglia: Schweizersche Mineralog. Petrog. Mitt., V. 41; pp. 157-254.
237. Paria, P., Bhattacharya, A. and Sen, S.K. (1988) The reaction garnet + clinopyroxene + quartz = 2 orthopyroxene + anorthite: A potential geobarometer for granulites. Contrib. Mineral. Petrol., V. 99; pp. 126-133.

238. Pattison, D.R.M. and Newton, R.C. (1989) Reversed experimental calibration of the garnet - clinopyroxene Fe-Mg exchange thermometer. *Contrib. Mineral. Petrol.*, V. 101; pp.87-103.
239. Pearce, T.H., Gorman, B.E. and Birkett, T.C. (1975) The TiO_2 - K_2O - P_2O_5 diagram a method of discriminating between oceanic and non-oceanic basalts. *Earth Planet. Sci. Lett.*, V. 24; pp.419-426.
240. Perchuk, L.L. (1967) Biotite - garnet geothermometer. *Academia Nauk, USSR Doklady*. V. 177; pp.131-134.
241. " (1970) Equilibrium of biotite with garnet in metamorphic rocks, *Geochim Int.*, V. 7; pp.157-179.
242. " (1981) correction of the biotite-garnet thermometer in case of the Mn = Mg + Fe isomorphism in garnet. *Dokl. USSR AS.*, V. 256; pp.38-41.
243. Perchuk, C.L. and Lavrent'eva, I.V. (1983) Experimental investigation of exchange equilibria in the system cordierite - garnet - biotite. In: *Kinetics and Equilibrium in Mineral Reaction*, Saxena S.K. (ed). Springer, Berlin, Heidelberg, Newyork, pp.199-239.
244. Perkins, D(III) and Chipera, S.J. (1984) Garnet - orthopyroxene - plagioclase - quartz barometry : refinement and application to the English river subprovince and the Minnesota river valley. *Contrib. Min. Petrol.*, V. 89; pp.69-80.
245. Perkins, D(III)., Essene, E.J. and Marcotty, L.A. (1982). Thermometry and barometry of some amphibolite - granulite facies rocks from the Otter Lake area, southern Quebec. *Canad. J. Earth. Sci.*, V. 19; pp.1759-1774
246. Perkins, D. and Newton, R.C. (1981). charnockite geobarometers based on coexisting garnet - pyroxene - plagioclase - quartz. *Nature.*, V. 292; pp. 144 -146.
247. Peterman, Z.E., Hedge, C.E., Coleman, R.G. and Snively, P.P., Jr (1967) Sr^{87}/Sr^{86} ratios in some eugeosynclinal sedimentary rocks and their bearing on the origin of granitic magma in orogenic belts. *Earth. Planet. Sci. Lett.*, V. 2; pp.433.

248. Pettijohn, F.J. (1949) Sedimentary Rocks. Harper, New York, 526 p.
249. " (1963) Chemical composition of sandstones-excluding carbonate and volcanic sands. In: Data of Geochemistry, U.S. Geol. Surv. Prof. Pap., 440-S, 19 p.
250. " (1975) Sedimentary Rocks, (3rd ed.), Harper & Row, 718 p.
251. Plank, T. (1987) Magmatic garnets from the Cardigon pluton and the Acadian thermal event in S.W. New Hampshire, Am.Mineral., V. 72; No.7&8. pp.681-688.
252. Plyusnina, L.P. (1982) Geothermometry and geobarometry of plagioclase-hornblende bearing assembles. Contrib. Mineral. Petrol., V. 80; pp. 140-146.
253. Poldervaart, A. (1955) Chemistry of the Earth's crust: Geol.Soc.Am. Spec. paper., V. 62; pp.119-144.
254. Powell, M. and Powell, R. (1977). Plagioclase, alkalifeldspar thermometry revisited. Mineral. Mag., V. 41; pp.253-256.
255. Pownceby, M.I., Victor J.W. and O'Neil, H.St.C. (1987) Fe-Mn partitioning between garnet and ilmenite : experimental calibration and applications. Contrib. Mineral. Petrol., V. 97; pp.116-126.
256. Price, J.G. (1985) Ideal site-mixing in solid solutions with applications to two-feldspar geothermometry. Am. Mineral., V. 70 pp.696-701
257. Putnis, A. and Bisch, D.L. (1983) The mechanism and kinetics of Al, Si ordering in Mg-cordierite. Am.Mineral., V. 68; pp.60-65
258. Radhakrishna, B.P. (1968) Geomorphological approach to the charnockite problem. Jour. Geol. Soc. India., V. 9; pp. 67 - 74.
259. " (1989) Suspect tectono-stratigraphic terrane elements in the indian sub - continent. Jour. Geol. Soc. India., V. 34; No.1,pp. 1-24.
260. Raheim, A. and Green, D.H. (1974) Experimental determination of the temperature and pressure dependence of the Fe-Mg partition coefficient for co-existing garnet and clinopyroxene. Contrib. Mineral. Petrol., V. 48; pp 179-203.

261. Raith, M., Raase, P., Ackerman, D. and Lal, R.K. (1982) Regional Geothermobarometry in the granulite facies terrane of South India. *Trans. Roy. Soc. Edin.(Earth Sci.)*, V. 73; part 4, pp.221-244.
262. Rajan, P.K., Santosh, M. and Ramachandran, K.K. (1984) Geochemistry and petrogenetic evolution of the diatexites of central Kerala, India. *Proc. Indian Acad. Sci (Earth & Planet Sci.)*, V.93; No.1, March.pp.57-69.
263. Rama Krishnan, M. (1988) Tectonic evolution of the Archaean high-grade terrain of south India. *Jour. Geol. Soc. India.*, V. 31; pp.118-120.
264. " (1991) Evolution of the high grade terrain of southern India and Srilanka. In: *Composition and Evolution of High Grade Gneiss Terrain, Srilanka (Abstr)*. pp. 57 - 59.
265. Rao, P.S. (1978) some aspects of structure and tectonics of Kerala region, India and related metallogeny. In: *Tectonics and metallogeny of South- East Asia. Geol. Surv. India. Misc. Publ.*, part III, V. 34; pp. 61-64.
266. Rao, P.S., Reddy, U.S. and Selvan, T.A. (1975) Crystalline limestone in Kerala with special reference to the occurrence and utilisation. *Proc. of the symp. Geoscience & Technology Assoc. Kerala*, 18-19 Oct., pp. 82-89.
267. Rao, P.S., Selvan T.A. and Pawar, S.D. (1974) Report on the prospecting and preliminary exploration for limestone, Pandarettu area, Walayar R.F, Palghat district, Kerala State (Unpublished report of the G.S.I.)
268. Raval, U. (1988) Electrical structure and its implication across the lower - and upper - crustal settings of south India. *Jour. Geol. Soc. India.*, V. 31; pp. 127 - 129.
269. Ravindra Kumar, G.R. and Chacko, T. (1986) Mechanism of charnockite formation at Ponmudi, Southern India: *Nature (London)*, V. 313; pp.207-209.
270. Ravindra Kumar, G.R., Srikantappa, C. and Hansen, E. (1985) Charnockite formation at Ponmudi in southern India. *Nature.*, V. 313; pp. 207-209.

271. Reddy, A.G.B., Mathew, M.P., Singh, B. and Naidu, P.B. (1988) Aeromagnetic evidence of crustal structure in the granulite terrane of Tamil Nadu, Kerala. *Jour. Geol. Soc. India.*, V. 32; pp. 368-381.
272. Rickwood, P.C. (1989) Boundary lines within petrologic diagrams which use oxides of major and minor elements. *Lithos.*, V. 22; pp. 247-263.
273. Robie, R.A, Bin, Z., Hemingway, B.S. and Barton, M.D. (1987) Heat capacity and thermodynamic properties of andradite garnet. $\text{CaFe}_2\text{Si}_3\text{O}_{12}$ between 10 and 1000 k and revised values of T.Gm. (298.15) of hedenbergite and Wollastonite. *Geochim Cosmochim. Acta.*, V. 51; pp.2219-2224.
274. Robinson, P., Ross, M. and Jaffe, H. (1971) composition of the anthophyllite - gedrite series. Comparisons of gedrite and hornblende and the anthophyllite - gedrite solvus. *Am. Mineral.*, V.56; pp.1005-1041.
275. Roedder, E. (1984) Fluid Inclusions. *Reviews in Mineralogy. Mineral. Soc. Am.*, V.12; 644 p.
276. Rossman, G.R., Grew, E.S. and Dullase, W.H. (1982) The colour of sillimanite. *Am. Mineral.*, V. 67; No. 7 & 8, pp. 749-761.
277. Russ, C.A. (1984). Contact metamorphism of mafic schists, Laramic anorthosite complex, Morton Pass, Wyoming (Master thesis), State University of New York, Stony Brook, IIIp.
278. Rutter. M.J., Van der Laan S.R. and Wyllie P.J. (1989), Experimental data for a proposed empirical igneous geobarometer: Aluminium in hornblende at 10 Kbar pressure. *Geology.*, V. 17; No. 10, pp. 897-900.
279. Santosh, M. (1984) Fluid inclusion petrography of charnockites from the granulite facies terrain of Kerala, south west India. *Neues. Jb. Miner. Mh.*, H-8, pp. 337 - 345.
280. " (1986) Carbonic metamorphism of charnockites in the south western Indian shield : a fluid inclusion study. *Lithos.*, V.19; pp. 1-10.

281. Santosh, M., Drury, S.A. and Iyer, S.S. (1988) Pan African alkali granites and syenites of Kerala as imprints of taphrogenic magmatism in the south Indian shield. Geol. Soc. India. Mem., V. 4; pp.130-132.
282. Santosh, M., Iyer, S.S. and Vasconcellos, M.B.A. (1987) Rb-Sr geochronology and REE geochemistry of alkali granites from the south-west Indian shield and their bearing on Pan Africa taphrogenic magmatism. Lithos.,
283. Santosh, M. and Thara K.G. (1984) The Mannapra syenite, central Kerala, India, Geochemistry, petrogenesis and bearing on anorogenic magmatism. Proc. Indian Acad. Sci. (Earth. Planet. Sci)., V. 94; No.1, pp.43-56.
284. Sarkar, S.N. (1968) Precambrian stratigraphy and geochronology of Peninsular India. Dhanbad publishers, pp. 1-33
285. Saxena, S.K. (1969) Silicate Solid solution and geothermometry. Distribution of Fe and Mg between co-existing garnet and biotite. Contrib. Mineral. petrol., V. 22; pp. 259-267.
286. " (1976) Two pyroxene geothermometer: a model with an approximate solution. Am. Mineral., Vol.61; No. 7&8, pp.643-652.
287. " (1979) Garnet - clinopyroxene geothermometer. Contrib. Mineral. petrol., V. 70; pp. 229-235.
288. Schmid, R., Cressey, G. and Wood B.J. (1978) Experimental determination of univariant equilibria using divariant solid - solution assemblages. Am. Mineral., V. 63; pp.511-515.
289. Seck, H.A. (1971 a). Koexistierendi Alkalifeldspate and plagioklase im system $\text{NaAlSi}_3\text{O}_8$ - $\text{CaAl}_2\text{Si}_2\text{O}_8$ - H_2O . bei Temperaturen Von 650°C bis 900°C . Neues. Jahrbuch fur Mineralogie Abundlungen., V. 115; pp.315-345.
290. " (1971 b) Der Einfluss des Drucks auf die Zusammensetzung Koexistierender Alkali-feldspate und Plagioklase. Contrib. Mineral. Petrol., V. 31; pp. 67-86.
291. Sederholm, J.J. (1907) On granite and gneiss. Bulletin. Commission. Geologique de Finlande., V. 23; pp. 1-110

292. Sederholm, J.J. (1913) Die Entstehung der migmatischen Gesteine. Geologische Rundschau., V. 4; pp.174-185.
293. " (1934) On migmatites and associated Precambrian rocks of south western Finland. Bulletin commission. Geologique de Finlande., V. 107; pp.1-68.
294. Senior, A. and Leake, B.E. (1978) Regional metasomatism and the geochemistry of the Dalradian metasediments of Connemara, Western Ireland. Jour. Petrol., V. 19; pp.585-625.
295. Sevigny, T.H.(1988) Geochemistry of Late Proterozoic amphibolites and ultramafic rocks, South eastern Canadian cordillera. Can.J.Earth. Sci., V. 25; pp. 1323-1337.
296. Shand, S.J. (1950) Eruptive Rocks. (4th edition) Wiley, New York. Shaw, D.M. (1956) Geochemistry of pelitic rocks. Part III. Major elements and general geochemistry. Geol. Soc. Am. Bull., V. 67; pp.919-934.
297. Sharma, R.S. (1988) Granulites from northwest Indian shield : Their differences and similarities with southern Indian granulite terrain . Jour. Geol. Soc. India., V. 31; pp. 136 - 138.
298. Shelley, D. (1975) Manual of optical mineralogy. Elsevier publishing company, 201 p.
299. Sighinolfi, G.P.(1969) K/Rb ratio in high- grade metamorphism : a confirmation of the hypothesis of continual crustal evolution. Contrib. Mineral. Petrol., V. 21; pp.346-356.
300. " (1971) Investigations into deep crustal levels : fractionating effects and geochemical trends related to high grade metamorphism. Geochim. Cosmochim. Acta., V. 35; pp.1005-1021.
301. " (1974) Geochemistry of early Precambrian carbonate rocks from the Brazilian shield: implications for Archean carbonate sedimentation. Contrib. Mineral. Petrol., V. 46; pp. 189-200.
302. Sinha Roy, S. (1979a) structural evolution of the Precambrian crystalline rocks in parts of the Trivandrum and Quilon Districts, kerala : professional paper, 7., Centre for Earth Science Studies, pp. 1-25.

303. Sinha Roy, S. (1979b) Laterite profiles in relation to geomorphology in parts of Trivandrum District, Kerala : Prof. Paper, Centre for Earth Science Studies.
304. " (1983) Structural evolution of the precambrian crystalline rocks of South Kerala In: Structure and Tectonics of precambrian rocks of india: S.Sinha-Roy (ed). Hindustan pub.co; Delhi, pp.127-143.
305. Soman, K. (1980) Geology of Kerala, professional paper, No.8; Centre for Earth Science studies.
306. Soman, K., Nair, N.G.K., Golubyev, V.N. and Arakelyan, M.M. (1982) Age data on pegmatites of south Kerala and their tectonic significance. Jour. Geol. Soc. India., V. 23(9); pp.458-462.
307. Soman, K., Santosh, M. and Golubyev, V.N., (1983). Early paleozoic I - type granite from central Kerala and its bearing on possible mineralization, india. Jour Earth. Sci., V. 10; pp.137-141.
308. Soman, K. Thara, K.G., Arakelyants, M.M. and Golubyer, V.N. (1990) Mineral ages of pegmatites from the Palghat Gap region in Kerala and their tectonic significance. Jour. Geol. Soc. India., V. 35; pp. 82 - 86.
309. Soman, K. Thara , K.G. and Motoyoshi, Y. (1992) Geothermobarometric conditions of formation of granulites in Palghat Gap region, Kerala. Proc. Kerala. Sci. Congr., Feb, pp. 193 - 195.
310. Sonder, L.L., England , P.C., Wernicke, B.P. and Christiansen, R.L. (1987) A physical model for Cenozoic extension of western North America. In: Continental Extensional tectonics. M.P. Coward, J.F. Dewey and P.L. Hancock (eds), Geol. Soc. Lond. Spec. Publ., No. 28, pp.187 - 201.
311. Srikantappa, C. (1987) Carbonic inclusions from the Nilgiri charnockite massif, Tamil Nadu, India . Jour. Geol. Soc. India., V. 30; pp. 72-76.
312. Srikantappa, C., Ashamanjari, K.G, Prakash Naramsimha, K.N. and Raith, M. (1988) Retrograde charnockite - gneiss relation in southern India. Jour. Geol. Soc. india., V. 31; pp. 112-113.

313. Srikantappa, C. and Prakash Narasimha, K.N. (1988) Retrogression of charnockites in Moyar shear zone, Tamil Nadu, India. Geol. Soc. India. Mem., No.11; pp. 117-124.
314. Srikantappa, C., Raith, M. Ashamanjari, K.G., Ackermant, D. (1986) pyroxenites and gabbroic rocks from the Nilgiri granulite terrane, southern India. Indian Mineral., V. 27; pp. 62-83.
315. Srikantappa, C., Raith, M. and Klatt, E. (1987) Fluid regime during charnockite formation in the granulite terrane of the Nilgiri Hills, Southern India. European current research on fluid inclusions (Abstr), 9th symposium, Univ. of Porto, Portugal.
316. Srikantappa, C., Raith, M. and Spiering, B. (1985) Progressive charnockitisation of a leptynite - khondalite suite in southern Kerala, India - evidence for formation of charnockite through decrease in fluid pressure?. Jour. Geol. Soc. India., V.26; pp.849-872.
317. Stellan, A. (1988) Interpretation of biotite - garnet - partitioning data from two sve cokarelian metamorphic rock units. lithos., V. 22; pp. 25 - 29.
318. Sterner, S.M. and Bodnar, R.J. (1989) synthetic fluid inclusion - VII. Re- equilibration of fluid inclusions in quartz during laboratory simulated metamorphic burial and uplift. Jour. Metamorph. Geol, V.7; No.2, pp. 242.
319. Stewart, D.B. and Ribbe, P.H. (1969) structural explanation for variations in cell parameters of alkali feldspars with Al/Si ordering. Am.Jour. Sci., V. 267 A; pp. 444-462
320. St - Onge, M.R. (1987). Zoned poikiloblastic garnets: P-T paths and syn-metamorphic uplift through 30 km of structural depth, Wopmay orogen, Canada: Jour. Petrol., V. 28; pp. 1-21.
321. Stormer. J.C. (1975), A practical two-feldspar thermometer. Am. Mineral., V. 60; pp.667-674.
322. Streckeisens, A., (1976) To each plutonic rock its proper name; Earth Sci. Review., V. 12; pp.1-33.

323. Subramanian, A.P. (1956) Mineralogy and petrology of the Sittampundi complex, Salem District, Madras state, India. Geol. Soc. Am. Bull., V. 67; pp. 317 - 423.
324. Subramanian, C. (1978) On the relation of gravity anomalies to geotectonics of the Precambrian terrains of the south Indian shield. Jour. Geol. Soc. India., V.19; No.6, pp.251.
325. Subramanian, K.S., Mani, G. and Prabhakara Rao, P. (1980) Geomorphological and geochemical aspects of some residual deposits in the southern part of the Indian peninsula. Geol. Surv. India. Spl. publ., No.5; pp.48-50.
326. Subramanian, K.S. and Muraleedharan, M.P. (1985) origin of the Palghat Gap in south India - A synthesis. Jour. Geol. Soc. India., V. 26; pp. 28-37.
327. Taylor, H.P., Jr. (1977) Water rock interaction and the origin of H₂O in granitic batholiths. Jour. Geol. Soc., V. 133; part 6, pp. 509-558.
328. Thara, K.G. (1989) Geology, metamorphism and tectonic evolution of a segment of Palghat Gap, Kerala (Unpublished report), CSIR, 74 p.
329. " (1992) Geological setting and geochemical characterisation of the Pandarettu limestone deposit, Walayar, Kerala. Proc. Kerala. Sci. Congr., Feb, pp. 11 - 14.
330. Thompson, A.B. (1975) Calc-silicate diffusion zones between marble and pelitic schist. Jour.Petrol., V. 16; pp.314-346.
331. " (1976). Mineral reactions in pelitic rocks: I. Prediction of P-T-X (Fe-Mg) phase relations. Am. Jour. Sci., V. 276; pp.401-24.
332. Tracy, R.J. (1982) Compositional zoning and inclusions in metamorphic mineral. Min. Soc. Am., Reviews in Min, V. 10; pp 355-397.
333. Turekian, K.K. and Wedepohl, K.H. (1961) Distribution of the elements in some major units of the Earth's crust. Geol. Soc. Am. Bull., V. 72; pp.175-192.
334. Tuttle, O.F. and Bowen, N.L. (1958) Origin of granite in the light of experimental studies in the system NaAlSi₃O₈ - KAlSi₃O₈ - H₂O. Geol. Soc. Am. Mem., V. 74; 153 p.

335. Urey, H.C. (1947). the thermodynamic properties of isotopic substances. J. Chem. Soc. (London)., pp. 562-581.
336. Vaidyanathan, R. (1967) An outline of the geomorphic history of India, south of 18° N latitude. Proc. Sem. on Geomorphological studies in India, Centre for Adv. Study, Univ. Sagar., pp. 121-130.
337. " (1977) Recent advances in geomorphic studies of Peninsular India. Jour. Geol. Soc. India: A Review. Indian Jour. Earth Sci., (Ray Volume), pp.17-20.
338. Van de Kamp, P.C. (1970) The green beds of the scottish Dalradian series; geochemistry, origin and metamorphism of mafic sediments. Jour. Geol., V. 78; pp. 281-303.
339. Venkata Rao, V. and Subramanian, K.S. (1979) Implications of geology and structure on the evolution of the high level disposition of the Nilgiri Hills. Geol. Surv. India. Rec., V. 112; pp.85-88.
340. Venkatasubramanian, V.S., Gopalan, K., Iyer, S.S. and Krishnan, R.S. (1967) Studies on the Rb-Sr and K-Ar dating of minerals from the Precambrian of India. Geochronology of Precambrian stratified rocks. Conference at Alberta (Abst.), pp.90.
341. Venkatasubramanian, V.S. and Krishnan, R.S. (1961). Radioactivity and geochronology of igneous and metamorphic rocks of the Precambrian Era of the Indian Peninsula. Proc. nat. Inst. Sci., V. 26; pp.89-99.
342. Vinogradov, A.P. and Tugarinov, A.I., (1964). Geochronology of the Indian Precambrians. (Report) 22nd Inter. Geol. Cong. (Report), New Delhi.
343. Virgo, D. and Hafner, S.S. (1969). Fe²⁺, Mg order-disorder in heated orthopyroxene. Mineral. Soc. Am. Spec. Paper., V. 2; pp. 67-81.
344. Walker, K.R., Joplin, G.A., Lovering, J.F. and Green, R. (1960) Metamorphic and metasomatic convergence of basic igneous rocks and lime-magnesia sediments of the Pre-cambrian of north-western Queensland: Jour. Geol. Soc. Australia. V. 6; pp.149-177.

345. Wedepohl, K.H. (1969) composition and abundance of common sedimentary rocks, In: Handbook of Geochemistry I Wedepohl, K.H.(ed) Springer verlag, Berlin- Heidelberg - Newyork, pp. 227-271.
346. Weisbrod, A. (1973) Refinements of the equilibrium conditions of the reaction Fe- cordierite= almandine + Sillimanite + quartz + (H₂O). Carnegie Inst. Washington Year Book., V. 72; pp.518-521.
347. Weisbrod (1973 b). Cordierite - garnet equilibrium in the system. Fe-Mn-Al-Si-O. Carnegie Inst. Washington Year Book, V.72; pp. 515-518.
348. Wells, P.R.A. (1977) Pyroxene thermometry in simple and complex systems. Contrib. Mineral. petrol, V. 62; pp.129-139.
349. " (1979) Chemical and thermal evolution of Archean sialic crust, southern West Greenland. Jour. petrol., V. 20; pp. 187-226.
350. " (1980) Thermal models for the magmatic accretion and subsequent metamorphism of continental crust. Earth. Planet. Sci. Lett., V. 46; pp. 253 - 265
351. White, A.J.R. (1966) Genesis of migmatites from the Palmer region of s. Australia. Chem.Geol., V. 1; pp. 165-200.
352. Wilcox, R.E. and Poldervaart, A. (1958) Metadolerite dyke swarms in Bakersville - Roan Mountain area, north Carolina. Geol. Soc. Am. Bull., V.69; pp.1323-1368.
353. Wilson, A.F., Compston, W., Jeffrey, P.M. and Riley, G.H. (1960). Radioactive ages from the Precambrian rocks of Australia. Jour. Geol. Soc. Australia., V. 6; pp. 179-195.
354. Winkler, H.G.F. (1961) Die Genese Von Granites und Migmatites unf Grund neuer Experimente. Geologische Rundschau., V. 61; pp. 347-364.
355. " (1979) petrogenesis of Metamorphic Rocks (4th edition). Springer-Verlag, 348 p.
356. Wood, B.J. (1975) The influence of presure, temperature and bulk compositions on the appearance of garnet in ortho-gneisses - an example from south Harris, Scotland. Earth. planet. Sci. Lett., V. 26; pp.299-311.

357. Wood, B.J. (1976). The partitioning of iron and magnesium between garnet and clinopyroxene. Carnegie Inst. Washington Year Book. V. 75; pp.571-574.
358. " and Banno, S. (1973). Garnet- orthopyroxene and orthopyroxene- clinopyroxene relationships in simple and complex systems. Contrib. Mineral. Petrol., V. 42; pp.100-124.
359. Wyllie, P.J. (1976). The Way the Earth Works. John Wiley & sons, New York, 234.P.
360. Yoder, H.S. Jr. and Tilley, C.E. (1962) Origin of basalt magmas: an experimental study of natural and synthetic rock systems: Jour. Petrol V. 3; pp. 342-532.